EXPLORING SMALL BITE-ANGLE PNP AND PCP LIGANDS FOR THE RHODIUM-CATALYSED INTERMOLECULAR HYDROACYLATION OF β-S-SUBSTITUTED ALDEHYDES WITH ALKENES AND ALKYNES

Indrek Pernik

A thesis submitted in partial fulfilment of the requirements for the degree of Doctor of Philosophy at the University of Oxford

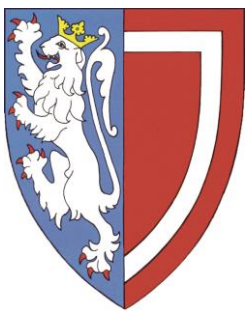

Balliol College
June 2014

The work presented in this thesis was carried out between October 2010 and May 2014 under the supervision of Professor Andrew S. Weller. All of the work is my own, unless otherwise stated and has not been submitted previously for any other degree at this, or any other, university.

Indrek Pernik
June 2014

ACKNOWLEDGEMENTS

I would like to thank my supervisor Prof. Andrew Weller for offering me a D.Phil. student position in his group. The Weller group has definitely been the best group I have ever worked in and this is all thanks to Andy's everyday efforts to keep the lab operating at a very high standard while remaining a fun place to be. His constant support and guidance over these years are very highly appreciated. Also, comments like "the Estonian g**p", and "where's my hammer" will never leave my memory.

During the years in the Weller group, there have been a number of great people there with me who have added their share to my development, and I will miss them all! The post-docs who I have had a pleasure to work with: Dr. Adrian Chaplin, he has become a great friend although I really struggled to understand him due to his tricky New Zeeland accent at first. Thanks for being a good motivator and for all the chemistry tricks and cycling knowledge he taught me. Dr. Miguel Huertos, thanks to whom I now know pretty much every Spanish person in the world – Spanish mafia! Dr. Rowan Young, part of team hydroacylation. I really miss those lab talks about changing the world him and I used to have. Dr. Tom Hooper, thanks for being my useful ally on the lab music front, otherwise my mind would be full of the latest TOP 40 hits rather than the stout Bruce Springsteen. Dr. Peng Ren, our half Willis post-doc, who always uses the lift to go to the 1st floor (*ps.* sorry about the X-ray structures taking so long). Dr. Mark Chadwick and Dr. Amparo Prades, the new post-docs in the Weller group, unfortunately we've only had a few pints together, but it has already been good fun. Amparo, good luck with HA chemistry, it's all on your shoulders now!

Over the years, a surprising number of D.Phil students have passed through the lab. When I joined the crew, the lab consisted of three D.Phils: Romaeo Dallanegra, Rebekah Pawley and Laura Sewell. Maeo was mainly writing up when I was there, so I know him just as a good friend, but I still do all my distillations exactly the way he taught me. Bex was part of team hydroacylation and hence will always have a special place in my heart, and I am thankful for the chance to see what happens when one holds on to a frozen catchpot. Laura, my original desk buddy, I have missed you and I have even missed the hugs (not tickling though). A bit after me, Sebastian Pike joined the lab – a fellow Balliol man, whose whole project was designed to break one of my main chemistry rules "never trust colours!" Thanks for being such a great friend in the lab, on the croquet field, on the tennis court, at the Megaron and even at 8 am in the Toulouse subway on our way to another chemistry talk, given by a man with the strongest French accent ever. Next in was Heather Johnson (also a part II in the Weller group). Hevz and I have had the longest overlap in the Weller group, and over these past four years we have managed to end up in a lot of interesting photos together. Hevz made sure that the Weller group

solvents were always kept ultra-pure and thanks to her there is always a big box of needles somewhere! The newest D.Phil in the Weller group is Amit Kumar (Mr.9). It was good fun teaching him all I know, and seeing all of that in use now – professional! I have always appreciated his self-sacrificing help whenever I needed it.

Part II-s have been an interesting bunch as even though they only spend about 9 months in the lab, they become an important part of it. There sure have been loads of them, all with their own unique characters: Will, Georgie, Molly, Tim, Mark, Rosie, Becky, Gemma and Lucy. Thanks to part II-s the lab has never been a boring place to be, including a liquid nitrogen fight, a fire bigger than my fires, destruction of glassware, variety of different music played (some not so desirable), interesting relationship dramas, very varied work schedules, and so on. Obviously the greatest thanks goes to Tim for being such a great student, for adapting to my ways of doing things and obviously for helping me to prove that lunging is necessary rather than just for fun. You have made me proud!

Thanks also to all the collaborators over the years, Prof. Michael Willis and the Willis group, in particular Joel, Milan, James and Manjeet. Working with Joel was an absolute pleasure and I hope that one day we'll team up again. Dr. Scott McIndoe and the McIndoe group, Rhonda, Robin and in particular Jingwei who put all his own work aside to help me for two weeks, thank you! Also, Kiwi-Mike from the Faulkner group and Andy and Rob from the Goicoechea group, thanks for helping me out whenever the Weller group knowledge was not enough.

Thanks to all the CRL support staff, in particular Dr. Nick Rees, Colin Sparrow, Dr. Amber L. Thompson, Alan Roper and Jude Nettleton, who always found time for me even at the busiest of times.

Massive thanks also to my Balliol family for making these last four years so amazing. In particular Phoebe, the first person I met after moving to Oxford, and still a dear friend of mine! I would like to thank her for always helping me out with all the paperwork that I could never understand, and she is probably the only English student who knows what hydroacylation is. Dan for making sure I did plenty of sports over the years and in general for being an awesome friend. Rahul, thanks for all the good times together, from whisky tasting to walking in Wales to filling in pension forms, and most of all keeping me involved when I was hiding writing my thesis. I would also like to thank Sarah for keeping a smile on my face during the stressful thesis writing times, for pointing out that I should eat less sugar and do more exercise and her constant reminders/examples that technology cannot be trusted and that all the data needs to be backed up.

And finally, thanks to my parents for their support and encouragement over the years even though I'm pretty sure they would prefer me working or studying in Estonia. Aitäh!

ABBREVIATIONS

Å	Angstrom
Ar	aryl
Ar^F	[3,5-$C_6H_3(CF_3)$]
atm	atmosphere
β_n	natural bite angle
b.p.	boiling-point
^{n}Bu	butyl
^{t}Bu	tert-butyl
calc.	calculated
cat.	catalyst
cod	cyclooctadiene
Cp	cyclopentadienyl
Cp*	(pentamethyl)-cyclopentadienyl
Cy	cyclohexyl
δ	chemical shift
dcpm	1,1-*bis*(dicyclohexylphosphino)methane
DMSO	dimethylsulfoxide
DPEphos	*bis*(2-diphenylphosphionophenyl)ether
dpp1	1,1-*bis*(diphenylphosphino)methane
dpp2	1,2-*bis*(diphenylphosphino)ethane
dpp3	1,3-*bis*(diphenylphosphino)propane
dpp4	1,4-*bis*(diphenylphosphino)butane
dpp5	1,5-*bis*(diphenylphosphino)pentane
ESI-MS	Electrospray Ionisation Mass Spectrometry
ESI-MS/MS	Electrospray Ionisation Mass Spectrometry/Mass Spectrometry
Et	ethyl
fac	facial
GC-MS	Gas Chromatography-Mass Spectrometry
HOMO	Highest Occupied Molecular Orbital
HPLC	High Performance Liquid Chromatography
Hz	Hertz
^{i}Pr	isopropyl
IR	infrared
J	coupling constant

LUMO	Lowest Unoccupied Molecular Orbital
Me	methyl
mer	meridinal
mod	modified
m/z	mass to charge ratio
nbd	norbornadiene
NMR	Nuclear Magnetic Resonance
OTf	$[CF_3SO_3]^-$
Ph	phenyl
POP	*bis*(2-diphentlphosphinoethyl)ether
ppm	parts per million
THF	tetrahydrofuran
TOF	turnover frequency
TON	turnover number
XANTphos	4,5-*bis*(diphenylphosphino)-9,9-dimethylxanthene

ABSTRACT

This thesis discusses the intermolecular hydroacylation reaction using cationic rhodium *bis*-phosphine complexes as catalysts. A series of small bite-angle rhodium *bis*-phosphine complexes have been prepared and characterised. The reactivity of these complexes has been investigated in order to gather information about the effect of subtle changes in the ligand design and they are compared to the previously reported catalysts.

Chapter 2 presents the challenges involved in the synthesis of small bite-angle isopropyl and cyclohexyl PNP and PCP *bis*-phosphine ligand containing rhodium complexes. These complexes have been fully characterised and screened in intermolecular hydroacylation reaction using 2-(methylthio)benzaldehyde (**E**) and 1-octene or 1-octyne as substrates. The formed complexes were shown to be very efficient and regioselective alkyne hydroacylation catalysts. The mechanism of the hydroacylation reaction was investigated using the isopropyl PNP complex [Rh($^{i}Pr_2$PNMeP$^{i}Pr_2$)(C_6H_5F)][BAr^F_4] (**11b**).

Chapter 3 concentrates on developing new rhodium *bis*-phosphine complexes that involve a ligand incorporating the small bite-angle motif with the one of hemilability. The PNP complex [Rh((2-OMe-C_6H_4)$_2$PNMeP(2-OMe-C_6H_4)$_2$)(C_6H_5F)][BAr^F_4] (**41**) was synthesised and analytically characterised. **41** was shown to be an active alkyne hydroacylation catalyst with more stability towards the catalyst deactivation pathway, reductive decarbonylation, compared to the previously investigated **11b**. Additionally mechanistic studies using **41** were carried out.

The final chapter moves on to study the C-S activation ability of small bite-angle rhodium *bis*-phosphine complexes to remove the sulfur tether from the hydroacylation products at the end of the hydroacylation reaction. A screening is conducted to compare the reactivity of different small bite-angle ligands. Additionally, a detailed investigation is carried out to see the effect the C-S activation has on the hydroacylation reaction.

CONTENTS

1. INTRODUCTION

1.1. Scope of Introduction

This thesis reports the synthesis, characterisation and reactivity of new *bis*-phosphine rhodium complexes, building upon previous results in hydroacylation catalysis. In this thesis, the mechanistic aspects of the hydroacylation reaction will be covered, as well as the properties of the rhodium phosphine complexes, and historical and latest advances in the hydroacylation catalysis.

1.2. General Overview of Transition Metal Complexes

Since the 1920's when Fischer and Tropsch produced a range of alkenes from syngas using the transition metals (cobalt and iron), the importance of the d-block metals has increased significantly.[1] The transition metals have proven to be useful for both highly specific organic "fine chemical" reactions and commodity scale industrial processes. The usefulness of the transition metals arises from the fact that they can coordinate and activate organic molecules. This is due to the ability of the transition metal to both donate and accept electrons. Transition metals in low oxidation states tend to coordinate the number of ligands needed to fill all the valence orbitals. In most cases, 16 and 18 valence electrons lead to the most stable complexes.[2-4]

1.2.1. General Overview of Rhodium Metal Properties

Rhodium is one of the rarest metals in the Earth's crust, making it expensive (approximately \$35/gram) to use.[5, 6] Although costly, it has found a great number of uses, including catalytic converters due to its ability to efficiently convert nitrogen oxides to oxygen and nitrogen (more than 90% of commercial rhodium goes into catalytic converter production),[7] and in many laboratory and industrial scale processes (*e.g.* production of acetic acid – Monsanto process[8], hydroformylation[9], and cyclohexane production[10]). Rhodium is a platinum group metal, with the electronic configuration of Rh [Kr]$4d^8 5s^1$. Although rhodium can exist in oxidation states –III to +VI, $[Rh(CO)_3]^{3-}$ and RhF_6 respectively, the most common oxidation states for rhodium are +I and +III.[11] This allows rhodium to be a useful catalyst to facilitate reactions that include steps that result in a 2 unit change in the oxidation state (*i.e.* oxidative addition and reductive elimination). Rhodium +I is has 8 d electrons, and due to being a 2nd row transition metal, the ligand field splitting energy is high, thus it generally adopts a square planar configuration. In this case the highest occupied molecular orbital (HOMO) is $2a_{1g}$ (d_z^2) and lowest unoccupied molecular orbital (LUMO) is the high energy orbital $2b_{1g}$ ($d_{x^2-y^2}$). Rhodium +III has 6 d electrons, which also due to high ligand field splitting energy prefers the low spin state, and the most stable configuration is octahedral, where the HOMO is the t_{2g} and the LUMO is the e_g set. The molecular orbital diagrams for octahedral and square planar complexes are depicted in Figure 1.1.

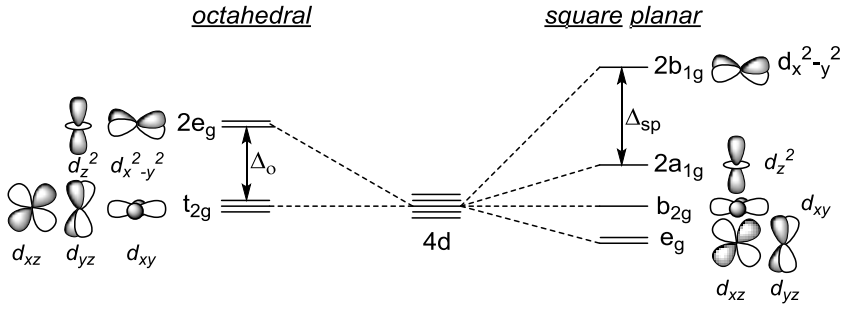

Figure 1.1. Molecular orbital diagram for octahedral and square planar complexes involving only the metal d orbitals.

Although occurring in ores, and often used (*i.e.* rhodium nanoparticles), pure rhodium is rarely used for homogeneous catalyst synthesis. A common rhodium precursor is rhodium chloride complex $RhCl_3 \cdot 3H_2O$. This starting material can easily be functionalised by reacting it with different olefins, phosphines and other potential ligands.

1.3. Phosphine ligands

1.3.1. General Considerations

Phosphine ligands are of great importance as their electronic and steric properties can be altered in a systematic and predictable way, which leads to different properties of the resulting transition metal complex. As many synthetic routes to phosphines are known, different phosphines with different properties can readily be synthesised and complexed to metals. In general, phosphine ligands are considered spectator ligands rather than actor ligands[3, 12] although they can participate in the reaction (*e.g.* hemilability[13, 14] or dehydrogenation of the phosphine ligand[15, 16]). Due to their ability to stabilise a broad range of oxidation states, they are considered to be very useful for catalytic reactions.[17]

1.3.2. Electronic Effects

Phosphines are "soft" 2 electron donor ligands. They are also π-acids, where the strength of the π-acidity is dependent on the R-groups on the PR_3 ligand. The effect of π-acidity is quite weak for alkyl groups, but can be much more profound in case of aryl, dialkylamino and alkoxy groups, and is particularly strong for the strongly electron withdrawing fluorides – PF_3 (Figure 1.2).[2]

$$\mathbf{PMe_3 \approx P(NR_2)_3 < PAr_3 < P(OMe)_3 < PCl_3 < PF_3 \approx CO}$$

Figure 1.2. Order of increasing π-acid character for phosphine ligands, with respect to carbon monoxide.

The bonding to the metal centre occurs in a synergic way (Figure 1.3, a), where the phosphorus centre donates its lone pair to the metal in a σ-bond (Figure 1.3, b). Additionally, due to phosphines having low energy LUMO-s, back-bonding also occurs. A classic approach considers the back-donation to the empty phosphorus d orbitals, which are low enough in energy to allow good overlap with the filled metal orbitals (Figure 1.3, d). More recent research implies that empty P-R σ* orbitals have an important role in back-bonding (Figure 1.3, c).[17]

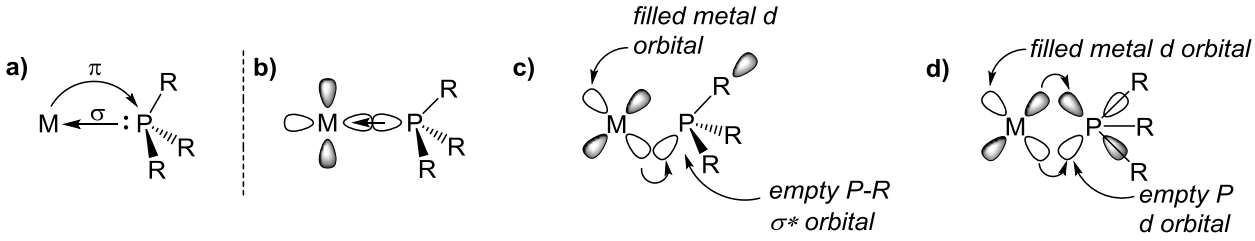

Figure 1.3. a) Synergic bonding between the metal and the phosphine ligand, where the phosphine acts as a σ-donor and π-acceptor. b) lone-pair donation to an empty metal d orbital. c and d) Two ways for back-bonding between a metal centre and the phosphine ligand.

If the R-group on phosphorus is more electronegative, the bonding orbital becomes lower in energy, implying that σ* orbital of the P-R bond has become more stable, thus making the phosphine to a better acceptor ligand (Figure 1.4).

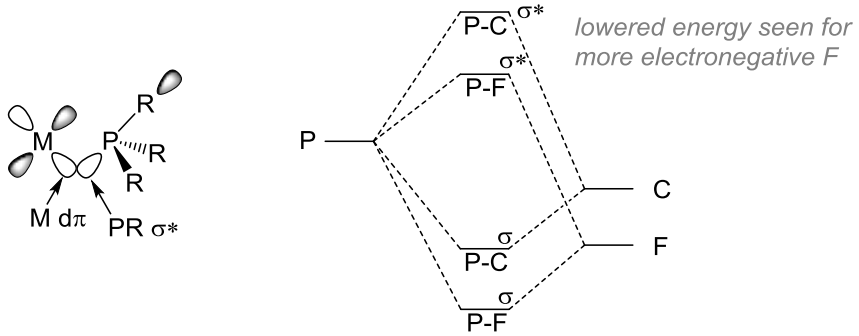

Figure 1.4. Left: Metal-phosphine back-bonding to the empty PR σ* orbital. Right: The stability of the PR antibonding σ* orbital depends on the atom attached to the phosphorus atom. More electronegative R allows for more stable σ* orbital and is lowered in energy.[3]

These electronic effects have been quantified by Tolman by using $Ni(CO)_3L$ complexes, where L is a different phosphine (or phosphite) ligand. Tolman's work relies on the fact that when a phosphorus centre bearing electron donating substituents is used, the metal centre becomes

more electron-rich, and thus there is more back-donation into the C-O σ*-orbital (LUMO) (Figure 1.5). This back-bonding leads to weaker C-O bond hence lowering the vibrational stretching frequencies of CO.[12, 18] These data can be used to compare the effects of different phosphine ligands and to design metal complexes with variable electronic properties at the metal centre (Table 1.1).

Table 1.1. CO stretching frequencies measured for $Ni(CO)_3L$. *cf.* υ(free CO) = 2143 cm^{-1}

Ligand	υ(CO) / cm^{-1}
P^tBu_3	2056
PCy_3	2056
P^iPr_3	2059
PMe_2Ph	2065
$P(C_6H_4\text{-}p\text{-}OMe)_3$	2066
PPh_3	2068
$P(O^iPr)_3$	2075
$P(C_6F_5)_3$	2090
PF_3	2110

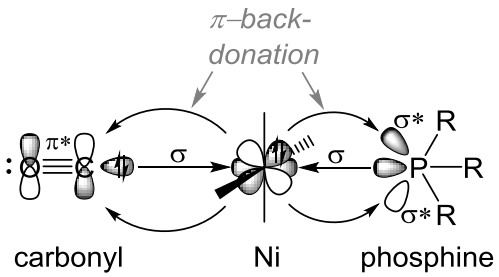

Figure 1.5. Schematic representation showing the electronic effect of the phosphine ligand on the C-O stretching frequency using a nickel complex.

1.3.3. Steric Effects

Although electronic effects have a substantial role to play in the reactivity of the metal-phosphine complexes, systematic studies have shown that steric effects are at least as important as electronic effects, and in terms of the stability of the complex or catalyst, can even be dominating.[17, 19] For example, if dissociation of one of the phosphine ligands leads to the formation of the active catalyst, the bulk can determine the position of this equilibrium. In some

cases bulky phosphines can be beneficial, as this can result in dissociation of one of the phosphines, leading to a vacant site and hence formation of an active catalyst (*e.g.* Wilkinson's catalyst[20]). At the same time, bulky ligands might inhibit the approach of the substrate to the metal centre. Hence for different catalytic reactions, metal-phosphines with different motifs can be chosen. Another case where bulky phosphines can be useful is for the formation of metal complexes with less than 18 valence electrons. If not enough phosphine ligands can fit around the metal-centre to form an 18-electron complex, an electron-poor or coordinatively unsaturated metal complexes can be formed. An example of a low coordinate, electronically unsaturated species is the palladium(0) complex $Pd[P(^tBu)_2Ph]_2$ which only has 2 ligands and 14 valence electrons.[21]

A way to quantify the phosphine ligand "size" was again proposed by Tolman. The steric bulk of the phosphine ligand was determined by taking a space-filling model of the metal-phosphine, and measuring the angle of the cone that will contain the ligand where the tip of the cone is at the metal centre. The angle formed at the tip of the cone was termed as the cone-angle, θ. The M-P distance is set at 2.28 Å, which corresponds to common metal phosphine bond length (Table 1.2). In the case of asymmetrically substituted phosphines an average of three substituents is taken.[12]

Table 1.2. Cone angle schematic representation, and cone angle values for some relevant ligands.

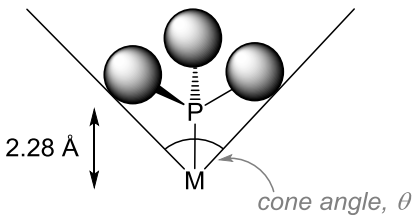

ligand	cone angle / °
PF_3	104
$P(OMe)_3$	107
PEt_3	132
PPh_3	145
PCy_3	170
P^tBu_3	182
$P(o\text{-}Tol)_3$	194

Tolman combined both the electronic data and the steric effects of the common phosphine ligands and plotted them on a "ligand map" which can be highly valuable for developing new catalysts for a catalytic transformation (Figure 1.6).

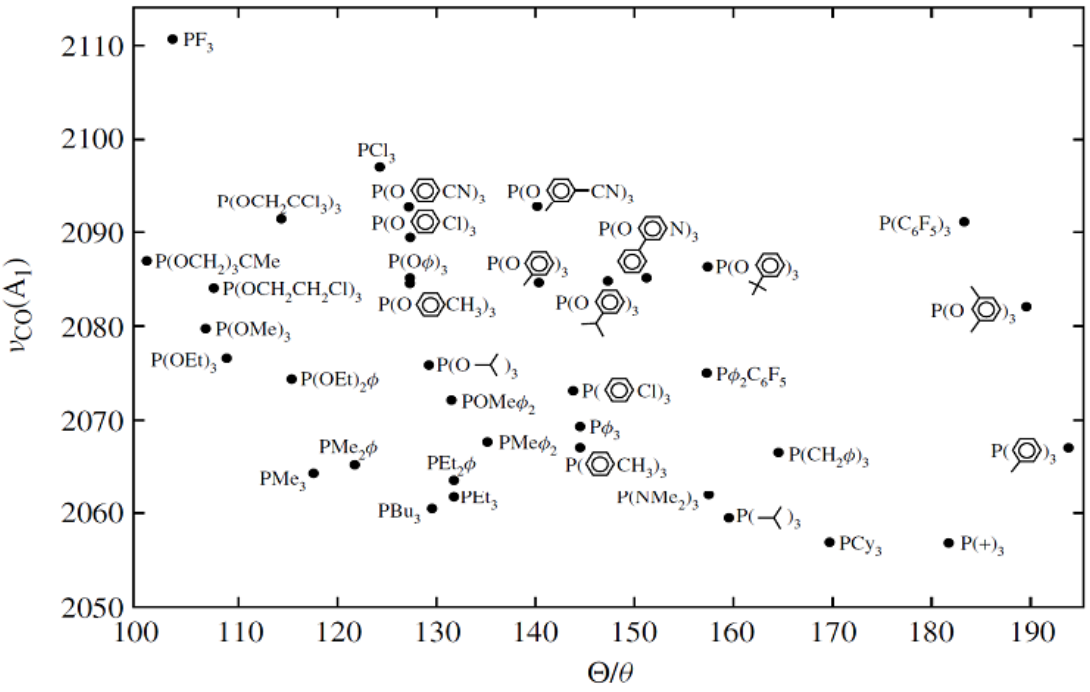

Figure 1.6. Tolman's "ligand map" that combines the steric and electronic effects. The figure is adapted from Tolman.[12]

1.3.4. Chelating Phosphine Ligands

Although mono-dentate phosphines were already regularly used in the 1960's[22, 23] the bidentate phosphines did not become popular until the 70's. The initial results using depe (1,2-*bis*(diethylphosphino)ethane) or dppe (1,2-*bis*(diphenylphosphino)ethane) indicated that the use of diphosphines led to lower catalytic activity than the corresponding monophosphines.[24, 25] This initial weakness proved to be a strength later, as the bidentate ligands were shown to be useful due to their constrained *cis* (mainly) geometry and greater resistance to dissociation.[26] In the 1970's Tolman introduced the *cone angle* parameter for the *bis*-phosphines. It was defined as the average cone angle as measured for the two substituents and the angle between the M-P bond and the bisector of the P-M-P angle. Other parameters for describing bidentate ligands have also been reported, including solid angle, pocket angle and bite angle.

The solid angle, Ω, developed by Hirota, White and Coville, is a measure of the "shadow" cast by a group of atoms when placed relative to an apex atom, the metal being the light source on a sphere centred around the metal.[27]

The pocket angle, established by Barron is calculated from the solid state X-ray structure by allowing free rotation of the substituents at phosphorus. This is used to determine the space available for substrates at a complex containing a bidentate ligand. Essentially for a bidentate complex this is 360° minus Tolman's cone angle. [28]

The most simple way and also more applicable in the case of this thesis is the *bite angle* concept. For this the sterics of a diphosphine are described by accounting the length of the bridging backbone connecting them. Based on these data the bite angle is calculated, which is the angle formed between the metal and the two phosphorus atoms. The "preferred" bite angle depends on the conformation of the metal complex. In the case of octahedral or square planar complexes, the preferred P-M-P angle is 90°, whereas for trigonal bipyramid this angle is 90° or 120° and for tetrahedral 109.5°. This can be beneficial because different bite angles can change the rate of certain steps in a catalytic cycle by changing the relative energies of the transition states.

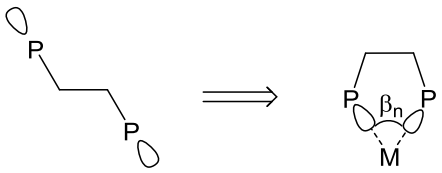

Figure 1.7. For flexibility range calculations a dummy metal is used to direct the lone pairs.

Casey and Whitaker have quantified the "preferred" bite angle, by introducing the concept of natural bite angle, β_n (Figure 1.7). This corresponds to the "flexibility range" where the change in the bite angle is no higher in energy than 3 kcal.mol^{-1}.[29] This data was plotted to show the general trend for a two carbon backbone complex at different bite angles (Figure 1.8).[19] This data indicates that for a two carbon backbone *bis*-phosphine ligand containing complex the preferred bite angle is between 95 and 135°.

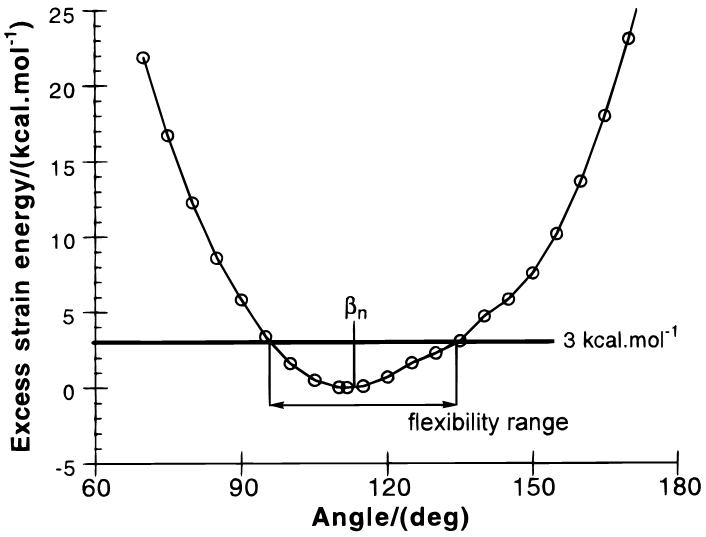

Figure 1.8. The change in excess strain energy at different bite angles. β_n – natural bite angle. Figure adapted from Casey and co-workers.[29]

A more recent work, carried out by Kiprof and co-workers concentrated on the bite angle effects in hydroformylation.[30] By using computational methods, the Cundari model, they analysed the bite angle effect on intermediate and transition state energies. In their calculations they use rhodium as the metal with a range of *bis*-diphenylphosphino ligands with different backbone lengths, and they fix the rhodium-phosphine distance to 2.315 Å. The data showed that the natural bite angle increased with every added carbon in the backbone, and the wider structures have more flexibility. The flexibilities in the case of four different *bis*-diphenylphosphino ligands with varied backbone are depicted in Figure 1.9. These results indicate that if flexibility in the bite angle is required during the catalytic process, then 1,4-*bis*(diphenylphosphino)butane (dpp4) (**i-83**) and 1,5-*bis*(diphenylphosphino)pentane (dpp5) are more suitable ligands, although this data does not shed light on to situations where a bite angle larger than 150° is required. In comparison, 1,2-*bis*(diphenylphosphino)ethane (dpp2) (**i-81**) and 1,3-*bis*(diphenylphosphino)propane (dpp3) (**i-82**) have much smaller range of preferred "flexibility range", particularly this is the case for dpp2, where above 110° bite angle energies higher than 80 kcal.mol^{-1} are required. This research by Kiprof and co-workers did not comment on the use of the smaller bite-angle dpp1 ligand (dpp1 = 1,1-*bis*(diphenylphosphino)methane).

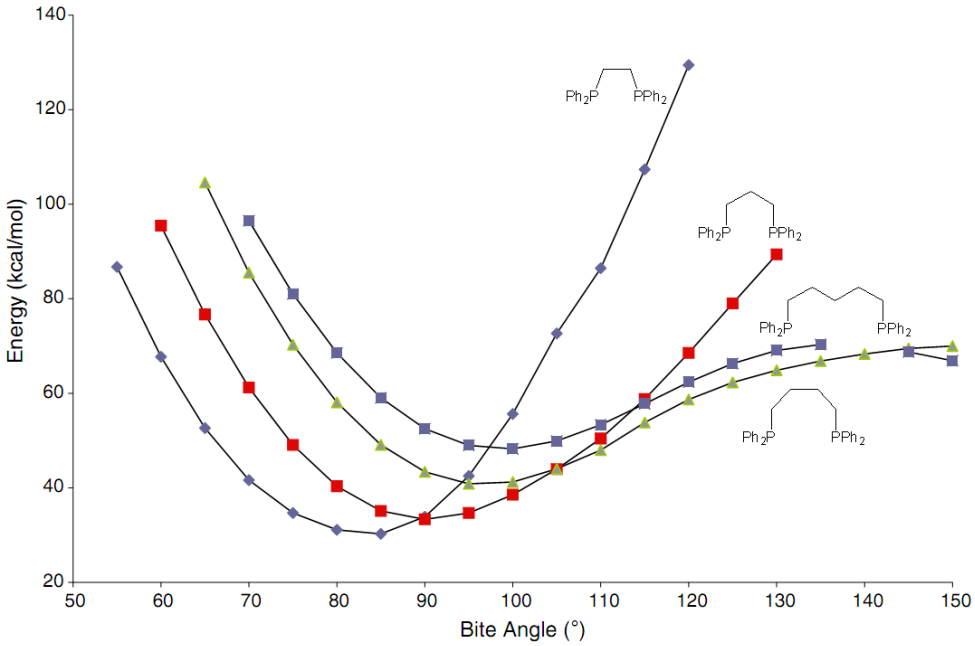

Figure 1.9. Natural bite-angles and the flexibility range of four *bis*-diphenylphosphino ligands with different backbones. Figure adapted from Kiprof and co-workers [30]

1.3.5. Hemilabile Phosphine Ligands

Hemilabile ligands have received a considerable amount of interest due to their ability to open up a coordination site at the metal readily during the reaction, but remain coordinated at other times. This ability has found use in many catalytic transformations, including hydrogenation, carbonylation, hydroformylation and different polymerisation reactions.[31, 32, 33] Hemilabile ligands are defined as polydentate ligands that contain at least two different atoms capable of coordinating to the metal centre.[31] Unlike monodentate ligands, more than one atom coordinates to the metal centre; whereas contrasting to classic homofunctional bidentate ligands, the bonding strength of one of the atoms is much lower than for the other, thus allowing for reversible coordination of that atom (Figure 1.10). Braunstein and Naud consider the energy differences involved in the dynamic process which form the basis of hemilability to be around 50 kJ.mol^{-1} (approx. 12 kcal.mol^{-1}).[31]

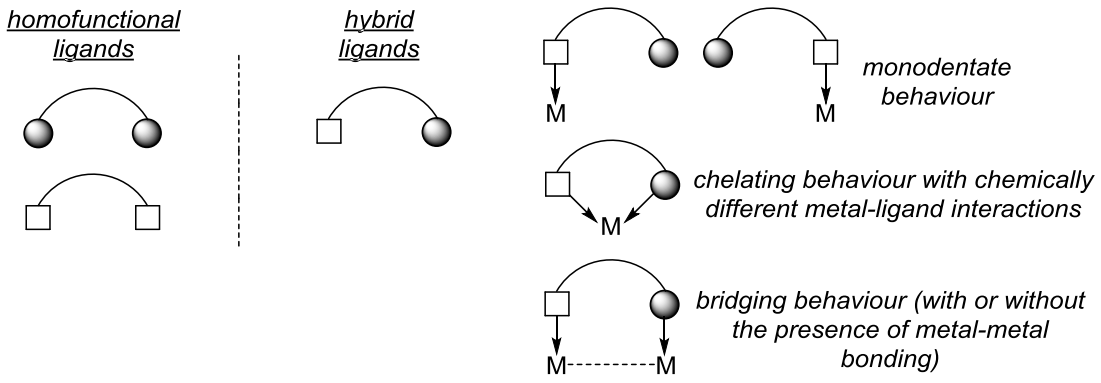

Figure 1.10. Left: homofunctional bidentate ligands. Right: general scheme of hybrid bidentate ligands and their different coordination modes.

A common, and extensively studied in the Weller group, motif is a ligand type where phosphorus atoms act as the anchoring part of the ligand, while an oxygen atom has the hemilabile functionality.[34-36] Typical ligands of this type are DPEphos, XANTphos and POP ligands, which all have different rigidity due to the lack or presence of aromatic groups in the backbone (Figure 1.11) and this rigidity affects the binding ability of the hemilabile group, which can be beneficial in systematically changing the binding strength of the hemilabile group.

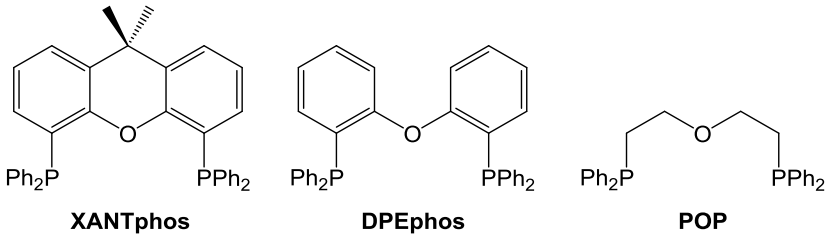

Figure 1.11. Commonly used hemilabile *bis*-phosphine ligands that incorporate an oxygen atom as the hemilabile group.

1.4. Hydroacylation – General Considerations and Key Mechanistic Steps

1.4.1. General Introduction

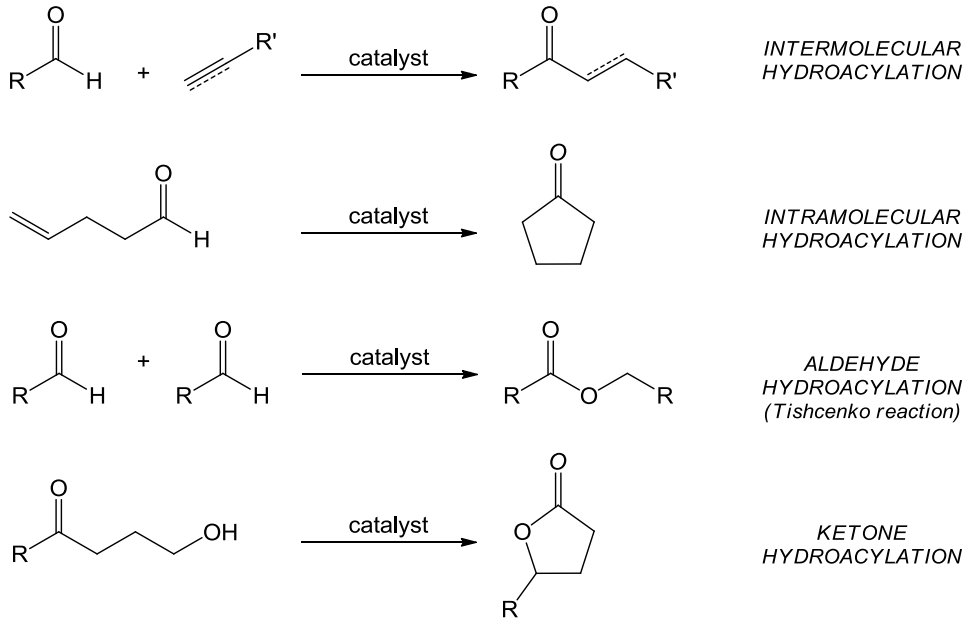

Scheme 1.2. Inter- and intramolecular alkene/alkyne hydroacylation reaction, aldehyde hydroacylation and ketone hydroacylation reaction.[37]

Hydroacylation is potentially an extremely useful reaction for obtaining ketones, forming a new carbon-carbon bond by adding an aldehyde across a multiple bond of an alkene or alkyne using a transition metal catalyst.[38, 39] It combines C-H activation with C-C bond formation. In general, hydroacylation can be divided into two categories: intra- and intermolecular hydroacylation, but also the unwanted aldehyde hydroacylation (unwanted in the case of this thesis) and the highly specific ketone hydroacylation (Scheme 1.2). The utility of hydroacylation arises from the 100% atom efficiency of the reaction, while also introducing versatile functionality, the carbonyl group, to the substrate. This efficiency means that during the reaction all the reagents are used and end up in the product, thus making it environmentally more desirable. The potential power of this reaction is illustrated by > 6 million possible combinations of commercially available substrates to give hydroacylation products and there is currently no conventional organic reaction to efficiently produce ketones from aldehydes.[38, 40] The main drawbacks with this

reaction are deleterious side-reactions, reductive decarbonylation, which leads to deactivation of the catalyst, and in some cases also occurrence of the side-reaction between two aldehydes is observed, aldehyde-hydroacylation (Tishcenko reaction)[34, 41] or the side-reaction between alkynes or alkenes to form the corresponding oligomeric by-products.

1.4.2. Organic Synthesis of Ketones

Although some large scale synthetic processes exist for making ketones, there is no single general organic method for ketone synthesis. The most common approach for synthesising ketones is via *oxidation of secondary alcohols*. There are many different reagents for this reaction, but commonly an acidic solution of chromium trioxide is used. This approach works well for secondary alcohols, whereas in the case of tertiary alcohols this procedure leads to cleavage of C-C bond.[42] Upon starting from an aldehyde, first a reaction with a Grignard reagent occurs, forming the corresponding alcohol which is then oxidised by the chromium trioxide reagent (Scheme 1.3).

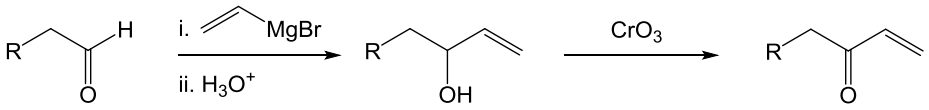

Scheme 1.3. Synthesis of ketones via oxidation of secondary alcohols.

Another often used approach to obtain ketones is the oxymercuration reaction which is used for *hydration of alkynes*. In this case the ketone is produced by reacting an alkyne with mercury(II)acetate under acidic conditions. This is a very useful method for making methyl ketones, but the substantial limitation of the reaction is the stoichiometric amount of mercury waste generated.

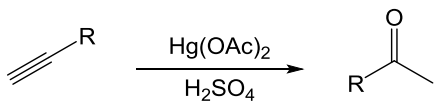

Scheme 1.4. Synthesis of ketones via hydration of alkynes.

In case of *synthesis of aromatic ketones*, the readily used reaction is the Friedel-Crafts acylation as the starting material can be a simple benzene ring. If the starting material contains an acid-chloride functional group, addition of lithium dialkylcuprate (Gilman reagent) leads to the formation of a ketone (Scheme 1.5).

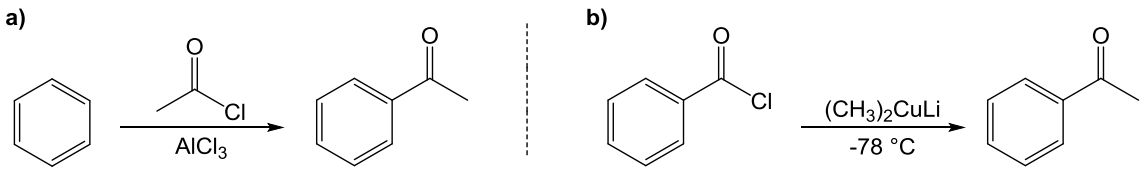

Scheme 1.5. Synthesis of aromatic ketones. **a)** Fiedel-Crafts acylation **b)** via the addition of Gilman reagent.

For aromatic species that do not react well under the Friedel-Crafts conditions, or in the case of some alkyls, there are other, more complicated routes via imines or nitrile complexes.

Although in small scale and in case of specific substrates these methods work well, but for most of the commonly used organic methods for synthesising ketones, there exist a range of limitations: lack of selectivity, stoichiometric amounts of waste (including metal-containing waste) and low functional group tolerance.[38, 42]

1.4.3. The Hydroacylation Reaction Mechanism

The hydroacylation reaction can be catalysed by a variety of transition metals (including cobalt[43, 44] and ruthenium[37, 45]), but rhodium catalysts have proven to be the most effective and most widely used, and in this thesis it is the main metal discussed.[38] In general the reaction formally involves the addition of an acyl unit across a C-C multiple bond.[38] The rhodium catalysed hydroacylation is generally considered to go through a 4-step reaction mechanism (Scheme 1.6). The C-H bond of an aldehyde is C-H activated to generate an acyl-metal-hydride (**i-1**), which can bind with an alkyne or alkene forming complex **i-2**, followed by a hydride migratory insertion which subsequently affords a ketone product through reductive elimination. Depending on the migration step, the formation of either branched or linear product is determined (**i-3**-bra *vs.* **i-3**-lin). Mechanistic evidence points to the rate limiting step

being in most cases the irreversible reductive elimination while all the other steps are reversible.[34, 46] It has been demonstrated previously that the rate limiting step can be hydride insertion instead.[47] The acyl-metal-hydride complex (**i-1**) can also undergo decarbonylation to form **i-4**, which either returns to the hydroacylation cycle or reductively eliminates to give the inactive metal-carbonyl complex (**i-5**) and an alkene or arene.

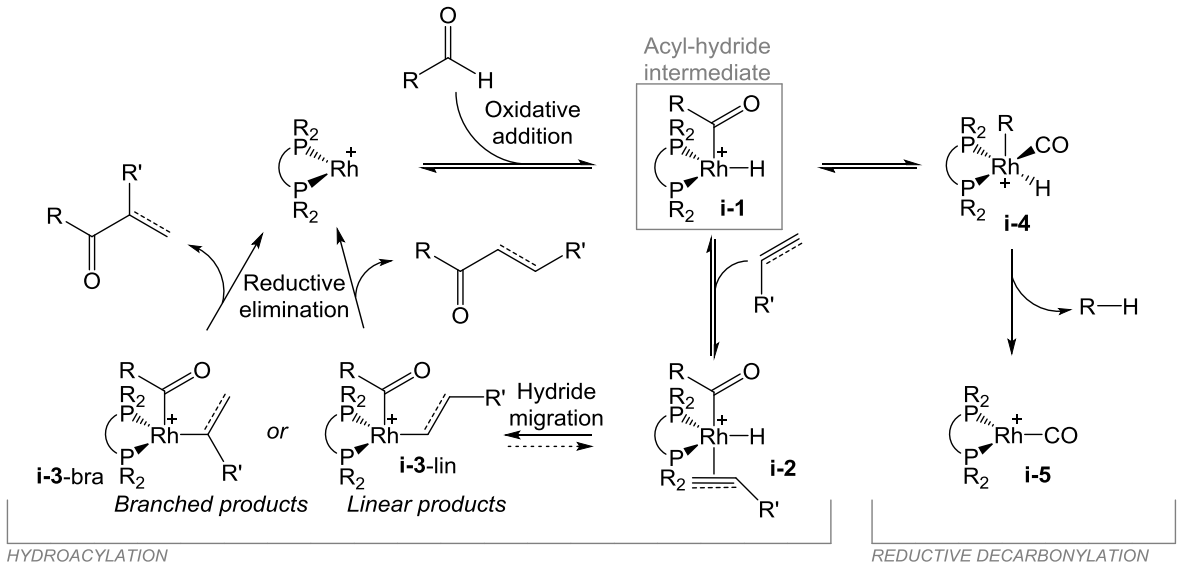

Scheme 1.6. General reaction mechanism for transition metal catalysed intermolecular hydroacylation reaction, and decarbonylation reaction that leads to the catalytically inactive metal-carbonyl complex (**i-5**).

1.4.4. Oxidative Addition

In general terms, during oxidative addition, two new metal-ligand bonds are formed by cleavage of a bond in an organic, main group or tethered reagent.[39] In the case of hydroacylation, the carbon-hydrogen bond of the acyl unit is cleaved and the acyl-metal-hydride intermediate (Scheme 1.6, **i-1**) is formed. During the oxidative addition step, oxidation state, number of valence electrons and coordination number of the metal increase by 2 units. Oxidative addition occurs when the metal centre is coordinatively unsaturated and the metal in oxidation state n has accessible n+2 oxidation state. In general oxidative addition tends to be more favoured by electron-rich, and by less-hindered metal centres.[17]

There are three mechanistic pathways for oxidative addition: the S_N2 mechanism, the ionic mechanism and the three-centred concerted mechanism.[2]

During the *S_N2 mechanism* the metal centre acts as a nucleophile. This mechanism requires a polar substrate (*e.g.* alkyl-halide). The rate of the reaction is dependent on the nucleophilicity of the metal centre and the leaving ability of the leaving group (*e.g.* halide) (Scheme 1.7).

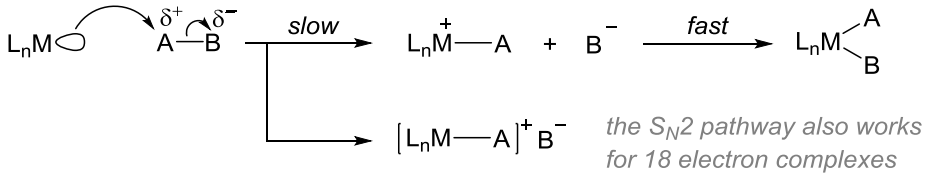

Scheme 1.7. Schematic representation of the S_N2 oxidative addition pathway. For the above mechanism, B^- can either add *cis* or *trans* with respect to A.

The ionic mechanism applies to strongly dissociating protic acids, H^+X^- (*e.g.* HCl). The reaction can occur via two different pathways, depending on the nature of the metal centre. Metal centres with high electron density (*i.e.* low oxidation state and good donor ligands) act as a nucleophile (Scheme 1.8, a), whereas if the metal centre has a high oxidation state, is positively charged and/or has good acceptor ligands, the metal acts as an electrophile (Scheme 1.8, b).

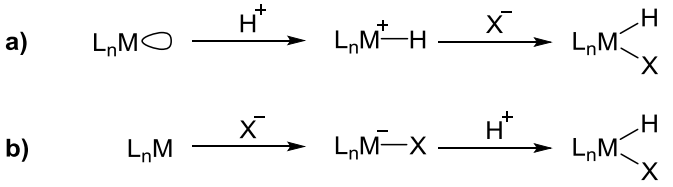

Scheme 1.8. Schematic representation of the two forms of ionic oxidative addition mechanisms. For mechanism **a**, the reaction stops after the first step if X^- is a non-coordinating counter ion. X^- can either add *cis* or *trans* with respect to H.

Three-centred concerted mechanism operates with apolar or weakly polarised substrates (*e.g.* C-H, H-H, Si-H, O-O). This is favoured by electron rich metal centres, particularly second and third row transition metals with low oxidation state, small donor ligands and vacant coordination site(s) which stabilise the resulting more crowded metal complex and higher oxidation state. In the concerted mechanism the metal can be considered as both a nucleophile and an electrophile. (Scheme 1.9)

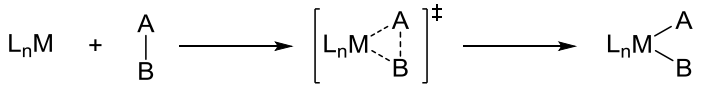

Scheme 1.9. Three-centred concerted oxidative addition mechanism. Initially A and B adopt *cis* geometry, but depending on the complex they may rearrange to give other geometries.

1.4.5. Oxidative Addition of H_2

The concerted mechanism is very common for the addition of H_2 to a metal complex. As hydrogen approaches the metal, it donates electron density from its filled σ-orbital to the metal's LUMO, weakening the H-H bond. There is also back-bonding from one of the filled d orbitals on the metal overlapping with the antibonding σ* orbital of dihydrogen, which weakens the H-H bond even further. Depending on the metal complex, this can result in two different bonding modes: dihydrogen complex or "classical" dihydride complex (Figure 1.12).[48, 49] Theoretical studies have shown that side on approach is favoured over the end-on approach, and that *cis*-addition has quite a low barrier (< 10 kcal.mol^{-1}) while *trans*-addition is forbidden because of the high energy barrier due to geometric constraints.[50]

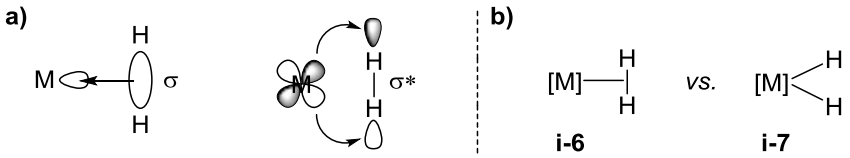

Figure 1.12. a) Bonding orbitals showing σ-donation by the hydrogen and metal back-bonding into the anti-bonding σ* orbital. b) metal-dihydrogen complex (**i-6**) and metal-dihydride complex (**i-7**).

Whether a dihydrogen or a dihydride complex has formed can be determined by different analytical methods, including crystallography, IR-spectroscopy and NMR spectroscopy.

1.4.6. C-H Activation

The oxidative addition (usually via the 3-centre concerted mechanism) of a C-H bond is termed C-H activation. C-H activation has become an increasingly important topic of study due to its

potential use for functionalising C-H bonds in substrate molecules selectively, but also due to its potential for reducing the amount of waste generated, hence allowing for greener chemistry.[51-55]

In general C-H activation can be divided into two categories: intra- and intermolecular C-H activation. The development of intramolecular C-H activation was more active in the late 20th century, as this is favoured kinetically and thermodynamically.[56] The intramolecular C-H activation reactions are known as cyclometallation.[57] In the case of a metal undergoing an addition of an *ortho* C-H bond of the aromatic group of the ligand the reaction is termed orthometallation.[39, 56] The earliest work related to cyclometallations was carried out by Kliman and Ducbeck, who activated the aryl C-H bonds of azobenzene (**i-8**), using a nickel complex $NiCp_2$ (Scheme 1.10, **I**).[58] Similar work conducted three years earlier, in 1960, also must have involved C-H activation, but was not reported as such (Scheme 1.10, **II**).[59]

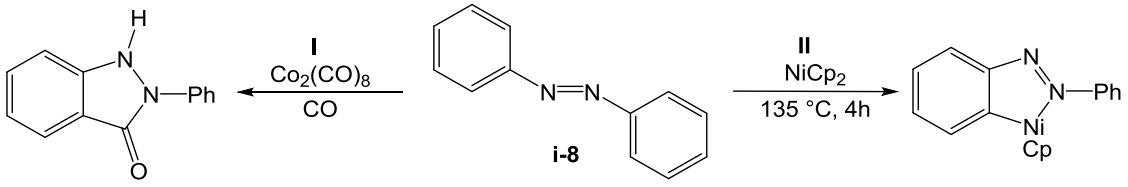

Scheme 1.10. Left: work conducted by Horiie and Murahashi (**I**). Right:. C-H bond activation work published by Kilman and Ducbeck (**II**).

The first C-H activation of an alkyl sp^3 C-H bond was reported by Chatt and Davidson.[60] They used $Ru(dmpe)_2$ {dmpe – 1,2-*bis*(dimethylphosphino)ethane} (**i-9**), as the metal complex and in a reaction with naphthalene it was noticed that both inter- and intramolecular C-H activation occurred. The metal centre carried out the intermolecular C-H activation by reacting with the methyl substituents on the phosphorus atom (Scheme 1.11, **I**), leading to the formation of the strained complex **i-10**. Also the reaction between the ruthenium metal centre and the naphthalene reagent was observed, leading to the formation of complex **i-11** (Scheme 1.11, **II**).

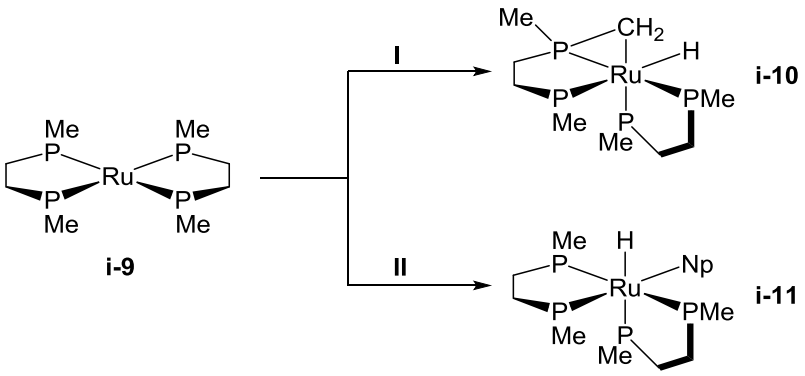

Scheme 1.11. The inter- and intramolecular reactions that resulted upon adding naphthalene to the ruthenium complex **i-9**.

The first reports of transition metal mediated C-H activation of a saturated hydrocarbon were made simultaneously by two separate research groups, Janowicz and Bergman[61] and Hoyano and Graham.[62] In both cases UV light was used to generate the free coordination site needed for the C-H activation reaction to occur. (Scheme 1.12)

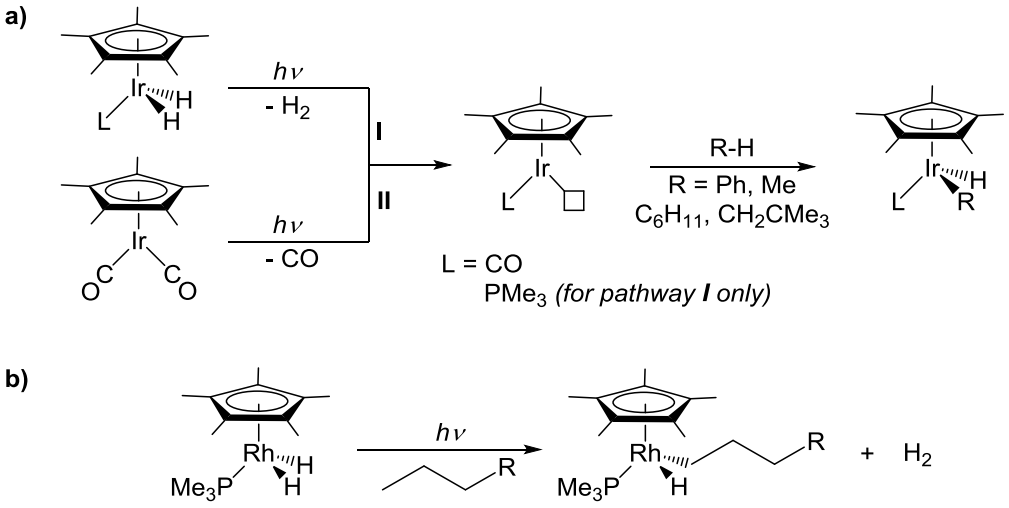

Scheme 1.12. a) Bergman and Janowicz used the iridium-hydride or –carbonyl complexes to mediate the C-H activation reaction. **b)** Hoyano and Graham used the analogous rhodium complex for the C-H activation.

Examples of C-H activation are known for group 7-10 transition metals, whereas the largest number of these reactions has been reported for iridium and rhodium complexes.[39]

1.4.7. The mechanism of C-H Activation

Although there are many examples of C-H activation, it has remained challenging. Inactivated C-H bonds, particularly alkanes, are very unreactive as they do not possess available lone pairs or empty orbitals, which is a reflection on the number of valence orbitals being equal to the number of valence electrons. The σ bonding HOMO is low in energy while the σ* bonding LUMO is very high in energy, thus leading to a strong carbon-hydrogen bond (Alkyl-H: 90 – 110 kcal.mol^{-1}; Aryl-H: 100 – 110 kcal.mol^{-1}). Also the small difference in electronegativity between carbon and hydrogen atoms leads to low reactivity. Furthermore, with respect to the H-H bond, the reactivity is limited by the steric factors; compare H-H and CR_3-H.[51] In order for C-H activation to occur, the metal complex has to be able to donate electron density to the C-H σ* orbital while also accepting C-H σ-bonding electrons. During the C-H activation process, first the formation of a σ complex (**i-12**) occurs, or in the case of an intramolecular C-H activation, an agostic complex (**i-13**) is formed, which can be a transition state or an intermediate. Then cleavage of the C-H bond results in the formation of the metal-alkyl-hydride (Scheme 1.13).

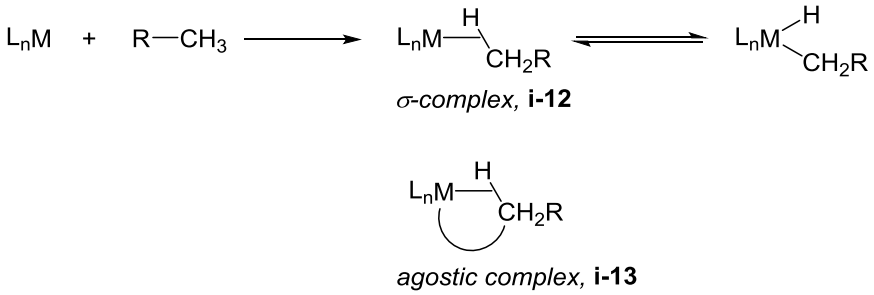

Scheme 1.13. C-H activation reaction via a σ-complex (**i-12**) or an agostic complex (**i-13**).

Crabtree and co-workers have calculated, based on structural data of agostic complexes (discussed further in Section 1.4.7.1), the trajectory of the approach of a C-H to a metal that leads to the oxidative addition. The calculations show that the C-H bond approaches the metal with the C-H bond pointing towards the metal with the M-H-C angle of 130°. Upon approaching, the bond rotates and elongates followed by cleavage and formation of the octahedral C-H activated metal complex containing the *cis* alkyl-hydride motif, with the angle of 90° for C-M-H (Figure 1.13).

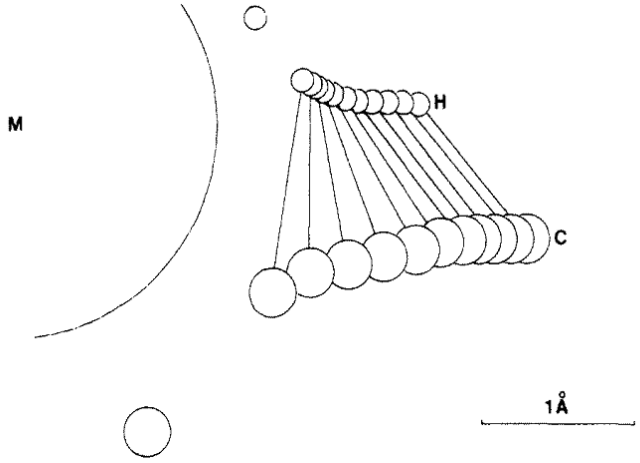

Figure 1.13. Schematic representation of the trajectory of the C-H approaching to the metal centre. Figure adapted from Crabtree.[51]

1.4.7.1. *Agostic Interaction*

The term, *agostic interaction*, was introduced by Green and Brookhart in early 1980s.[63] This came about due to observations which showed that in many cases a C-H bond that was part of the ligand interacted with the transition metal centre in a three-centre two electron configuration. It was also noted, that this interaction had a noticeable effect on the molecular and electronic properties and hence reactivity of the metal complex (Figure 1.14)

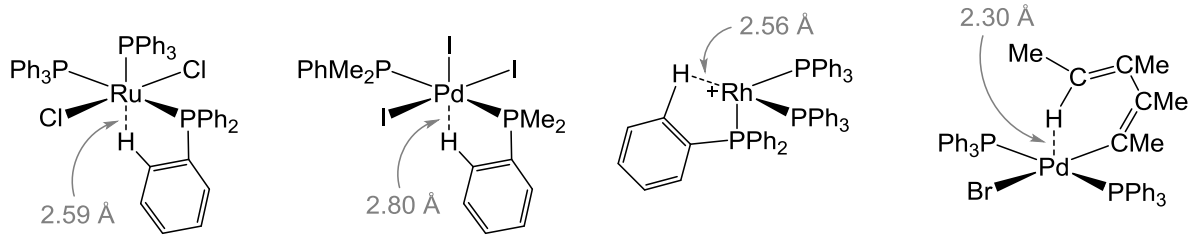

Figure 1.14. Early examples of agostic complexes (**i-14** – **i-16**) and the hydrogen-bonding anagostic complex **i-17** due to high energy LUMO of the metal.[63-67]

For determining the presence of an agostic interaction, three main analytical approaches are used: crystallography, NMR spectroscopy and infrared (IR) spectroscopy. Based on neutron diffraction data, some trends can be observed. The bridging C-H bond distances are 5 – 10% longer than for analogous non-bridging C-H bonds. Also the M-H bond distances are 15 – 20%

longer than normal metal hydride bonds.[63] NMR spectroscopy, in particular ^{1}H and ^{13}C NMR spectra, can also be an useful tool for determining agostic interactions. The coupling constant, *J*(C-H) is lower for the bridged C-H groups (around 80 – 100 Hz *vs*. 120 Hz), and agostic complexes show high field shifts in ^{1}H and ^{13}C NMR spectra. As agostic compounds can often be fluxional at room temperature, frequently useful data is obtained using variable temperature NMR spectroscopy. In particular low temperature spectra are commonly acquired as this allows for these intermediates to be "frozen out".[68, 69] The usefulness of IR spectroscopy arises from the fact that due to longer C-H bond lengths, the stretching frequency bands are expected in a different region compared to normal C-H bonds. Indeed, the agostic C-H stretching bands are at υ(C-H) approx. 2350 – 2700 cm^{-1} (*cf*. normal C-H has a characteristic absorption of 2850 – 3000 cm^{-1}).[70] Furthermore, as the relative time scale of IR spectroscopy is much faster than of NMR spectroscopy, these fast processes can be followed more readily.

1.4.7.2. *Sigma-complexes*

σ-C-H complexes are transition metal alkane complexes, where the alkane donates electron density from its C-H sigma bond to the metal.[71] Unlike the agostic complexes, there is no additional stabilisation to the complex by additional coordination to the metal centre, and hence, examples of σ-complexes are rare. Before 2009, only two examples of solid state σ-complexes, where a saturated hydrocarbon has been located within the coordination sphere of a metal centre, had been reported – a heptane interacting with an iron(II)-porphyrin complex (**i-18**)[72] and a cyclic alkene interaction with a uranium(III) complex (**i-19**)[73] (Figure 1.15). In both of these cases the incorporation of the alkane solvent molecule in the metal coordination sphere involves potential host-guest interactions.[71]

Within the last decade, Ball, Brookhart and Weller have shed some light on the crystallographic and other analytical properties of these intermediates. Ball characterised the rhenium complexes $[CpRe(CO)_2(\eta^2(CH)\text{-}C_5H_{10})]$ and $[CpRe(CO)_2(\eta^2(CH)\text{-}C_5H_{14})]$ using IR and a range of NMR spectroscopy techniques at low temperatures (–100 °C) by irradiating $[CpRe(CO)_3]$ with cyclopentane or pentane used as solvents.[74, 75]

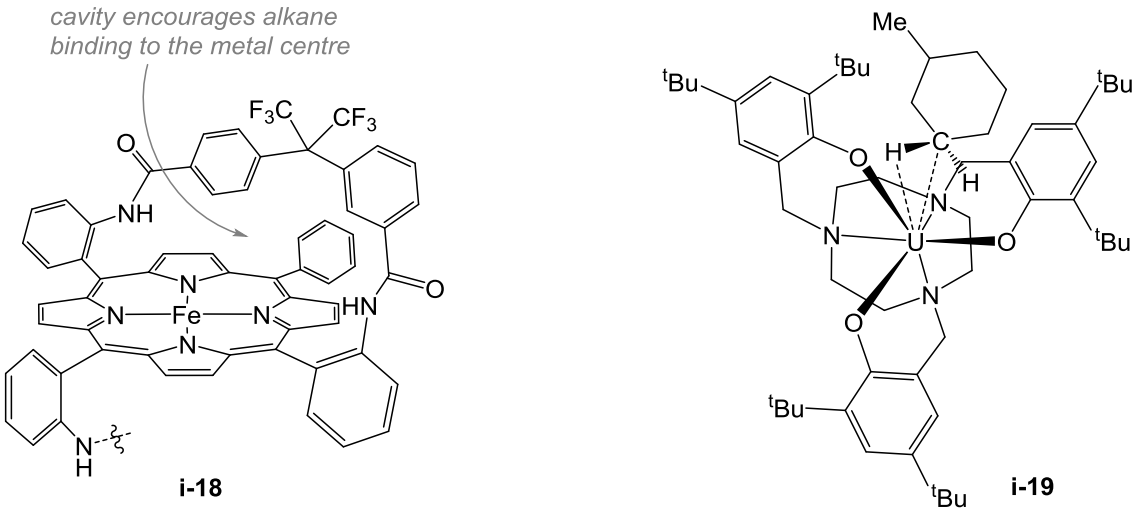

Figure 1.15. Examples of sigma complexes with potential host-guest character.

Brookhart and co-workers reported a full spectroscopic characterisation of a rhodium(I) pincer complex σ-bound to a methane molecule (**i-21**). The reaction was carried out by protonating a rhodium-methyl precursor (**i-20**) in CD_3CCl_2F at –110 °C, and was followed by low temperature nuclear magnetic resonance studies (Scheme 1.14, a). Although full characterisation was achieved, even at temperatures as low as –87 °C, the half-life of the σ-complex is only around 83 minutes, leading to the dissociation of the methane.[76] This rapid decomposition did not allow for the crystal structure of the σ-bound complex to be obtained. Recently, in 2012, another piece of the puzzle was found, when Weller and co-workers reported a crystal structure of a rhodium alkane complex (**i-24**) (Scheme 1.14, b).[71] The Weller approach was concentrated on increasing the stability of the formed alkane complex. Hence, solvent use was avoided, and the formation of the rhodium(I) alkane complex was carried out via a solid-gas reaction. A rhodium norbornadiene (nbd) complex (**i-22**) was hydrogenated in the crystalline state, and due to the retained crystallinity during that step, it was possible to obtain the crystal structure of the resulting rhodium-bound alkane intermediate (**i-24**).

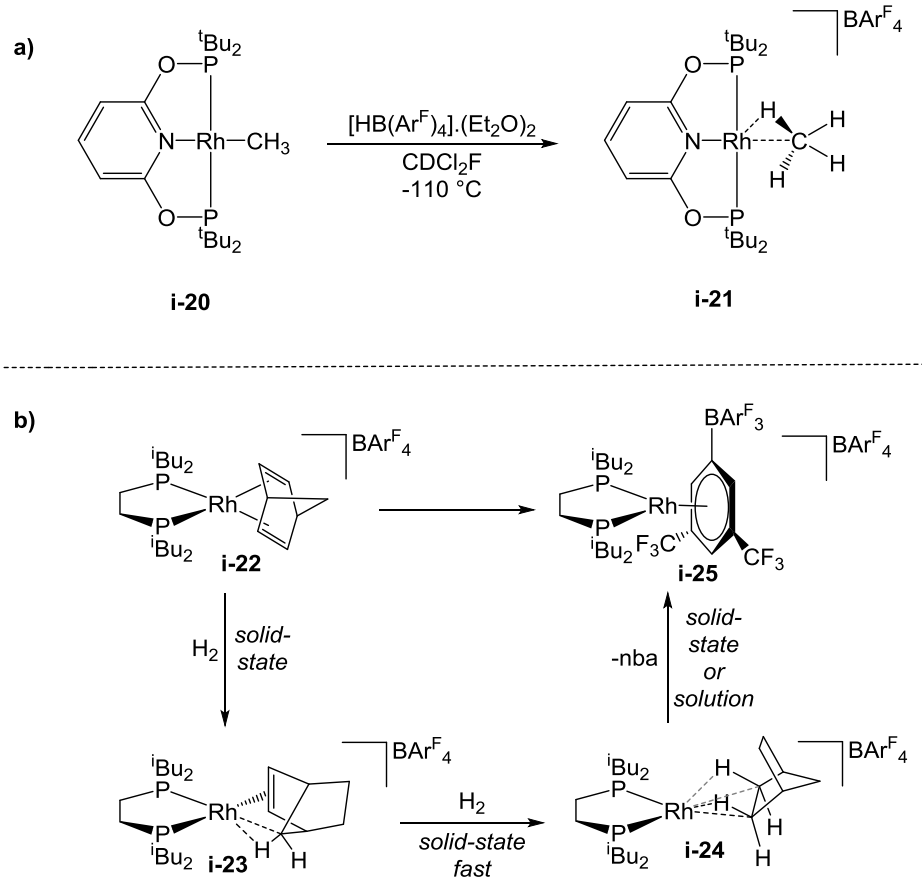

Scheme 1.14. a) Brookhart's synthetic approach to prepare the σ-bound complex **i-21**. **b)** Solid state reaction leading to the σ-bound complex **i-24** and its decomposition route to **i-25**.

1.4.7.3. *Oxidative Addition of Aldehydes*

For aldehydes an extra aspect for oxidative addition is considered. Compared to hydrocarbons, aldehydes can undergo C-H activation more readily due to the aldehylic carbonyl oxygen's ability to coordinate to the metal centre. This initial coordination of the oxygen creates the tethered metal-complex **i-26**, which promotes intramolecular C-H activation (Scheme 1.15).[77] The C-H activation is affected by both the ligands and the aldehyde itself. For example, in complex **i-26** the more electron rich PMe_3 ligands led to higher rates of dissociation of the aldehyde (*i.e.* reorganisation of the aldehyde coordination mode to form the transition state **i-27**) and faster C-H activation compared to electron poorer $P(OMe)_3$ ligands. The more electron rich phosphines stabilise the metal centre during the oxidative addition step. Similarly, the electronic effects of the aldehyde affect the reaction. More electron-deficient aldehydes led to

faster rates of dissociation of the oxygen bound aldehyde and faster C-H activation (fastest for X = CF_3; slowest for X = OMe). This is due to the fact that electron donating X stabilises the aldehyde adduct and hence inhibits the C-H activation step that would result in the formation of **i-28**.

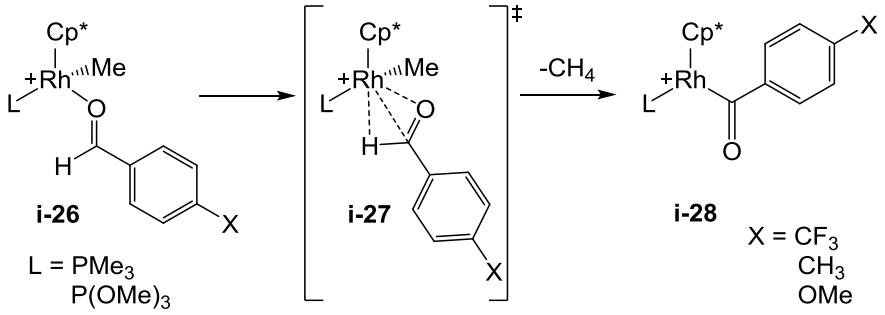

Scheme 1.15. Schematic representation of the C-H activation of an aldehyde. The $[BAr^F_4]^-$ counter-anion is not pictured for clarity.

1.4.8. Coordination of Olefins

1.4.8.1. *Coordination of Alkenes*

The step following the oxidative addition of an aldehyde during the hydroacylation reaction is the coordination of an alkene or alkyne (Scheme 1.6). Olefins and related unsaturated organic molecules are an important class of π-acceptors, but also they act as good σ-donors. The bonding mode for metal-olefin complexes considers both σ-donating and π-accepting interactions.[78]

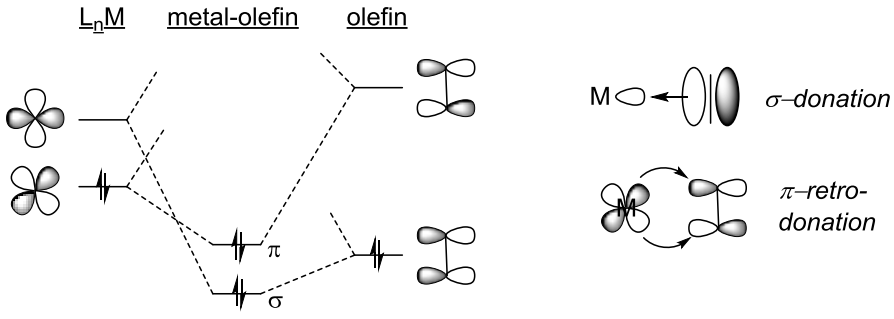

Figure 1.16. Chatt-Dewar-Duncanson model for transition-metal olefin bonding. Figure adapted from ref 33.

The σ-donation occurs from the π-bonding orbital of the olefin to an unoccupied metal d orbital. The back-bonding occurs from an occupied metal d orbital to an antibonding π* orbital of the olefin (Figure 1.16). This donation into the antibonding orbital, along with the σ donation, weakens the double bond and can result in the metallacyclopropane structure (Figure 1.17).

The olefin σ donation and π acceptor abilities are highly dependent on the metal complex. Metals with significant positive charge or high oxidation state make the coordinated olefin behave mainly as a σ donor. For such complex the C-C bond lengths differ only slightly from the free olefin bond (*cf*. ethylene C-C bond length, 1.33 Å).[42] This leads to the olefin being more susceptible to nucleophilic attacks.[39] Metal complexes with low oxidation state or an electron-rich metal centre can donate more electron density into the unoccupied π* orbital of the olefin and thus making the olefin to predominantly act as a π-acceptor. This leads to significant reduction of the bond order of the olefin; hence the C-C bond is lengthened. This back-donation also leads to hybridisation of the olefin orbitals from sp^2 towards sp^3, which in turn makes the olefin more susceptible to electrophilic attack.

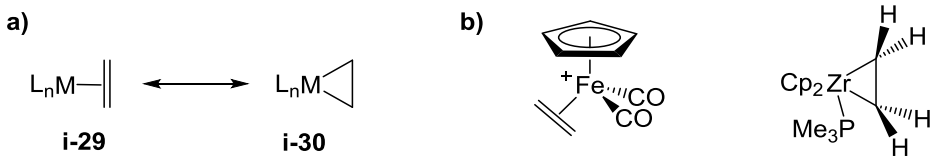

Figure 1.17. a) Olefin complex (**i-29**) *vs.* metallacyclopropane complex (**i-30**) **b)** examples of both motifs respectively.

1.4.8.2. *Coordination of Alkynes*

In general the binding of an alkyne to the metal centre is analogous to the one of alkene. The bonding occurs via synergic σ donation from the alkyne and π back-donation from the metal.[39] As for alkenes, both the alkyne complex (**i-31**) and the corresponding metallacyclopropene complex (**i-32**) can form (if the alkyne is a good π acceptor). The ability of being good π acceptors has been demonstrated by Kasai and Kurosawa, who have shown that there can be a high barrier for the rotation of the metal-acetylene bond even if the ligands on the alkyne are not sterically demanding.[79]

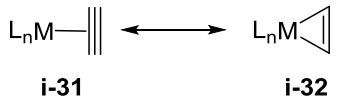

i-31 **i-32**

Figure 1.18. Alkyne complex (**i-31**) *vs.* metallacyclopropene complex (**i-32**).

1.4.9. Migratory Insertion

The migratory insertion reaction is known for all of the transition metals.[39] In general, the transition metal reacts by insertion of an unsaturated ligand Y into an adjacent metal-ligand bond (M-X). As this behaviour creates a free coordination site, often the migratory insertion step is followed by a coordination of a donating ligand (*i.e*. Lewis base, L) (Scheme 1.16).[39]

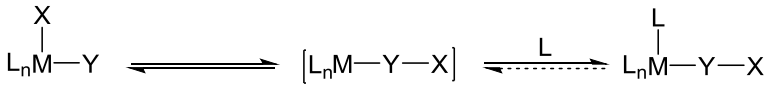

Scheme 1.16. Schematic representation of the migratory insertion.

During the migratory insertion, the oxidation state of the metal remains unchanged, but it leads to a change in valence electron count (decrease by two) and coordination number (decrease by one) of the metal. For the migration reaction to occur, the migrating ligand (*i.e*. X) has to be *cis* to the ligand it is migrating on to (*i.e*. Y). The migratory insertion process can be reversible, and the position of the equilibrium depends on the bond strengths of the starting and product compounds, also, for the reversible reaction (*i.e.* β-elimination) to occur, a vacant site is required. The mechanism of the insertion can be described as two extremes: a concerted mechanism (three and four centred) or an intramolecular nucleophilic attack (in the case of more polar intermediates). In reality the mechanism is considered to be somewhere in the middle.[39]

In hydroacylation the migratory insertion follows the coordination of the olefin, but as this reaction is reversible, the microscopic reverse of migratory insertion must be considered (Scheme 1.6). As the ligand, L, can dissociate, de-insertion of Y can occur leading to the formation of the product containing the unsaturated ligand Y and M-X fragment (Scheme 1.16).

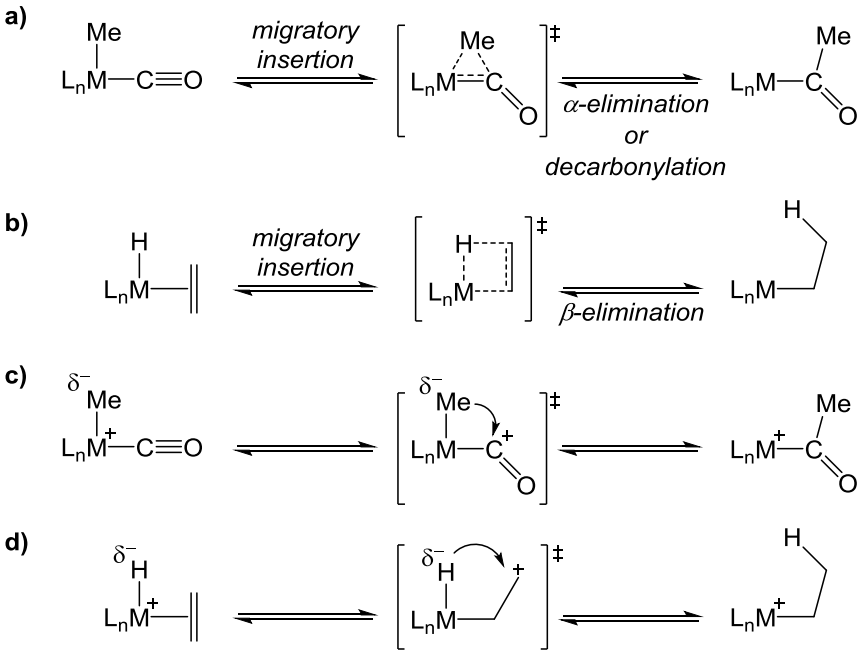

Scheme 1.17. Mechanism of migratory insertion: **a**) Three centred concerted mechanism, **b**) four-centred concerted mechanism, **c** and **d**) examples of the intramolecular nucleophilic attack mechanism.

The reversible step of the hydride migration is termed as β-hydrogen elimination (Scheme 1.17, b). When Y = CO, then the reversible reaction is termed de-insertion of CO, or more conventionally decarbonylation (Scheme 1.17, a) (discussed further in section 1.4.12).

1.4.10. Reductive Elimination

Reductive elimination is the last step in the hydroacylation reaction mechanism (often, but not always, considered as the rate limiting step) (Scheme 1.6).[38] It is the microscopic reverse of the oxidative addition, where the product is formed by the coupling of two ligands at a transition metal centre.[39] In general, during the reductive elimination reaction a strong A-B bond (new C-C bond in hydroacylation) is formed. This prevents the reaction from being reversible (*i.e.* prevents oxidative addition from occurring). The reaction generally proceeds via a 3-centred intermediate leading to a decrease in the oxidation state (from n + 2 to n) and coordination number (by two) of the metal centre (Scheme 1.18). The concerted pathway results in the retention of configuration of a stereocentre directly attached to the metal.[80] In rare occasions the reaction can also occur through cationic or radical intermediates. The mechanism is

dependent on the metal centre and the ligands that undergo the elimination reaction. For example, the reductive elimination of ligands that form a bond to an hydrogen tend to be faster than those that form a bond to a heavy atom.[39] Upon forming new C-C bonds, the slower relative rate is due to a higher-energy transition state. This is due to the sterically hindered conformation that the alkyl groups need to take in order to reductively eliminate.

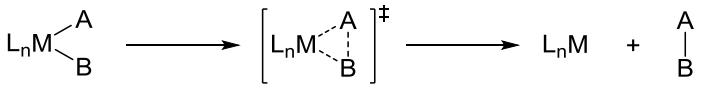

Scheme 1.18. Reductive elimination process proceeding via a 3-centred intermediate.

The rate of reductive elimination is affected by many factors, but overall it can be rationalised that the properties that promote the rate of oxidative addition inhibit the rate of reductive elimination.

The *identity of the metal* influences the rate of reductive elimination. The first row metals promote the reductive elimination over the second and particularly the third row metals, as the bonds between 3rd row transition metals and the ligands tend to be much stronger. The electronics of the metal centre also play an important role. Reductive elimination occurs faster for electron-poor metal centres, as during the reductive elimination reaction the oxidation state of the metal is reduced by 2 units, hence creating a more electron-rich metal centre at the end of the reaction. For electron-rich metal centres, reductive elimination would lead to high energy metal complexes. In cases of electron-rich metal centre, the promotion of the metal into a higher oxidation state, prior to the reductive elimination step, can make the reductive elimination take place more readily.[80]

Another factor that determines the rate of reductive elimination is the properties of the *ligands that are not participating* in the reductive elimination reaction. The sterically more demanding ligands tend to lead to faster rates in reductive elimination in comparison to sterically less demanding ligands.[3] As long as the required conformation can be obtained, sterically demanding ligands result in a sterically hindered metal centre, which in turn leads to faster reductive elimination to relieve the steric congestion. This has even shown to be the case for relatively small benzene molecule elimination (Scheme 1.19). Faster reaction rates were

determined when bulkier phosphine ligands were used.[81] Under the same reaction conditions, also sterically similar, but electronically different phosphine ligands were tested. The results indicated that the phosphines that donate less electron density to the metal result in a faster reductive elimination reaction. For example, when PMe_3 was used as the phosphine ligand, a slower rate of reductive elimination was observed compared to the sterically similar, yet electronically different, PMe_2Ph ligand.

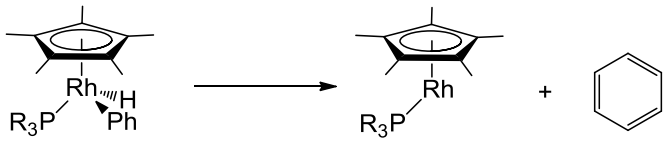

PR_3	Cone angle / °
PMe_3	118
P^nBu_3	132
$PMe_2{}^tBu$	139
PMe_2Ph	122

Scheme 1.19. Reductive elimination of benzene using a rhodium phosphine complex with sterically different phosphine ligands.

Reductive elimination is also shown to be affected by the *ligand-metal-ligand bite angle*. Brown has shown, using palladium(II) species, that the P-Pd-P bite angle has an effect on the rate of reductive elimination. During the reductive elimination, the Pd(II) complex is reduced to Pd(0), and as the preferred geometry of Pd(0) is linear, reductive elimination occurs faster if the bite angle is closer to 180° (Scheme 1.20, a).[82] Also, Brown argues that ancillary ligands with larger bite-angle result in smaller distances between the ligands that undergo reductive elimination, hence increasing the rate of the reaction. Interestingly, an opposite trend was seen by Fink, using similar palladium *bis*-phosphine complexes.[83] Fink reports a comparative reductive elimination reaction study, where he compares the reactivity of two palladium(II) phosphine complexes that only differ by the P-Pd-P bite angle. The results indicate the reductive elimination to be faster when the phosphine back-bone linker was one carbon compared (**i-36**) to a phosphine ligand with two carbon back-bone (**i-35**) (Scheme 1.20, b). Also in the case of three and four carbon back-bone ligands, the reductive elimination was not observed under the given conditions. The reductive elimination also occurs when one carbon backbone ligand (analogues to **i-36**) with *tert*-butyl substituents on phosphorus atoms were used instead of the *cyclo*-hexyl.

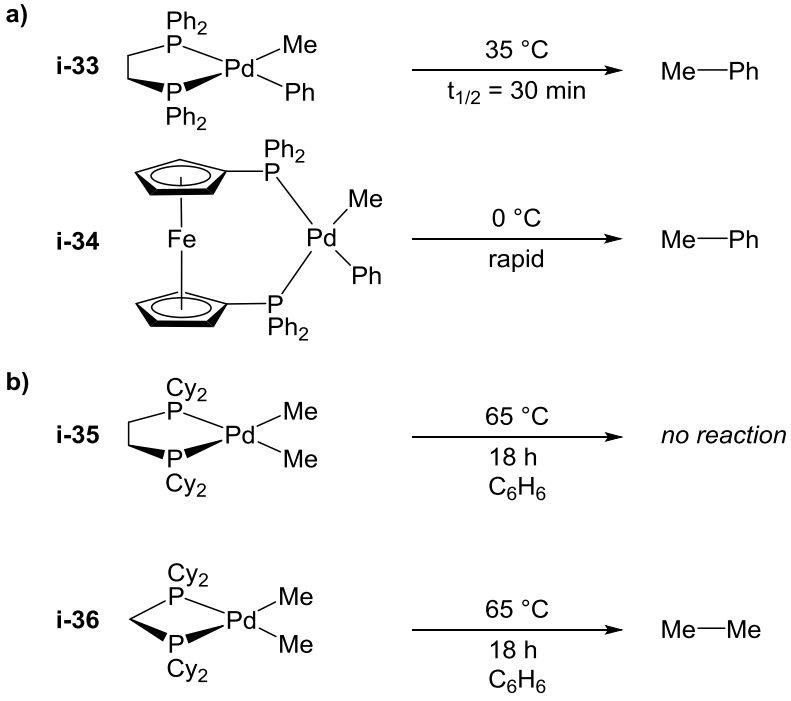

Scheme 1.20. Reductive elimination reactions using *bis*-phosphine ligands with different bite angles on palladium. a) reported by Brown, b) reported by Fink.

As the reductive elimination of C-C bonds occurs usually via a concerted three-centred mechanism, for the reaction to occur a *cis* orientation of the eliminated ligands is required (Scheme 1.18). When the ligands undergoing reductive elimination step are *trans* to each other, the reductive elimination can still occur, but prior to that isomerisation to the *cis* isomer must occur. If the ancillary ligand cannot facilitate the formation of the required *cis* orientation, then the reductive elimination reaction does not occur (Scheme 1.21).[80]

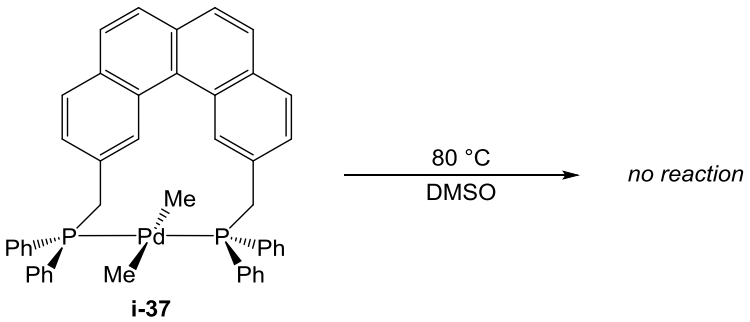

Scheme 1.21. An example of a ligand (transphos) forcing the metal to keep the *trans* conformation, hence inhibiting the reductive elimination reaction.

Ligands like transphos (**i-37**) can be highly useful for mechanistic studies where information about the intermediate directly before the reductive elimination step is required.[84]

The rate of reductive elimination is also affected by the *coordination number*. Three- or five-coordinate metal centres tend to undergo reductive elimination faster than those of four- and six-coordinate metal centres.[85] This effect is caused by the changes in energies of the frontier orbitals during the reductive elimination step (*i.e.* the fate of the additional two electrons that need to be accommodated in the metal d orbitals).[39] For four- and six-coordinate complexes, reductive elimination leads to occupation of a strongly antibonding metal-ligand orbital, whereas for three- and five-coordinate systems (bipyramidal and trigonal complexes) lead to occupation of a nonbonding orbital (Figure 1.19). This explanation is further strengthened by examining oxidative addition, the microscopic reverse reaction, which also occurs faster for odd coordination numbers.

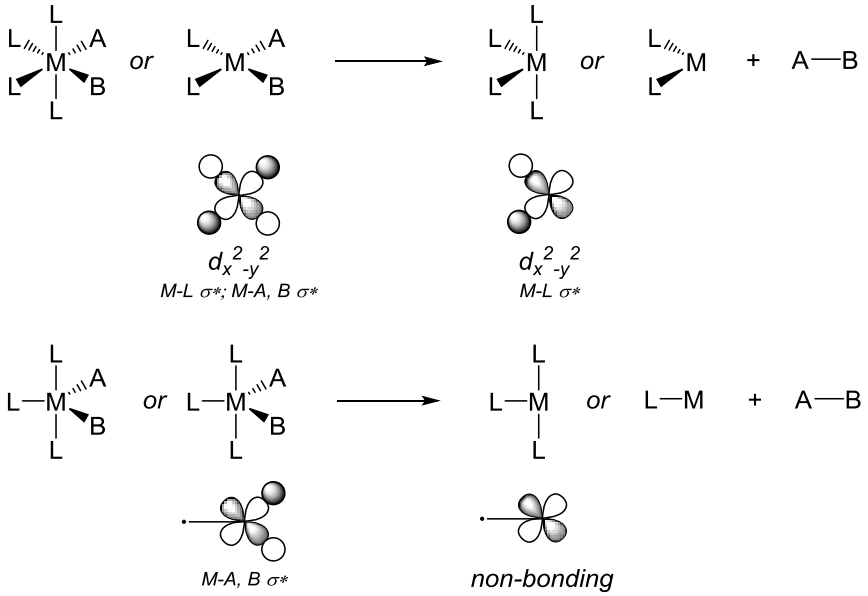

Figure 1.19. Schematic representation of the origin of different rates for reductive elimination depending on the coordination number. Figure adapted from ref. 33.

Milstein used a relatively stable *cis*-hydridoalkylrhodium complex (**i-38**) to study the mechanism of reductive elimination. Based on kinetic studies and reactions with different amounts of free phosphine ligand (PMe_3), it was determined that the reductive elimination of **i-38** occurs by a dissociative mechanism, involving a rate-determining loss of PMe_3, where the reductive elimination step is irreversible (Scheme 1.22).[86] The need for the loss of a ligand for the reductive elimination to proceed faster has also been reported by other research groups.[87-90] Based on these results and other corresponding results, it was concluded that reductive

elimination of 4-coordinate d^8 complex and 6-coordinate d^6 complex are more difficult than for 3- and 5-coordinate complexes.

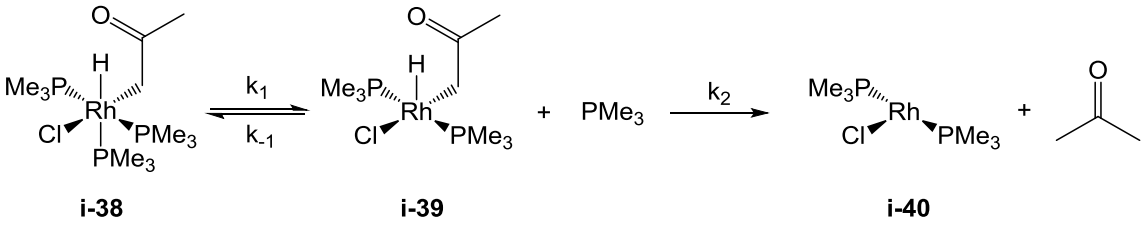

Scheme 1.22. Relatively stable *cis*-hydridoalkyl rhodium complex (**i-38**) used by Milstein to study the reductive elimination reaction. The rate limiting step in this mechanism was found to be the dissociation of the phosphine.

1.4.11. β-hydrogen Elimination

β-elimination is the microscopic reverse of the migratory insertion step (Scheme 1.23). If the eliminating group is hydrogen, the reaction is termed as β-hydrogen elimination. β-hydrogen elimination is usually kinetically and thermodynamically more favourable than the β-alkyl elimination.[91]

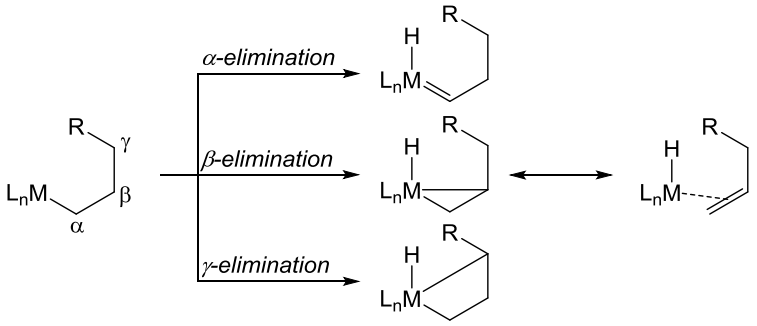

Scheme 1.23. Comparison of α-, β- and γ-hydrogen elimination.

For β-hydrogen elimination to occur, the metal centre must have a vacant coordination site and the metal-alkyl complex must be able to adopt the *syn* coplanar arrangement of the metal and the hydride groups. Using these requirements the metal centre can be designed so that no vacant coordination sites are available, or they cannot adopt the geometry required for the elimination reaction (*e.g.* metallacyclic complexes).[92] Also, electron-rich metal centres lead to faster β-hydrogen elimination, as there is more π-back-donation available to break the C-H

bond. Electron-poor metals tend to prefer the formation of the agostic complex (Scheme 1.24).[93] Also the substrate itself affects the β-hydrogen elimination. If the R-groups at the α-position are electron withdrawing, the carbon-metal σ-bond is strengthened and thus β-hydrogen elimination suppressed.[3] Similarly, electron-withdrawing R-groups at the β-position inhibit the reaction as they lead to less donating β-C-H bond, hence reducing the initial agostic effect needed for the C-H unit to approach the metal centre.[91]

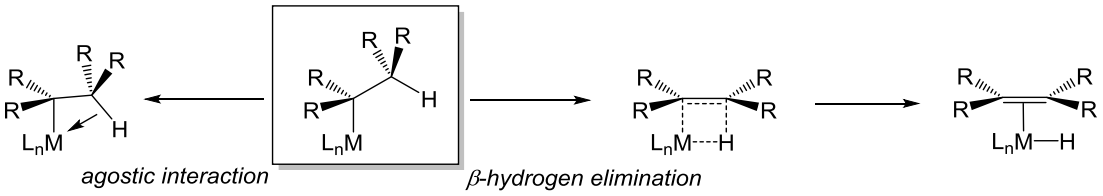

Scheme 1.24. β-hydrogen elimination reaction occurring through migratory de-insertion process. In case of electron-poor metals that are not capable of back-donating into the antibonding C-H orbital result in formation of the agostic complex.

The ancillary ligands, other than electronically affecting the metal centre, can also influence the β-hydrogen elimination sterically. For example bulky or hemilabile ligands can block the coordination site needed for the metal-hydride formation (Scheme 1.25).

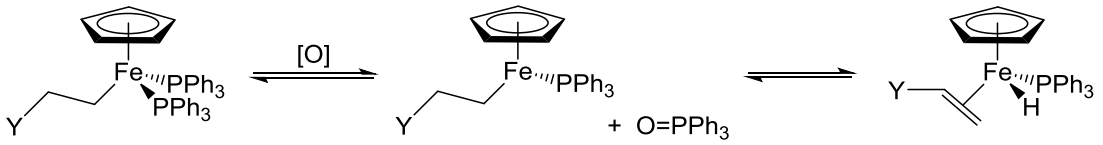

Scheme 1.25. Example of a phosphine ligand blocking a vacant site needed for β-hydrogen elimination. Without oxidation of the phosphine the β-hydrogen elimination reaction does not occur.[94]

1.4.12. Decarbonylation

Decarbonylation is the transition metal promoted pathway for cleaving the C-H bond in aldehydes in order to produce acyl-metal-hydrido intermediates followed by the migration of the carbonyl group. The importance of this reaction comes from its ability to remove a functional group from organic molecules.[95, 96] This is beneficial in natural product synthesis; removal of CO can act as an *in situ* source of CO gas in the reaction mixture, and it is an useful way for synthesising alkanes and alkenes from fatty aldehydes.[97-100]

In hydroacylation, decarbonylation is an unwanted side-reaction that reversibly leads to the formation of the corresponding metal carbonyl complex (**i-4**), which can then continue to irreversibly reductively eliminate the hydrocarbon fragment leading to the formation of the catalytically inactive metal-carbonyl complex (Scheme 1.6, **i-5**).[38]

As for reductive elimination, Milstein has shown that for decarbonylation reaction to occur, a dissociation of a ligand (*e.g.* PR_3) must first take place to provide a free coordination site.[86] A reaction was conducted between rhodium complex **i-41** and acetaldehyde resulting in a complex **i-42** which is stable at room temperature. Upon heating the reaction mixture to 70 °C the dissociation of the phosphine ligand was observed and the complex **i-43** was obtained. This 5-coordinate intermediate could then reductively eliminate the aldehyde and recoordinate the phosphine ligand reforming the starting rhodium complex **i-41** or decarbonylate to form **i-45** which can then rearrange and reductively eliminate to result in the metal carbonyl complex **i-46** (Scheme 1.26).

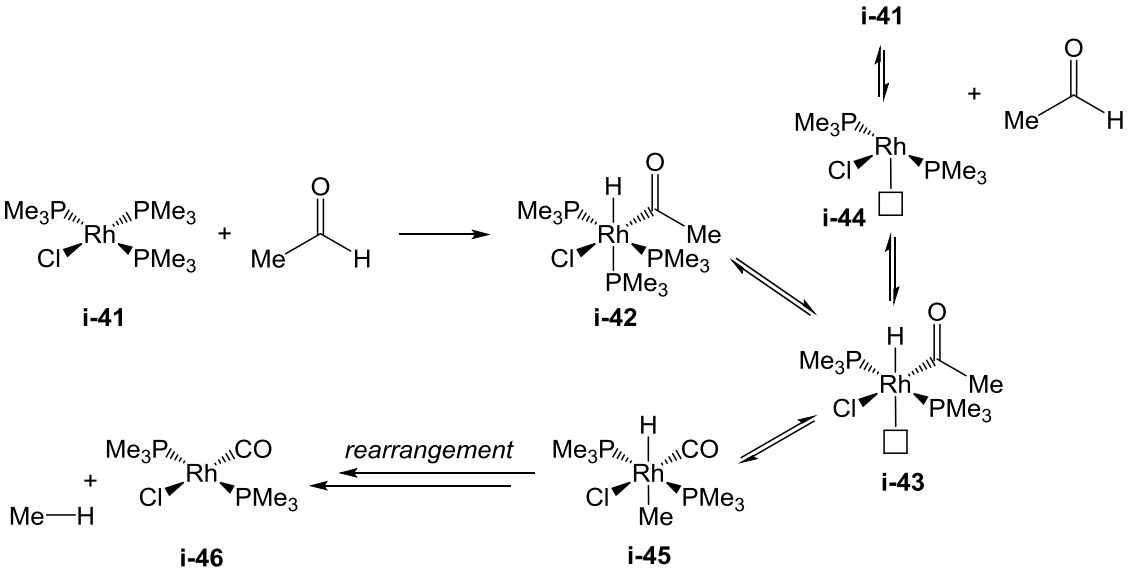

Scheme 1.26. Decarbonylation reaction from a 6-coordinate rhodium complex. For the dissociation of the phosphine, elevated temperature (70 °C) was needed.

This reactivity was also shown using the same complex, **i-42**. If no additives were added to the reaction mixture, no decarbonylation was observed at room temperature. Upon adding $AgPF_6$ to the reaction to abstract the halogen, spontaneous decarbonylation was observed from the formed 5-coordinate complex. This extra stability gained from 6-coorndinate intermediates has

been used by many research groups, to reduce the effect of decarbonylation during the hydroacylation catalysis (section 1.5.1.3).

1.5. Hydroacylation Reaction – Catalyst Systems

This potentially extremely useful catalytic transformation has been studied extensively over the last few decades. During this period, initial stoichiometric reactions have eventually led to catalytic processes where the catalyst loading can be dropped to 0.1 mol%, and very specific reactions been upgraded to more general substrates. Nevertheless, hydroacylation still attracts significant interest, as even lower catalyst loadings are needed, more selective and robust and catalysts that work on any aldehyde/olefin combinations are desired.

1.5.1. Historic Advances in Hydroacylation Catalysis

1.5.1.1. *Intramolecular Hydroacylation*

The first example of the hydroacylation reaction using a transition metal complex was published by Sakai in the early 1970's.[101] Studying the stoichiometric reactions to eventually synthesise 2,3-disubstituted cyclopentanone derivatives, they carried out a range of reactions with different 4-enals using Wilkinson's catalyst – $[Rh(PPh_3)_3Cl]$. Although up to 34% yield for the hydroacylation product (the cyclic ketone) was observed, in all cases equivalent amounts of the unwanted decarbonylation product (the cyclopropane derivative) were also obtained (Scheme 1.27).

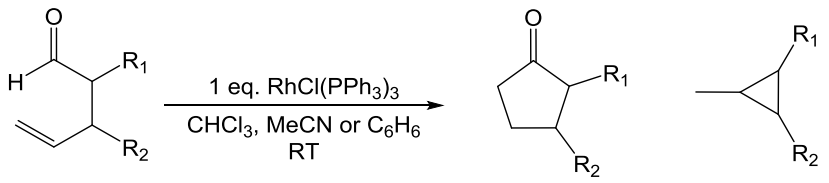

Scheme 1.27. First example of the hydroacylation reaction carried out by Sakai and co-workers *101*

Milstein further studied this reaction using a methyl substituted rhodium complex **i-41**.[102] Upon reacting **i-41** with 4-pentenal at room temperature, he was able to isolate the acyl-rhodium-hydride intermediate (**i-47**) (Scheme 1.28). The intermediate was fully characterised and this motif was subsequently confirmed by other research groups.[102-105] Only when the reaction mixture was heated to 50 °C, the phosphine dissociated, and allowed for the reaction to continue resulting in intramolecular hydroacylation process leading to the formation of the cyclopentanone product in good yield (72%). However, the metal-carbonyl complex (**i-46**) and but-1-ene were also formed via the decarbonylation process.[106]

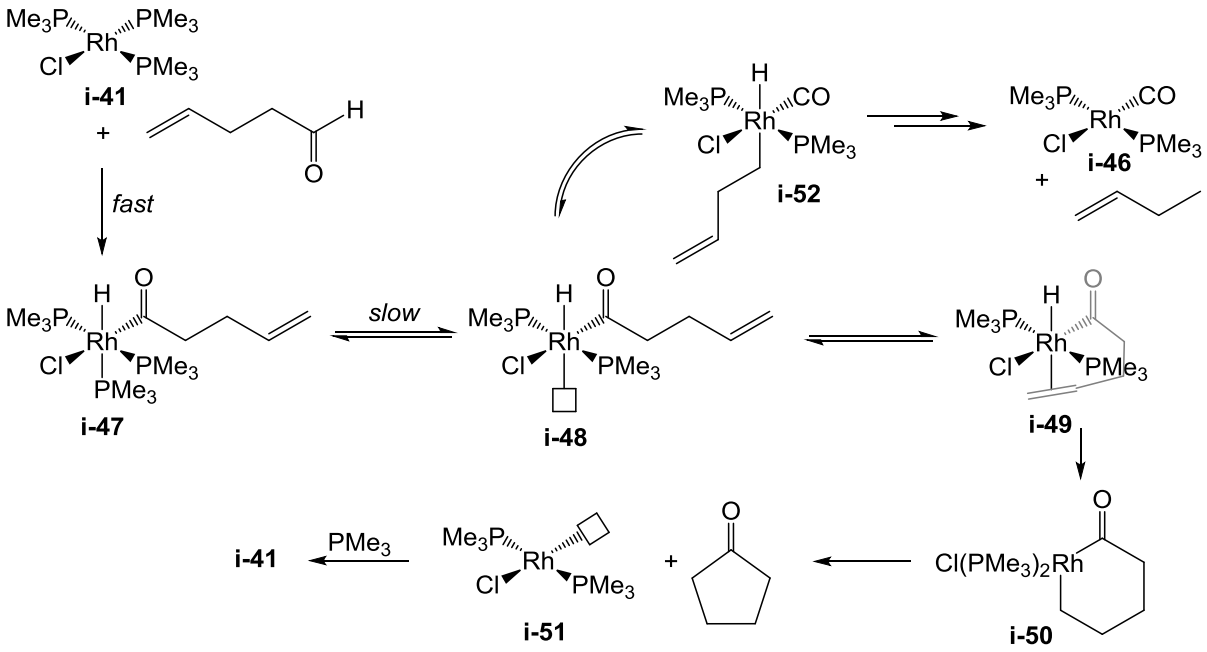

Scheme 1.28. Milstein's proposed reaction mechanism for intramolecular hydroacylation of 4-pentenal using a rhodium phosphine catalyst.

In order to accommodate the coordination of the double bond *trans* to the hydride (**i-49**), a dissociation of a phosphine ligand was expected to occur. To test this hypothesis, Milstein carried out a study using a $P(CD_3)_3$ ligand. Isolated (**i-47**) was allowed to react at 40 °C for 1h in the presence of excess of $P(CD_3)_3$, which led to an observation where the ^1H NMR spectra signals for the PMe_3 *trans* to the hydride disappeared (due to being replaced with the $P(CD_3)_3$), whereas the shifts for the *cis*-phosphines had not been affected proving the hypothesis that the *trans* phosphine dissociates in order for the hydroacylation reaction to be carried out. The

observation that only the phosphine *trans* to the hydride was affected is thought to be because of the high *trans*-effect of the hydride ligand.[106]

Another breakthrough of this work carried out by Milstein, was the reporting of the first catalytic hydroacylation reaction that was not carried out under ethylene (ethylene gas was used by some pioneering research groups in order to block vacant coordination sites). Although the first example, it was far from efficient; even though the reaction was carried out at relatively high catalyst loading (10 mol%), only 3 turnovers were observed and during the reaction the formation of but-1ene (the decarbonylation product) was determined.[102]

A substantial leap forward in the hydroacylation of 4-pentenal was reported by Vinogradov in the 1980's.[107] They found that the cyclisation of 4-pentenal using $Co(dpp2)(PPh_3)_2$ (dpp2 – 1,2-*bis*(diphenylphosphino)ethane) (**i-81**) as the catalyst led to 95% conversion at only 3 mol% catalyst loading (70 °C, 1 h). Interestingly, they report that the reaction was 100% selective towards hydroacylation, but the mechanistic studies indicate the formation of $[Co(dpp2)(CO)]_2$. If instead of $Co(dpp2)(PPh_3)_2$, the monodentate $CoCl(PPh_3)_3$, was used, no catalytic transformation was observed, hence it was proposed that the active species during the catalytic cycle were cobalt(0), d^9, and cobalt(II), d^7. The mechanism was proposed to resemble the one suggested for rhodium. The reaction involves an initial oxidative addition step resulting in an acyl-metal-hydride species (rate limiting step), which rearranges to acyl-alkyl-cobalt derivative that goes through a reductive elimination step in order to yield the desired ketone. Although this complex acts as a very good catalyst for the intramolecular hydroacylation of 4-pentenals, the activity towards other substrates was shown to be limited.

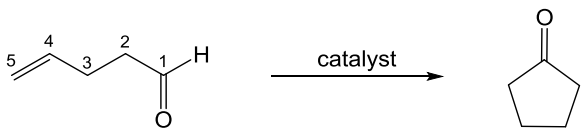

Scheme 1.29. General scheme of 4-pentenal and its intramolecular hydroacylation product, with labelled positions.

The first example of catalytically active intramolecular hydroacylation catalysts that can catalyse the coupling of a range of substrates was reported by Bosnich in two papers.[108, 109] In

this tandem-publication the use of rhodium *bis*-phosphines as catalysts for intramolecular hydroacylation of 4-pentenals to cyclopentanones was discussed. From the range of [Rh(*bis*-phosphine)]$^+$ fragments tested as catalysts, where the counterion used was $[ClO_4]^-$, it was determined that the best conversions were seen upon using dpp2 as the ligand (**i-81**). The catalyst existed as a dimeric species in the solid state or in non-coordinating CH_2Cl_2 (**i-54**), or as a *bis*-substituted solvent-complex in acetone solvent (**i-53**) (Figure 1.20). The catalysts have been shown to be relatively stable and can be conventionally stored. Both of these complexes rely on the weak coordination towards the aromatic ring or the solvent molecules which are displaced by the coordination of the 4-pentenal.

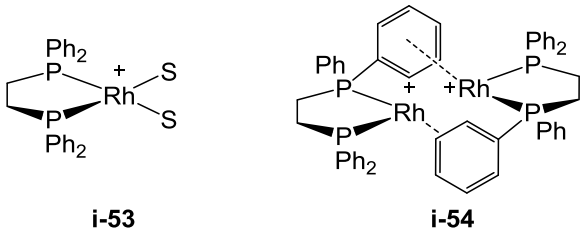

i-53 **i-54**

Figure 1.20. Two forms of the Bosnich's catalyst. S – solvent molecule in case of coordinating solvent (acetone or methanol). Upon dissolving the dimer **i-54** in a coordinating solvent, the corresponding *bis*-solvent complex (**i-53**) was observed.

These catalysts were capable of converting a range of 4-pentenals to the desired ketones. Substituted 4-pentanals with substituents in positions 2, 3, 4 and 5 were also tested (Scheme 1.29). It was determined that substituents in positions 3 and 4 do not have a significant effect on the catalytic rate, but substitution at position 2 slowed down the catalysis substantially and substitution at position 5 (*i.e.* not primary alkene) lead to no catalytic activity at all. In the case of non-inhibiting substrates, the turnover numbers were between 80 and 100 when catalyst loading of 1 mol% was used. The turnover frequency was reported for 4-pentenal to be 6 turnovers per second. After 80-100 turnovers the catalyst becomes slower and the formation of the metal-carbonyl species, [Rh(*bis*-phosphine)$(CO)_2$]$^+$, was observed. The catalytic reactivity was also found to be highly sensitive to the solvent used. The best results were obtained when CH_3NO_2 or CH_2Cl_2 were used as the reaction medium. In the case of acetone also good catalytic activity was observed initially, but the catalyst was found to be more susceptible towards decarbonylation in acetone. Also methanol and acetonitrile were tested as solvents, but it was

determined that in methanol the formation of hemiacetal (via the reaction between alcohol and aldehyde groups) occurred. Acetonitrile led to inactive catalysts, which was explained by the formation of catalytically inactive [Rh(*bis*-phosphine)$(MeCN)_2]^+$ species.

To probe the fine balance between the hydroacylation reaction and the reductive decarbonylation, Bosnich tested other *bis*-phosphine ligands in order to develop a hydroacylation catalyst that would increase the rate of hydroacylation relative to the rate of decarbonylation. A range of *bis*-phosphines with different chelate ring sizes were prepared to study the effect of the P-Rh-P bite-angle on the hydroacylation reaction {dpp2, dpp3 and dpp4, (**i-81** – **i-83**)}. The catalyst precursors were generated by hydrogenating the [Rh(*bis*-phosphine)(nbd)]$[ClO_4]$. In cases other than dpp2, a much faster rate of decarbonylation was observed, particularly that was seen to be the case with the widest bite-angle complex containing the dpp4 ligand. The catalytic activity of the [Rh(*bis*-phosphine)(nbd)]$[ClO_4]$ (nbd = norbornadiene) complexes before the hydrogenation step was also studied, showing quite slow activity. It was rationalised to be due to the strong rhodium-nbd bonding, and hence the dissociation of nbd substantially inhibits the rate of catalysis.

To study the reasons behind this increased activity of the dpp2 complex, a comparison reaction using the fluorinated ligand dpf2 {1,2-*bis*(diperfluoroarylphosphino)ethane} was performed. The use of this electron-poor *bis*-phosphine led to decrease in catalytic rate. Interestingly the rate of decarbonylation was also seen to decrease by the same amount, hence leaving the hydroacylation to decarbonylation ratio roughly the same. Another comparison reaction was conducted using non-aromatic substituted 1,2-*bis*(dicyclohexylphosphino)ethane (dcpe) as the ligand. The use of this rhodium-dcpe complex resulted in the fastest turnover frequency for the first 20 turnovers, but also a faster rate of decarbonylation was observed and hence after approximately 20 turnovers fully decarbonylated complex was seen.

As the data indicated that the phenyl-groups were necessary to obtain good catalytic conversions, the monodentate $[Rh(PPh_2Me)_2(acetone)_2][ClO_4]$ complex was synthesised to study the effect of the chelation. This complex proved to be catalytically inactive towards hydroacylation reaction and instead rapid double-bond migration of 4-pentenal to 3-pentenal

was observed. The proposed mechanism for that was reported to be via a π-allyl intermediate. Overall it was commented that the chelation is crucial, and in particular the bite-angle of the metal phosphine complex is important in order to obtain an active hydroacylation catalyst.[108]

Bosnich also carried out a fundamental mechanistic study to further explore the individual steps of the hydroacylation reaction.[109] The problem they encountered was that for this fast hydroacylation catalyst none of the catalytic intermediates are formed in high enough quantities to be detected, and hence they consider the system as "black box" into which reagents enter and products emerge from, but no intermediates are visible. For this they used deuterated reagents to study the deuterium-scrambling processes which would shine light towards reversibility of different steps and any rate data (Scheme 1.30).

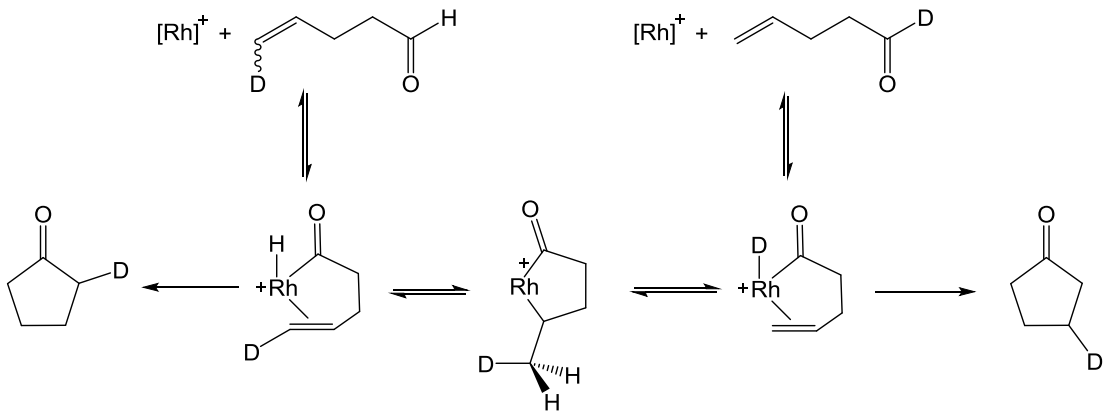

Scheme 1.30. The proposed mechanism for deuterium transfer.

When *mono*-deuteriated aldehyde was used (deuterium in the aldehylic position), it was observed that at the end of the reaction the cyclopentanone products contain deuterium in either the α- or β-position, in approximately 1:1 ratio (depending on the substrate). Mass spectrometry data showed that only one deuterium per product is observed, thus indicating the deuterium source to be intramolecular. When the same reaction was carried out in deuterated solvent, identical final products ratio was seen. During the reaction, ^{1}H NMR spectroscopy showed a signal growing in for the protic aldehyde, showing reversibility in all the steps before reductive elimination (Scheme 1.30). From the deuterium scrambling data they determined that

the oxidative addition, hydride migration and all the other steps are much faster than the reductive elimination, as at the beginning of the catalysis almost 90% of the catalytic activity generated different deuterated 4-pentenals and the remaining 10% led to product. Overall the rate determining step was proposed to be reductive elimination, with all the other steps being reversible, and the reverse steps are faster than the forward steps.

Another mechanistically relevant study carried out by Bosnich was a comparison of the hydroacylation reaction comparing the reactivity of 1-pentenal and 1-pentanal. Using 1-pentanal, no hydroacylation reaction occurred as expected, but also after several hours at 20 °C no decarbonylation was noted. Only after heating the solution at 60 °C for hours, decarbonylation was observed, indicating that the binding of the olefin group acts as a tether bringing the aldehyde closer to the metal centre and hence aids the oxidative addition step, but also it reduces the effect of reductive decarbonylation.[56, 108, 109]

For a number of years, different groups have used different cationic rhodium phosphine complexes of the general structure [Rh(*bis*-phosphine)(solvent)$_2$]$^+$ to carry out hydroacylation.[38] A new approach was reported by Peters using zwitterionic complexes instead of the established cationic ones.[110] Zwitterionic complexes are formally regarded as mesoionic species, as no direct interaction between the negatively charged atom (boron in the Peters case) and the central metal exist.[111]

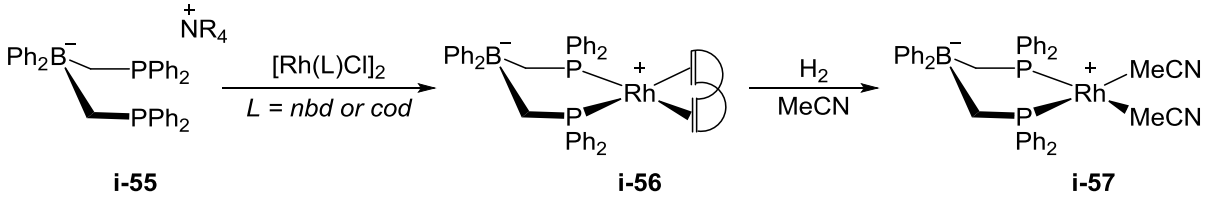

i-55 **i-56** **i-57**

Scheme 1.31. Synthesis of the zwitterionic catalyst **i-57**. R = butyl.

The zwitterionic complex used as the catalyst was [Rh(PCBCP)(MeCN)$_2$] (**i-57**). Based on X-ray crystallography data it was deduced that the borate unit was locked rigidly in the backbone and the distance between the boron atom and the rhodium metal was > 4 Å, hence no close molecular ion-pairing was observed. Peters describes this zwitterionic motif to have some of the charge of the borate unit dissipated through the space and/or the ligand framework to the metal

centre. This is expected to lead to a more electron-rich rhodium centre compared to the analogous cationic complexes. This was backed-up by IR spectroscopy data, where the stretching frequencies of the zwitterionic [Rh(PCBCP)$(CO)_2$] (2080 and 2029 cm^{-1}) were significantly lower than the data for the cationic [Rh(dpp3)$(CO)_2$][PF_4] or [{$Ph_2Si(CH_2PPh_2)_2$}Rh$(CO)_2$][PF_6] (2100 and 2056 cm^{-1}; and 2099 and 2056 cm^{-1} respectively).[18] Based on work carried out by Bosnich and considering that the rate determining step being reductive elimination, it would be expected that an electron-rich metal centre would inhibit the rate of hydroacylation.[39, 80, 109] Catalytic data on the other hand shows the zwitterionic ligand to be beneficial.[110] The intramolecular hydroacylation reaction was carried out using 4-methyl-4-pentenal as the substrate. A range of cationic and zwitterionic catalysts were tested, and the results showed an advantage in using the zwitterionic catalyst over the cationic analogues. At 0.5 mol% catalyst loading at room temperature in acetone, full conversion was seen using the zwitterionic **i-57** whereas cationic complexes [Rh(dpp3)$(MeCN)_2$][PF_4], **i-58**, [Rh(dpp2)$(MeCN)_2$][PF_4], **i-53** and direct comparison complex [{$Ph_2Si(CH_2PPh_2)_2$}Rh$(MeCN)_2$][PF_6] reached to about 70 – 80% conversions. Also significant difference in rate was determined, where turnover frequency for **i-57** of 2400 h^{-1} was observed, compared to quite sluggish 40-60 h^{-1} for the cationic complexes. As an added benefit, the zwitterions were capable in carrying out the hydroacylation reaction in a range of solvents where cationic catalysts were inhibited, including benzene, acetonitrile (which in the case of cationic complexes can be used as a reaction quencher during catalysis) and THF.[41, 108]

1.5.1.2. *Intermolecular Hydroacylation*

Based on how many different combinations of products could be synthesised via intermolecular hydroacylation, it must be considered as a more important reaction to achieve than the intramolecular hydroacylation. Unfortunately it is also a much more challenging target, as the C-H activation of the aldehyde is made more difficult by not being promoted by a chelating olefin, while the decarbonylation reaction is also promoted by the absence of a chelating alkene/alkyne.[38, 109] Hence the first publications on intermolecular hydroacylation appeared

almost 10 years after the intramolecular hydroacylation.[112] Miller used [Rh(acac)(C_2H_4)$_2$] as the catalyst for the hydroacylation reaction of 4-pentenal in ethylene saturated chloroform. At 10 mol% catalyst loading full consumption of the starting material was observed, leading to the formation of a range of products of up to 39% yield (Scheme 1.32). Interestingly, the intramolecular hydroacylation product, cyclopentanone, was produced as a minor product (1 %).

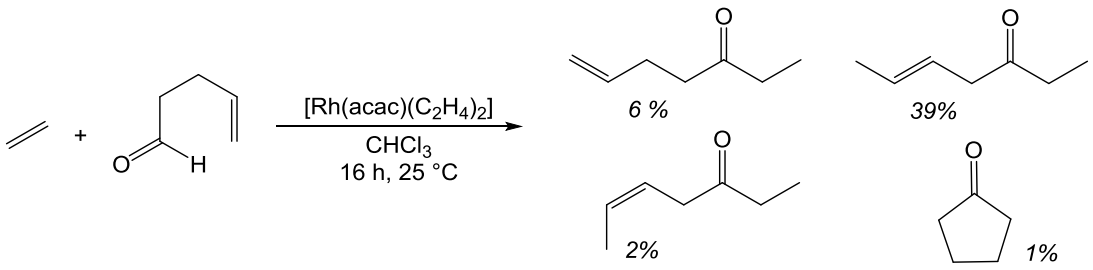

Scheme 1.32. Intermolecular hydroacylation reaction carried out by Miller, and the relative ratios of products formed.

Although this was the first example of intermolecular hydroacylation, the catalyst can definitely not be considered as useful one, as only 6% of the desired 1-en-product was formed (with 47% overall conversion to the intramolecular hydroacylation products). The catalyst was shown to be more useful for 4-hexenals, as in that case the double bond of the starting material is already at the preferred non-terminal position.

The intermolecular hydroacylation conversions were improved by Milstein and Marder.[113] They used the indenyl complex, [(η^5-C_9H_7)Rh(C_2H_4)$_2$], for intermolecular hydroacylation. Their strategy was to use the ethylene to block the vacant sites needed for decarbonylation to occur. The reaction was carried out under relatively harsh conditions: 100 °C, 1000 psi of ethylene with benzene as the solvent. Although the reaction was quite slow (TOF < 4 h^{-1}), high conversions were seen when benzaldehyde was used as the starting aldehyde, with catalyst loading as low as 3.6 mol% (Scheme 1.33). This exceptional stability was reported to be due to no decarbonylation occurring during the reaction and also no decomposition of the catalyst was observed. The obvious limitation of this reaction is the lack of scope. Only ethylene was used as the olefin source, and also the choice of aldehyde is limited. When formaldehyde was used

instead of benzaldehyde, reduced conversion, even slower rate (2-3 turnovers in 24 h) and deactivation of the catalyst were seen.

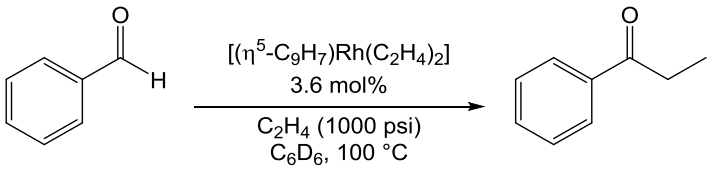

Scheme 1.33. Milstein's early catalytic system for intermolecular hydroacylation of benzaldehyde and ethylene under high ethylene pressure.

In attempts to use this method for intramolecular hydroacylation, using 4-pentenal,[108, 109] no formation of the expected cyclopentanone was seen, instead rapid alkene isomerisation occurs and 3-pentenal was observed as the main product.[112, 113]

Brookhart reported an elegant methodology to dramatically reduce the effect of decarbonylation using rhodium(I) and cobalt(I) Cp*-based ((pentamethyl)-cyclopentadienyl) catalysts to mediate the intermolecular hydroacylation reaction between benzaldehyde and vinylsilyltrimethylsilane.[44, 114] The catalytic process is carried out under mild conditions and the vinylsilane acts as both, substrate and ligand. The uniqueness of this reaction is the fact that although decarbonylation from the acyl-metal-hydride (**i-62**) species is occurring (via **i-63** or **i-64**), the catalyst is not deactivated. This is due to the formation of a 6-coordinate complex (**i-65** or **i-66**) after the decarbonylation step, which cannot reductively eliminate, hence the carbonyl inserts into the alkyl group, generating a 5-coordinate complex, **i-67** or **i-68**, which may then reductively eliminate to give the desired hydroacylation product.

The studies revealed the mechanism to be as follows: the initial dissociation of olefin forms a 16-electron intermediate that rapidly binds aldehyde to form a reactive rhodium aldehyde olefin complex. Oxidative addition of the aldehylic C-H bond is fast and reversible forming a Rh(III)-acyl-hydride intermediate. During olefin insertion a linear or branched rhodium-acyl intermediate can be generated. Next, the de-insertion of CO generates Rh(III) complexes, from which CO insertion occurs generating the rhodium-acyl-aryl intermediate that then reductively eliminates ketone in the rate limiting step of the reaction (Scheme 1.34).

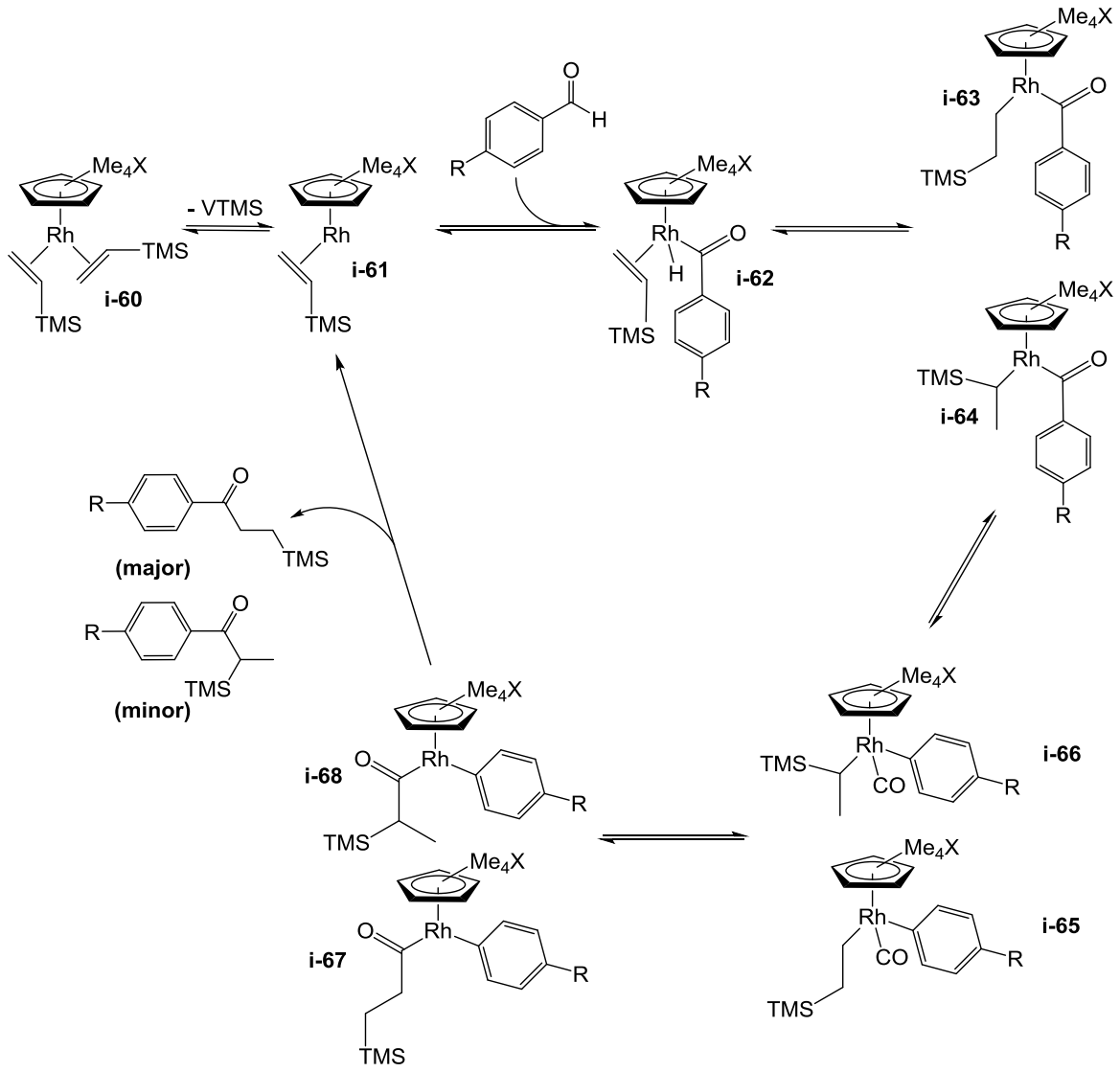

Scheme 1.34. Proposed mechanism for the hydroacylation using benzaldehyde and vinylsilyltrimethylsilane as substrates and a rhodium catalyst. TMS – trimethylsilyl, VTMS – vinyltrimethylsilane, X – Me or CF_3.

It was also found that the catalysis was affected by the electronics of the Cp* ligand. Upon changing one of the methyl groups on the Cp* ligand for a more electron withdrawing CF_3, the conversion and selectivity changed significantly. If X = CH_3, at 5 mol% catalyst loading, 14% conversion was seen, with 3:2 linear:branched product ratio. When the reaction was carried out under the same conditions with X = CF_3, 98% conversion was observed with the linear:branched ratio improved to 22:1. This is consistent with the rate limiting step being reductive elimination.

1.5.1.3. *Chelating Substrates in Hydroacylation*

Many catalysts have been developed for intermolecular hydroacylation, but for catalysts that promote coupling for a wide range of substrates, the decarbonylation side-reaction still remain problematic, resulting in catalyst deactivation. To reduce the effect of decarbonylation, while still allowing for a good scope, the use of a tethering heteroatom emerged. Suggs first demonstrated the benefit of an heteroatom in the 4-position using the Wilkinson's complex and quinolone-8-carboxaldehyde as the reagents (Scheme 1.35).[103, 115] While studying the decarbonylation reaction, he was interested in designing a complex that would allow for oxidative addition reaction to occur and result in the formation of a stable acyl-hydride intermediate that would not undergo reductive elimination. Suggs carried out the reaction between Wilkinson's complex and quinolone-8-carboxaldehyde. The formed acyl-metal-hydride (**i-69**) was found to be stable even at elevated temperatures (around 170 °C) for a number of reasons: the chelation effect, due to being a six-coordinate complex and as the decarbonylation reaction would lead to a strained 4-membered ring formation.[86, 103] Upon reacting **i-69** with $AgBF_4$, complex **i-70** was formed, which also, presumably due to the formation of the strained 4-membered ring, does not decarbonylate, but when an olefin is added, the aldehyde C-H bond is added across the olefin resulting in a formation of a ketone **i-71**. If an olefin was added to the 6-coordinate **i-69**, no reaction occurred (Scheme 1.35).

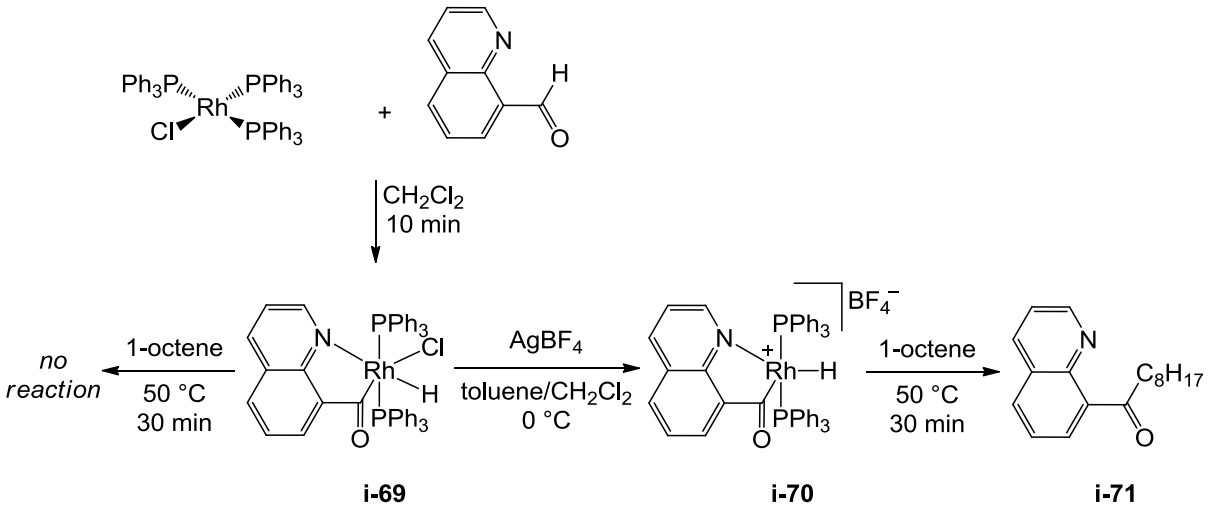

Scheme 1.35. The first stable acyl-hydride isolated from a $RhCl(PPh_3)_3$ promoted aldehyde addition, and its reactivity.

Jun took Suggs's idea, but changed the heteroatom unit to picolyl imine.[116, 117] The advantage in using the picolyl imine is that it can be formed *in situ* and removed at the end of the reaction[118]

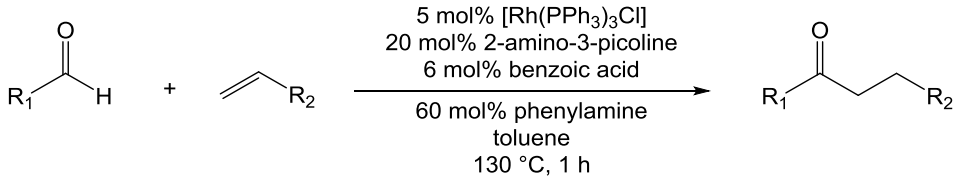

Scheme 1.36. Optimised reaction conditions required for Jun's hydroacylation reaction. R_1 – aryl group, R_2 – aryl or alkyl group.

Jun reported a general approach to intermolecular hydroacylation using Wilkinson's catalyst and 2-amino-3-picoline as the co-catalyst. The intermediate forming during the reaction between the aldehyde and 2-amino-3-picoline, the picolyl imine, has a key importance in promoting the C-H activation step by acting as an extra coordination site for the substrate to interact with the metal. Also, the extra coordination has an effect on suppressing the decarbonylation. The problematic step in the reaction was initially the formation of the picolyl imine (aldimine). This formation step was promoted by additives and the step was seen to be occurring faster and also better conversions were obtained when additional benzoic acid and phenylamine were added. This result suggested the transamination step (the formation of imine) to be catalysed by the acid. Under the conditions given in Scheme 1.36, 71 – 98% yield was seen.

The mechanism is expected to follow the general hydroacylation mechanism, but decarbonylation does not affect the reaction as there is no carbonyl unit. The proposed mechanism involving the organic fragments is depicted in Scheme 1.37.

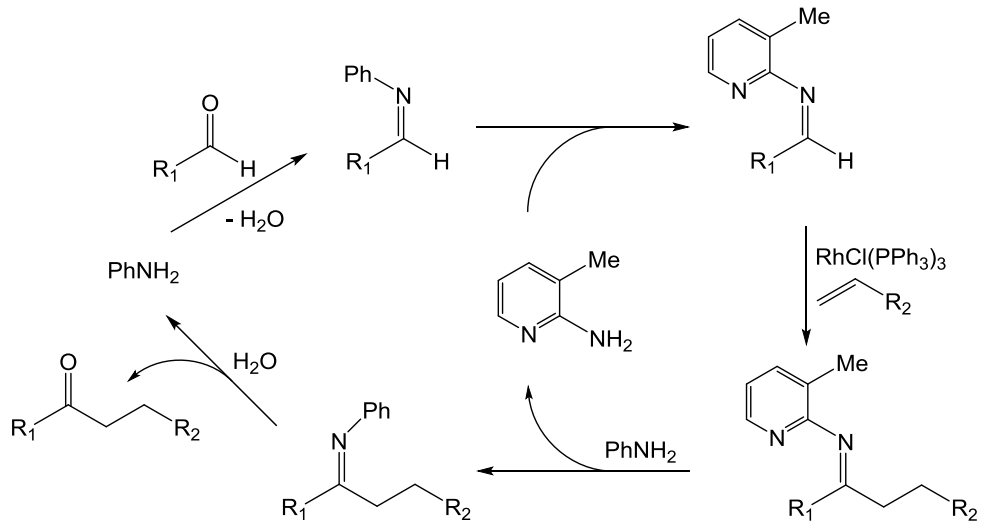

Scheme 1.37. The postulated mechanism for the hydroacylation reaction. The Scheme is a modified version of Jun's mechanism[119] as depicted by Willis[38]

Jun has continued to successfully employ the general approach of forming the aldimines to overcome decarbonylation in different hydroacylation reactions. An example of Jun's recent work is a double hydroacylation reaction. Using a "masked form of dialdehyde", they have been able to carry out double hydroacylation reactions.[120] During the reaction one of the carbon-carbon bonds gets broken, and via a range of rearrangement reactions the fragments lead to the formation of two products (Scheme 1.38), which can be separated.

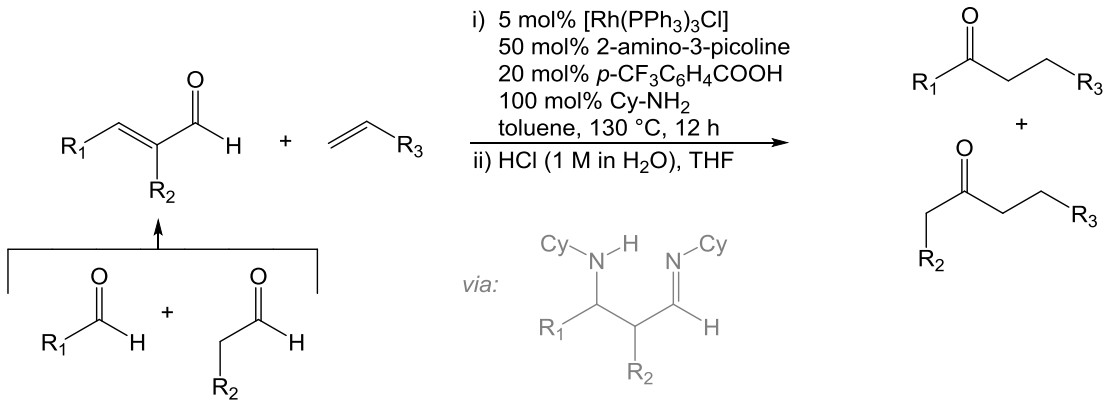

Scheme 1.38. Jun's example of double hydroacylation reaction starting from a "masked dialdehyde"

Attempting to make the reaction more general and more applicable, Jun has developed a tandem-reaction where the starting substrate can be an alcohol. During the catalysis, the rhodium catalyst, $[Rh(PPh_3)_3Cl]$ or $RhCl_3.H_2O$ + PPh_3, first performs alcohol oxidation to the required aldehyde, and then acts as the hydroacylation catalyst. During the oxidation of the

alcohol an equivalent of alkene is also used as the oxidant. This method can be used for a range of alcohols, including allyl alcohols[121] and simple alcohols (although based on their reported data, only aromatic alcohols can be used)[122] but recently Jun has reported a hydroacylation reaction using methanol as the starting point.[123] First the rhodium catalyst oxidises the methanol to formaldehyde which then goes through N-methylation and dehydrogenation forming the N-methylimine compound **i-72**. The formation of N-methylimine is followed by double chelation-assisted hydroamination of alkene with the imine to give the imine-product, which is hydrolysed to result in the desired ketone (Scheme 1.39).

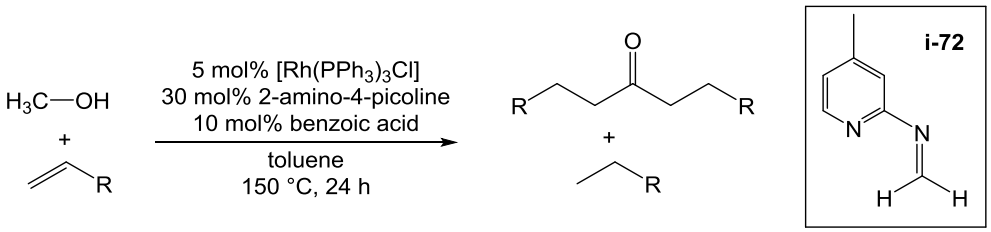

Scheme 1.39. Tandem process where the alcohol is first oxidised and then hydroacylated via the N-methylimine intermediate **i-72** using the Wilkinson's catalyst and 2-amino-4-picoline as the co-catalyst. During the reaction, the olefin acts as the substrate and the oxidant.

Although the catalyst loadings used by Jun are not very low (> 3 mol%), they have shown that the catalyst can be recycled. To make this recycling viable, a set-up was needed which would allow recycling of both the rhodium catalyst and the co-catalyst 2-amino-4-picoline. For that Jun explored biphasic systems for the reaction mixture which would allow for the separation of the catalysts and the reagents.[124] A mixture of solvents (phenol and 4,4'-dipyridil) was used to achieve this goal, where the products end up in the non-polar phase and the catalyst and the co-catalyst end up in the polar phase (Figure 1.21).

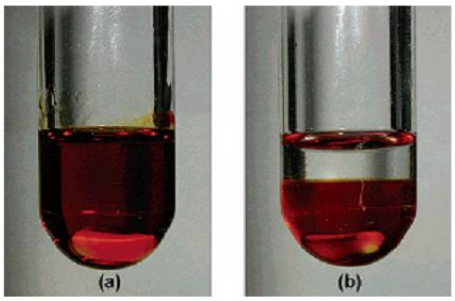

Figure 1.21. A one phase solution at high temperature (120 °C), and the formation of two phases at room temperature. Figure adapted from Jun.[124]

This phase separation allowed for the catalyst and co-catalyst to be recycled with only trace amounts of rhodium (0.01%) and up to 5% of 2-amino-4-picoline was found in the non-polar phase. This excellent separation allowed for no noticeable drop in catalytic activity for 8 runs for a range of hydroacylation reactions.

The use of tethering heteroatom has attracted significant attention from many research groups. For example Suemune,[125, 126] Miura[127] and Dong have studied hydroacylation reactions where an alcohol (phenol) group acts as the tether on the aldehyde. In most cases this approach has led to reactions with low conversions and high catalyst loadings required. However, over the last few years Dong has published some promising results using salicylaldehyde derivatives as the aldehydes and unactivated alkenes, with rhodium catalyst loadings as low as 2 mol% (Scheme 1.40).[47, 128]

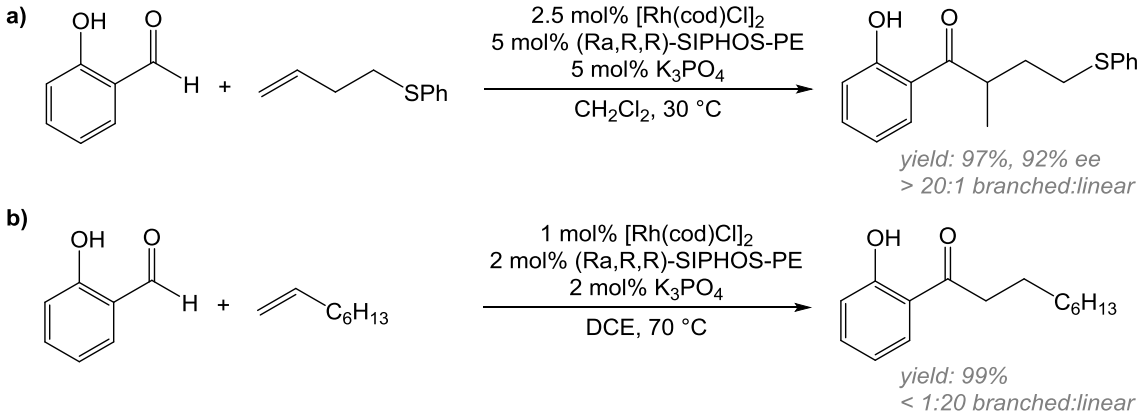

Scheme 1.40. Two examples of Dong's hydroacylation reaction leading to either the formation of branched or linear product. The base is required to deprotonate the salicylaldehyde in order to aid the coordination.

Using $[Rh(cod)Cl]_2$ as the rhodium precursor and (R_a,R,R)-SIPHOS-PE as the ligand (Figure 1.22), they were able to obtain a range of ketone products in good yields. Also excellent regioselectivity for the linear:branched ratios were observed (Scheme 1.40, a). If instead of a 4-carbon thio-alkene, an analogous sulfur-tethered 3-carbon olefin was used, selectivity of the product changes to linear. This selectivity was rationalised by the formation of an intermediate during the hydride insertion. To form a five-membered ring after the insertion step, instead of

4- and 6-membered rings, alkenes with different chain lengths end up preferring linear or branched pathway (Scheme 1.41).

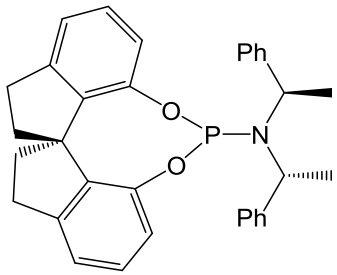

Figure 1.22. (R_a,R,R)-SIPHOS-PE ligand.

Although both the aldehyde and olefin have tethered heteroatoms, which allow for better coordination and by blocking vacant sites reduce the decarbonylation effect, still 2.5 – 10 mol% catalyst loading is needed for the reaction to go to completion. The control reaction with the 2-methoxybenzaldehyde showed no reactivity, hence proving that the –OH group is required for the reaction to proceed.

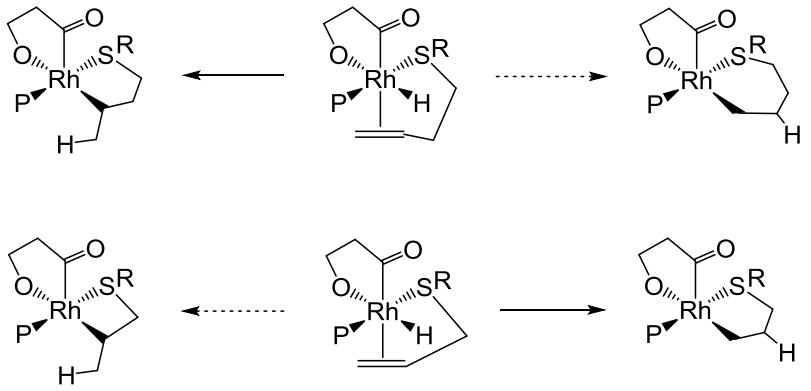

Scheme 1.41. The hydride migration step leading to different regioselectivity. Full arrows indicate the preferred pathway through the 5-membered ring, whereas the dashed arrows lead to the formation of less desirable 4- and 6-membered intermediates. P = (R_a,R,R)-SIPHOS-PE ligand

Dong further developed the use of the salicylaldehyde based hydroacylation by reporting the catalytic reaction where the sulfur-tether was not necessary for the reaction to proceed (Scheme 1.40, b).[128] Under similar conditions to the sulfur-ligand based reaction, at higher temperatures, they were able to use untethered olefins as the alkene source. Also under these conditions, the catalyst loading was dropped to 1 mol%. The mechanism was thoroughly

studied using deuterated substrates, and following the reaction rates under varied conditions. Based on the gathered data it was concluded that the oxidative addition and the alkene coordination steps are fast and reversible. The hydride insertion step was found to be fast and fully reversible for the branched hydride insertion, whereas linear hydride insertion is fully (with some exceptions) irreversible. The resting state for the linear pathway was reported to be the ligand-bound metal complex with somewhat surprisingly hydride insertion being the rate-limiting step. This was suggested based on the labelling studies and the relative ratios of deuteration during the reaction process. While often reductive elimination is reported as the rate limiting step, previously the hydride elimination step has also been observed as being rate limiting.[129] Based on the mechanistic studies the mechanism depicted in Scheme 1.42 was proposed. Although catalyst loadings were lowered and good activity observed, the side-reaction, reductive decarbonylation, was still seen and catalyst decomposition occurred.

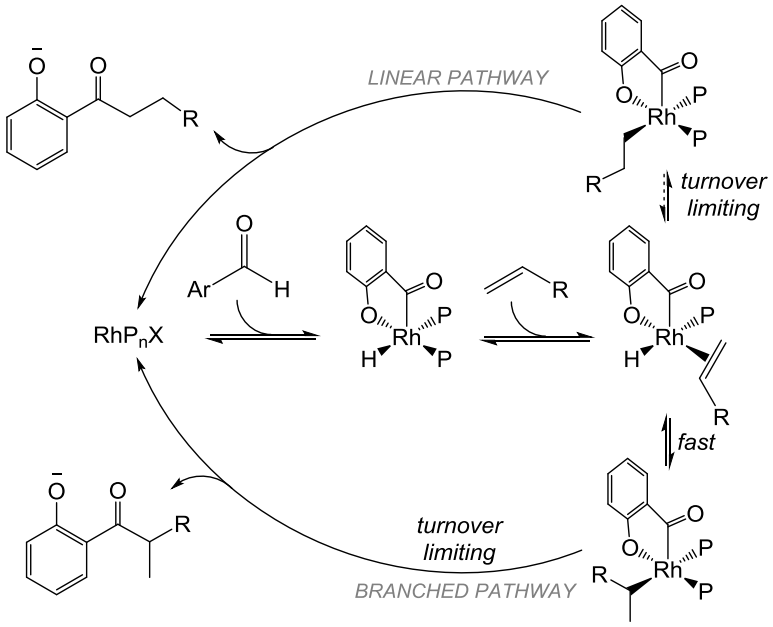

Scheme 1.42. Proposed catalytic mechanism for the hydroacylation reaction using salicylaldehyde and unactivated alkenes. X = leaving group, P = (R_a,R,R)-SIPHOS-PE.

Weller and Willis have also explored the tethered intermolecular hydroacylation reaction using β-sulfur tethered aldehydes first developed by Bendorf for intramolecular hydroacylation.[130] Initially these substrates were tested under Bosnich's developed conditions using [Rh(dpp2)][ClO_4] as the catalyst (Scheme 1.43).[108]

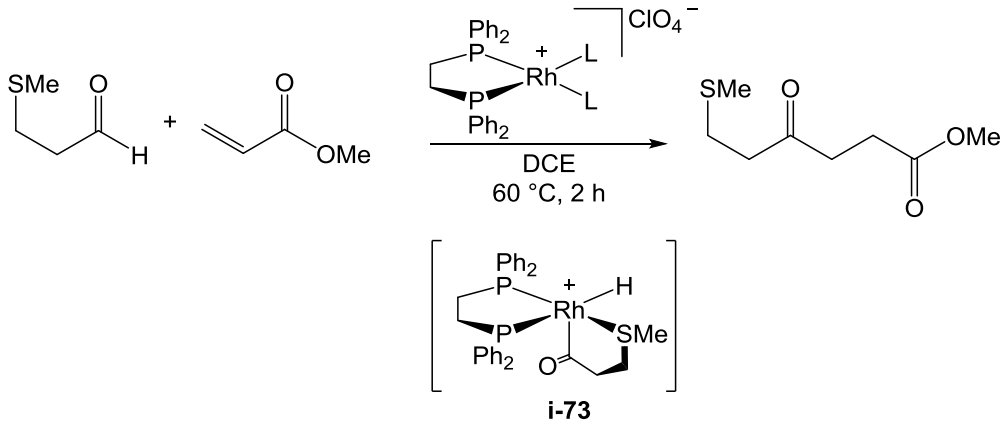

Scheme 1.43. Hydroacylation using β-S tethered aldehydes and Bosnich's catalyst. The reaction proceeds via the 5-coordinate acyl-hydride intermediate **i-73** which can readily decarbonylate. L = solvent molecule. In the intermediate. The $[BAr^F{}_4]^-$ counter-anion is not pictured for clarity.

The use of [Rh(dpp2)][ClO_4] as the catalyst allowed for the combination of a range of β-sulfur tethered aldehydes with functionalised alkenes under mild conditions, but still 10 mol% catalyst loadings were required and the catalyst rapidly decarbonylated under the reaction conditions.[131-133] This rapid deactivation was reported to be due to the 5-coordinate intermediate (**i-73**), which allows the catalyst to readily undergo reductive decarbonylation leading to the inactive metal-carbonyl species.[46] To test these results, Weller and Willis reasoned that the use of reversibly binding hemilabile ligands for the hydroacylation reaction would allow for a more stable 6-coordinate intermediate that does not readily reductively decarbonylate, while still allowing for olefin coordination. Based on a study involving a range of hemilabile ligands, it was concluded that the use of DPEphos as the hemilabile ligand on rhodium (**i-74**) allows for the best conversion under the conditions given in Scheme 1.44. Furthermore, the use of DPEphos allowed a wide range of functionalised and unfunctionalised olefins to be used as reagents.[46] The reaction mechanism was investigated by Weller and co-workers [13] Although the use of DPEphos as the ligand still only allowed reactions to be carried out at 10 mol% catalyst loading, the extra stability due to the hemilabile oxygen allowed for characterisation of the reaction intermediates during the catalytic cycle (Scheme 1.44). The substrates used for studying this reaction were 2-(methylthio)benzaldehyde and the electron deficient $HCCAr^F$ (Ar^F = 3,5-$(CF_3)_2C_6H_3$). Upon reacting the catalyst (**i-74**) with the aldehyde, the formation of the acyl-hydride intermediate (**i-75**) was observed. It was possible to fully

characterise **i-75** due to the significantly reduced rate of decarbonylation while using DPEphos ligand. Subsequent addition of the alkyne led to the formation of linear product via the linear pathway that allows for fast reductive elimination, but also the formation of the stable branched intermediate (**i-77**-bra) was seen, which was also isolated as a pure material. It was determined that the reductive elimination of the linear product was at least 3 orders of magnitude faster than that of the branched. This phenomenon has been shown to occur due to steric crowding in the branched intermediate slowing down the C–C reductive elimination as the rotation of the vinyl group to the required orientation is inhibited[134, 135] The isolation of **i-77**-bra allowed the authors to probe the rate of reductive elimination of the final product to further understand the regioselectivity of intermolecular alkyne hydroacylation to give the resulting linear or branched products.

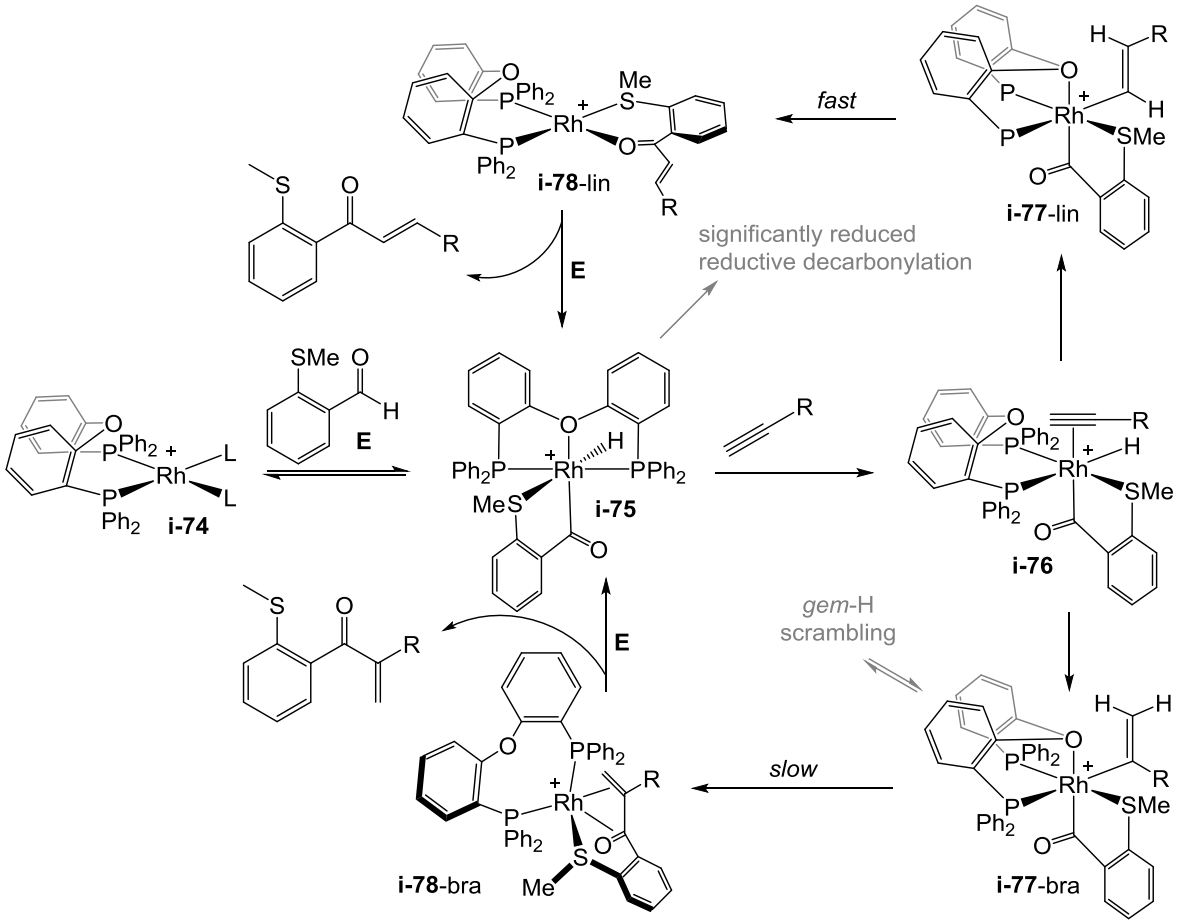

Scheme 1.44. Intermolecular hydroacylation using DPEphos ligand and β-S tethered aldehyde. The $[CB_{11}H_6Br_6]^-$ counter-anion is not pictured for clarity. R = 3,5-$(CF_3)_2C_6H_3$.

The extra coordination via oxygen in the DPEphos ligand significantly reduced the effect of decarbonylation (*i.e*. the formation of the inactive metal carbonyl complex), but also the use of DPEphos ligand led to 6-coordinate intermediate **i-77** before the rate limiting reductive elimination step, hence resulting in much slower catalysis. For the hydroacylation reaction to occur using this ligand, relatively high catalyst loadings were needed.[35]

More recently Weller and Willis have concentrated on development of catalysts that would increase the relative rate of the rate-limiting reductive elimination step. Based on studies carried out using a range of diphenylphosphino ligands on rhodium with different P-M-P bite angles (dpp2 – dpp5), it was found that the bite angle has a significant effect in hydroacylation catalysis. The general trend of preference for alkene hydroacylation was observed when small bite-angle ligands (dpp2 and dpp3) were used, whereas when large bite-angle ligands (dpp4 and dpp5) were used, undesired aldehyde hydroacylation was preferred (Scheme 1.45).[34, 136]

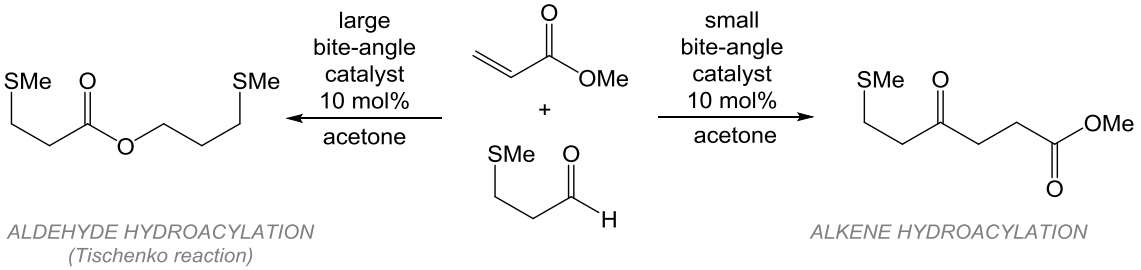

Scheme 1.45. Two competing reactions in different ratios were seen depending on the bite angle of the diphenylphosphino ligands used.

Based on this data, Weller and Willis moved on to investigate the catalytic activity of rhodium *bis*-phosphine complexes with even smaller bite angles.[41] The potential benefit of using small bite-angle complexes has also been reinforced by a number of research groups who have reported interesting changes in reactivity when these ligands were used, while inhibition of the reaction using small bite-angle systems have also been reported. An example of a negative effect caused by using a small bite-angle dpp1 ligand (**i-80**) in comparison to dpp2 (**i-81**) and dpp3 (**i-82**) (Figure 1.23) was reported by Iwamoto and Yuguchi[24] who were using iron-phosphine catalysts for co-dimerisation of 1,3-butadiene and ethylene. The bite angle effect was studied at relatively high temperatures and pressures (approximately 60 bar, 80 °C) and it was observed that the desired *cis*-1,4-hexadiene was the more preferred product for larger bite-angle

catalysts, whereas small bite-angle ligands led to poor conversions with the main product being polymeric or oligomeric material (Table 1.3).

Table 1.3. Hexadiene formation using different *bis*-phosphine ligands.[19]

ligand	bite angle / °	conversion of butadiene / %	selectivity for 1,4-hexadiene / %
dpp1	72	42.3	6
dpp2	85	78.2	81
dpp3	91	100	96

Conditions: chlorobenezene (20 mL), 0.5 – 1.0 mmol $FeCl_3$, 7.3 mmol of TEA, ethylene (60 bar), 1,3-butadiene (67 g), 80 – 85 °C.

A similar trend was seen by Drent using cationic palladium *bis*-phosphine complexes as catalysts for co-polymerisation of ethylene and CO.[137, 138] He noted that, while palladium complexes with dpp2 – dpp4 ligands (**i-80** – **i-83**) acted as highly efficient and selective catalysts (TOF up to 6000 h^{-1}), the use of dpp1 (**i-80**) was reported with TOF being 1 h^{-1} (Figure 1.23). Although the above examples are not highly relevant to the hydroacylation reaction, as the mechanism of co-polymerisation relies on different individual steps, it is still worth noting the degree of change in reactivity when these strained small bite-angle ligands are used in catalysis.

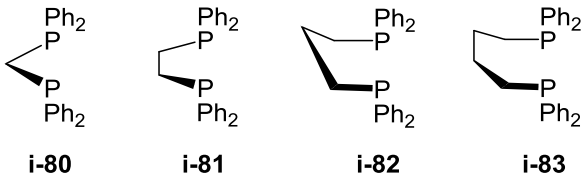

Figure 1.23. *Bis*-phosphine ligands dpp1 (**i-80**), dpp2 (**i-81**), dpp3 (**i-82**) and dpp4 (**i-83**).

More positive results using small bite-angle systems for polymerisation reactions, in particular for olefin oligomerisation reactions, have been show by Wass and co-workers In 2002, remarkable success in ethylene trimerisation was seen using small bite-angle *bis*-phosphine PNP ligand, (*o*-OMe-C_6H_4)$_2$PNMeP(*o*-OMe-C_6H_4)$_2$ (Figure 1.24) on chromium metal (Scheme 1.46).[139] Use of these catalysts allowed for excellent activity (more than a million grams of product for a gram of chromium per hour) in very high selectivities for 1-hexene (> 99.9 wt%) which is highly useful as a co-monomer for the polyolefin industry. Also, these catalysts were

shown to be extremely stable and robust; no deactivation occurred during the catalytic run. During this study a range of similar small bite-angle ligands (Y = CH_2 or NMe, Figure 1.24) were tested and compared with the larger bite-angle ligands (Y = CH_2CH_2). Furthermore, the small bite-angle ligands were systematically modified to further understand the effect of subtle changes in the ligand design upon the oligomerisation reaction (Figure 1.24).

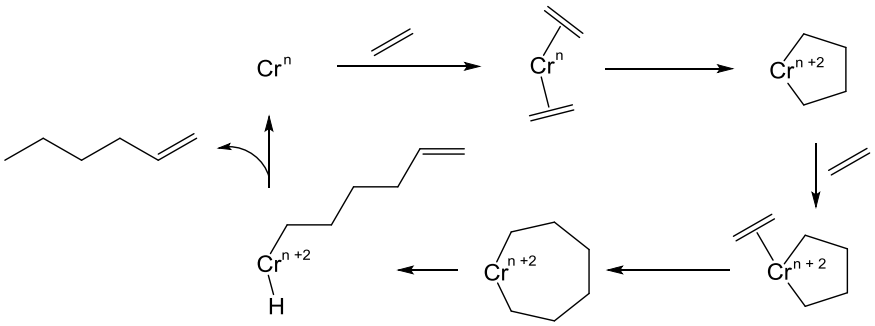

Scheme 1.46. Postulated mechanism of the ethylene trimerisation reaction.

The systematic modification of the backbone and the R-groups revealed that the best results were seen upon using the PNP motif containing ligands, plus the OMe at the R^1 position proved to be essential. The reasons for the *ortho*-OMe were investigated by replacing the OMe with an ethyl group. This resulted in no catalytic activity, indicating that this is not a simple steric effect provided by the OMe group. Similarly placing the OMe group in the *para*-position (*i.e.* R^3 = OMe) led to an inactive catalyst. It is postulated that the OMe groups behave as donors to the metal centre and increase the coordinative saturation. The Wass group continued to further investigate these types of ligands in a range of transformations, and additionally new motifs have also been developed, including ligands with a two nitrogen based backbone linker.[140]

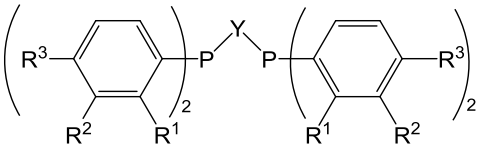

Figure 1.24. General structure of the ligand used by Wass for the ethylene trimerisation studies. Y = NMe, CH_2 or CH_2CH_2, R^1 – R^3 = H, Et, OMe or F. In case of Y = CH_2 or CH_2CH_2, R^2 and R^3 = H and R^1 = OMe.

The small bite-angle ligands have also been shown to promote reductive elimination – the postulated rate limiting step for the hydroacylation reaction using β-sulfur substituted

aldehydes.[38] Dubois has shown rhodium small bite-angle complexes to favour rhodium(I) over rhodium(III) thus promoting the reductive elimination step.[141] Dubois carried out a range of oxidative addition reactions of H_2 using rhodium *bis*-phosphine complexes with different electronic properties and bite angles (Figure 1.25). The authors comment that full understanding of the ligand effect can be limited, and lead to contradictory results, but in general from these studies a trend can be seen. The use of dpp2 led to no oxidative addition even at increased pressures (2-3 atm of H_2) while dmpe, depe and depx showed some oxidative addition and an equilibrium between the rhodium(I) and rhodium(III) species was observed (Figure 1.25). The affinity for the oxidative addition in the case of the alkyl-substituted phosphine ligands is expected due to their relatively high electron-richness. In comparison, the larger bite-angle ligand depp readily allowed for complete irreversible reaction to form the dihydride rhodium(III) species. This result indicates that there is an increased driving force to form the dihydride rhodium(III) species upon increasing the bite angle.

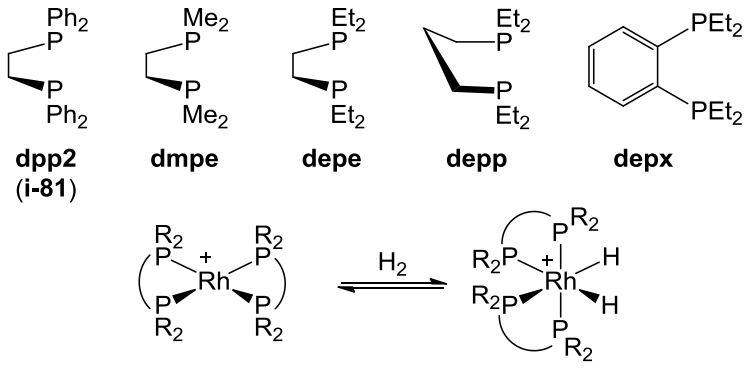

Figure 1.25. Range of different *bis*-phosphine ligands screened by Dubois on rhodium, resulting in the complexes of [Rh(*bis*-phosphine)$_2$][CF_3SO_3].

This preference for oxidative addition has been explained by the lowering of the energy of the lowest unoccupied molecular orbital (LUMO) of a d^8 square planar metal complex as the bite angle increases.[142]

As reductive elimination is a microscopic reverse reaction of oxidative addition, the small bite-angle complexes are expected to aid the reductive elimination step. This was experimentally shown by Fink, who showed the correlation between the small bite-angle and preferred reductive elimination using palladium *bis*-phosphine complexes (Scheme 1.20, b).[83] The use of

small bite-angle ligands has also been enforced by Werner, who found that $[Rh(PR_2CH_2PR_2)]^+$ complexes promote reductive elimination due to the ring strain imposed by the four-membered chelate ring.[143]

Encouraged by the results presented using small bite-angle ligands, Willis and Weller investigated the hydroacylation reaction using ligands developed by Hofmann, with general structure of $R_2P(CH_2)PR'_2$, (where R, R' = ^{t}Bu and/or Cy).[144-146] Hofmann has carried out a range of mechanistic studies using these ligands, and he argues that the usefulness of these small bite-angle complexes arises due to the strain set on the metal centre, resulting in the change in reactivity.[147] Hofmann has also reported these small bite-angle ligand containing catalysts to be useful for a range of catalytic transformations.[145, 148] These transformations include ethylene polymerisation, olefin metathesis and hydrosilylation.[149] Due to the similarity to hydroacylation, the hydrosilylation reaction is of the greatest interest with respect to the topic of this thesis. Hofmann has shown that for the hydrosilylation of but-2-yne with $HSi(OEt_3)$ to form triethoxysilyl-but-2-ene, catalyst loadings as low as 0.1 mol% can be used in the case of small bite-angle ligand containing catalysts (25 °C, 30 min). More specifically, for this transformation, the most efficient catalyst was found to be $[Rh(P^tBu_2CH_2P^tBu_2)(PMe_3)(CH_3)]$. The mechanism proposed is depicted in Scheme 1.47.

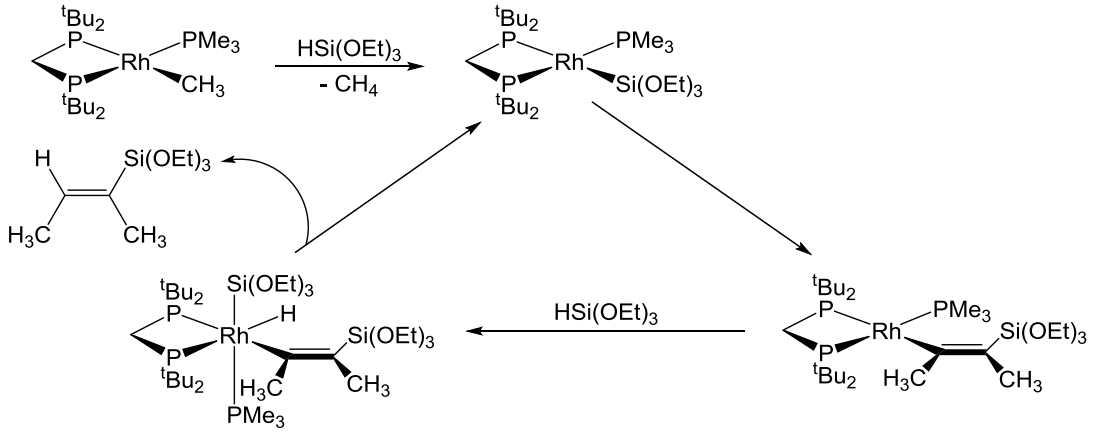

Scheme 1.47. Hydrosilylation reaction mechanism using small bite-angle rhodium *bis*-phosphine catalyst proposed by Hofmann.

The catalyst initially forms the silyl complex by oxidative addition of $HSi(OEt_3)$ followed by an elimination of methane. This is proposed to be followed by an insertion of but-2-ene into the

Rh–Si bond resulting in the vinyl intermediate. This vinyl intermediate can then undergo another oxidative addition of the silane molecule yielding the Rh(III) intermediate which allows for the formation of the desired product via reductive elimination.

Based on these results Weller and Willis postulated that the use of these electron-rich small bite-angle ligands would allow for improved reductive elimination and hence relative reduction of the destructive effect caused by the side reaction, reductive decarbonylation. Therefore, a range of bench stable precatalysts with the general structure of $[Rh(PR_2CH_2PR_2)(C_6H_5F)][BAr^F_4]$ were synthesised, analytically characterised and used in catalytic hydroacylation reactions, allowing a range of alkenes and aldehydes to be used as substrates. Although the reductive decarbonylation process was still observed, impressive conversions into the desired ketone product were seen. Using 2-(methylthio)benzaldehyde as the aldehyde and 1-octene, catalyst loadings as low as 0.1 mol% were established (*cf*. 10 mol% using cationic rhodium dpp2 (**i-81**) complexes as catalysts). The mechanism, using the small bite-angle cationic rhodium *bis*-phosphine complexes, was studied by NMR spectroscopy, ESI-MS, labelling and kinetic studies. The proposed mechanism is depicted in Scheme 1.48, and is discussed further in Chapter 2.

The mechanistic studies revealed that all the steps other than reductive elimination are reversible, including the migratory insertion step that leads to the intermediate which would allow for the formation of the branched product. This intermediate is proposed based on deuterium incorporation to the α-carbonyl when deuterated aldehyde was used as the starting material. Interestingly, no branched product was seen at the end of the reaction. This is suggested to be due to the considerably higher barrier for reductive elimination from the branched intermediate (as was previously observed to be the case upon using DPEphos ligand).

The use of these highly effective and selective catalysts was improved further by recent research by the same groups, where the same rhodium complexes with small bite-angle motif can be used to cleave the C-S bond at the end of the hydroacylation reaction, allowing for much more general reactivity.[150, 151] The C-S activation is discussed more thoroughly in Chapter 4.

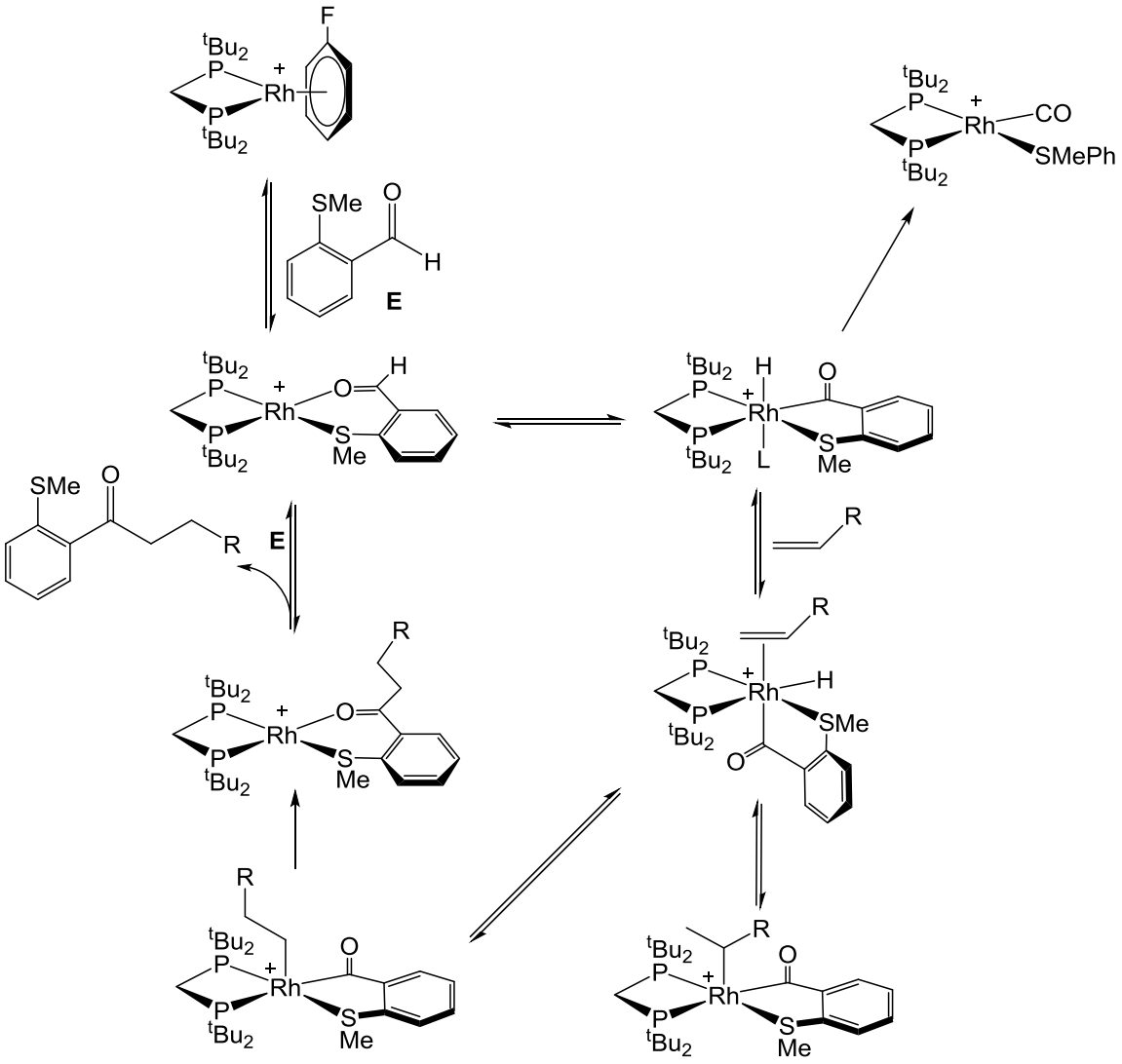

Scheme 1.48. The mechanism of the alkene hydroacylation reaction using the small bite-angle cationic rhodium *bis*-phosphine complex. The $[BAr^F_4]^-$ counter-anion is not pictured for clarity. L – coordinating solvent.

The usefulness of small bite-angle ligands was recently also realised by Dong,[152] who reported a method for high branched product selectivity (> 20:1 branched:linear ratio) and high reactivity using neutral [Rh(dcpm)(X)] complexes as hydroacylation catalysts. Using this neutral catalyst under the conditions in Scheme 1.49, they were able to carry out the hydroacylation reaction using non-tethered aldehydes and vinyl-phenols as starting materials, where the phenol group acts as an anionic directing group reducing the effect of decarbonylation by forming a coordinatively saturated acyl-metal-hydride intermediate (**i-84**) (Scheme 1.49). Although the

need for the vinyl-phenol limits the scope of this reaction, they were able to use a wide range of aldehydes, including aryl, alkenyl and alkyl aldehydes.

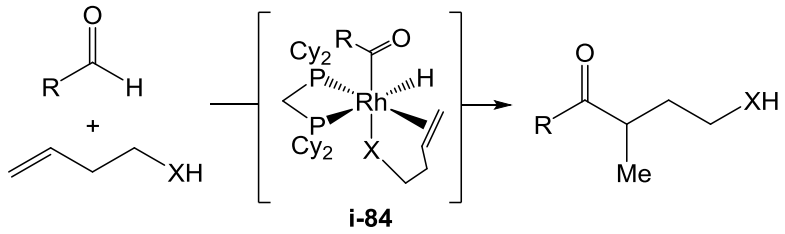

Scheme 1.49. Proposed intermediate for hydroacylation reaction using alkenes with an anionic directing group. *Conditions: [Rh(OMe)Cl]$_2$ (2 mol%), dcpm (4 mol%), THF, 1 M.* X = phenol.

The work has been continued by replacing the current anionic directing group for other directing groups (anilines, sulfonamides, hydroxyl groups and carboxylic acids) to expand the scope of this reaction, also mechanistic studies are currently being performed.

1.6. Summary

Over the period from the 1970's until the present, there have been substantial advances in hydroacylation catalysis. Over these years, the low yielding stoichiometric reactions that led to not just the desired hydroacylation product, but also to a range of side-products (often as major products), have been replaced with high yielding and highly selective reactions, where low catalyst loadings can be applied. Furthermore, in some cases, catalysts that are recyclable have been developed. This progress has relied on a range of different approaches, including trial and error and screening reactions, but has developed hand-in-hand with fundamental investigations, also including information gathered from other catalytic transformations that shed light on hydroacylation. Based on these studies individual steps of the hydroacylation reaction have been probed by a number of research groups, allowing for further understanding of the mechanism. Although the mechanisms of hydroacylation and the reductive decarbonylation are now well understood, this catalyst deactivating pathway (reductive decarbonylation) has remained the Achilles' heel for the hydroacylation reaction. At least, this is the case for producing a catalyst system capable of catalysing any aldehyde and alkene/alkyne. Hence, more than 40 years later, hydroacylation reaction is still actively studied.

Based on the work carried out by a range of research groups an approach to carry out productive intermolecular hydroacylation catalysis was devised. The most successful results have been obtained using tethered reagents and the work is continued using β-sulfur tethered aldehydes developed by Willis. These substrates can be combined with the small bite-angle research recently published by the Weller group to investigate the effect the bite angle resulting from a *bis*-phosphine ligand, and how other changes in the ligand design can affect hydroacylation catalysis. As discussed above, hemilability is also a key mediator in order to improve the hydroacylation reaction. Hence, the advances seen using DPEphos ligand can be combined with the Wass's work with PNP ligands to develop new catalysts for hydroacylation reaction that allow for fast reactivity, while still providing stability against reductive decarbonylation. Also, in order to expand the scope, the removal of the tether on the substrate is discussed.

1.7. References

1. H. Schulz, *Appl. Catal., A*, 1999, **186**, 3-12.
2. J. D. Atwood, *Inorganic and Organometallic Reaction Mechanisms, Wiley-VCH, 2nd Edition*, 1997.
3. R. H. Crabtree, *The Organometallic Chemistry of the Transition Metals, John Wiley and Sons, 5th Edition*, 2011.
4. C. A. Tolman, *Chem. Soc. Rev.*, 1972, **1**, 337-353.
5. K. Barbalace, Periodic Table of Elements. www.environmentalchemistry.com.
6. www.kitco.com.
7. www.pmrrefiner.com.
8. J. F. Roth, *Platinum Met. Rev.*, 1975, **19**, 12-14.
9. D. Evans, J. A. Osborn and G. Wilkinson, *J. Chem. Soc. A*, 1968, **33**, 3133-3142.
10. S. B. Halligudi, H. C. Bajaj, K. N. Bhatt and M. Krishnaratnam, *React Kinet Catal Lett*, 1992, **48**, 547-552.
11. E. E. N.N. Greenwood, *Elsevier*, 1997.
12. C. A. Tolman, *Chem. Rev.*, 1977, **77**, 313-348.
13. R. J. Pawley, M. A. Huertos, G. C. Lloyd-Jones, A. S. Weller and M. C. Willis, *Organometallics*, 2012, **31**, 5650-5659.
14. R. Barrios-Francisco, E. Balaraman, Y. Diskin-Posner, G. Leitus, L. J. W. Shimon and D. Milstein, *Organometallics*, 2013, **32**, 2973-2982.
15. S. Moret, R. Dallanegra, A. B. Chaplin, T. M. Douglas, R. M. Hiney and A. S. Weller, *Inorg. Chim. Acta*, 2010, **363**, 574-580.
16. A. B. Chaplin, A. I. Poblador-Bahamonde, H. A. Sparkes, J. A. K. Howard, S. A. Macgregor and A. S. Weller, *Chem. Commun.*, 2009, 244-246.
17. J. M. Winter, *d-Block Chemistry, Oxford Univeristy Primers 27*, 1994.
18. C. A. Tolman, W. C. Seidel and L. W. Gosser, *J. Am. Chem. Soc.*, 1974, **96**, 53-60.
19. P. W. N. M. van Leeuwen, P. C. J. Kamer, J. N. H. Reek and P. Dierkes, *Chem. Rev.*, 2000, **100**, 2741-2770.
20. C. O'Connor and G. Wilkinson, *Tetrahedron Lett.*, 1969, **10**, 1375-1377.
21. S. Otsuka, T. Yoshida, M. Matsumoto and K. Nakatsu, *J. Am. Chem. Soc.*, 1976, **98**, 5850-5858.
22. R. D. Cramer, E. L. Jenner, R. V. Lindsey and U. G. Stolberg, *J. Am. Chem. Soc.*, 1963, **85**, 1691-1692.
23. J. F. Young, J. A. Osborn, F. H. Jardine and G. Wilkinson, *Chem. Commun.*, 1965, 131-132.
24. M. Iwamoto and S. Yuguchi, *J. Org. Chem.*, 1966, **31**, 4290-4291.
25. R. S. Coffey, *Chem. Comm.* 1967, 923a-923a.
26. J. A. Osborn and R. R. Schrock, *J. Am. Chem. Soc.*, 1971, **93**, 3089-3091.
27. D. White, B. C. Taverner, N. J. Coville and P. W. Wade, *J. Organomet. Chem.*, 1995, **495**, 41-51.
28. Y. Koide, S. G. Bott and A. R. Barron, *Organometallics*, 1996, **15**, 2213-2226.
29. C. P. Casey and G. T. Whiteker, *Isr. J. Chem.*, 1990, **30**, 299-304.
30. P. D. Achord, P. Kiprof and B. Barker, *J. Mol. Struct. THEOCHEM*, 2008, **849**, 103-111.
31. P. Braunstein and F. Naud, *Angew. Chem. Int. Ed.*, 2001, **40**, 680-699.
32. A. Bader and E. Lindner, *Coord. Chem. Rev.*, 1991, **108**, 27-110.
33. J. C. Jeffrey and T. B. Rauchfuss, *Inorg. Chem.*, 1979, **18**, 2658-2666.
34. R. J. Pawley, G. L. Moxham, R. Dallanegra, A. B. Chaplin, S. K. Brayshaw, A. S. Weller and M. C. Willis, *Organometallics*, 2010, **29**, 1717-1728.
35. G. L. Moxham, H. Randell-Sly, S. K. Brayshaw, A. S. Weller and M. C. Willis, *Chem. Eur. J.*, 2008, **14**, 8383-8397.
36. R. Dallanegra, A. B. Chaplin and A. S. Weller, *Organometallics*, 2012, **31**, 2720-2728.

37. S. K. Murphy and V. M. Dong, *J. Am. Chem. Soc.*, 2013, **135**, 5553-5556.
38. M. C. Willis, *Chem. Rev.*, 2010, **110**, 725-748.
39. J. Hartwig, *Organotransition Metral Chemistry From Bonding to Catalysis*, University Science Books, 2010.
40. www.sigma-aldrich.com.
41. A. B. Chaplin, J. F. Hooper, A. S. Weller and M. C. Willis, *J. Am. Chem. Soc.*, 2012, **134**, 4885-4897.
42. N. G. Jonathan Clayden, and Stuart Warren, *Organic Chemistry, OUP Oxford*, 2001.
43. Q.-A. Chen, D. K. Kim and V. M. Dong, *J. Am. Chem. Soc.*, 2014, **136**, 3772-3775.
44. C. P. Lenges, P. S. White and M. Brookhart, *J. Am. Chem. Soc.*, 1998, **120**, 6965-6979.
45. F. Shibahara, J. F. Bower and M. J. Krische, *J. Am. Chem. Soc.*, 2008, **130**, 14120-14122.
46. G. L. Moxham, H. E. Randell-Sly, S. K. Brayshaw, R. L. Woodward, A. S. Weller and M. C. Willis, *Angew. Chem. Int. Ed.*, 2006, **45**, 7618-7622.
47. M. M. Coulter, K. G. M. Kou, B. Galligan and V. M. Dong, *J. Am. Chem. Soc.*, 2010, **132**, 16330-16333.
48. E. Clot and O. Eisenstein, *J. Phys. Chem. A*, 1998, **102**, 3592-3598.
49. G. J. Kubas, R. R. Ryan, B. I. Swanson, P. J. Vergamini and H. J. Wasserman, *J. Am. Chem. Soc.*, 1984, **106**, 451-452.
50. S. Niu and M. B. Hall, *Chem. Rev.*, 2000, **100**, 353-406.
51. R. H. Crabtree, *Chem. Rev.*, 1985, **85**, 245-269.
52. R. H. Crabtree, *Chem. Rev.*, 1995, **95**, 987-1007.
53. D. Alberico, M. E. Scott and M. Lautens, *Chem. Rev.*, 2007, **107**, 174-238.
54. J. E. B. Jay A. Labinger, *Nature*, 2002, **417**, 507-514.
55. M. Matsushita, K. Kamata, K. Yamaguchi and N. Mizuno, *J. Am. Chem. Soc.*, 2005, **127**, 6632-6640.
56. A. D. Ryabov, *Chem. Rev.*, 1990, **90**, 403-424.
57. O. Schuster, L. Yang, H. G. Raubenheimer and M. Albrecht, *Chem. Rev.*, 2009, **109**, 3445-3478.
58. J. P. Kleiman and M. Dubeck, *J. Am. Chem. Soc.*, 1963, **85**, 1544-1545.
59. S. Horiie and S. Murahashi, *Bull. Chem. Soc. Jpn.*, 1960, **33**, 247-251.
60. J. Chatt and J. M. Davidson, *J. Am. Chem. Soc.*, 1965, 843-855.
61. A. H. Janowicz and R. G. Bergman, *J. Am. Chem. Soc.*, 1982, **104**, 352-354.
62. J. K. Hoyano and W. A. G. Graham, *J. Am. Chem. Soc.*, 1982, **104**, 3723-3725.
63. M. Brookhart and M. L. H. Green, *J. Organomet. Chem.*, 1983, **250**, 395-408.
64. N. A. Bailey, J. M. Jenkins, R. Mason and B. L. Shaw, *Chem. Commun.* 1965, 237-238.
65. Y. W. Yared, S. L. Miles, R. Bau and C. A. Reed, *J. Am. Chem. Soc.*, 1977, **99**, 7076-7078.
66. S. J. La Placa and J. A. Ibers, *Inorg. Chem.*, 1965, **4**, 778-783.
67. D. M. Roe, P. M. Bailey, K. Moseley and P. M. Maitlis, *J. Chem. Soc., Chem. Commun.*, 1972, 1273-1274.
68. M. Brookhart, M. L. H. Green and G. Parkin., *PNAS*, 2007, **104.17**, 6908-6914.
69. P. M. Morse, M. D. Spencer, S. R. Wilson and G. S. Girolami, *Organometallics*, 1994, **13**, 1646-1655.
70. www2.ups.edu/faculty/hanson/Spectroscopy/IR/IRfrequencies.html.
71. S. D. Pike, A. L. Thompson, A. G. Algarra, D. C. Apperley, S. A. Macgregor and A. S. Weller, *Science*, 2012, **337**, 1648-1651.
72. D. R. Evans, T. Drovetskaya, R. Bau, C. A. Reed and P. D. W. Boyd, *J. Am. Chem. Soc.*, 1997, **119**, 3633-3634.
73. I. Castro-Rodriguez, H. Nakai, P. Gantzel, L. N. Zakharov, A. L. Rheingold and K. Meyer, *J. Am. Chem. Soc.*, 2003, **125**, 15734-15735.
74. S. Geftakis and G. E. Ball, *J. Am. Chem. Soc.*, 1998, **120**, 9953-9954.
75. D. J. Lawes, S. Geftakis and G. E. Ball, *J. Am. Chem. Soc.*, 2005, **127**, 4134-4135.

76. W. H. Bernskoetter, C. K. Schauer, K. I. Goldberg and M. Brookhart, *Science*, 2009, **326**, 553-556.
77. B. K. Corkey, F. L. Taw, R. G. Bergman and M. Brookhart, *Polyhedron*, 2004, **23**, 2943-2954.
78. J. Chatt and L. A. Duncanson, *J. Am. Chem. Soc.*, 1953, 2939-2947.
79. K. Miki, Y. Kai, N. Kasai and H. Kurosawa, *J. Am. Chem. Soc.*, 1983, **105**, 2482-2483.
80. D. Milstein and J. K. Stille, *J. Am. Chem. Soc.*, 1979, **101**, 4981-4991.
81. W. D. Jones and V. L. Kuykendall, *Inorg. Chem.*, 1991, **30**, 2615-2622.
82. J. M. Brown and P. J. Guiry, *Inorg. Chim. Acta*, 1994, **220**, 249-259.
83. S. M. Reid, J. T. Mague and M. J. Fink, *J. Am. Chem. Soc.*, 2001, **123**, 4081-4082.
84. A. Gillie and J. K. Stille, *J. Am. Chem. Soc.*, 1980, **102**, 4933-4941.
85. K. Tatsumi, R. Hoffmann, A. Yamamoto and J. K. Stille, *Bull. Chem. Soc. Jpn.*, 1981, **54**, 1857-1867.
86. D. Milstein, *Acc. Chem. Res.*, 1984, **17**, 221-226.
87. A. T. Luedtke and K. I. Goldberg, *Inorg. Chem.*, 2007, **46**, 8496-8498.
88. G. S. Hill and R. J. Puddephatt, *Organometallics*, 1998, **17**, 1478-1486.
89. U. Fekl and K. I. Goldberg, *J. Am. Chem. Soc.*, 2002, **124**, 6804-6805.
90. J. Procelewska, A. Zahl, G. Liehr, R. van Eldik, N. A. Smythe, B. S. Williams and K. I. Goldberg, *Inorg. Chem.*, 2005, **44**, 7732-7742.
91. N. Koga, S. Obara, K. Kitaura and K. Morokuma, *J. Am. Chem. Soc.*, 1985, **107**, 7109-7116.
92. T. M. Miller and G. M. Whitesides, *Organometallics*, 1986, **5**, 1473-1480.
93. D. L. Thorn and R. Hoffmann, *J. Am. Chem. Soc.*, 1978, **100**, 2079-2090.
94. H. Kurosawa, T. Majima and N. Asada, *J. Am. Chem. Soc.*, 1980, **102**, 6996-7003.
95. M. A. Garralda, *Dalton Trans.*, 2009, 3635-3645.
96. A. Modak, A. Deb, T. Patra, S. Rana, S. Maity and D. Maiti, *Chem. Commun.*, 2012, **48**, 4253-4255.
97. K. Sen and J. C. Hackett, *J. Am. Chem. Soc.*, 2010, **132**, 10293-10305.
98. T. Morimoto, K. Fuji, K. Tsutsumi and K. Kakiuchi, *J. Am. Chem. Soc.*, 2002, **124**, 3806-3807.
99. A. Schirmer, M. A. Rude, X. Li, E. Popova and S. B. del Cardayre, *Science*, 2010, **329**, 559-562.
100. N. Li, H. Nørgaard, D. M. Warui, S. J. Booker, C. Krebs and J. M. Bollinger, *J. Am. Chem. Soc.*, 2011, **133**, 6158-6161.
101. K. Sakai, J. Ide, O. Oda and N. Nakamura, *Tetrahedron Lett.*, 1972, **13**, 1287-1290.
102. D. Milstein, *J. Am. Chem. Soc.*, 1982, **104**, 5227-5228.
103. J. W. Suggs, *J. Am. Chem. Soc.*, 1978, **100**, 640-641.
104. R. E. Campbell Jr and R. G. Miller, *J. Organomet. Chem.*, 1980, **186**, C27-C31.
105. R. E. Campbell, C. F. Lochow, K. P. Vora and R. G. Miller, *J. Am. Chem. Soc.*, 1980, **102**, 5824-5830.
106. D. Milstein, *J. Chem. Soc., Chem. Commun.*, 1982, 1357-1358.
107. M. G. Vinogradov, A. B. Tuzikov, G. I. Nikishin, B. N. Shelimov and V. B. Kazansky, *J. Organomet. Chem.*, 1988, **348**, 123-134.
108. D. P. Fairlie and B. Bosnich, *Organometallics*, 1988, **7**, 936-945.
109. D. P. Fairlie and B. Bosnich, *Organometallics*, 1988, **7**, 946-954.
110. T. A. Betley and J. C. Peters, *Angew. Chem. Int. Ed.*, 2003, **42**, 2385-2389.
111. R. R. Schrock and J. A. Osborn, *Inorg. Chem.*, 1970, **9**, 2339-2343.
112. K. P. Vora, C. F. Lochow and R. G. Miller, *J. Organomet. Chem.*, 1980, **192**, 257-264.
113. T. B. Marder, D. C. Roe and D. Milstein, *Organometallics*, 1988, **7**, 1451-1453.
114. C. P. Lenges and M. Brookhart, *J. Am. Chem. Soc.*, 1997, **119**, 3165-3166.
115. J. W. Suggs, M. J. Wovkulich and S. D. Cox, *Organometallics*, 1985, **4**, 1101-1107.
116. J. Chul-Ho, H. Jong-Soo, K. Jung-Bu and K. Sun-Il, *J. Organomet. Chem.*, 1994, **474**, 183-189.
117. J. Chul-Ho, K. Jung-Bu and K. Jin-Yong, *J. Organomet. Chem.*, 1993, **458**, 193-198.
118. C.-H. Jun, H. Lee and J.-B. Hong, *J. Org. Chem.*, 1997, **62**, 1200-1201.
119. C. H. Jun, D. Y. Lee, H. Lee and J. B. Hong, *Angew. Chem. Int. Ed.*, 2000, **39**, 3070-3072.

120. K.-M. Cha, H. Lee, J.-W. Park, Y. Lee, E.-A. Jo and C.-H. Jun, *Chem. Asian J.*, 2011, **6**, 1926-1930.
121. D.-Y. Lee, C. W. Moon and C.-H. Jun, *J. Org. Chem.*, 2002, **67**, 3945-3948.
122. C.-H. Jun, C.-W. Huh and S.-J. Na, *Angew. Chem. Int. Ed.*, 1998, **37**, 145-147.
123. E.-A. Jo, J.-H. Lee and C.-H. Jun, *Chem. Commun.*, 2008, 5779-5781.
124. D.-H. Chang, D.-Y. Lee, B.-S. Hong, J.-H. Choi and C.-H. Jun, *J. Am. Chem. Soc.*, 2003, **126**, 424-425.
125. M. Tanaka, M. Imai, Y. Yamamoto, K. Tanaka, M. Shimowatari, S. Nagumo, N. Kawahara and H. Suemune, *Organic Letters*, 2003, **5**, 1365-1367.
126. M. Imai, M. Tanaka, K. Tanaka, Y. Yamamoto, N. Imai-Ogata, M. Shimowatari, S. Nagumo, N. Kawahara and H. Suemune, *J. Org. Chem.*, 2004, **69**, 1144-1150.
127. K. Kokubo, K. Matsumasa, M. Miura and M. Nomura, *J. Org. Chem.*, 1997, **62**, 4564-4565.
128. M. von Delius, C. M. Le and V. M. Dong, *J. Am. Chem. Soc.*, 2012, **134**, 15022-15032.
129. C. P. Casey and L. M. Petrovich, *J. Am. Chem. Soc.*, 1995, **117**, 6007-6014.
130. H. D. Bendorf, C. M. Colella, E. C. Dixon, M. Marchetti, A. N. Matukonis, J. D. Musselman and T. A. Tiley, *Tetrahedron Lett.*, 2002, **43**, 7031-7034.
131. M. C. Willis, S. J. McNally and P. J. Beswick, *Angew. Chem. Int. Ed.*, 2004, **43**, 340-343.
132. M. C. Willis, H. E. Randell-Sly, R. L. Woodward, S. J. McNally and G. S. Currie, *J. Org. Chem.*, 2006, **71**, 5291-5297.
133. M. C. Willis, H. E. Randell-Sly, R. L. Woodward and G. S. Currie, *Org. Lett.*, 2005, **7**, 2249-2251.
134. A. H. Roy, C. P. Lenges and M. Brookhart, *J. Am. Chem. Soc.*, 2007, **129**, 2082-2093.
135. R. Ghosh, T. J. Emge, K. Krogh-Jespersen and A. S. Goldman, *J. Am. Chem. Soc.*, 2008, **130**, 11317-11327.
136. S. D. Pike, R. J. Pawley, A. B. Chaplin, A. L. Thompson, J. A. Hooper, M. C. Willis and A. S. Weller, *Eur. J. Inorg. Chem.*, 2011, 5558-5565.
137. E. Drent, J. A. M. Van Broekhoven and M. J. Doyle, *J. Organomet. Chem.*, 1991, **417**, 235-251.
138. E. Drent and P. H. M. Budzelaar, *Chem. Rev.*, 1996, **96**, 663-682.
139. A. Carter, S. A. Cohen, N. A. Cooley, A. Murphy, J. Scutt and D. F. Wass, *Chem. Commun.*, 2002, 858-859.
140. L. E. Bowen, M. Charernsuk, T. W. Hey, C. L. McMullin, A. G. Orpen and D. F. Wass, *Dalton Trans.*, 2010, **39**, 560-567.
141. D. L. DuBois, D. M. Blake, A. Miedaner, C. J. Curtis, M. R. DuBois, J. A. Franz and J. C. Linehan, *Organometallics*, 2006, **25**, 4414-4419.
142. A. Miedaner, R. C. Haltiwanger and D. L. DuBois, *Inorg. Chem.*, 1991, **30**, 417-427.
143. M. Manger, J. Wolf, M. Teichert, D. Stalke and H. Werner, *Organometallics*, 1998, **17**, 3210-3221.
144. P. Hofmann, C. Meier, U. Englert and M. U. Schmidt, *Chem. Ber.*, 1992, **125**, 353-365.
145. P. Hofmann, C. Meier, W. Hiller, M. Heckel, J. Riede and M. U. Schmidt, *J. Organomet. Chem.*, 1995, **490**, 51-70.
146. F. Eisentrager, A. Gothlich, I. Gruber, H. Heiss, C. A. Kiener, C. Kruger, J. U. Notheis, F. Rominger, G. Scherhag, M. Schultz, B. F. Straub, M. A. O. Volland and P. Hofmann, *New J. Chem.*, 2003, **27**, 540-550.
147. P. Hofmann, H. Heiß and G. Müller, *Z. Naturforsch.*, 1987, **42**, 395-409.
148. M. Schultz, F. Eisenträger, C. Regius, F. Rominger, P. Hanno-Igels, P. Jakob, I. Gruber and P. Hofmann, *Organometallics*, 2011, **31**, 207-224.
149. P. Hofmann, M. A. O. Volland, S. M. Hansen, F. Eisenträger, J. H. Gross and K. Stengel, *J. Organomet. Chem.*, 2000, **606**, 88-92.
150. J. F. Hooper, R. D. Young, I. Pernik, A. S. Weller and M. C. Willis, *Chemical Science*, 2013, **4**, 1568-1572.
151. J. F. Hooper, R. D. Young, A. S. Weller and M. C. Willis, *Chem. Eur. J.,* 2013, **19**, 3125-3130.
152. S. K. Murphy, A. Bruch and V. M. Dong, *Angew. Chem. Int. Ed.*, 2014, **53**, 2455-2459.

2. SMALL BITE-ANGLE COMPLEXES

2.1. Introduction

Previous research within the Weller group has reported on a range of *bis*-diphenylphosphino ligands (**i-80** – **i-83**) and their use in the intermolecular hydroacylation reaction.[1] To understand the effect of the bite angle on intermolecular hydroacylation catalysis, rhodium complexes with the general motif of $[Rh(Ph_2PCH_2(CH_2)_nPPh_2)(acetone)_2][BAr^F_4]$ (where n = 1 – 4) were synthesised and tested as catalysts in the hydroacylation reaction of $MeSCH_2CH_2COH$ (**A**) with methyl acrylate (**B**) (Scheme 2.1).

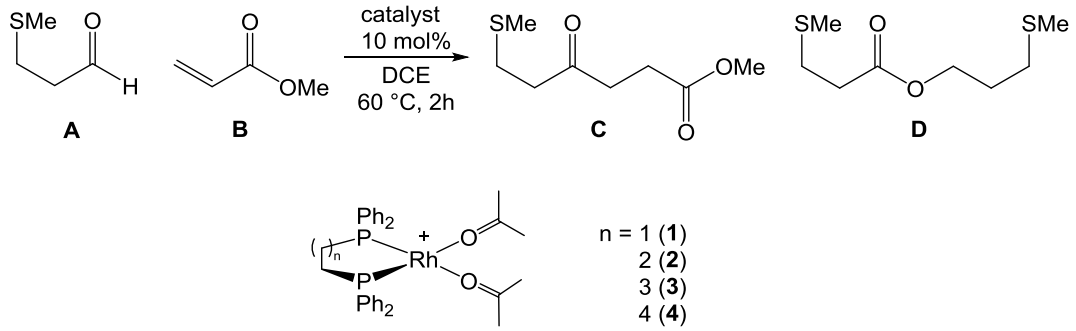

Scheme 2.1. The hydroacylation reaction between $MeSCH_2CH_2COH$ (**A**) and methyl acrylate (**B**) using $[Rh(Ph_2PCH_2(CH_2)_nPPh_2)(acetone)_2][BAr^F_4]$ (where n = 1 – 4) as the catalyst (**1** – **4**). The $[BAr^F_4]^-$ counter-anion is not pictured for clarity. DCE = 1,2-dichloroethane.

The change in the backbone length showed substantial change in the reactivity of these catalysts (**1** – **4**). The data collected indicated that the phosphine ligands with longer backbones led to faster rate of catalysis {full conversion in 60 h (**1**) *vs.* 6 h (**4**)}; but also the use of larger bite-

angle ligands resulted in aldehyde hydroacylation (Tishcenko reaction, formation of **D**) over the desired alkene hydroacylation (**C**), whereas the small bite-angle complex **1** resulted in alkene hydroacylation. This change from alkene hydroacylation to the Tishcenko reaction was gradual over the increase in backbone length, indicating that a change in the P-Rh-P bite-angle has an incremental effect on the hydroacylation reaction. It was argued that this is probably a steric effect as the higher number of atoms in the backbone brings the substituents on the phosphorus atoms closer to the coordination sphere of the metal and this determined the relative rates of hydride insertion and/or reductive elimination. The catalytic data has been summarised in Table 2.1.

Table 2.1. Comparison of the catalytic activity of a range of rhodium *bis*-diphenylphosphino complexes with different bite angles in the hydroacylation reaction of **A** and **B**.

Catalyst	Bite angle[2] / °	Total Conversion of **A** / %	Alkene hydroacylation **C** / %	Aldehyde hydroacylation **D** / %	Time / h
1	83.7	99	91	8	60
2	90.7	100	38	62	40
3	97.1	100	50	50	8
4	98.9	100	13	87	6

Conversions determined by ^{1}H NMR spectroscopy.

When the hydroacylation reaction was conducted using **B** and the aromatic aldehyde, 2-(methylthio)benzaldehyde (**E**) instead of **A**, similar trends were seen. The use of the aromatic substrate **E** allows the reaction to be followed by HPLC. Additionally, the use of aromatic substrate led to smaller amounts of aldehyde hydroacylation (1 – 8 %), and as before, the fastest catalysts were shown to be the larger bite-angle complexes (**3** and **4**).

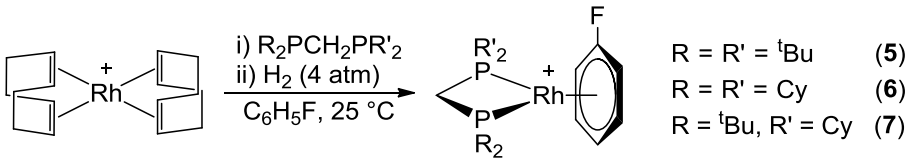

Scheme 2.2. Synthetic approach to the small bite-angle rhodium PCP complexes. The $[BAr^F_4]^-$ counter-anion is not pictured for clarity.

Another approach to speed up the hydroacylation reaction by increasing the rate of reductive elimination (the expected rate-limiting step for these systems), was to use the small bite-angle ligands that have previously been shown to be beneficial in promoting reductive elimination reactions.[3] Based on these results, and other success using small bite-angle systems discussed in the introduction, Willis and Weller investigated the effect of small bite-angle rhodium *bis*-phosphines on the hydroacylation reaction. The reactions were carried out using electron-rich alkyl phosphine ligands with a methylene backbone, developed and catalytically utilised by Hofmann.[4-6] The ligands contained the general motif of $R_2PCH_2PR_2$ where R was ^tBu or Cy. These ligands were complexed to a rhodium centre by a reaction between $[Rh(cod)_2][BAr^F_4]$ and the corresponding *bis*-phosphine, followed by hydrogenation of the formed complex in fluorobenzene which resulted in the desired precatalyst – $[Rh(\textit{bis}\text{-phosphine})_2(\eta^6\text{-}C_6H_5F)][BAr^F_4]$ (**5** – **7**) (Scheme 2.2).[7] These complexes proved to be highly active alkene hydroacylation catalysts, allowing catalyst loadings as low as 0.1 mol% and unique linear selectivity with a wide scope of substrates (example of the benchmark reaction, Scheme 2.3). It was also shown, that although decarbonylation still occurs, it was attenuated relative to the hydroacylation.

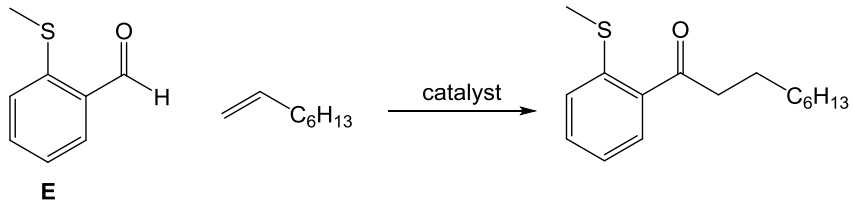

Scheme 2.3. Hydroacylation benchmark reaction using 2(methylthio)benzaldehyde and 1-octene. *Conditions: $ClCH_2CH_2Cl$ solvent, 80 °C; acetone solvent, 55 °C. Aldehyde (1.0 equiv) and alkene (1.5 equiv). Catalyst loading 0.1 – 10 mol%, concentration 0.075 M – 2.0 M.*

Combining the results from both of these studies carried out by Weller and Willis, it was important to understand the impressive activity behind the methylene-bridged complexes **5** – **7** *vs.* the previously reported complexes **1** – **4** containing diphenylphosphino based ligands 1,2-bis(diphenylphosphino)ethane (dpp2) – 1,5-bis(diphenylphosphino)pentane (dpp5). Furthermore, the activity of the small bite-angle catalysts was also shown to be dependent on the substituents on the phosphorus atoms. The best results were obtained using the tert-butyl substituted complex **5**, while the cyclohexyl substituted **6** resulted in lower catalytic

conversions. The mixed ligand complex **7** (tert-butyl/cyclohexyl) afforded an intermediate result, indicating that steric factors must be considered. Tolman has shown that upon measuring the CO stretching frequencies of $Ni(CO)_3P^tBu_3$ and $Ni(CO)_3PCy_3$ species, the same frequencies were seen ($\upsilon(CO)$ = 2056 cm^{-1}), while there is a difference in the size of the cone angle which for PCy_3 is 170° and for P^tBu_3 is 182°.[8] To further investigate this, a range of ligands were needed that allow for us to systematically change the phosphine ligands in order to make it possible to compare both the backbone identity and the PR_2 groups.

2.2. Ligands

Based on prior literature reports it was concluded that a good range of ligands that allow for different P-M-P bite angles (1 to 3 carbon backbone linker) had been reported for *bis*-phosphine ligands with isopropyl substituents on phosphorus atoms (*i.e.* $^iPr_2P(CH_2)_nP^iPr_2$ where n = 1 – 3). In order to further understand the small bite-angle complexes, a PNP(^{i}Pr) ligand **8b** and the novel PNP(Cy) ligand (**8a**) were also synthesised. The PNP(Cy) ligand **8a** would allow direct comparison to the analogues PCP(Cy) complex (**6**, Scheme 2.2) previously investigated in the Weller group.[7] Also these PNP ligands were targeted, in particular, due to previous reports showing the changes in catalytic activity towards ethylene trimerisation seen upon changing the carbon in the ligand backbone for nitrogen.[9, 10]

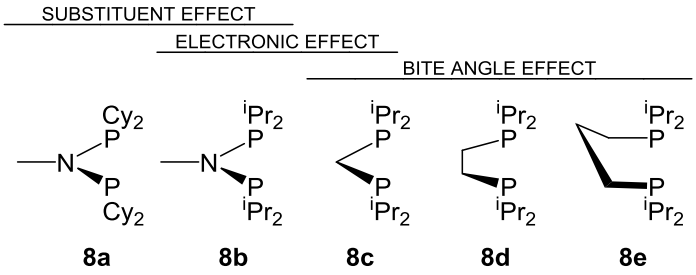

Figure 2.1. Isopropyl substituted *bis*-phosphine ligands (**8b** – **8e**) synthesised to investigate the effect of bite angle on hydroacylation catalysis and the cyclohexyl substituted phosphine (**8a**) to study the effect of the substituents on phosphorus atoms.

In order to obtain direct comparison to the best alkene hydroacylation catalyst reported previously (**5**), the synthesis of PNP(^{t}Bu) ligand, $^tBu_2PNMeP^tBu_2$, was attempted, but all

approaches led to the formation of partially substituted phosphine compounds (discussed in Section 2.2.2). A sterically less demanding PNP(Et) ligand was synthesised, $Et_2PNMePEt_2$ (**8f**), but attempts to complex this ligand on rhodium were unsuccessful (discussed in Section 2.2.3). Overall the five ligands depicted in Figure 2.1 were used to investigate how specific changes in the *bis*-phosphine ligand design affect the intermolecular hydroacylation reaction using 2-(methylthio)benzaldehyde (**E**) and 1-octene or 1-octyne.

2.2.1. Ligand Synthesis

Although previously reported,[11] the synthetic routes to these phosphine ligands were non-trivial, and in particular obtaining analytically pure ligands, which proved to be essential for rhodium complexation, was challenging. Maumela has reported synthesis of a range of diphosphinoamines from alkylamines and chlorophosphines under basic conditions, including the synthesis of **8b** (Scheme 2.4).[11]

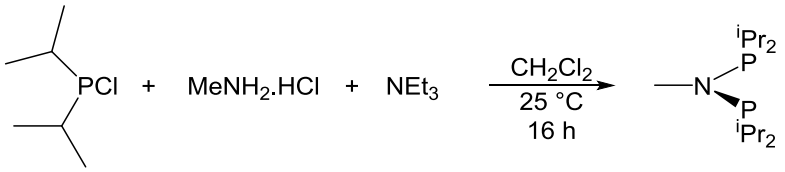

Scheme 2.4. The synthesis of PNP(^{i}Pr) ligand **8b**, based on the method reported by Maumela.[11] The ligand **8a** was synthesised via the same route using dicyclohexylchlorophosphine as the starting material.

The synthetic route allowed for the formation of the desired phosphine **8b**, but due to the poor solubility of the $MeNH_2$.HCl and the presence of the formed salts, the reaction mixture was not homogeneous leading to a range of by-products being produced. These by-products are proposed to be partially substituted phosphines (*e.g.* $^i Pr_2PNMeH$) (based on the N*H* proton chemical shifts seen in ^{1}H NMR spectrum and multiple peaks seen in ^{31}P NMR spectrum). Maumela proposed an efficient way to remove the impurities by eluating the ligand through an alumina column under an inert atmosphere. This proved to be an effective way to remove the more polar chlorine-containing by-products. Unfortunately alumina can oxidise the phosphine

ligands, but it was also found that the oxidised products can be removed using the same alumina column. To obtain pure ligand in good yield a highly specific synthetic and purification approaches were established concerning the concentration of the reaction, the amount of alumina used and the rate at which the ligand containing solution was allowed to go through the column (these are detailed in the Chapter 6). Based on this established route, the previously unknown ligand **8a** was also synthesised.

Similar synthetic problems were also encountered when synthesising the PCP(^{i}Pr) ligand **8c** and the PCCP(^{i}Pr) ligand **8d**, which were both synthesised by addition of the isopropyl-Grignard to the relevant 1,2-*bis*(dichlorophosphanyl) reagent (*i.e.* ethylene or methylene bridged). Under the established work-up conditions, pure ligands (**8b – 8d**) were isolated as colourless oils in good yields (50 – 70%) while **8a** was obtained as a white solid in 50% yield. Being a solid is beneficial in particular for *in situ* catalytic reactions, as this bench-stable solid can be much more easily handled than the air sensitive oils. The purity of the ligands was confirmed by ^{1}H and ^{31}P NMR spectroscopy. The PCCCP(^{i}Pr) ligand **8e** is a commercially available. All these ligands were stored under argon in a refrigerator. To use these ligands, a fluorobenzene or dichloromethane standard solution was prepared, from which the solvent was removed under reduced atmosphere after use to recover the unused phosphine avoiding any reactivity that might be occurring over time. Over prolonged storage of these phosphine compounds a change in colour from colourless to yellow was observed, but based on NMR spectroscopy no visible impurities had formed and the reactivity of these ligands remained unchanged.

2.2.2. Attempted Ligand Synthesis

Encouraged by the established route described above, synthesis of the bulky $^{t}Bu_2PNMeP^{t}Bu_2$ ligand was attempted to allow direct comparison with complex **5** (Scheme 2.2). Upon using the

conditions that were suitable for the synthesis of the isopropyl and cyclohexyl substituted ligands **8b** and **8a** (Scheme 2.4), at the end of the reaction a range of products were observed.

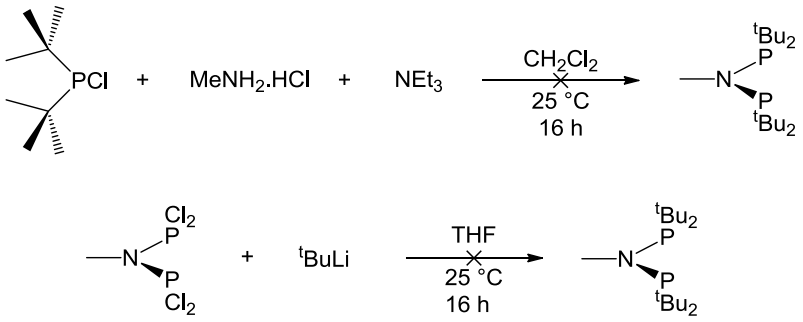

Scheme 2.5. Attempted synthesis of $^{t}Bu_2PNMeP^{t}Bu_2$.

These products corresponded to the partially substituted products (in the ^{1}H NMR spectra resonances corresponding to $^{t}Bu_2PNMeH$ were observed, and the $^{31}P\{^{1}H\}$ NMR spectra showed a number of species formed) similar to those partially substituted products observed in small quantities for **8b**, but no evidence for the formation of the desired tert-butyl product was observed. No product was isolated from column chromatography. Synthesis of $^{t}Bu_2PNMeP^{t}Bu_2$ was also attempted by a reaction between $Cl_2PNMePCl_2$ and $^{t}BuLi$ but, as before, no formation of the desired phosphine was seen. Overall these results indicate that the tert-butyl groups are too bulky to promote formation of PNP ligands of this type.

Similar problems, arising from the bulk of the substituents, were observed when attempts were made to vary the substituent on the nitrogen atom of the PNP backbone. There were two aims for developing these ligands with different R-groups on the backbone nitrogen: to further understand the effect of the nitrogen in the backbone, by changing electronics, and to develop N-chiral catalysts.[a] Our initial objective was set on isopropyl substituted PNP complexes, with modified backbone. Using the reaction procedure discussed above (Scheme 2.4), the aim was to

[a] Research concentrating on developing N-chiral ligands was carried out in the Willis group in order to develop ligands with the general structure of $Ph_2PN(R^*)PPh_2$ (where R* = chiral substituent).

synthesise two ligands with electron-withdrawing substituents on nitrogen (**8g** and **8h**) and the N-chiral ligand (**8i**) (Scheme 2.6).

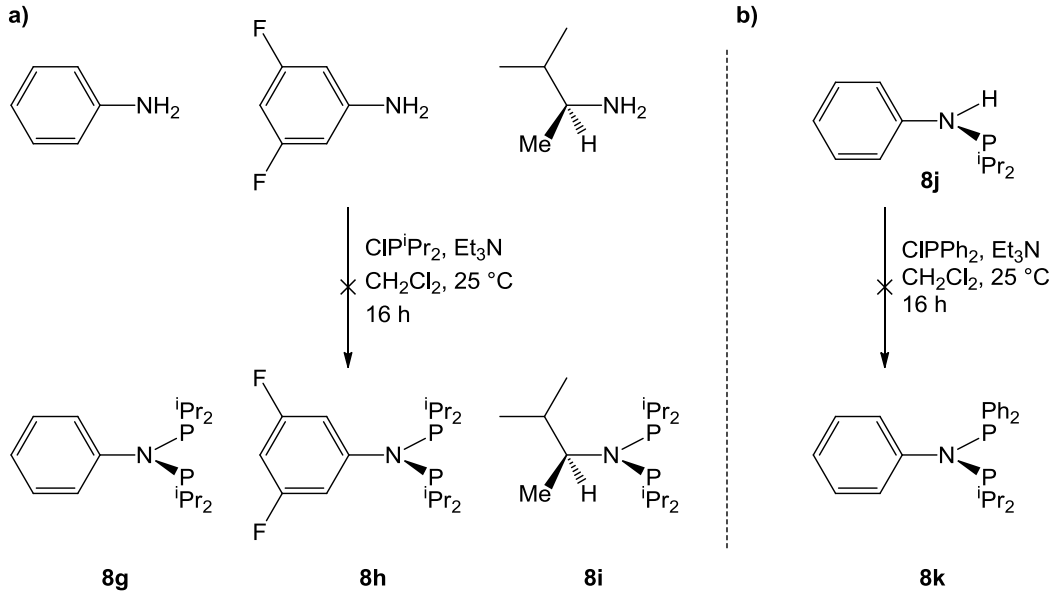

Scheme 2.6. a) Proposed ligands (**8g** – **8i**) that would allow the backbone effect of the PNP ligands to be investigated. b) The attempted reaction between monosubstituted **8j** and sterically less demanding diphenylchlorophosphine to form **8k**.

In all of these cases (**8g** – **8i**), only partial substitution was observed (similarly to the discussed $^{t}Bu_2PNMeP^{t}Bu_2$ attempted synthesis, products containing $^{i}Pr_2PNMeH$ moiety were observed by ^{1}H NMR spectroscopy and remaining $ClP^{i}Pr_2$ was observed at the end of the reaction). This reactivity was probed by adding 1 eq. of diisopropylchlorophosphine to the benzylamine, resulting in **8j**. In order to obtain **8k**, to this monosubstituted amine (**8j**) 1 eq. of sterically less demanding diphenylchlorophosphine was then added, but no reactivity was observed (Scheme 2.6, b). Overall the ligand synthesis is highly nuanced, as both the substituents on the nitrogen and the phosphorus atoms must be considered in order to synthesise the desired small bite-angle PNP ligands.

2.2.3. Rhodium Complexes Containing Small Bite-Angle Ligands

Initial attempts to form the desired rhodium-phosphines, via routes commonly used by the Weller group, failed and pure materials were not obtained. These routes involved the use of $[Rh(X)Cl]_2$ starting materials, where X is norbornadiene (nbd) or 1,5-cyclooctadiene (cod) (Scheme 2.7).[12-15] This approach led to the formation of various oily product mixtures, including doubly substituted rhodium complexes, assigned as $[Rh(\textit{bis}\text{-phosphine})_2][BAr^F{}_4]$ based on data from ^1H NMR spectroscopy and ESI-MS.

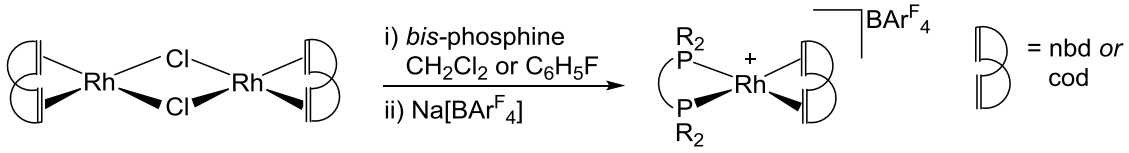

Scheme 2.7. Common approach to the synthesis of cationic rhodium *bis*-phosphine complexes which can subsequently be hydrogenated to form the fluorobenzene coordinated hydroacylation precatalysts. Coordinated olefin = cod or nbd. R = aryl group, *bis*-phosphine = dpp2, dpp3, dpp4 or dpp5.[12-16] The $[BAr^F{}_4]^-$ counter-anion is not pictured for clarity.

This was assumed to occur due to the second step in the reaction (Scheme 2.7), where the formed rhodium phosphine solution was transferred to solid $Na[BAr^F{}_4]$, thus not allowing for a controlled, slow, addition of the reagents. To avoid this troublesome $Na[BAr^F{}_4]$ addition step, cationic rhodium precursors were synthesised to which the phosphine ligand could be added slowly, hence keeping the rhodium complex in excess during the whole addition step. The rhodium precursors synthesised were $[Rh(cod)_2][BAr^F{}_4]$ (**9**) and $[Rh(nbd)_2][BAr^F{}_4]$ (**10**), as these had been shown to be useful in previous synthetic routes.[7, 17] Using the nbd precursor **10**, it was found that even when exactly one equivalent of the phosphine ligand was added slowly, *bis*-substituted rhodium complexes were observed during the reaction. In contrast the use of the **9** led to analytically pure $[Rh(\textit{bis}\text{-phosphine})(cod)][BAr^F{}_4]$ complexes, which could be isolated as microcrystalline solids. This change in reactivity was attributed to stronger binding affinity of the cod ligand compared to the nbd.

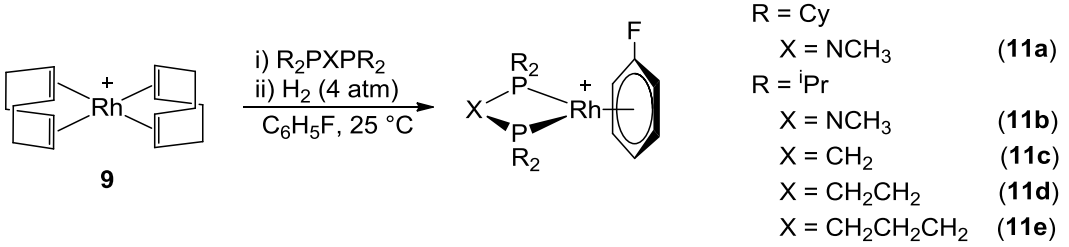

Scheme 2.8. Synthesis of rhodium(I) *bis*-phosphine precatalysts **11a** – **11e**. The $[BAr^F_4]^-$ counter-anion is not pictured for clarity.

In order to synthesise the desired 18-electron precatalysts with the general structure of [Rh(*bis*-phosphine)(η^6-C_6H_5F)][BAr^F_4] (**11**), the cod complex, [Rh(*bis*-phosphine)(cod)][BAr^F_4], was placed under a hydrogen atmosphere (4 atm) in fluorobenzene solvent. The synthetic utility of these fluorobenzene complexes has been demonstrated previously; they are stable towards air and moisture as solids, are highly reactive upon dissolving in various solvents due to the lability of the fluorobenzene ligand, and the liberated fluorobenzene that is formed during the reaction has no effect on the hydroacylation reaction.[7]

The use of **9** as the starting material also allows direct two step route to the fluorobenzene complexes (**11a – 11e**) without the need for isolation of the cod-intermediate (Scheme 2.8). Although the use of cyclooctadiene (cod) is beneficial in controlling the formation of the desired product during the addition of the phosphine to the rhodium starting material, it does complicate the hydrogenation step. Unlike nbd, which is hydrogenated under the conditions in Scheme 2.8 within a few minutes,[15] the hydrogenation of cod only occurs after an hour of vigorous stirring under 4 atm of H_2. This time-scale is problematic for these isopropyl substituted phosphine complexes, as after 1-2 hour(s) under 4 atm of hydrogen gas, decomposition of the rhodium complexes is observed. During this decomposition colloidal rhodium was formed (indicated by black precipitation in the reaction mixture), leading to the formation of excess phosphine in the reaction mixture and in turn the formation of *bis*-substituted rhodium phosphine complexes were formed. These impurities are very difficult to separate from the desired fluorobenzene complexes. Therefore to yield full conversion to the fluorobenzene complexes while avoiding any decomposition, hydrogenation should be carried out for 1 hour after which the reaction should be halted if conversion from orange to yellow has

occurred or if any indication of decomposition is seen. Small amounts of decomposed product may be separated by recrystallisation and colloidal rhodium can be filtered off. In the case of the propane-bridged PCCCP(^{i}Pr) complex **11e** the colour of the final product is pale orange instead of yellow. Interestingly, for complexes **5** – **7** this decomposition was not observed and the hydrogenation step was carried out overnight.[7] In all cases (**11a** – **11e**), upon using this methodology, full conversions into pure compounds were seen and the compounds were fully characterised using a range of analytical methods (solution NMR spectroscopy, ESI-MS, X-ray crystallography and elemental analysis).

The ^{1}H NMR spectra (CD_2Cl_2 solvent) show expected shifts for the ligand environments and the η^6-coordination of the fluorobenzene ring (pattern corresponding to three chemical environments at δ 5.5 – 6.2 with integration showing 2:2:1 ratio, *cf.* free fluorobenzene is seen as two multiplets at δ 7.1). The ^{31}P{^{1}H} NMR spectra show the expected rhodium phosphine coupling for *bis*-phosphine complexes of *J*(RhP) = 175 – 205 Hz, and also phosphorus fluorine coupling of *J*(PF) = 2 – 3 Hz.[18] The phosphorus chemical shifts of ^{31}P{^{1}H} NMR spectra are interesting, as small changes in the ligand lead to substantial changes in the chemical shifts. For the PNP(^{i}Pr) complex **11b** the ^{31}P{^{1}H} NMR shift is observed at δ 80.9, while the shift for the analogous PCP complex **11c** is at δ 0.7. The ^{31}P{^{1}H} NMR chemical shifts for larger bite-angle complexes **11d** and **11e** were observed at δ 107.5 and δ 46.7 respectively, while the chemical shift for the cyclohexyl PNP(^{i}Pr) complex **11a** was similar to the PNP(^{i}Pr) complex **11b** at δ 73.5. The exact reasons for this significant change in chemical shifts is unclear, but it is likely to be due to electronic effect resulting in the change from C to N and the strain forced upon the phosphorus atom by changing the bite angle.[19] ^{19}F NMR spectra (in CD_2Cl_2 solvent) showed similar fluorine environments in case of all complexes with the chemical shifts at δ –120 to –123 and a shift at δ –62.9 corresponding to the BAr^F_4 counterion. All of these complexes (**11a – 11e**) were isolated as yellow or pale orange solids by addition of hexane to fluorobenzene solutions, subsequent sonication and removal of supernatant (yield 70 – 80%). These precatalysts are air and moisture stable materials (there is no change in NMR spectroscopy after exposure of the solid to air for 24 h), although the compounds were stored under an inert atmosphere in an argon-filled glovebox to ensure no decomposition.

The coordination of the fluorobenzene to the rhodium phosphine fragment was further probed by ESI-MS studies which confirmed the masses of complexes **11a** – **11e** with the correct isotope patterns.[20, 21] Crystals of **11a** – **11e** suitable for single crystal X-ray diffraction were obtained by layering a fluorobenzene solution of the appropriate complexes with hexane, and slow diffusion at 2 °C.

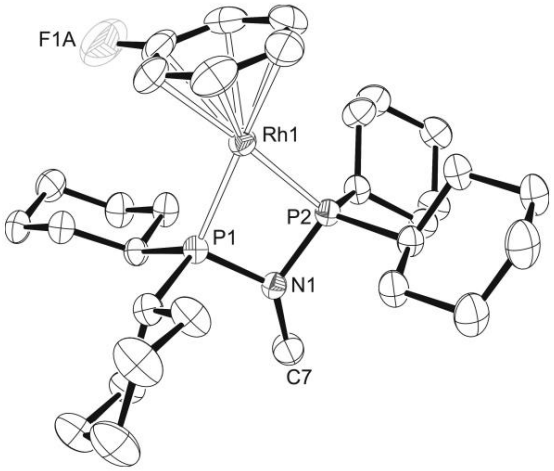

Figure 2.2. Solid state structure of the cation **11a**. Displacement ellipsoids depicted at the 50% probability level. Hydrogen atoms, $[BAr^F{}_4]^-$ anion and disordered component (C_6H_5F ligand) are omitted for clarity. All unlabelled atoms are carbon atoms. Key bond lengths (Å) and angles (°): Rh1-P1, 2.2250(11); Rh1-P2, 2.2267(11); Rh1-C, 2.282(4)-2.339(5); P1-Rh1-P2, 70.49(4); P1-N1-P2, 98.33(17).

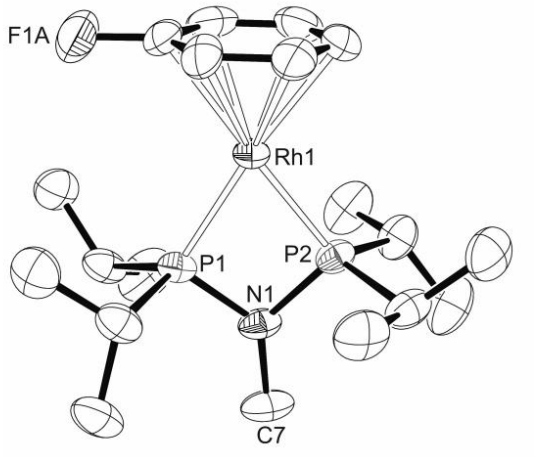

Figure 2.3. Solid state structure of the cation **11b**. Displacement ellipsoids are depicted at 50% probability level. Hydrogen atoms, $[BAr^F{}_4]^-$ anion and disordered component (C_6H_5F ligand) are omitted for clarity. All unlabelled atoms are carbon atoms. Key bond lengths (Å) and angles (°): Rh1-P1, 2.2365(8); Rh1-P2, 2.2103(8); Rh1-C, 2.297(4)-2.329(4); P2-Rh1-P1, 70.36 (3); P2-N1-P1, 98.33(13).

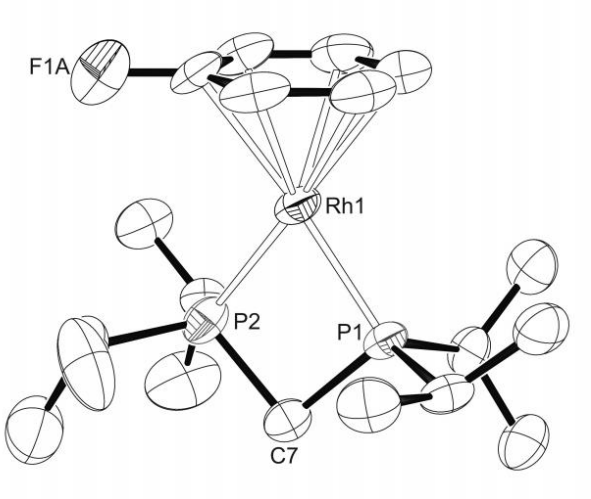

Figure 2.4. Solid state structure of the cation **11c**. Displacement ellipsoids depicted at the 50% probability level. Hydrogen atoms, $[BAr^F_4]^-$ anion and disordered component (C_6H_5F ligand) are omitted for clarity. All unlabelled atoms are carbon atoms. Key bond lengths (Å) and angles (°): Rh1-P1, 2.2244(11); Rh1-P2, 2.2362(15); Rh1-C, 2.313(8)-2.362(8); P2-Rh1-P1, 72.64(5); P1-C7-P2, 91.8(2).

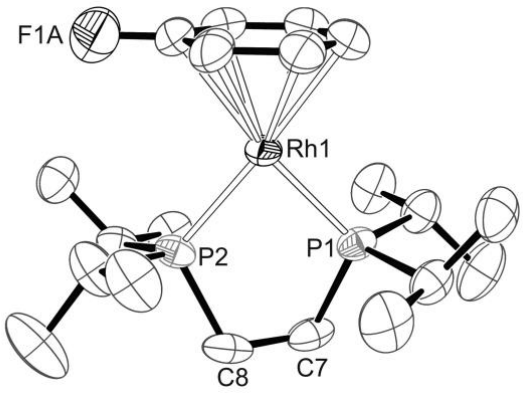

Figure 2.5. Solid state structure of the cation **11d**. Displacement ellipsoids depicted at the 50% probability level. Hydrogen atoms, $[BAr^F_4]^-$ anion and disordered component (C_6H_5F ligand) are omitted for clarity. All unlabelled atoms are carbon atoms. Key bond lengths (Å) and angles (°): Rh1-P1, 2.2352(8); Rh1-P2, 2.2399(8); Rh1-C, 2.297(4)-2.353(4); P1-Rh1-P2, 84.81(3).

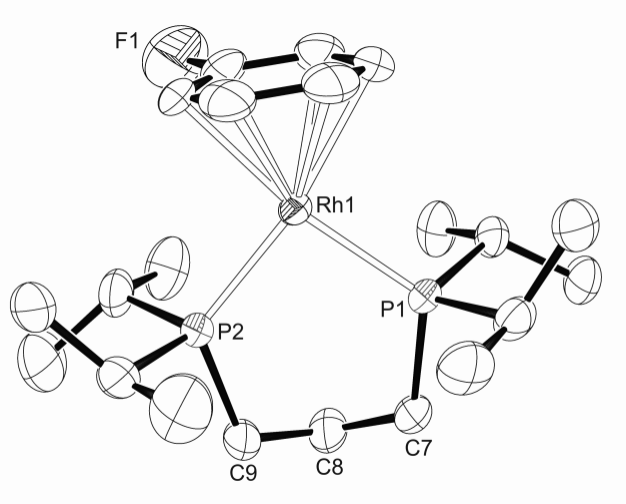

Figure 2.6. Solid state structure of the cation **11e**. Displacement ellipsoids depicted at the 50% probability level. Hydrogen atoms, $[BAr^F{}_4]^-$ anion and disordered component (C_6H_5F ligand) are omitted for clarity. All unlabelled atoms are carbon atoms. Key bond lengths (Å) and angles (°): Rh1-P1, 2.2556(8); Rh1-P2, 2.2481(8); Rh1-C, 2.285(3)-2.395(3); P2-Rh1-P1, 93.78(3).

The crystallographic data demonstrates that placing a nitrogen atom in the backbone leads to smaller P-Rh-P bite-angles than that those with the methylene linker. The bite angles of the PNP(^{i}Pr) complex **11b** and the PNP(Cy) complex **11a** are 70.36(3)° and 70.49(4)°, respectively, whereas the angle for the PCP(^{i}Pr) complex **11c** and the previously reported PCP(Cy) complex **6** are 72.64(5)° and 72.78(3)°.[7] In comparison, the P-Rh-P bite angle reported for the PCP tert-butyl complex **5** is 74.44(5)°.[7] The bite angles for the PCCP(^{i}Pr) and the PCCCP(^{i}Pr) complexes **11d** and **11e**, respectively are 84.81(3)° and 93.78(3)° (Table 2.2).

Table 2.2. Rh-C/P bond lengths relative to the P-Rh-P bite angle.

Complex	Bite angle / °	Rh-C bond length / Å	Rh-P bond length / Å
PNP(^{i}Pr) **11b**	70.36(3)	2.297(5) – 2.329(5)	2.2365(8), 2.2103(8)
PNP(Cy) **11a**	70.49(4)	2.282(4) – 2.339(5)	2.2250(11), 2.2267(11)
PCP(^{i}Pr) **11c**	72.64(5)	2.313(8) – 2.362(8)	2.2344(11), 2.2362(15)
PCP(Cy) **6**	72.78(3)	2.287(2) – 2.365(15)	2.2325(7), 2.2459(7)
PCP(^{t}Bu) **5**	74.44(5)	2.298(4) – 2.341(4)	2.263(2), 2.2711(15)
PCCP(^{i}Pr) **11d**	84.81(3)	2.297(4) – 2.353(6)	2.2352(8), 2.2399(8)
PCCCP(^{i}Pr) **11e**	93.78(3)	2.285(3) – 2.395(3)	2.2556(8), 2.2481(8)

The data show smaller bite angles in the case of shorter backbone linkers, but also upon comparing PNP and PCP complexes, for both the isopropyl and cyclohexyl species, the nitrogen in the backbone leads to slightly reduced bite angle.

To understand the effect the nitrogen has on the metal centre, the rhodium-carbon bond-lengths (carbon atoms of the η^6-coordinated fluorobenzene ring) were examined. This comparison relies on the fact that a phosphine ligand with different electronic properties can affect the rhodium centre's bonding to other ligands.[8] For PNP(^{i}Pr) complex **11b** the Rh-C lengths are 2.297(5) – 2.329(5)Å, whereas in case of PCP(^{i}Pr) complex **11c** slightly longer Rh-C bond lengths were observed [2.313(8) – 2.362(8)Å] (*cf.* Rh-C bond lengths for the analogous PNP(Cy) and PCP(Cy) complexes (**11a** and **6**) show similar slight increase in the bond lengths upon changing from N to C; 2.282(4) – 2.339(5)Å *vs.* 2.287(2) – 2.365(15)Å respectively.[7] These small changes in rhodium-carbon bond lengths do not allow us to discuss the effect of the change between nitrogen and carbon in the backbone.

The effect of backbone was further probed using ESI-MS (ESI-MS = Electrospray Ionisation Mass Spectrometry). Seb Pike (former D.Phil. student in the Weller group) carried out a range of ESI-MS measurements to probe the binding strength of different fluorinated aryl ligands. During this study, the binding strength of the fluorobenzene ligand to the isopropyl substituted complexes (**11b** – **11e**) was also investigated. The fragmentation of the fluorobenzene species in the ESI-MS experiment can be achieved in a controlled manner, allowing for direct comparisons to be drawn between metal-ligand fragments. For determining the ESI-MS spectra of these air-sensitive solutions the previously described experimental set-up of ESI-MS interfaced with argon-filled glovebox was used.[20]

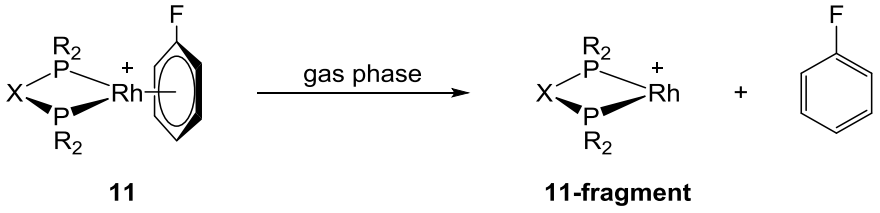

11 **11-fragment**

Scheme 2.9. Schematic representation of the fragmentation occurring in the ESI-MS during the increase of the exit voltage. X = CH_2 or NMe, R = isopropyl or tert-butyl. The $[BAr^F{}_4]^-$ counter-anion is not pictured for clarity.

During the sample transfer into the spectrometer, the exit voltage can be changed which determines the degree of fragmentation by collision induced processes. Exit voltage is used to accelerate the ions relative to the neutral fragments (*i.e.* solvents) in the electrospray.[21] Increasing the exit voltage encourages the dissociation of weakly bound ligands (*i.e.* fluorobenzene) from the [Rh(*bis*-phosphine)(C_6H_5F)]$^+$ parent ion and leads to the formation of the [Rh(*bis*-phosphine)]$^+$ fragment (Scheme 2.9). At different exit voltages (approximately 60 – 250 V) different ratios of **11** and **11-fragment** are seen which can be plotted relative to one-another (Figure 2.7) and based on these data the 50% dissociation voltages (summarised in Table 2.3) were obtained.

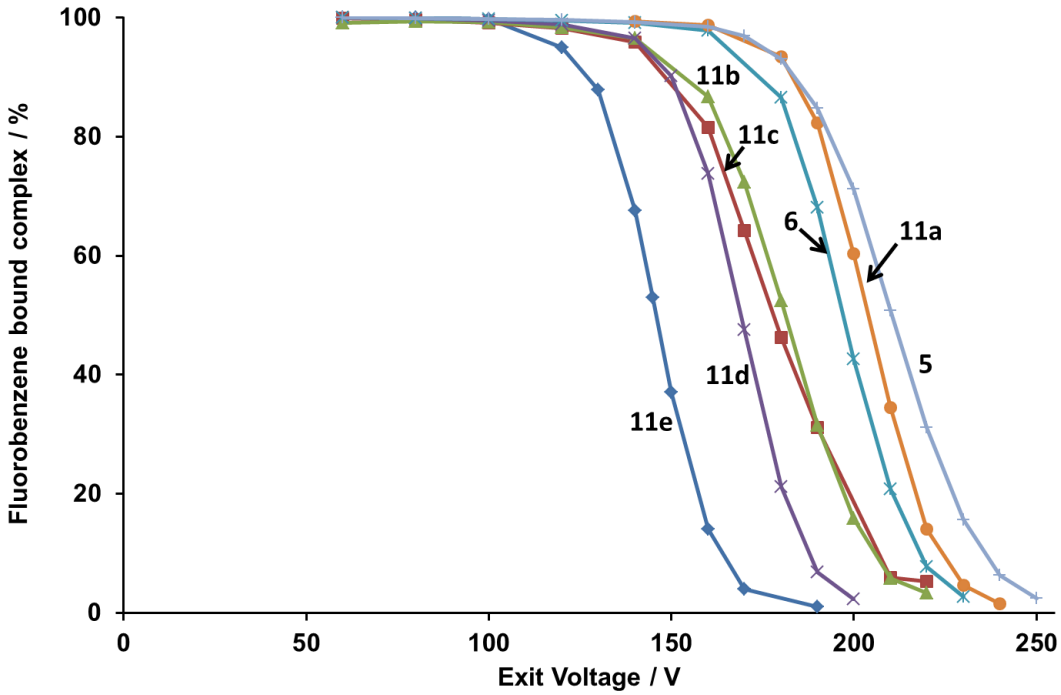

Figure 2.7. Fluorobenzene binding affinity towards different rhodium bis-phosphine complexes measured by varying the exit voltage of the ESI-MS. **11a** = [Rh($Cy_2PN(CH_3)PCy_2$)(C_6H_5F)][BAr^F_4], **11b** = [Rh($^iPr_2PN(CH_3)P^iPr_2$)(C_6H_5F)][BAr^F_4], **11c** = [Rh($^iPr_2PCH_2P^iPr_2$)(C_6H_5F)][BAr^F_4], **11d** = [Rh($^iPr_2PCH_2CH_2P^iPr_2$)(C_6H_5F)][BAr^F_4], **11e** = [Rh($^iPr_2PCH_2CH_2CH_2P^iPr_2$)($C_6H_5F$)][$BAr^F_4$], **5** = [Rh($^tBu_2PCH_2P^tBu_2$)($C_6H_5F$)][$BAr^F_4$], **6** = [Rh($Cy_2PCH_2PCy_2$)($C_6H_5F$)][$BAr^F_4$].

Based on the combined data in Figure 2.7 and Table 2.3 different trends can be identified. Upon comparing nitrogen and carbon containing backbones (*i.e.* PNP *vs.* PCP) it is seen, that both small bite-angle PNP(^{i}Pr) and PCP(^{i}Pr) complexes **11b** and **11c** result in very similar 50% dissociation voltage (181 V *vs.* 178 V). An analogous difference is observed for PNP(Cy) and

PCP(Cy) complexes **11a** and **6** that show 50% dissociation at 204 V and 197 V respectively. Both these results show that changing the backbone carbon for nitrogen allows for a small, yet consistent, change in the fluorobenzene binding affinity.

Table 2.3. The 50% dissociation of the fluorobenzene and rhodium-carbon bond-lengths with respect to the P-Rh-P bite angle. The $[BAr^F{}_4]^-$ counter-anion is not pictured for clarity.

Complex	50% dissociation / V	Rh-C bond length / Å	Bite angle / °
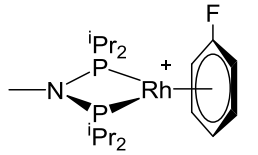 **11b**	181	2.297(5) – 2.329(5)	70.36(3)
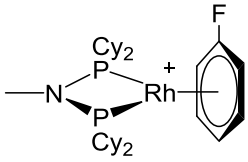 **11a**	204	2.282(4) – 2.339(5)	70.49(4)
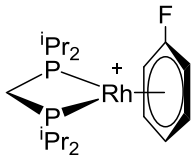 **11c**	178	2.313(8) – 2.362(8)	72.64(5)
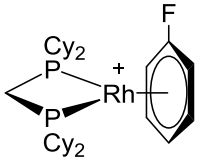 **6**	197	2.298(4) – 2.341(4)	72.78(3)
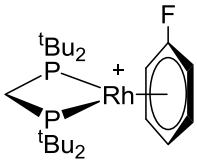 **5**	210	2.287(2) – 2.365(15)	74.44(5)
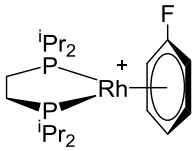 **11d**	169	2.297(4) – 2.353(6)	84.81(3)
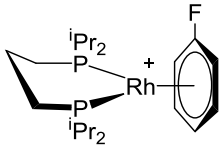 **11e**	143	2.285(3) – 2.395(3)	93.78(3)

A more pronounced effect is seen upon changing the bite angle (*i.e.* $CH_2CH_2CH_2$ *vs.* CH_2CH_2 *vs.* CH_2 linker in the backbone of the *bis*-phosphine). There is a clear trend indicating lower binding affinity with increasing bite angle, showing **11c** > **11d** > **11e**. This trend is probably due to a

combination of steric (the larger bite-angle allows for isopropyl groups to be closer to the reaction centre)[1, 22] and electronic effects (the bite angle difference changes the degree of orbital overlap between the metal centre and the ligands).[4]

To allow for further comparison, the ESI-MS study was also carried out using the bulky PCP(^{t}Bu) complex **5**. Unlike the analogous PCP(^{i}Pr) complex (**11c**), the PCP(^{t}Bu) complex (**5**) fragments at much higher exit voltages, showing for much stronger relative binding affinity for the fluorobenzene ligand, even though the bite angles are very similar (72.64(5) *vs.* 74.44(5) respectively). Similarly to the PCP(^{t}Bu) complex (**5**) both cyclo-hexyl species (**6** and **11a**) showed strong relative binding towards fluorobenzene and overall a trend of ^{i}Pr < Cy < ^{t}Bu was observed. This data is further complicated as it is undetermined whether the formed [Rh(*bis*-phosphine)]$^+$ fragment relies on any stabilisation. For example, if there are any agostic interactions in the dissociated product then it can be argued that the isopropyl groups are more likely to interact with the rhodium centre in an agostic manner, while the bulky tert-butyl groups might be more restricted thus stabilising the isopropyl fragment relative to the tert-butyl congener. This kind of agostic interaction was also seen upon probing the decarbonylation reaction using the PCP(^{i}Pr) complex **11c** (Section 2.3.2.1), whereas no agostic interaction were reported for the PCP(^{t}Bu) complex **5**.[7] At the same time, it has been shown using [Ir(H)$_2$(PR$_3$)$_3$]$^+$ fragments (where R = ^{t}Bu or ^{i}Pr) that agostic interaction is occurring for the tert-butyl complex, while no agostic interaction is seen for the isopropyl complex.[23] The agostic interaction theory is strengthened upon using the PCP(^{i}Bu) complex [Rh(^{i}Bu$_2$PCH$_2$P^{i}Bu$_2$)(C$_6$H$_5$F)][BAr$^F_4$]. Isobutyl groups have previously been shown to form agostic complexes with Rh(I).[24, 25] The relative binding affinity for fluorobenzene for this isobutyl complex (50% dissociation at 167 V) is similar to the one seen for the analogous isopropyl complex **11c** (50% dissociation at 178 V).

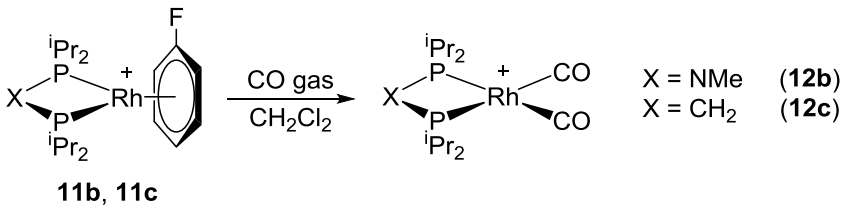

11b, **11c**

Scheme 2.10. Synthesis of the *bis*-CO rhodium phosphine complexes **12b** and **12c**. The [BAr$^F_4$]$^-$ counter-anion is not pictured for clarity.

To probe the ligand backbone further an infrared spectroscopy study of the corresponding *bis*-CO complexes was conducted. For this, two *bis*-carbonyl complexes (PNP(^{i}Pr) complex **12b** and PCP(^{i}Pr) complex **12c**) were synthesised (Scheme 2.10). These *bis*-CO complexes would allow the backbone effect to be probed by comparison of the CO stretching frequencies. **12b** and **12c** were synthesised by dissolving the fluorobenzene complexes **11b** and **11c** in CH_2Cl_2 and bubbling CO gas through the system for 1 minute. This resulted in slight colour change from yellow to pale yellow, and some decomposition material indicated by a black precipitate that appeared during the reaction. As the formed complex was the major product and remained stable in the solution, this decomposition was posited to be the result of some minor impurities in the CO gas. The decomposition materials were removed from the product via filtration. By layering this fluorobenzene solution with hexane pure, crystalline, solid was obtained. The $^{31}P\{^{1}H\}$ NMR spectra and ESI-MS show full conversion into new *bis*-CO products **12b** and **12c**. A Nujol mull of each sample was prepared in an argon filled glovebox, and IR data were recorded. Peaks for CO-stretches were seen at υ(CO) = 2100 and 2058 cm^{-1} for **12b** and 2102 and 2057 cm^{-1} for **12c**. This data suggests that the electron density at the metal centre that is available to backbond with the CO is very similar for both complexes and is in line with the ESI-MS and X-ray studies discussed above.

2.2.4. Attempted Synthesis of Sterically Different Rhodium *bis*-Phosphines

Upon establishing these fruitful conditions for the synthesis of rhodium complexes (**11a** – **11e**), synthesis of complexes with different substituents on phosphorus atoms was attempted. Upon reacting $Et_2PNMePEt_2$ (**8f**) with $[Rh(cod)_2][BAr^F{}_4]$ it was possible to synthesise the cod-complex $[Rh(Et_2PNMePEt_2)(cod)][BAr^F{}_4]$ (**11f**) but upon hydrogenation decomposition alongside formation of the *bis*-substituted complex $[Rh(Et_2PNMePEt_2)_2][BAr^F{}_4]$ was observed. A similar scenario was seen upon using the nbd-containing starting material (**10**).

In the case of the phenyl substituted $Ph_2PNMePPh_2$ ligand,[26, 27] it was not possible to synthesise the cod-complex $[Rh(Ph_2PNMePPh_2)(cod)][BAr^F{}_4]$. Even under the reaction conditions where 1 eq. of $Ph_2PNMePPh_2$ was added to $[Rh(cod)_2][BAr^F{}_4]$, $[Rh(Ph_2PNMePPh_2)_2][BAr^F{}_4]$ was seen as

the major product with no formation of the desired [Rh($Ph_2PNMePPh_2$)(cod)][BAr^F_4]. Similar trends were also seen using the commercially available $Ph_2PCH_2PPh_2$ (dpp1) or other similar phenyl-substitued complexes ($Ph_2PCMeHPPh_2$ and $Ph_2PCMe_2PPh_2$). In collaboration with the Willis group (between myself and visiting students David Fabry and Edgar Christobal), a project was carried out using $Ph_2PN(R^*)PPh_2$ type ligands, in which ligands with a chiral substituent on the nitrogen (*i.e.* R* = chiral group) were synthesised. Unfortunately any attempts to complex these PNP ligands to rhodium led to formation of mixtures, which were mostly (some cases uniquely) assigned, using NMR spectroscopy and ESI-MS, as *bis*-substituted rhodium complexes with general structure of [Rh(*bis*-phosphine)$_2$][BAr^F_4], with a range of unidentified products also observed (Scheme 2.11).

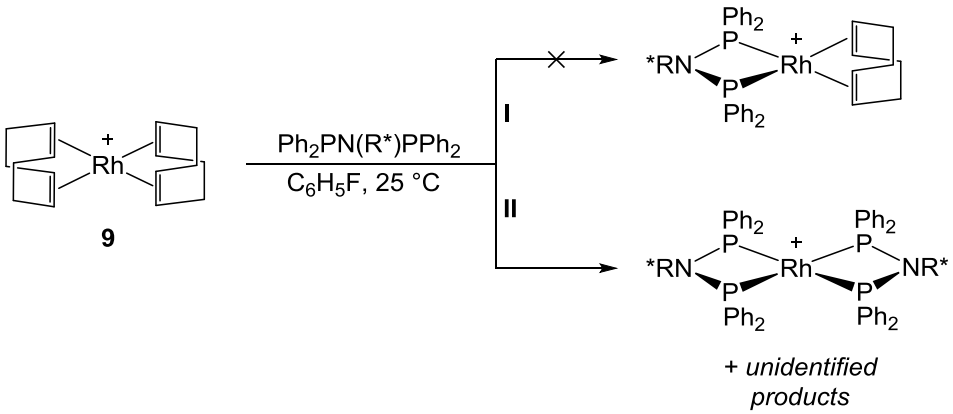

Scheme 2.11. Synthetic approach using chiral $Ph_2PN(R^*)PPh_2$ ligands. The desired pathway (**I**) and the occurring pathway (**II**). The [BAr^F_4]$^-$ counter-anion is not pictured for clarity.

In general it can be concluded, that a very fine balance exists on which of the rhodium *bis*-phosphine complexes can be synthesised. If the substituents on the phosphorus atoms are too bulky, then problems are encountered during the synthesis of ligands, whereas if the ligands are not bulky enough, the formation of unwanted rhodium *bis*-substituted species is seen.

2.2.5. Modification of the Counterion

In order to reduce to cost and time required to synthesise the [BAr^F_4]$^-$ anion-containing rhodium *bis*-phosphine fragments, we also investigated the potential use of cheaper and readily available [BF_4]$^-$ anion (1 g of Na[BAr^F_4] = £264.00; 1 g of Ag[BF_4] = £17.70).[28] Synthetically, a

similar approach to the [BAr^F_4] complex can be taken, by first synthesising the [$Rh(cod)_2$][BF_4] precursor by a reaction between [Rh(cod)Cl]$_2$ and Ag[BF_4] in CH_2Cl_2.[17] To this isolated precursor the *bis*-phosphine ligand can be slowly added and the resulting complex hydrogenated to yield the desired [Rh(*bis*-phosphine)(C_6H_5F)][BF_4] complex. It was determined that the [BF_4]$^-$ complex is useful for *in situ* reactions, where the rhodium precursor is mixed with the phosphine, and subsequently added to the catalysis (*i.e*. the catalyst is not isolated). Also it has been previously shown in the Weller group using [Rh(dpp3)(acetone)$_2$][X] complex (where X = counterion), that for the hydroacylation reaction using the β-sulfur tethered aldehyde, there is no counterion effect upon changing [BAr^F_4]$^-$ for [BF_4]$^-$.[29] Unfortunately, in our hands, isolating the fluorobenzene complex, [Rh(^{i}Pr$_2$PN(CH_3)P^{i}Pr$_2$)(C_6H_5F)][BF_4], led to significantly lower isolated yield (30 %), thus all mechanistic work was continued using [BAr^F_4] complexes. Also lower stability (*i.e.* not bench stable) of the formed [Rh(^{i}Pr$_2$PN(CH_3)P^{i}Pr$_2$)(C_6H_5F)][BF_4] was observed.

2.2.6. Variation of the Labile Ligand

Although the 18-electron fluorobenzene coordinated complexes were used as the precatalysts due to their stability and ease of use, *bis*-acetone complexes were also synthesised (Scheme 2.12, **16a** – **16e**). It is important to explore these acetone complexes, as hydroacylation catalysis is often performed in acetone solution, while Willis and Weller have previously shown that acetone can provide stabilisation towards the undesirable reductive decarbonylation by reversibly blocking a vacant site.[1, 7, 15, 30] Also the use of these acetone complexes as precatalysts would allow for us to completely avoid the presence of fluorobenzene in the reaction mixture. The acetone complexes (**16a – 16e**) were synthesised by dissolving the fluorobenzene complexes **11a** – **11e** in acetone (Scheme 2.12).

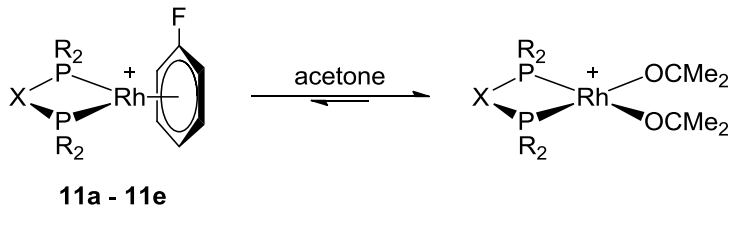

R = Cy
X = NCH_3 (**16a**)
R = ^{i}Pr
X = NCH_3 (**16b**)
X = CH_2 (**16c**)
X = CH_2CH_2 (**16d**)
X = $CH_2CH_2CH_2$ (**16e**)

Scheme 2.12. Synthesis of rhodium *bis*-acetone complexes. The $[BAr^F_4]^-$ counter-anion is not pictured for clarity.

It was possible to isolate the acetone complex but obtaining solid material was demanding and the yield was substantially reduced compared to the corresponding fluorobenzene complexes. Hence any further attempts to isolate the acetone complexes were not pursued. *In situ* experiments using the fluorobenzene complexes (**11a** – **11e**) in acetone-d_6 showed dissociation of the fluorobenzene ligand (based on ^{1}H NMR spectra) and slight change in shift in $^{31}P\{^1H\}$ NMR spectra with Rh-P coupling analogous to the fluorobenzene complex ($^{31}P\{^1H\}$ NMR spectrum (in acetone-d_6) shows Rh-P coupling constant of J(RhP) = 181 Hz for **11b** and **16b**). Interestingly, the larger bite-angle complexes **16d** and **16e** show only one environment in the $^{31}P\{^1H\}$ NMR spectra (assigned as the *bis*-acetone complexes), whereas **16a – 16c** are in equilibrium with the fluorobenzene adducts (**11a – 11c** respectively) with the acetone complex significantly favoured (ratios: **11a**:**16a** = 25:75; **11b**:**16b** = 24:76; **11c**:**16c** = 13:87).

Attempts to synthesise *bis*-acetonitrile complexes $[Rh(^iPr_2PNMeP^iPr_2)(MeCN)_2][BAr^F_4]$ and $[Rh(^iPr_2PCH_2P^iPr_2)(MeCN)_2][BAr^F_4]$, analogues to **16b** and **16c**, were carried out. MeCN has proven to be beneficial in hydroacylation catalysis due to its ability to stabilise the 5-coordinate acyl-hydride reaction intermediate and hence reduce the reductive decarbonylation effect even more than acetone.[7] Similarly to the acetone adduct, it was found that the isolation of the solid material was complicated and yield was significantly reduced (30 – 40 %). Also it was noted that the stability of the solid precatalyst was reduced, compared to the fluorobenzene complex, upon handling it in air.

In general, the acetone and acetonitrile substituted complexes can be synthesised and used in the hydroacylation catalysis. However due to the synthetic problems (reduced yield, complicated isolation process) and the ease of using the bench stable fluorobenzene complexes,

it was concluded that the catalytic reactions will be carried out using the fluorobenzene precatalysts **11a** – **11e**.

2.3. Catalysis

2.3.1. Catalytic Screening and Optimisation

In order to determine whether the small bite-angle isopropyl and cyclohexyl PNP or PCP motif can be used for hydroacylation catalysts a set of test reactions under relatively high catalyst loadings (10 mol%) were carried out and compared to those previously reported for PCP(^{t}Bu) complex **5** and PCP(Cy) complex **6**. As **5** and **6** showed particularly good conversions in alkene hydroacylation reactions, the initial screening was carried out using 2-(methylthio)benzaldehyde (**E**) and 1-octene (Scheme 2.13). The reaction was conducted at 10 mol% catalyst loading in DCE or acetone as the solvent (DCE allows for higher reaction temperature, b.p. = 84 °C, *cf.* acetone b.p. = 56 °C), at 0.075 M substrate concentration and **E**:1-octene ratio of 1:1.5. Based on the conversions measured by HPLC, it was established that these isopropyl and cyclohexyl substituted small bite-angle complexes **11a** – **11c** are not effective alkene hydroacylation catalysts for these β-sulfur substituted aldehydes as only up to 4 – 6.6 turnovers were seen (40 – 66% conversion) even after 1 h at 80 °C (Table 2.4). The general trend seen from the experimental results indicates that bulkier ligands are better alkene hydroacylation catalysts with PCP(^{t}Bu) complex **5** being the best with PCP(Cy) complex **6** closely following (94% and 91% conversions respectively). There was an effect of the nitrogen backbone in which isopropyl ligated complexes **11b** (PNP) and **11c** (PCP) yield very similar conversions (66% and 67% respectively), but the analogous cyclohexyl complexes **11a** (PNP) and **6** (PCP) led to considerably different conversions (40% and 95% respectively).

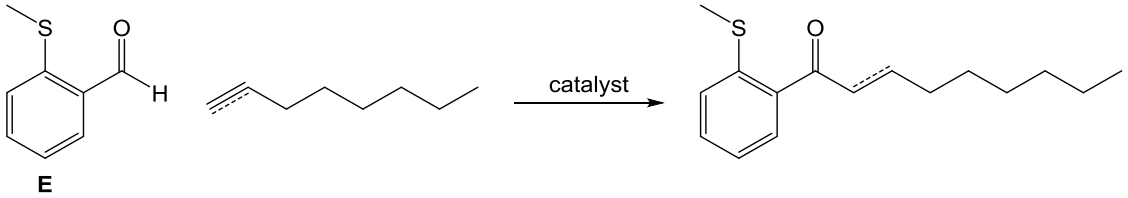

E

Scheme 2.13. Hydroacylation reaction using 2-(methylthio)benzaldehyde (**E**) and 1-octene or 1-octyne as the substrates.

Table 2.4. Comparison of a range of small bite-angle rhodium *bis*-phosphine catalysts in hydroacylation reaction of 2-(methylthio)benzaldehyde (**E**) and 1-octene or 1-octyne.

Catalyst	Substrate	Conversion / %	Time / min	Solvent	Temperature / °C
PNP(^{i}Pr) **11b**	1-octene	66	60	DCE	80
PNP(^{i}Pr) **11b**	1-octyne	100	5	DCE	25
PCP(^{i}Pr) **11c**	1-octene	67	60	DCE	80
PCP(^{i}Pr) **11c**	1-octyne	100	5	DCE	25
PNP(Cy) **11a**	1-octene	40	120	DCE	80
PNP(Cy) **11a**	1-octyne	97	5	DCE	25
PCP(^{t}Bu) **5**	1-octene	94	15	DCE	80
PCP(^{t}Bu) **5**	1-octyne	90	360	DCE	25
PCP(Cy) **6**	1-octene	91	60	DCE	80
PCP(Cy) **6**	1-octyne	95	15	DCE	25
PNP(^{i}Pr) **11b**	1-octene	64	60	acetone	55
PNP(^{i}Pr) **11b**	1-octyne	100	5	acetone	25

Conditions: 0.075M aldehyde, 10 mol% catalyst. Aldehyde:alkene/alkyne ratio = 1:1.5. Conversions measured by HPLC.

Upon screening the catalysts for their activity in alkyne hydroacylation using 2-(methylthio)benzaldehyde (**E**) and 1-octyne as substrates (Scheme 2.13), noticeably different reactivity was observed. The sluggish alkene hydroacylation catalysts, the isopropyl-substituted **11b** and **11c**, showed both high conversions and turnover frequencies. Within 5 minutes 100% conversion to the product was seen (10 mol% catalyst loading, 25 °C, DCE or acetone (**11b**), **E**:1-octyne 1:1.5). Furthermore, higher sampling frequency studies showed that at 10 mol% catalyst loading full conversion to the product is seen within 30 sec (*i.e.* turnover frequency > 1200 h^{-1}). Compared to alkene hydroacylation, the opposite trend in reactivity was observed, with less bulky isopropyl groups leading to the best conversions while bulkier cyclohexyl and tert-butyl-substituted catalysts showing slightly lower activities, with **5** giving the lowest conversion and rate. The screening reactions also included non-tethered aldehydes (*e.g.*

benzaldehyde) but this resulted in no conversion, which is presumably due to rapid decarbonylation possibly coupled with the lack of C-H activation of these untethered substrates.

Based on the screening data, it was concluded that the low bulk isopropyl substituted catalysts are useful for alkyne hydroacylation reaction, and further testing was carried out using 1-octyne. It was shown by Willis and Weller that although the above conditions are useful for screening; these are not the optimal conditions for the hydroacylation reaction using the small bite-angle catalysts.[7] In order to reduce the effect of decarbonylation, a higher concentration is beneficial, as then more alkene or alkyne is present to bias the reaction towards intermolecular hydroacylation over the decarbonylation. This is due to decarbonylation being a first order process that does not include alkene/alkyne in the rate equation, whereas the productive hydroacylation reaction is dependent on alkene/alkyne concentration. Based on this, the concentration of the aldehyde (**E**) was increased to 2 M (and the concentration of alkyne respectively to the 1:1.5 ratio). Also, as 100% conversions were seen under the screening conditions, the catalyst loading was dropped to 1 mol%. Since high temperatures are not needed for the alkyne hydroacylation reaction (Table 2.4) the studies were continued using acetone as the solvent at room temperature.[30] The optimised conditions for studying the alkyne hydroacylation reaction between **E** and 1-octyne are depicted in Scheme 2.14. The alkyne hydroacylation reaction using **E** and 1-octyne results in two products, the linear product (**F**) and the branched product (**G**).

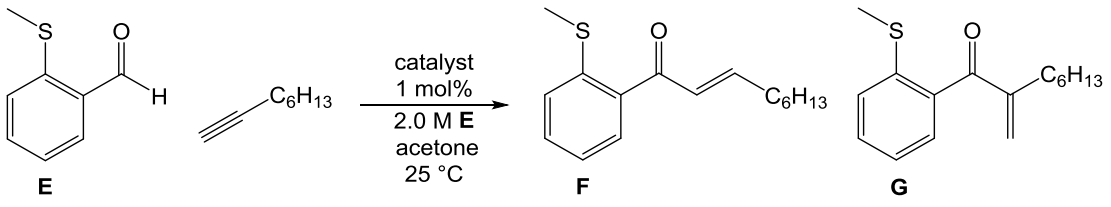

Scheme 2.14. Alkyne hydroacylation reaction using 2-(methylthio)benzaldehyde (**E**) and 1-octyne as the substrates under optimal conditions. The ratio of **E**:1-octyne is 1:1.5. At the end of the reaction linear (**F**) and branched product (**G**) were seen, while the ratio of the products is dependent on the catalyst used.

The catalytic conversions were followed using HPLC and the results are depicted in Figure 2.8. In all cases, other than the bulky PCP(^{t}Bu) catalyst (**5**) and the larger bite-angle three carbon backbone PCCCP(^{i}Pr) complex **11e**, rapid hydroacylation is initially seen, but then presumed

decarbonylation of the catalyst occurs and no further conversion of the aldehyde to the desired ketone was observed. In the case of **5** and **11e**, slightly slower initial hydroacylation reaction is observed, but the catalysts seem to have extra stability towards the reductive decarbonylation. It is posited this is due to a more sterically crowded reaction centre. For example, in direct comparison between PCP(^{t}Bu) complex **5** and the analogous PCP(^{i}Pr) complex **11c**, the tert-butyl substituents allow for a longer lived hydroacylation catalyst.

Catalyst	50% dissociation of fluorobenzene / V	Bite angle / °
11b	181	70.36(3)
11a	204	70.49(4)
11c	178	72.64(5)
6	197	72.78(3)
5	210	74.44(5)
11d	169	84.81(3)
11e	143	93.78(3)

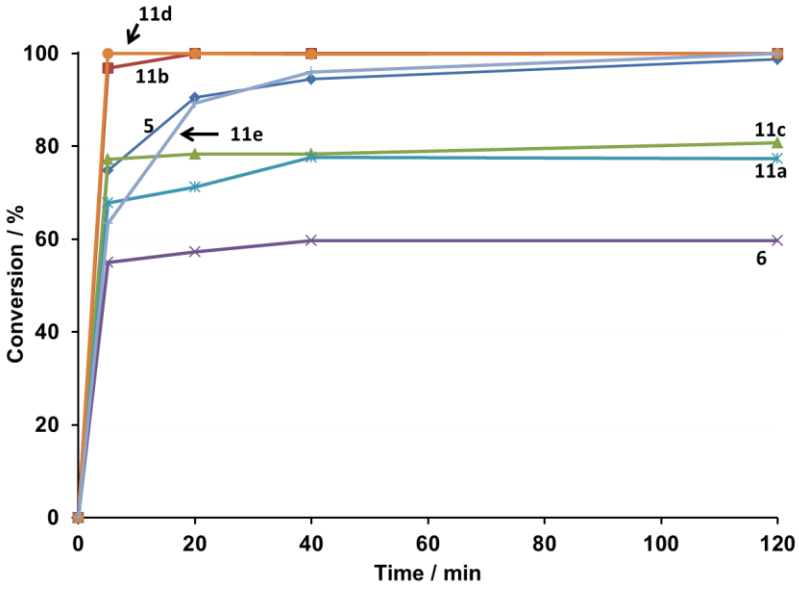

Figure 2.8. Comparison of a range of rhodium bis-phosphine small bite-angle catalysts (**11a** – **11e**, **5** and **6**) for the hydroacylation reaction of **E** and 1-octyne over time. *Conditions: 1.0 mol% catalyst loading, acetone, 25 °C, 2.0 M aldehyde, **E**:1-octyne ratio = 1:1.5. Conversions were measured by HPLC*

Table 2.5. Comparison of the catalytic activity dependence on the substituents on phosphorus atoms and the P-Rh-P bite angle.

Catalyst	P-Rh-P bite angle / °	conversion / % (after 5 min)	conversion / % (after 120 min)	linear:branch ratio (**F**:**G**)
PNP(^{i}Pr) **11b**	70.36(3)	97 (1164)[a]	100 (98)[b]	21:1
PNP(Cy) **11a**	70.49(4)	68 (816)[a]	77	69:1
PCP(^{i}Pr) **11c**	72.64(5)	77 (924)[a]	81	12:1
PCP(Cy) **6**	72.78(3)	55 (660)[a]	60	10:1
PCP(^{t}Bu) **5**	74.44(5)	74 (888)[a]	99	6:1
PCCP(^{i}Pr) **11d**	84.81(3)	100 (1200)[a]	100 (98)[b]	16:1
PCCCP(^{i}Pr) **11e**	93.78(3)	63 (756)[a]	100 (96)[b]	11:1

Conditions: 1.0 mol% catalyst loading, acetone, 25 °C, 2.0 M aldehyde, aldehyde:alkyne ratio = 1:1.5. Conversions were measured by HPLC. [a] – TOF after 5 min.[31] [b] – isolated yield.

These catalytic data allow for an interesting comparison to the ESI-MS data discussed previously (Figure 2.7). Both, the PCP(^{t}Bu) complex **5** and the PCCCP(^{i}Pr) complex **11e**, have different binding affinities towards the η^6-bound fluorobenzene ring, in comparison to **11c**. The large bite-angle complex **11e** is sterically different, hence different reactivity was expected, while based on the bite angle **5** would be expected to behave similarly to PCP complex **11c** but this is not seen experimentally. This stronger binding affinity of **5** seen using ESI-MS could be mirroring the activity during the hydroacylation catalysis, leading to slower reaction times and more stable intermediates, including more preferred binding of the alkenes or the solvent molecules, hence reducing the effect of the reductive decarbonylation and slower catalytic rate. However care must be taken in comparing the ESI-MS data from the fluorobenzene complexes with the different motifs [Rh(I) and Rh(III)] likely present during the hydroacylation reaction.

Under these conditions, all of these catalysts lead to fast hydroacylation initially, but the overall conversion depends on the initial rate in comparison to the rate of decarbonylation. Within the first 5 minutes the highest conversions were observed for the small bite-angle PNP(^{i}Pr) complex **11a** and the wider bite-angle PCCP(^{i}Pr) complex **11d**. These catalysts allow for full conversion within 5 – 10 minutes with turnover frequencies of 1164 and 1200 h^{-1}, respectively (based on the data during the first 5 min.).[31] Upon comparing PCP(^{i}Pr) and PCCCP(^{i}Pr) (**11c** and **11e** respectively) no trend with respect to the bite angle is observed. PCP(^{i}Pr) catalyst **11c** allows for 77% conversion within the first 5 minutes after which the catalyst is essentially inactive, while the use of PCCCP(^{i}Pr) catalyst **11e** results in 63% conversion within the first 5 minutes, but the catalyst remains active and allows for full conversion over 2 h whereas **11c** does not (Table 2.5). A more pronounced effect is seen upon using the catalysts containing the nitrogen backbone. In the case of both, isopropyl and cyclohexyl substituted catalysts approximately 20% increase in activity is seen: catalysts **11c** and **6** led to 81% and 60% conversion, whereas the analogous PNP catalysts **11b** and **11a** led to 100% and 77% conversions respectively. Also the effect of the substituents on the phosphorus atoms may be considered as isopropyl complexes **11b** and **11c** led to the best conversions compared to considerably lower conversions observed using cyclohexyl substituted complexes **11a** and **6**, while tert-butyl substituted **5** led to a slower yet more stable catalyst.

In order to form a comparison with the previously developed diphenylphosphino ligand based catalyst, the alkyne hydroacylation reaction was carried out using [Rh(dpp2)(C_6H_5F)][BAr^F_4] (dpp2 = bis-(1,2-diphenylphosphino)ethane) as the catalyst under the same conditions described in Figure 2.8. During the catalytic transformation, rapid decomposition of the catalyst was observed (including the possible formation of colloidal rhodium). Even over the period of 2 hours, less than 10% conversion was seen. Additionally the sterically similar, yet electronically different [Rh(1,2-bis(di(perfluorophenyl)phosphanyl)ethane)(C_6H_5F)][BAr^F_4] was used as the catalyst under the same conditions. As for the dpp2 complex, this species also led to much reduced catalytic activity compared to the alkyl PCCP catalyst **11c** (30 % conversion). These low conversions further prove the usefulness of these alkyl-substituted electron-rich *bis*-phosphine complexes (**5**, **6** and **11a** – **11e**) for the hydroacylation reaction.

As the alkyne hydroacylation can result in the formation of two regio-isomers, during the catalytic reactions, the ratio of linear to branched product was monitored (Scheme 2.14, Table 2.5). Again, the NMe in the backbone had a positive effect in comparison to CH_2; NMe containing backbones led to higher linear selectivity, with the best linear:branced ratios seen with **11a** (61:1) and **11b** (21:1), compared to the less selective analogous PCP catalysts **6** (10:1) and **11c** (12:1). The larger bite-angle catalysts **11d** and **11e** gave ratios of 16:1 and 11:1 respectively while the worst linear to branched ratio was seen with the PCP(^{t}Bu) catalyst **5** (6:1). Overall the best conversion, selectivity and overall rate was seen for the PNP(^{i}Pr) catalyst **11b**.

It is unclear why the nitrogen in the backbone aids the catalytic conversions. Previously small bite-angle PNP ligands have been used in olefin oligomerisation reactions with good catalytic results.[9, 32, 33] The authors suggest the extra activity might be due to delocalisation of the nitrogen lone pair, but so far no mechanistic insights have been found.

In order to test the catalytic activity of the highly efficient small bite-angle hydroacylation catalysts further the catalyst loading was decreased to 0.1 mol%. Unfortunately **11b** results in only 30% conversion (*i.e.* 300 turnovers). It has been demonstrated previously that the addition of 2 equivalents of acetonitrile (with respect to the catalyst) to the catalytic mixture stabilises the catalyst against decarbonylation and allows for better overall conversion.[7] Therefore the

hydroacylation reaction was carried out at 0.1 mol% catalyst loading (**11b**) plus 2 equivalents of acetonitrile. This improved the catalytic activity somewhat and 50% conversion was observed. Full conversion was obtained when catalyst loading was raised to 0.5 mol%, while 0.4 mol% still resulted in 87% conversion (both cases with 2 equivalents of acetonitrile added to the reaction mixture) (Table 2.6).

Table 2.6. Hydroacylation using **E** and 1-octyne as substrates, and **11b** as catalyst.

Catalyst loading:	0.1 mol%	0.4 mol%	0.5 mol%
Conversion / %	30	-	-
Conversion / % (2 eq. of MeCN)	50	87	100

*Conditions: **11b**, 2.0 M aldehyde, acetone, 25 °C, **E**:1-octyne ratio 1:1.5.*

The effect of changing substrate concentration was also studied using **11b**. A decrease in rate is seen upon reducing the concentration of the reaction mixture (1 mol% catalyst loading, 0 °C, acetone, 1:1.5 **E**:1-octyne). At 1.0 M of aldehyde solution the reaction results in 100 turnovers in 60 min, whereas slight drop in reactivity is observed for 0.4 M solution (94 turnovers in 60 min), while 0.1 M yields 85 turnovers in 60 min, and almost full conversion is seen only after 3.5 h (97 turnovers) (Figure 2.9).

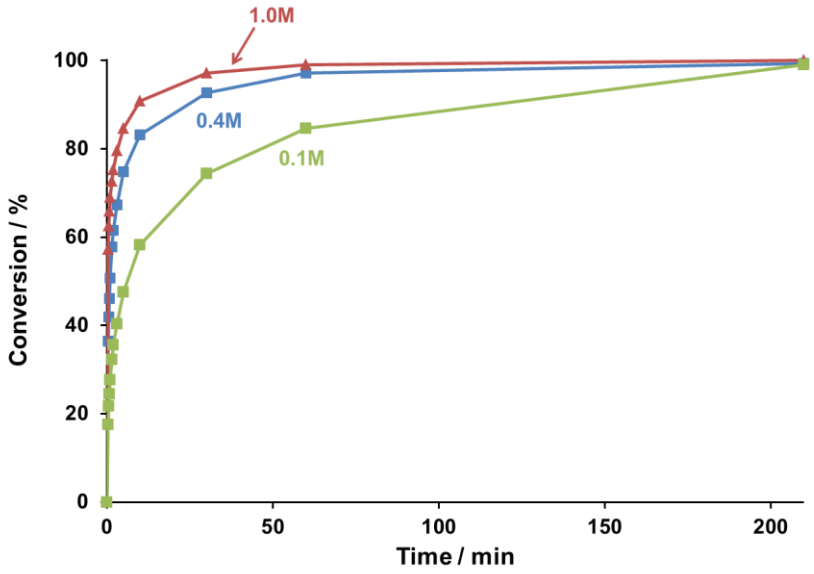

Figure 2.9. Comparison of reaction rate under different concentrations of **E** and 1-octyne. 1.0 mol% **11b**, 0 °C, **E**:1-octyne 1:1.5. The conversions were measured using HPLC.

As hydroacylation reaction is dependent on the concentration of both the aldehyde and the alkyne, the trend in the reaction rate (1.0 M > 0.4 M > 0.1 M) was expected; but also the longer lifetime of the catalyst at low concentration can be explained, as the reductive decarbonylation is dependent on the aldehyde concentration. The kinetic data does not follow any simple kinetic scenarios which presumably can be attributed to the effect of reductive decarbonylation.[7]

Even though these screening and optimising reactions did not allow us to determine the reasons behind different ligands leading to different reactivity, it was determined that the small bite-angle ligands with low steric isopropyl substituents allow for very fast and selective alkyne hydroacylation catalysis, but they also are readily deactivated.

2.3.2. Mechanistic studies

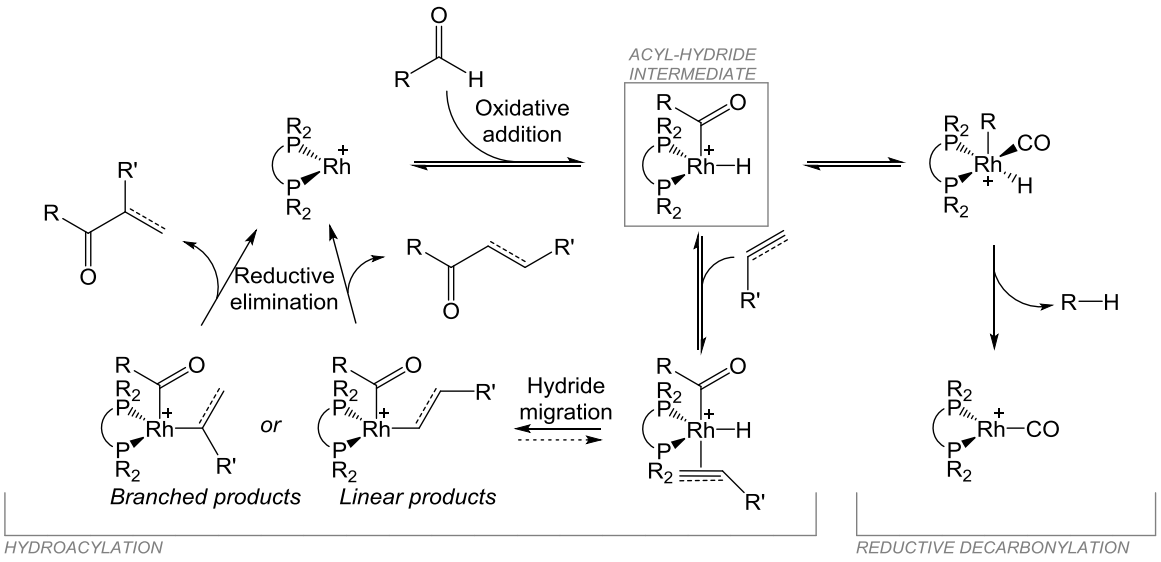

Scheme 2.15. General mechanism of hydroacylation reaction and the side reaction – reductive decarbonylation.

To understand the catalytic activity, selectivity and decomposition pathways of these catalysts, a mechanistic investigation was carried out, involving labelling studies, variable temperature NMR spectroscopy, ESI-MS and kinetic studies. The studies were based on the knowledge about general mechanism of the hydroacylation mechanism depicted in Scheme 2.15.[30]

2.3.2.1. *Reductive Decarbonylation*

The catalytic data show that the complexes **11a** – **11e** are very fast hydroacylation catalysts, but it was also observed that inactive catalysts are formed during the catalysis. As decarbonylation using rhodium *bis*-phosphine complexes has been shown to occur previously,[30] decarbonylation studies using **11a** – **11e** and **E** were undertaken in acetone-d_6.

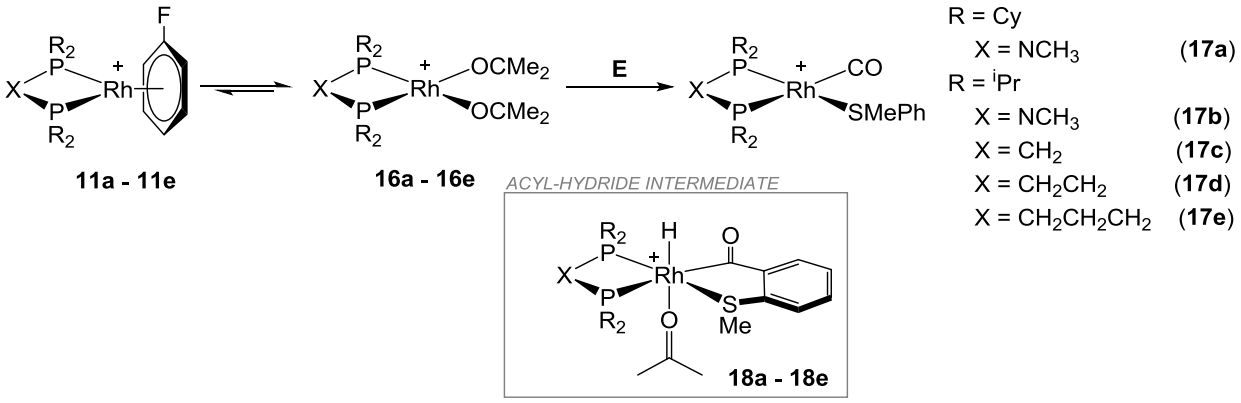

Scheme 2.16. Synthesis of the decarbonylation products (**17a** – **17e**) via the initial formation of the *bis*-acetone complexes (**16a** – **16e**) followed by the formation of the acyl-hydride intermediate (**18a** – **18e**), which can then undergo the reductive decarbonylation reaction to yield the desired product. The $[BAr^F_4]^-$ counter-anion is not pictured for clarity.

The absence of 1-octyne allows for the decarbonylation pathway to occur more cleanly yielding the expected reductive decarbonylation products of [Rh(*bis*-phosphine)(SMePh)(CO)][BAr^F_4], **17a** – **17e** (Scheme 2.16) and the formation of $[Rh(bis\text{-phosphine})(CO)_2]^+$ in small quantities can be detected by ESI-MS. Formation of the rhodium carbonyl complexes **17a** – **17e** was confirmed by NMR spectroscopy (which also showed the formation of unidentified products), ESI-MS, and in case of **17b**, an X-ray structure and ESI-MS/MS data were obtained. The crystal structure shows a pseudo square planar Rh(I) structure (Figure 2.10), analogous to the previously reported structure [Rh($^tBu_2PCH_2P^tBu_2$)(SMePh)(CO)][BAr^F_4].[7]

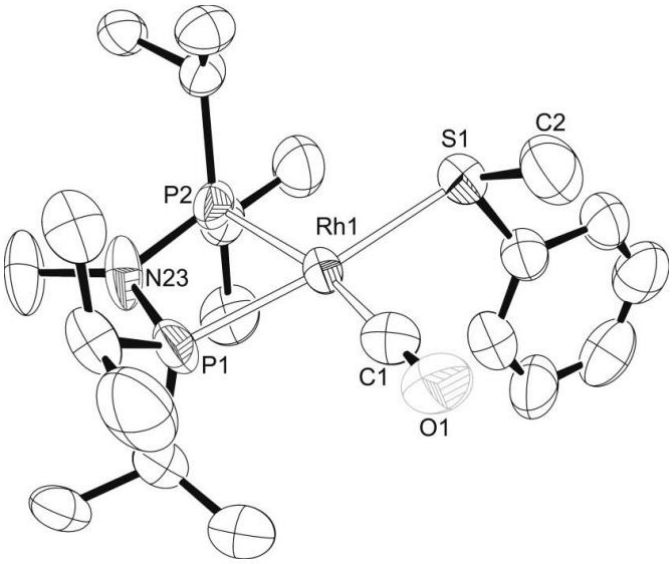

Figure 2.10. Solid state structure of the cation **17b**. Displacement ellipsoids depicted at the 50% probability level. Hydrogen atoms, $[BAr^F{}_4]^-$ anion and disordered components (CO ligand) omitted for clarity. All unlabelled atoms are carbons. Key bond lengths (Å) and angles (°): Rh1-P1, 2.2394(14); Rh1-P2, 2.3310(15); Rh1-C1, 1.889(10); Rh1-S1, 2.3753(16); P1-Rh1-P2, 70.24(6); P1-N23-P2, 102.7(2).

The $^{31}P\{^1H\}$ NMR spectra of the decarbonylation products **17a** – **17e** showed a distinctive set of doublet of doublets [*e.g.* for **17b**, δ 91.4 *J*(RhP) 125, *J*(PP) 59 Hz; δ 69.5 *J*(RhP) 114, *J*(PP) 59 Hz] while no hydride resonances were observed in the ^1H NMR spectra. The isolated rhodium carbonyl complex **17b** was inactive as a catalyst for hydroacylation. To confirm the formation of the decarbonylation products via the C-H activated acyl-metal-hydride intermediate **18b** (Scheme 2.16), *in situ* NMR spectroscopy experiments were performed. Following the reaction of **11b** with **E** (using ^1H NMR spectroscopy) at room temperature in acetone-d_6 the acyl-hydrido species **18b** immediately formed and was identified by a broad hydride signal at δ –20.22 which parallels to the result obtained using the tert-butyl complex **5** and **E** [δ –20.29].[7] Upon mixing the reagents at –78 °C, followed by warming the sample to the room temperature for 5 seconds and then placing the sample into a pre-cooled NMR spectrometer (–60 °C), the ^1H NMR spectrum shows a distinctive hydride environment at δ –20.09 as a doublet of doublet of doublets, due to coupling to ^{103}Rh and two *cis* ^{31}P environments. The $^{31}P\{^1H\}$ NMR spectra at –60 °C, showed two phosphorus resonances, δ 92.2 [*J*(RhP) 133 Hz, *J*(PP) 36 Hz, *J*(PH) 13 Hz)], δ 83.5 [*J*(RhP) 63 Hz, *J*(PP) 36 Hz, *J*(PH) 9 Hz)]. These data are consistent with a Rh(III) centre and

with one phosphorus environments being *trans* to a high *trans* influence acyl ligand which leads to a weaker rhodium-phosphine bond, and hence smaller *J*(RhP) value is seen.[34] These data are very similar to those previously reported for the analogous system using complex **5** as the starting material.[7, 19, 35] It was not possible to isolate **18a** – **18e** or to obtain clean NMR spectra due to the rapid decay of these acyl-hydride intermediates. Intermediate **18b** decays readily at room temperature to give **17b** (50% consumption after 5 min) and similar decay is also seen upon using **18a** and **18c** – **18e**. A significantly longer time scale for the same process was reported for the tert-butyl substituents containing complex **5**, where the $t_{1/2}$ = 1.79 h for a first order process. This difference in the rate of decarbonylation reflects the difference in the hydroacylation reaction rate of **5** as shown in Figure 2.8. These decay times are particularly noteworthy upon comparison with the hemilabile [Rh(DPEphos)]$^+$ fragment that significantly slows down the decarbonylation pathway ($t_{1/2}$ = 160 h) due to the formation of the 6-coordinate acyl-rhodium-hydride intermediate.[36, 37] During the decarbonylation step of **18b** and **18c** another set of hydride signals were seen in the ^{1}H NMR spectrum which were speculated to correspond to C-H activation or agostic interactions between the metal centre and the isopropyl substituents.[38, 39] This extra reactivity did not allow for the observation of simple first order kinetics for the decarbonylation process, as would be expected.[7] The reasons for this fast decarbonylation of **18** are not straightforward, but by comparing the PNP(^{i}Pr) and PCP(^{i}Pr) ligands with the analogous PCP(^{t}Bu), it is expected that steric factors are the primary cause. Caulton has also demonstrated, using an iridium phosphine complex, that reductive elimination can be aided by formation of an agostic interaction which could point towards the reasons behind the relative instability of these isopropyl substituent containing complexes.[40] Furthermore the observation of additional hydride signals may point to C-H activation that would follow from an agostic intermediate.

2.3.2.2. *Kinetic Studies*

Due to the fast rate of decarbonylation and hence reduction in catalyst concentration during the catalytic reaction, no simple kinetic scenarios about the product formation were obtained.

Similar to Bosnich's "Black box" problem, it was proposed that the use of labelled reagents would allow insight into the kinetics of this system.[41] The reactions were carried out at 0 °C and at low concentration (0.1 M) in order to permit the reaction to be followed by NMR spectroscopy and HPLC at 1.0 mol% catalyst loading (**11b**). The use of **E** and 1-d-octyne resulted in essentially no change in overall rate compared to non-deuterated alkyne (100 turnovers in 3.5 h). Whereas the use of deuterated aldehyde (d-**E**) significantly reduced the rate, resulting in 68 turnovers in 5 h.

During the first 30 seconds of the reaction the decomposition of the catalyst was proposed to be negligible, thus the initial stages of the reaction between **E** and 1-octyne using **11b** as the catalyst were probed. Under the comparison conditions (1.0 mol% catalyst loading, *i.e.* 0.001 M **11b**, **E**:1-octyne ratio of 1:1.5, 0 °C) the initial rate of 1.3 ± 0.4 x 10^{-3} M.s^{-1} and 100 overall turnovers were seen. If a 10 fold excess of 1-octyne was used, the increase in initial rate to 4.0 ± 0.2 x 10^{-3} M.s^{-1} was observed and the reaction essentially reached completion (96 turnovers). 10 fold excess of aldehyde (**E**) reduced the rate of catalysis to 0.4 ± 0.2 x 10^{-3} M.s^{-1} and led to only 79 turnovers. The reduction in conversion is observed due to excess aldehyde promoting the irreversible reductive decarbonylation (previously commented on by Dong *et. al.*).[42] while the excess of alkyne allows for it to be more readily coordinated and hence increase the relative rate of hydroacylation. However, these initial rates do not show simple order relations, suggesting a more complex mechanistic scenario. Based on initial rates and by using deuterated substrates the kinetic isotope effect k_H/k_D, of 1.6 ± 0.2 was calculated. This small KIE is consistent with the previously reported results: the PCP(^{t}Bu) catalyst **5** that works under pseudo first order conditions for alkene hydroacylation shows a KIE of 1.4 ± 0.2 upon using d-**E**, while the $[Rh(DPEphos)]^+$ fragment led to a negligible KIE of 1.1 ± 0.1 for alkyne hydroacylation reaction using d-**E**.[7, 36] This data does not allow us to discriminate between reductive elimination or hydride migration step being turnover limiting. Both steps have been reported as rate limiting for hydroacylation in the literature previously.[7, 30, 43] What can be determined, is that irreversible oxidative addition is not rate limiting for the hydroacylation reaction upon using these small bite-angle catalysts, as for this to be the case a much higher KIE would be expected.[44]

2.3.2.3. *Selectivity Studies*

Based on previous publications and the results above it was proposed that the deuterated reagents used in the kinetic studies can also be helpful in understanding the origin of the selectivity of the small bite-angle isopropyl-substituted catalysts. Based on the position of the deuterium in the starting material, and where it ends up in the product, it is possible to further understand the individual steps in the reaction mechanism (Figure 2.11).

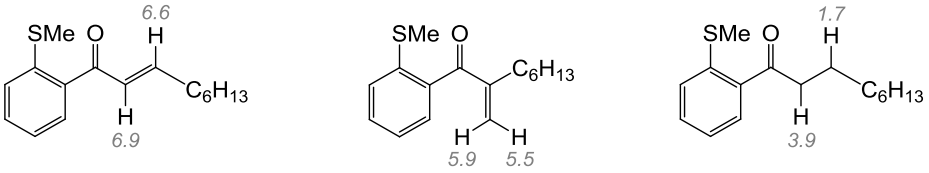

Figure 2.11. Characteristic ^{1}H NMR shifts for alkyne and alkene hydroacylation products. The coupling pattern of these shifts is affected by any deuteration occurring in these positions.

The first reactions were carried out using linear selective catalyst **11b** (linear:branched ratio of 21:1). Using d-**E** and 1-octyne, deuteration only in the β-position of the product was observed and the oppositely labelled reaction using **E** and d-1-octyne, resulted in the formation of the product with deuterium exclusively in the α-position (Scheme 2.17). These data indicate that no deuterium scrambling is occurring during the formation of the linear product.

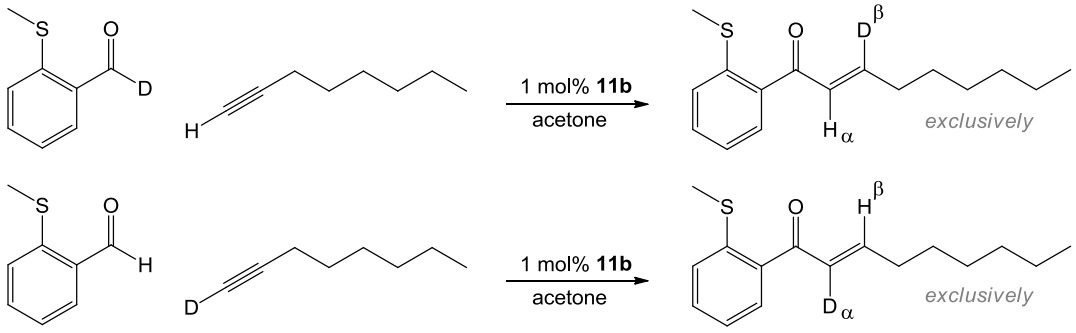

Scheme 2.17. Deuterium labelling experiments using d-**E** and d-1-octyne as substrates and the linear selective catalyst **11b**.

These results echo the deuterium labelling studies carried out for the linear alkyne hydroacylation reaction using $[Rh(DPEphos)]^{+}$ fragment as the catalyst.[36] At the same time, it

has been shown that for alkene hydroacylation reaction using **5** and d-**E**, deuterium could be in both the α- and β-position due to reversible insertion and β-elimination.[7] Even if this reversibility were occurring, for linear alkyne hydroacylation it cannot be demonstrated using deuterated substrates, as in the case of linear selectivity, even if the reverse process (β-hydrogen elimination) is occurring, the deuterium would end up in the same position (Scheme 2.18).

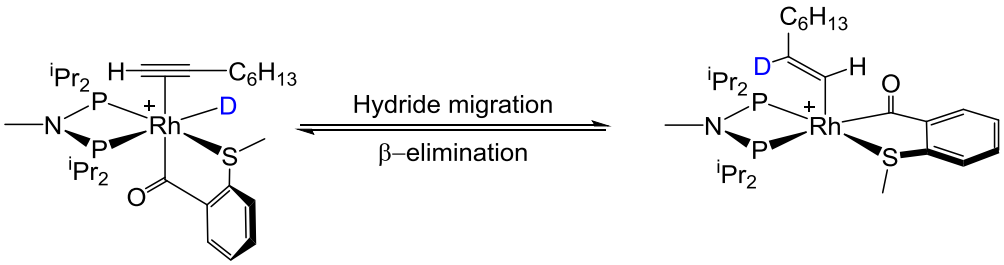

Scheme 2.18. Deuterium labelling study for the reversibility of the hydride migration step in alkyne hydroacylation. The $[BAr^F_4]^-$ counter-anion is not pictured for clarity.

In contrast to the linear pathway, deuterium scrambling for the branched pathway is observed. The mechanism and reversibility of the migration step can be studied using a catalyst that allows for the formation of both linear and branched products in observable quantities. To probe this complex **5** was used as the catalyst (linear:branced ratio of 6:1). Using **5**, d-**E** and 1-octyne, scrambling was observed in the case of the branched product, but in the linear ketone product only β-deuteration was observed (Scheme 2.19). This is presumably occurring via the branched-alkenyl intermediate undergoing the isomerisation process that scrambles the *gem*-H/D (Scheme 2.19, **19**). As the scrambling can be seen experimentally, but no deuterium in the α-position of the linear product, it can be determined that β-elimination from the branched intermediate is not occurring. If it were it would allow for the insertion to the linear product which would in turn lead to the formation of some α-deuterium containing linear product. The combination of these experimental data show that isomerisation in the branched product is occurring while β-elimination is not.

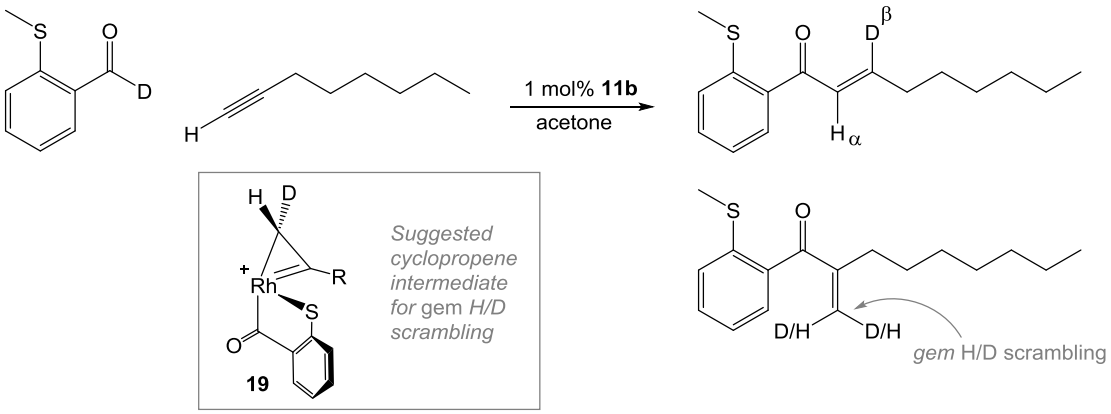

Scheme 2.19. Deuterium labelling studies using d-**E** and 1-octyne, and a small bite-angle catalyst. The $[BAr^F_4]^-$ counter-anion is not pictured for clarity.

The kinetic modelling for $[Rh(DPEphos)]^+$ supports the insertion for the linear and the branched pathways being irreversible for alkyne hydroacylation. It has also been possible to use the $[Rh(DPEphos)]^+$ fragment to suggest that the deuterium scrambling occurring in the branched route is due to a metallacyclopropene intermediate (Scheme 2.20, **19**). During the studies of $[Rh(DPEphos)(acetone)_2][BAr^F_4]$ as a hydroacylation catalyst (Scheme 1.44), a stable intermediate *anti*-d-**20** was synthesised by using **E** and the deuterated electron-deficient alkyne $DCCAr^F$ {Ar^F = 3,5-$(CF_3)_2C_6H_3$} and no deuterium scrambling was observed. Similarly, the reverse labelled reaction, using **d-E** and $HCCAr^F$, led exclusively to the *syn*-d-**20** intermediate. Upon heating the reaction mixture to 60 °C, the reaction proceeded to give the expected branched product, but with deuterium being in both *syn*- and *anti*-positions. A mechanism suggested for this isomerisation is via the metallacyclopropane intermediate (Scheme 2.19, **20**). This motif has been observed previously for intramolecular alkyne hydroacylation and alkene hydrosilylation.[45, 46]

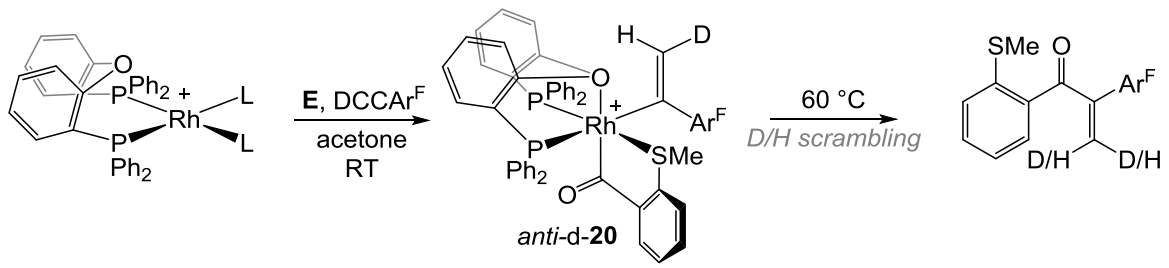

Scheme 2.20. Formation of the stable complex *anti*-d-**20** and the subsequent deuterium scrambling that leads to branched product. L = acetone. The $[BAr^F_4]^-$ counter-anion is not pictured for clarity.

In order to further understand the selectivity, and in particular the reversibility of the migration step for the linear pathway of the alkyne hydroacylation reaction using these small bite-angle complexes, an investigation using an acyl-rhodium-chloride intermediate was carried out. The acid chloride reagent (Cl-**E**) has been used previously to mimic the acyl-metal-hydride intermediate (**18b**) and in particular to obtain crystal structures, as unlike the acyl-hydride intermediate (**18b**), **21b** is a highly stable complex (*i.e.* it does not undergo reductive decarbonylation). It was postulated that the acyl-chloride intermediate (**21b**) could react with hex-1-en-1-yllithium allowing for the linear hydroacylation product if the elimination step is not occurring (*i.e.* hydride migration is not reversible). Whereas if the step was reversible the formation of the branched product would also be expected (Scheme 2.21).

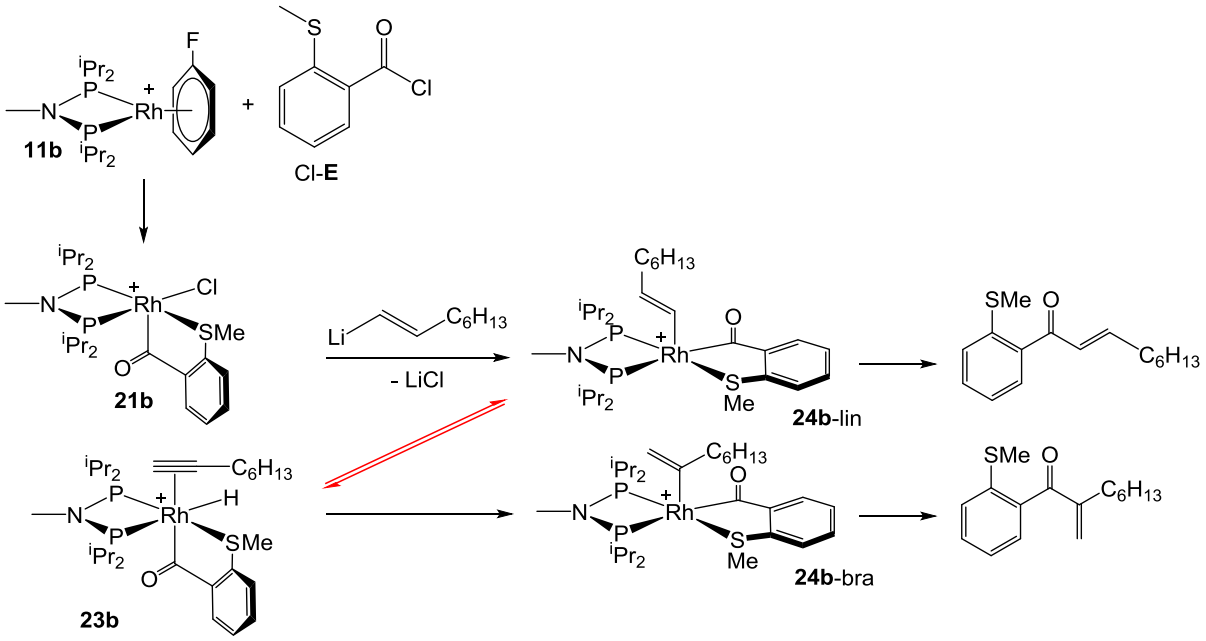

Scheme 2.21. Postulated reactivity of the acyl-chloride intermediate (**21b**) with the hex-1-en-1-yllithium. The $[BAr^F_4]^-$ counter-anion is not pictured for clarity.

As the mechanistic studies were carried out using the PNP(^{i}Pr) complex **11b**, the acyl-chloride PNP(^{i}Pr) complex **21b** was synthesised by a reaction of **11b** with the acid-chloride, 2-(methylthio)benzoyl chloride (Cl-**E**) (Figure 2.12) in CH_2Cl_2.[7] The formed complex was isolated as yellow solid and characterised using standard analytical methods. The $^{31}P\{^1H\}$ NMR spectrum exhibits two doublets of doublets at δ 73.2 [J(RhP) = 120 Hz and J(PP) = 36 Hz] and δ 69.8 [J(RhP) = 120 Hz and J(PP) = 36 Hz]. Crystals suitable for X-ray crystallography were obtained

by layering the fluorobenzene solution of **21b** with hexane (Figure 2.12). Unfortunately the crystals were not high enough quality to obtain publishable data, but it did confirm connectivity. The solid state structure is in agreement with the solution data acquired. **21b** adopts a 5-coordinate rhodium(III) *pseudo*-square based pyramidal structure where one of the phosphorus atoms is *trans* to the thio-ether and the other phosphorus atom is *trans* to the chloride, while the acyl group is *trans* to the vacant site. This leads to the Rh-P bond lengths of Rh1-P1, 2.2270(2); Rh1-P2, 2.2264(18) reflecting to the ^{31}P NMR data showing the same Rh-P coupling constants for both phosphorus atoms.

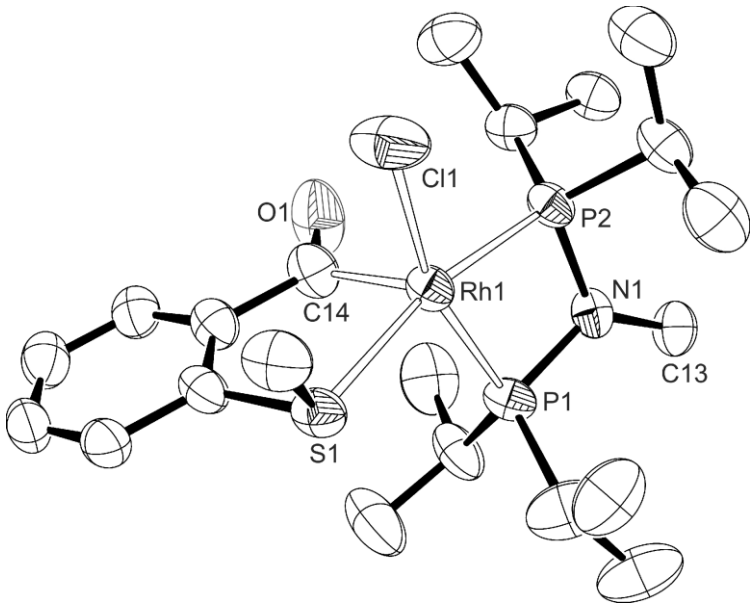

Figure 2.12. Solid state structure of the cation **21b**. Displacement ellipsoids depicted at the 50% probability level. Hydrogen atoms and $[BAr^F_4]^-$ anion and are omitted for clarity. All unlabelled atoms are carbon atoms. Key bond lengths (Å) and angles (°): ; Rh1-Cl, 2.318(2); Rh1-S1, 2.3975(18); Rh-C14, 1.962(8); P2-Rh1-P1, 70.92(7); C14-Rh-S1, 86.7(2). The X-ray data is poor quality and the structure presented here is only to confirm the bonding modes.

ESI-MS shows a peak at m/z = 552.08 (calc. m/z = 552.09) showing the correct isotopic pattern characteristic to a chlorine containing species. Analogous data have been observed previously upon using $[Rh(dpp2\text{-}o\text{-}^iPr)(acetone)_2][BAr^F_4]$ [where dpp2-*o*-^{i}Pr = 1,2-bis(bis(2-isopropylphenyl)phosphanyl)ethane].[22] The lithium reagent was synthesised from the corresponding 1-iodo-octene using ^{t}BuLi (this reaction does not occur upon using ^{n}BuLi or lithium metal instead). Unfortunately, upon addition of the acyl-chloride complex (**21b**) to the

lithium reagent (in benzene or Et_2O solvent), no reaction was observed. This lack of reactivity can probably be attributed to high stability of the acyl-chloride complex (**21b**).

2.3.2.4. *Proposed mechanism*

Based on the above catalytic and mechanistic studies and previous work reported,[7, 41-43, 47] a mechanism for the alkyne hydroacylation reaction using β-S tethered aldehyde **E** and 1-octyne and the small bite-angle PNP(^{i}Pr) catalyst **11b** is proposed in Scheme 2.22. The first step of dissolving the fluorobenzene complex **11b** in acetone (**i**) leads to an equilibrium between the *bis*-acetone complex **16b** and **11b**. The former complex (**16b**) readily reacts with the sulfur-tethered aldehyde **E** (**ii**), indicated by instant colour change of the solution from pale yellow to deep brown. It was not possible to confirm the formation of the aldehyde coordinated intermediate (**22b**) by any analytical methods, but following the reactions using ^{1}H NMR spectroscopy an immediate formation of an acyl-rhodium-hydride complex **18b** was observed (**iii**) (only if there is no alkyne present in the reaction mixture).

During the catalytic process (*i.e.* alkyne in the reaction mixture) there is no sign of acyl-hydride intermediate **18b** by ^{1}H and ^{31}P{^{1}H} NMR spectroscopy, even at reduced temperature. As discussed above, the acyl-hydride intermediate can then either reductively decarbonylate (**viii**) to form the inactive rhodium-carbonyl complex (**17b**) or via the coordination of the alkyne (**iv**) to form the alkyne bound complex **23b**. **23b** can then result in either the branched intermediate **24b**-bra or the linear intermediate **24b**-lin. This occurs via hydride migration (**v**) which is irreversible in the case of branched pathway (based on labelling studies), while the reversibility of the linear pathway cannot be confirmed, but based on literature reports, it also is expected to be irreversible as reversible hydride insertion for alkynes is rare.[48]

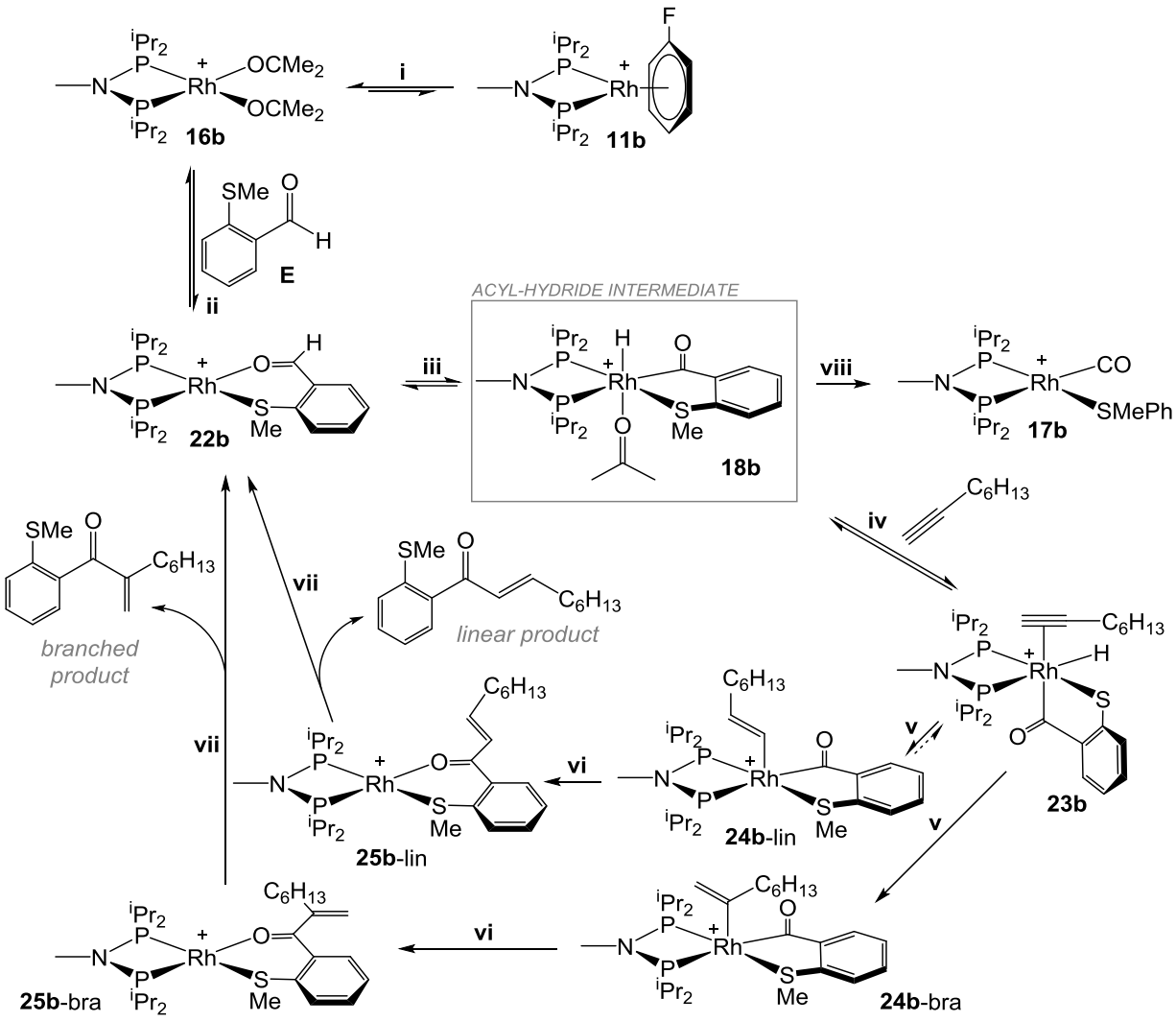

Scheme 2.22. Proposed mechanism of intermolecular alkyne hydroacylation of **E** and 1-octyne using **11b** as the catalyst. The $[BAr^F_4]^-$ counter-anion is not pictured for clarity.

The hydride migration is followed by reductive elimination (**vi**) which results in the product bound complex (**25b**). This was found to be the resting state of the catalytic cycle (**vii**). The $^{31}P\{^1H\}$ NMR spectrum, at –80 °C, of a sample where the reagents were mixed at –78 °C (10 mol% **11b**, acetone-d_6, 0.075M) and allowed to react for 10 seconds at room temperature, shows a pair of doublet of doublets with coupling to ^{103}Rh and ^{31}P [δ 75.7, *J*(RhP) 132Hz, *J*(PP) 65Hz; δ 65.9, *J*(RhP) 125Hz, *J*(PP) 65Hz] suggesting the formation of the product bound to the metal centre, $[Rh(^iPr_2PNMeP^iPr_2)(\kappa^2\text{-}O,S\text{-}CO(C_6H_4SMeCH{=}CH(CH)_5Me)][BAr^F_4]$ (**25b**). This data was re-enforced by ESI-MS data showing only one organometallic species during the catalytic process with the m/z = 628.21 (calc. for **25b**, m/z = 628.24). Furthermore the ESI-MS isotopic

pattern is fully consistent with the proposed molecular formula. Analogous complexes have been identified previously in the Weller group using (*o*-^{i}PrC$_6$H$_4$)$_2$PCH$_2$CH$_2$(*o*-^{i}PrC$_6$H$_4$)$_2$ and (^{t}Bu)$_2$PCH$_2$(^{t}Bu)$_2$ ligands.[7, 22] Upon allowing the solution containing the product bound intermediate **25b** to reach room temperature, full conversion of the aldehyde **E** to ketone product was observed by NMR spectroscopy (with some decarbonylation product also present). Confirmation of the product bound complex **25b** was achieved by addition of the isolated linear hydroacylation product, (E-1-(2-methylthio)-phenyl)non-2-ene-1-one to **11b**. At –80 °C ^{31}P{^{1}H} NMR showed a spectrum identical to the one obtained for the ^{31}P{^{1}H} NMR spectrum acquired (at –80 °C) during the catalytic reaction (Figure 2.13).

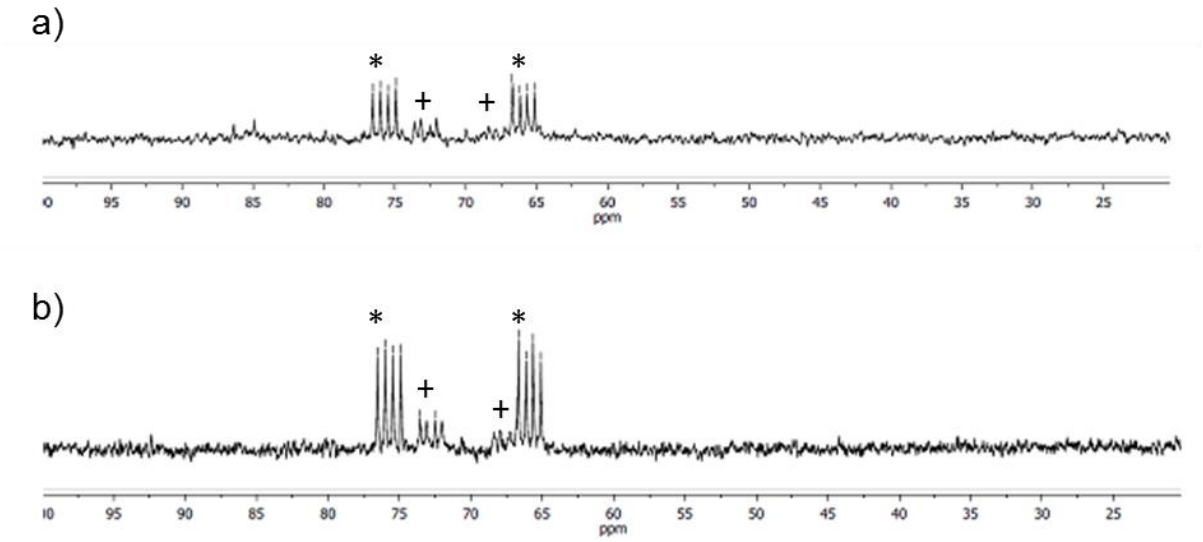

Figure 2.13. The direct comparison reaction between a) **11b** and the isolated hydroacylation product b)^{31}P{^{1}H} NMR spectrum (–80 °C) of the resting state. * - major isomer, + - minor isomer.

The extra resonances seen in the spectra were assigned to a minor isomer; possibly a stereoisomer due to the SMe group or coordination between the metal centre and the double bond present in the product. The ESI-MS data shows the formation of one product in both cases. Although the product-bound species is the resting state of the catalytic transformation, the reaction is not inhibited by the product. This was shown by addition of the product (**F**) to the catalytic mixture under the optimal conditions (1 mol% **11b**, 2.0 M aldehyde, **E**:1-octyne:isolated hydroacylation product ratio 1:1.5:1, acetone, 25 °C), and no change in reactivity or rate was observed (essentially full conversion was observed in 5 minutes, *cf.* Figure 2.8).

2.3.2.5. *Real-time ESI-MS Studies*

Under the catalytic conditions we were not able to follow the formation of the resting state or any other intermediates during the course of reaction at room temperature. Therefore a collaborative project between the Weller group and the McIndoe group (University of Victoria, Victoria, BC) was established. The McIndoe group are interested in organometallic catalysis and synthesis, but in particular the use of novel mass spectrometric-led techniques for catalyst discovery, mechanistic information and reaction optimisation.[49, 50] In order to follow the reaction by mass-spectrometry, a modified tagged version of the aldehyde was synthesised (mod-**E**). By using this charged aldehyde it was possible to follow the fate of the aldehyde (Scheme 2.23), the cationic catalyst fragment and the formation of the product (or any side products) or intermediates during the reaction.

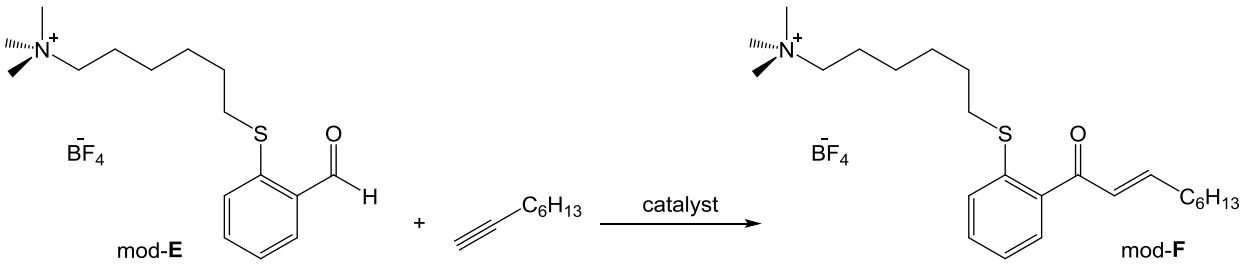

Scheme 2.23. Hydroacylation reaction using charged aldehyde (mod-**E**) as the starting aldehyde. *Conditions: 10 mol% catalyst loading, acetone, 25 °C, 0.015 M aldehyde, mod-**E**:1-octyne ratio = 1:1.5.*

Obtained data helped us confirm some previously studied intermediates, which was not possible using conventional analytical methods (*i.e.* HPLC and NMR spectroscopy) due to the relatively long times needed to sample and due to the lower dynamic range (*i.e.* ESI-MS can cover 3 orders of magnitude).

For ESI-MS, very dilute conditions are needed, hence the first challenge was to change from the established concentrated systems (as high as 2 M) to diluted catalytic reactions with concentration as low as 0.015 M (with respect to the aldehyde). At 10 mol% catalyst loading (0.0015 M catalyst), at room temperature, the reaction still allowed for full conversion. Initial tests were carried out by dissolving the fluorobenzene complex **11b** in acetone, and immediately the formation of the *bis*-acetone complex **16b** was seen by ESI-MS (m/z = 482.18).

Additionally, the species corresponding to the *mono*-acetone complex was observed (m/z = 424.14) at half the relative concentration compared to **16b**, presumably due to the low stability of the *bis*-acetone complex under ESI-MS conditions. No signal for the fluorobenzene precatalyst **11b** was observed by ESI-MS upon dissolving **11b** in acetone.

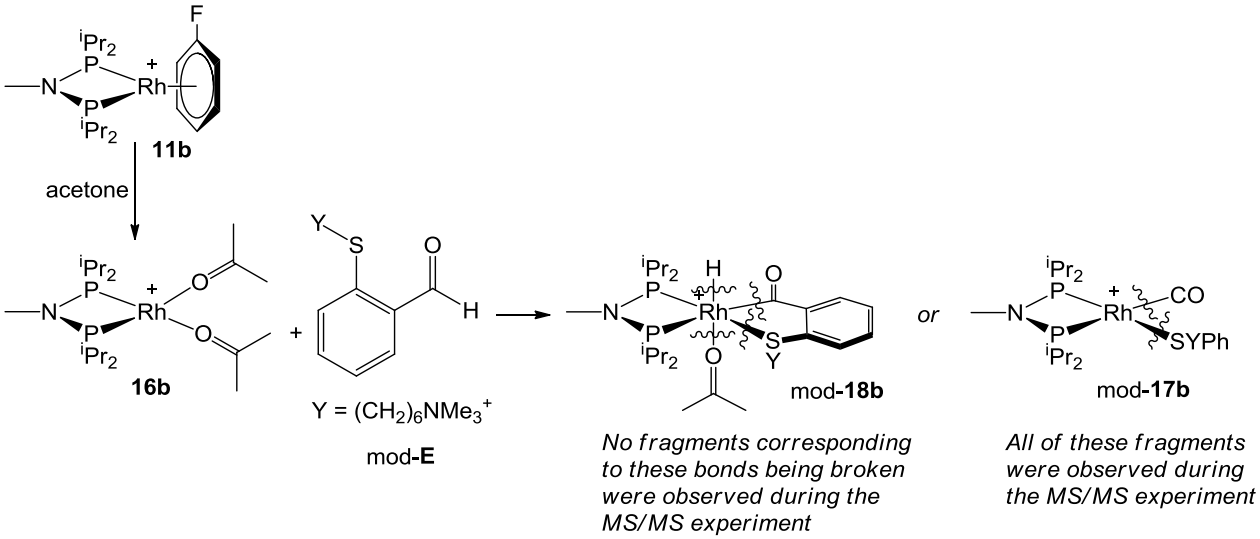

Scheme 2.24. ESI-MS/MS experiment following the reaction between mod-**E** and catalyst **11b**. The $[BAr^F_4]^-$ and $[BF_4]^-$ counter-anions are not pictured for clarity.

If only aldehyde (mod-**E**) was added to the reaction mixture in acetone, the formation of the acetone complexes (*mono* and *bis*-acetone complexes) and a complex with mass of m/z = 323.13 was observed, which can correspond to aldehyde bound (mod-**22b**), acyl-hydride (mod-**18b**) or decarbonylation product (mod-**17b**) as the calculated masses for all of these species are m/z = 323.13. Upon carrying out MS/MS experiments using this mixture (in particular on the peak at 323.13) fragmentation occurs and the following signals were observed: m/z = 252.16, 366.07 and 394.07. The peak at m/z = 252.16 corresponds to the starting aldehyde (mod-**E**) missing a CO-group, *i.e.* $[C_6H_5S(CH_2)_6NMe_3]^+$ (calc. m/z = 252.18) while the peak at 394.07 corresponds to the remaining rhodium *bis*-phosphine fragment with one carbonyl group, $[Rh(^iPr_2PNMeP^iPr_2)(CO)]^+$ (calc. m/z = 394.09). The peak at 366.07 corresponds to the mass of the $[Rh(^iPr_2PNMeP^iPr_2)]^+$ fragment (calc. m/z = 366.10). These three fragments correspond to the potential bonds broken in the case of the decarbonylation product mod-**17b**, while these results would not be expected in the case of fragmentation of mod-**18b** or mod-**22b** (Scheme 2.24). No peaks corresponding to potential fragments from the acyl-hydride intermediate (mod-

18b) were identified, but this was expected as under these alkyne free conditions, using **11b** as the catalyst, decarbonylation proceeds rapidly (Scheme 2.24).

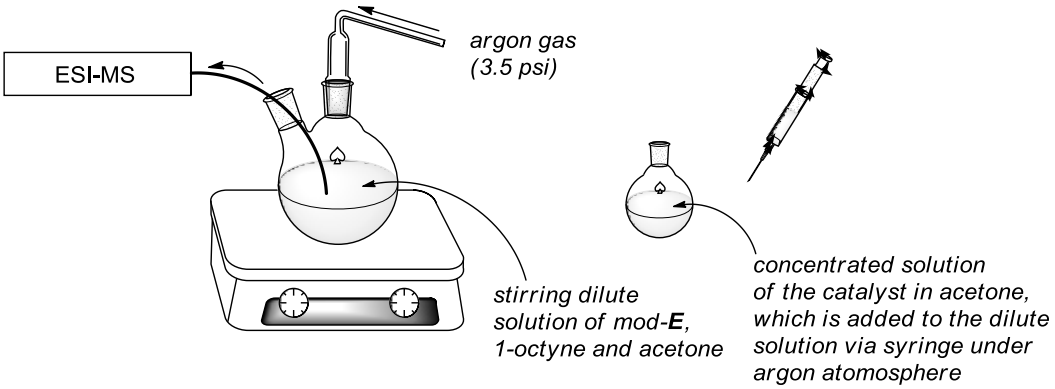

Figure 2.14. Set-up of the *in situ* in time ESI-MS experiments.

To follow the hydroacylation reaction *in situ* by ESI-MS, the reaction was set up initially with a solution of aldehyde (mod-**E**) and 1-octyne in acetone. This was allowed to run through the ESI-MS, and when stabilised conditions were seen (during the first 2 minutes), the catalyst (dissolved in a small amount of acetone) was added to the mixture (Figure 2.14). Immediately upon injection of the catalyst signals corresponding to the *bis*- and *mono*-acetone complexes were seen (m/z = 482.18 and 424.14 respectively). Also a signal for the product bound species, mod-**25b** was observed (m/z = 378.13), this had been shown previously to be the resting state of the catalytic cycle (Section 2.3.2.4). Additionally, the formation of the decarbonylation product (mod-**17b**) (m/z = 323.13) and the final metal-free ketone product (**F**) were noted (m/z = 390.21). The combined data from this reaction is depicted in Figure 2.15.

Figure 2.15 shows that immediately after the addition of the catalyst, a small amount of the decarbonylation product (mod-**17b**) is seen, but over time this peak disappears. A similar scenario was observed when only the aldehyde (mod-**E**) was added to the catalyst (*i.e.* no 1-octyne in the reaction mixture). The reasons behind this reactivity are not fully understood as the ESI-MS data did not show conversion of mod-**17b** to any new identifiable products. It has been demonstrated that the decarbonylation product (**17b**) is affected by water in the reaction mixture. Separate ESI-MS studies showed that adding water to the reaction mixture (1 – 10 eq. with respect to the aldehyde) led to the substantial reduction of the intensity of the

decarbonylation product peak, and the formation of unidentified species, while water in the reaction mixture was not seen to affect the hydroacylation catalysis. Water for these *in situ* ESI-MS experiments is a likely additive, as under such low concentrations, even 99.99% pure acetone has enough water in it to affect the results (approximately 4 eq. of water with respect to the rhodium species). A control-reaction using non-cation-tethered aldehyde (**E**) showed similar behaviour.

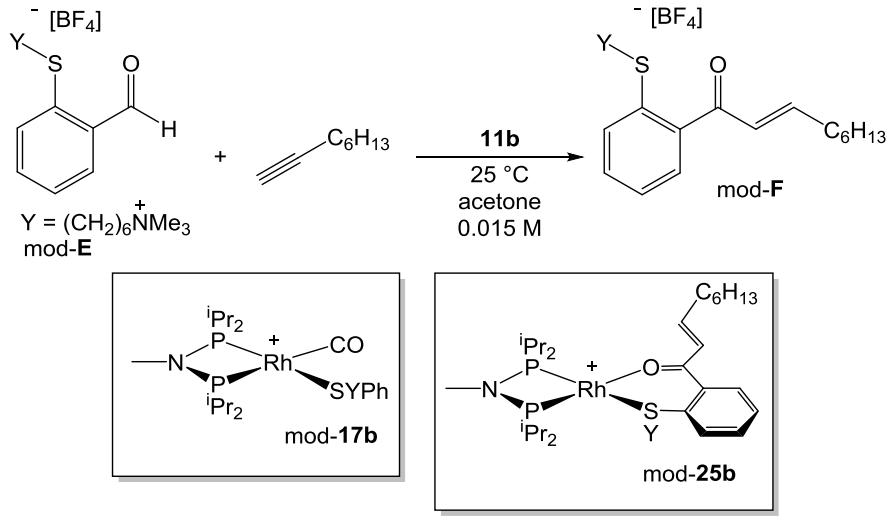

Scheme 2.25. Hydroacylation reaction using the cationic aldehyde, mod-**E** and 1-octyne as the substrates and **11b** as the catalyst. Decarbonylation mod-**17b** and the product bound resting state mod-**25b** are visible during the hydroacylation reaction by ESI-MS. The $[BAr^F_4]^-$ counter-anion is not pictured for clarity.

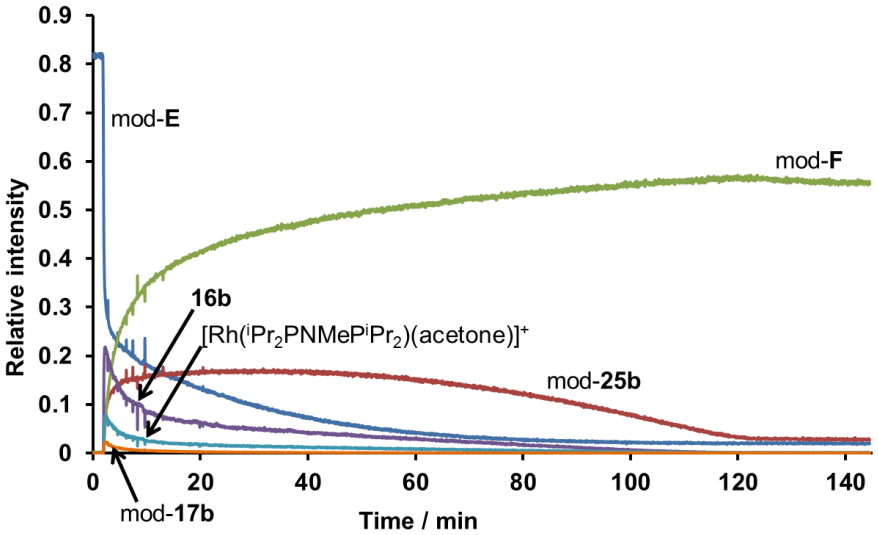

Figure 2.15. ESI-MS data of the hydroacylation reaction of mod-**E** and 1-octyne with **11b** as the catalyst. The sudden changes in relative intensities during the first 10 min are due to small blockages in the system.

During the first hour of the catalysis, the relative concentration of the resting state (mod-**25b**) remains more or less constant. Presumably there is a balance between deactivation of the catalyst via reductive decarbonylation and the formation of new product bound catalyst from the so far unreacted *mono*- and *bis*-acetone complexes. After 120 minutes, no more product (mod-**F**) was formed and the concentration of the product bound species (mod-**25b**) drops presumably due to the formation of the unobserved decarbonylation product.

The experiment was also carried out using a different mod-**E** to 1-octyne ratio of 1:3. Under these conditions the desired hydroacylation product (mod-**F**) was formed as the main species, however the formation of a small quantity of an additional product at m/z = 696.43 was also observed. This signal corresponds to $[Rh(^{i}Pr_2PNMeP^{i}Pr_2)(trihexylbenzene)]^+$ species. Upon carrying out MS/MS experiments on this peak, a fragment corresponding to $[Rh(^{i}Pr_2PNMeP^{i}Pr_2)]^+$ (m/z = 366.10) was observed, while species that correspond to the mass of a loss of only one or two octynes were not detected. Similar results have been obtained using a $[Rh((o\text{-}OMe\text{-}C_6H_4)_2PNMeP(o\text{-}OMe\text{-}C_6H_4)_2)(C_6H_5F)]^+$ species, where the formation of this trimer is more pronounced. This is discussed in more detail in Chapter 3.

The real-time ESI-MS experiments were also carried out using the PCP(^{i}Pr) complex **11c** and the PCP(^{t}Bu) complex **5** as the catalysts. The data acquired was analogous to the results obtained using **11b** as the catalyst. Overall, the ESI-MS data compliments the HPLC and NMR spectroscopy studies, and underscores that resting state of the reaction being the product-bound species (*e.g.* **25b**), and that these small bite-angle catalysts readily form the decarbonylation product (*e.g.* **17b**).

2.3.2.6. *Alkene vs. Alkyne Catalytic and Mechanistic Studies*

It has been observed that the complex **11b** acts as a highly effective alkyne hydroacylation catalyst even at low temperature (0 °C) and low catalyst loading (1 mol%). At the same time, initial screening studies showed that even at 10 mol% loading and at high temperatures (up to 80 °C) **11b** is a sluggish alkene hydroacylation catalyst. It was decided to carry out direct

comparison reactions with a 1:1 mixture of 1-octyne and 1-octene with **11b** as the catalyst (1 mol% catalyst loading, 0.4 M aldehyde, 0 °C, **E**:1-octene:1-octyne 1:0.5:0.5) to probe this. This resulted in no alkene hydroacylation product, while the full conversion of the alkyne (50 turnovers) was seen in 30 minutes (Figure 2.16). The same impressive selectivity was seen when an excess of alkene and alkyne (**E**:1-octene:1-octyne 1:5:5) were used.

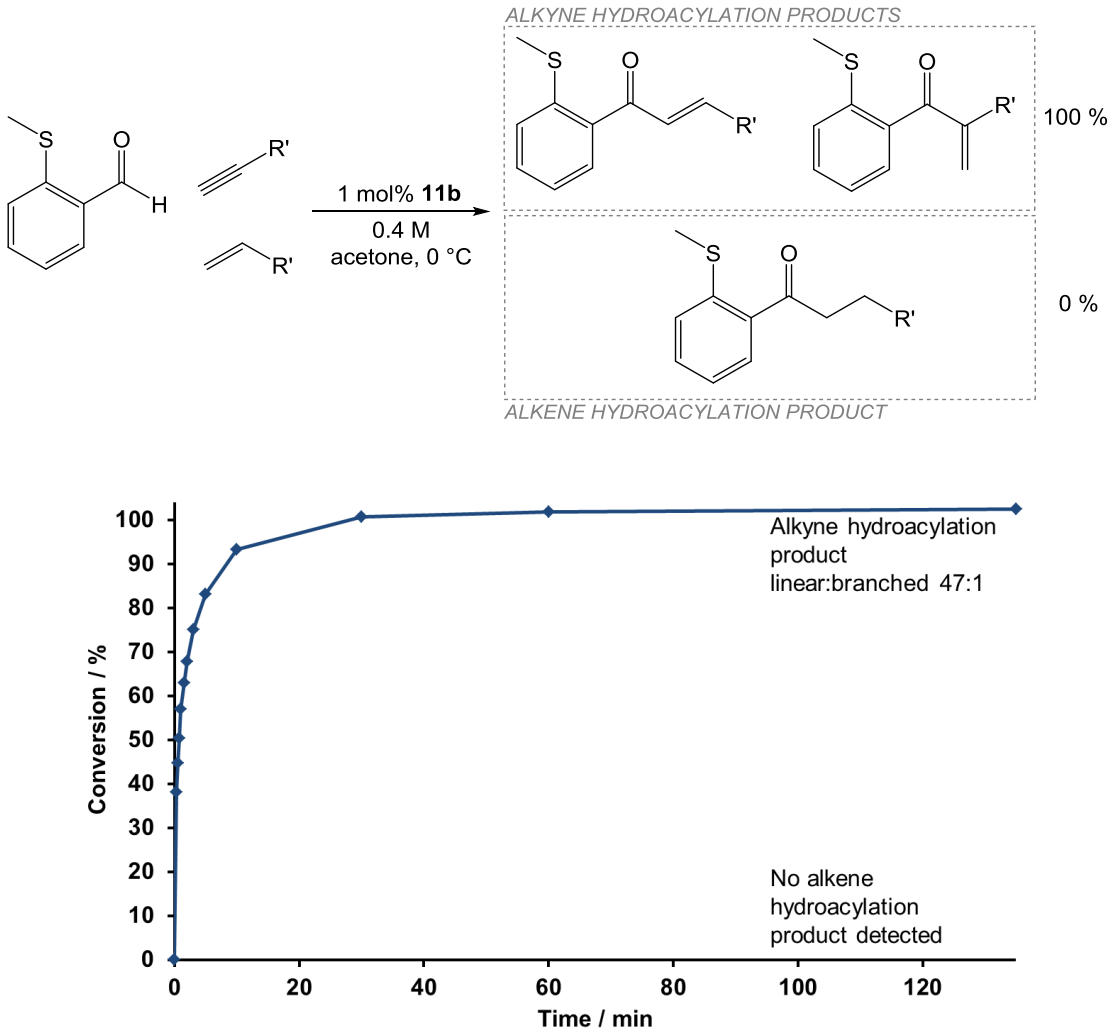

Figure 2.16. 1 mol% **11b**, 0.4M aldehyde (aldehyde:alkene:alkyne 1.0:0.5:0.5), 0 °C. No alkene hydroacylation product is observed. The conversions are measured using HPLC.

Upon raising the temperature to 25 °C, while keeping the rest of the variables the same as above (1 mol% cat, 0.4 M aldehyde, 25 °C, **E**:1-octene:1-octyne 1:0.5:0.5), a small amount of alkene hydroacylation product was seen (< 5%, after 2 h). The formation of alkene hydroacylation product was only observed after most of the alkyne (90%) was consumed (Figure 2.17).

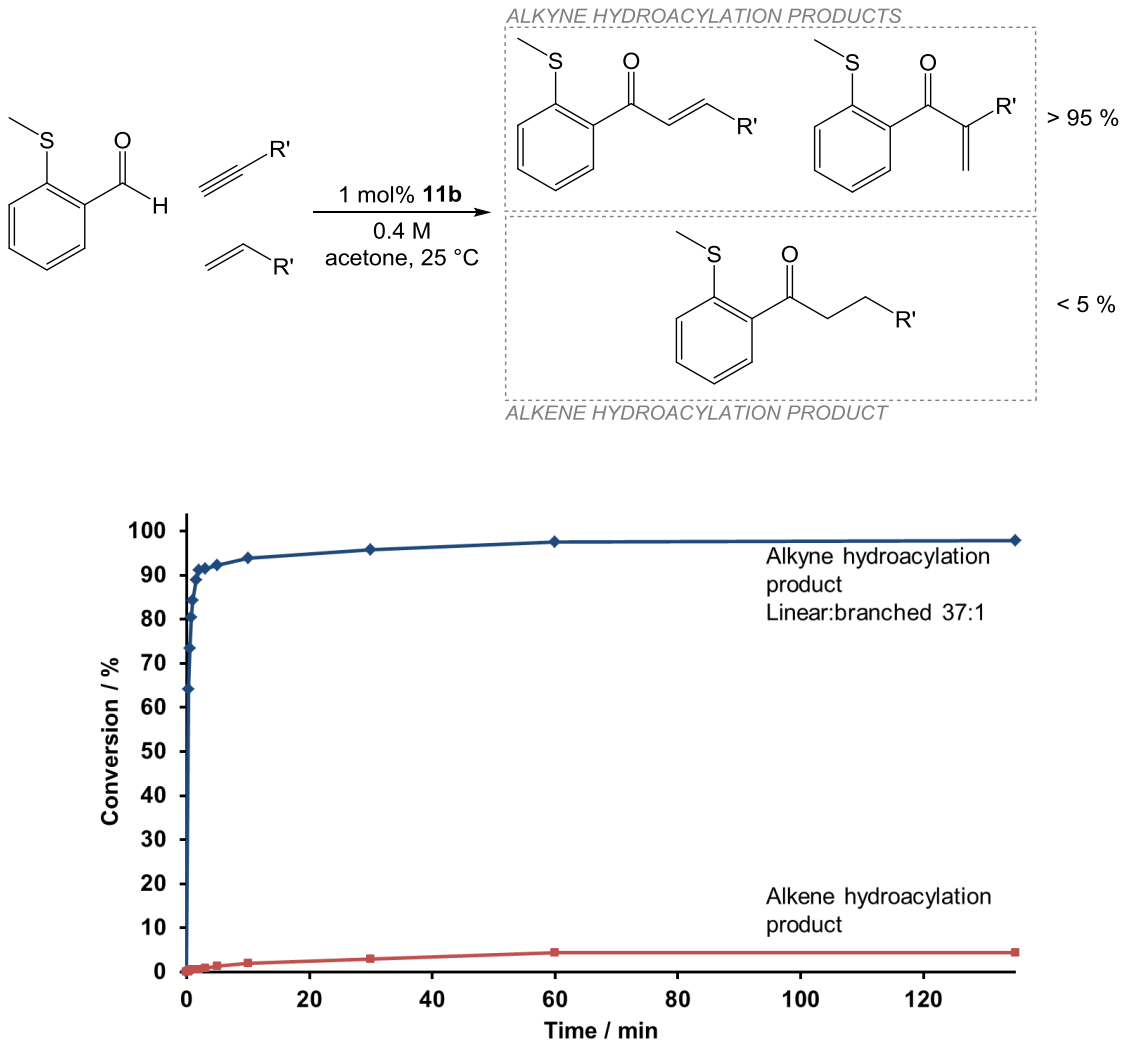

Figure 2.17. 1.0 mol% **11b**, 0.4M aldehyde (aldehyde:alkene:alkyne 1.0:0.5:0.5), 25 °C. Less than 5% of alkene hydroacylation product is observed. The conversions were measured using HPLC.

A control experiment with no alkyne in the reaction mixture (1 mol% **11b**, 0.4 M, **E**:1-octene 1:1.5, 0 °C, acetone) shows slightly higher alkene consumption over 2 h, with 20% alkene hydroacylation product formed, and upon placing the reaction mixture into a 55 °C oil-bath (after 2 h at 0 °C), results in approximately 50 % conversion to the alkene hydroacylation product. The data suggest that the alkyne is effectively competing with alkene for the metal centre coordination. Using a similar $[Rh(PR_3)_2(H)_2(solvent)_2]^+$ catalyst, analogous results have been shown by Schrock and Osborne for alkene/alkyne hydroacylation.[51]

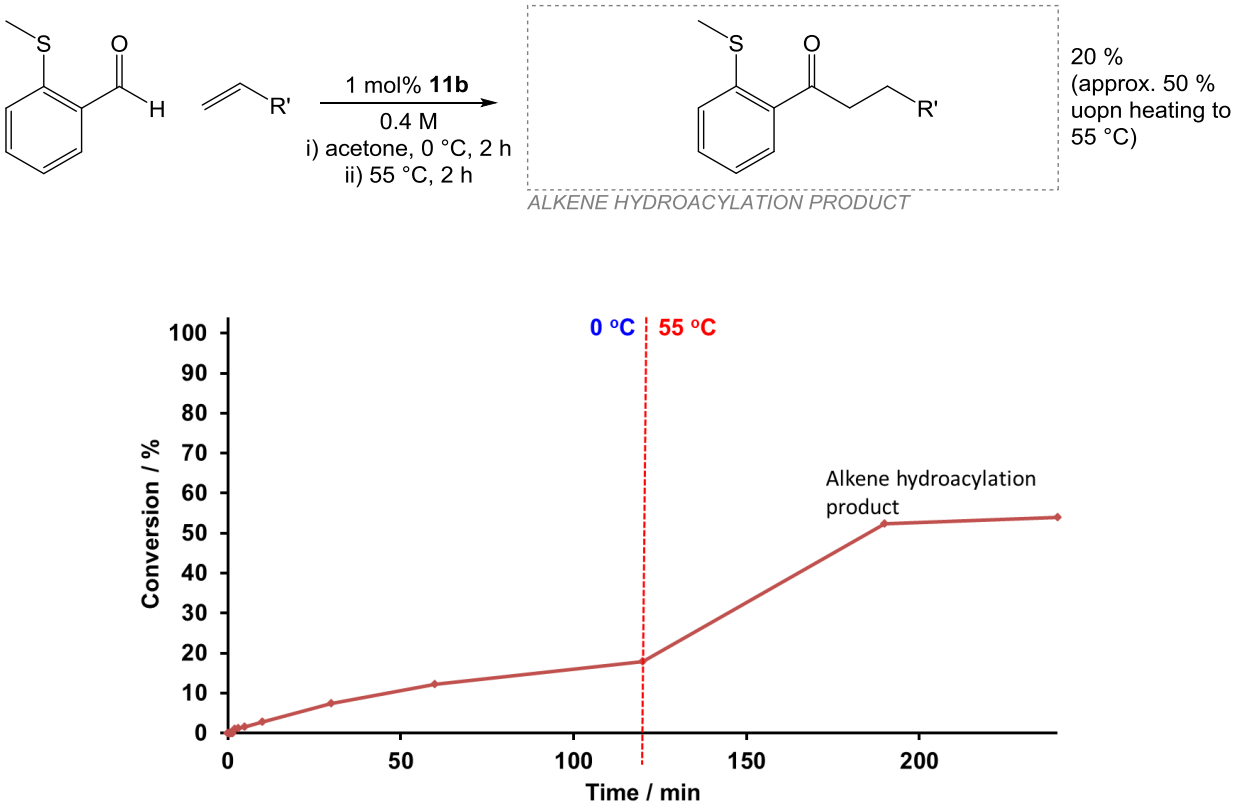

Figure 2.18. Control reaction with no alkyne present. 1.0 mol% **11b**, 0.4M aldehyde (aldehyde:alkene:alkyne 1.0:1.5:0.0), 0 °C. After 120 min the reaction mixture was placed into a pre-heated oil-bath (55 °C). The conversions were measured using HPLC.

To further investigate the reasons behind this selectivity, labelling studies were conducted using the deuterated aldehyde (d-**E**) and mixture on 1-octene and 1-octyne (d-**E**:1-octene:1-octyne 1:0.5:0.5, 1 mol% **11b** (linear selective catalyst), 0.4 M aldehyde, 0 °C). Based on ^{1}H and ^{2}H NMR spectra, this resulted in exclusive deuteration in the β-position of the linear alkyne hydroacylation product (Scheme 2.26).

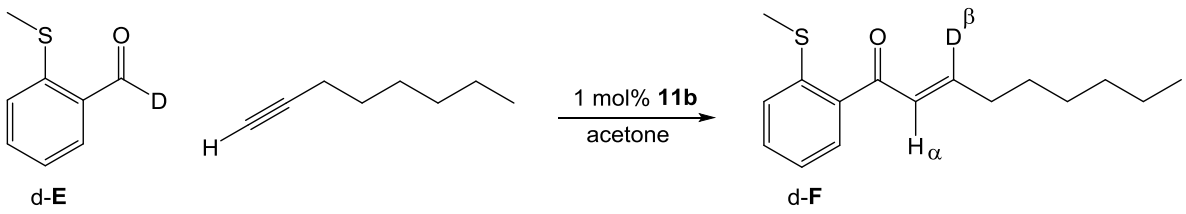

Scheme 2.26. Hydroacylation reaction using d-**E** and 1-octyne as the substrates and **11b** as the catalyst.

If reversible alkene coordination and hydride insertion were occurring, it would result in hydrogen appearing at the β-position (via incorporation of hydrogen into the acyl hydride), as

has been established for **5**, d-**E** and 1-octene.[7] To test this, a reaction under the same conditions, but without any alkyne (d-**E**:1-octene:1-octyne 1:0.5:0) was carried out using **5** as the catalyst. This reaction led to the incorporation of deuterium into both α- and β-position of the final alkene hydroacylation product and thus reversible alkene insertion in the absence of alkyne. These data support the hypothesis that the selectivity for alkyne over alkene is due to the competitive binding to the metal centre (Scheme 2.27).

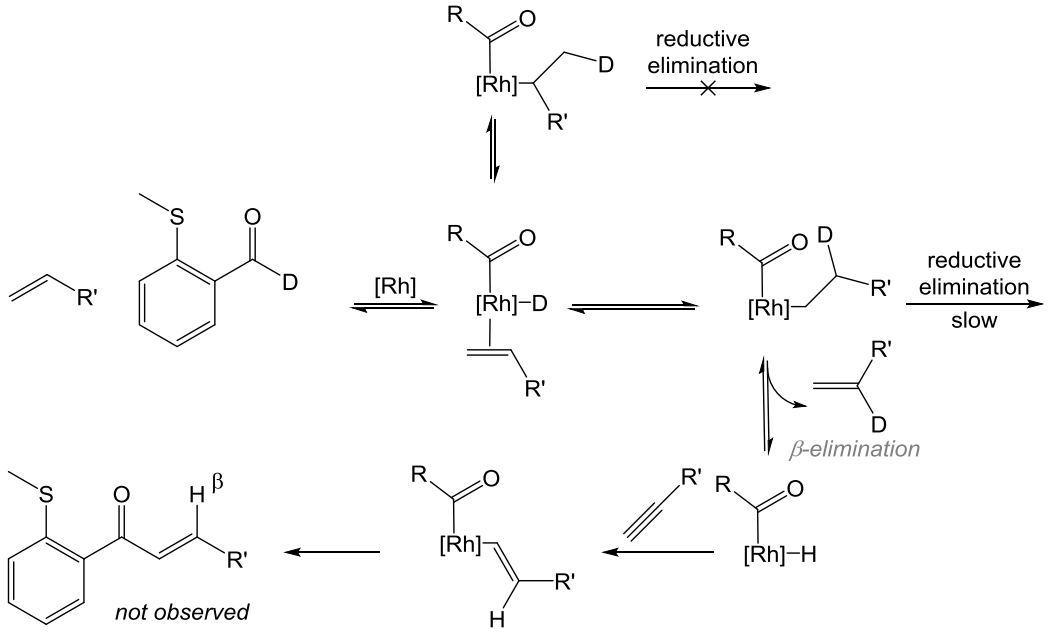

Scheme 2.27. Schematic representation of a scenario where initial coordination takes place, leading to the H/D-scrambling via the migration step, hence allowing for hydrogen at the β-position of the alkyne hydroacylation product.

Additionally, data from these experiments showed that the alkene hydroacylation reaction using **5** at effectively 2 mol% (*i.e.* **5**:1-octyne ratio of 1:50) allowed for full conversion after 30 min (*cf.* 94 turnovers after 1 h upon 1 mol% of **5**) and is consistent with the doubling of the catalyst loading and hence indicating that there is no reaction inhibition from the coordination of excess alkene.

2.4. Zwitterionic complexes

2.4.1. Introduction

Based on the successful intramolecular hydroacylation using zwitterionic rhodium-based catalysts reported by Peters (Section 1.5.1.1.), a research project together with a Part II student in the Weller group, Tim Shuttleworth, was carried out to investigate the efficiency of zwitterionic systems using β-S tethered aldehydes in the hydroacylation reaction. In particular we were interested in small bite-angle phosphorus-boron-phosphorus (PBP, *cf.* PNP and PCP ligands **8a** – **8c**) zwitterionic systems, but as there were no published synthetic routes to these ligands, the initial tests were carried out using the Peters' catalyst (**i-57**, Figure 2.19), which was synthesised based on the published route.[52] To directly compare the zwitterionic complex to a previously used cationic rhodium *bis*-phosphine complex an analogous cationic catalyst, [Rh(dpp3)(C_6H_5F)][BAr^F_4] (dpp3 = 1,3-(bisdiphenylphosphino)propane) (**26**), was synthesised (P-Rh-P bite angle for **i-57** is 88.8° and 90.8° for **26**). Both complexes were isolated as pure materials, and the analytical data (^{1}H and ^{31}P NMR spectra) were consistent with the previous reports.[1, 52]

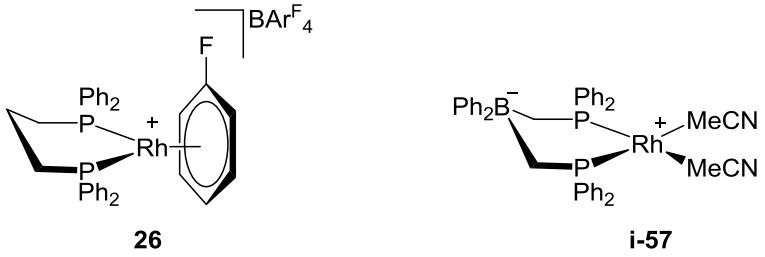

Figure 2.19. Cationic rhodium dpp3 complex **26** and the sterically analogous zwitterionic rhodium PCBCP complex **i-57**.

As discussed in Section 2.3.1, addition of MeCN to the catalyst allows for further stability towards the decarbonylation and thus using **i-57** and **26** would not allow for a direct comparison. Unfortunately it was not possible to isolate the corresponding fluorobenzene and acetonitrile complexes [Rh(PCBCP)(C_6H_5F)] (where PCBCP = $Ph_2PCH_2BPh_2CH_2PPh_2$) and [Rh(dpp3)$(MeCN)_2$][BAr^F_4] respectively. Therefore, during the catalytic reactions two

equivalents of MeCN (with respect to the catalyst) were added to **26**, which was shown to increase the catalytic activity of **26** by approximately 10% (*vide infra*).

2.4.2. Catalysis

The catalytic monitoring of the hydroacylation reaction was carried out using the same benchmark reaction already established previously by Weller and Willis using 2-(methylthio)benzaldehyde (**E**) as the aldehyde and 1-octene or 1-octyne (Scheme 2.28).

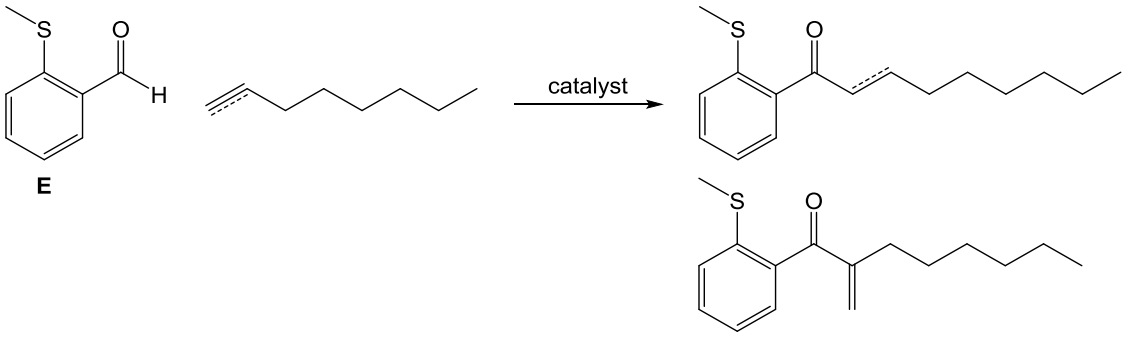

Scheme 2.28. The benchmark hydroacylation reaction using 2-(methylthio)benzaldehyde (**E**) and 1-octene or 1-octyne as the substrates. In the case of alkyne hydroacylation additionally the branched product is seen.

2.4.2.1. *Intermolecular Alkene Hydroacylation*

As for the small bite-angle systems discussed earlier with the general formula of $[Rh(R_2PXPR_2)(C_6H_5F)][BAr^F_4]$ (**11a** – **11e**), the initial catalytic screening reactions were carried out at 10 mol% catalyst loading (0.075 M, **E**:1-octene 1:1.5, acetone) at different temperatures using aldehyde **E** and 1-octene (Scheme 2.28). Both, the **26** and **i-57**, proved to be sluggish alkene hydroacylation catalysts, as even at 10 mol% catalyst loading full conversions to the ketone product were not obtained (Figure 2.20).

The cationic complex (**26**) promoted only 5 turnovers after 2 h at 55 °C (compared to 2.5 turnovers achieved at 25 °C). It did show some stability towards decarbonylation, as only 2 turnovers were seen after 5 min, and the catalyst remained active for more than 20 minutes

(Entry 3, Table 2.7). The zwitterionic complex (**i-57**) showed almost identical initial reactivity (2.3 turnovers after 5 min at 55 °C), but almost no further activity was observed.

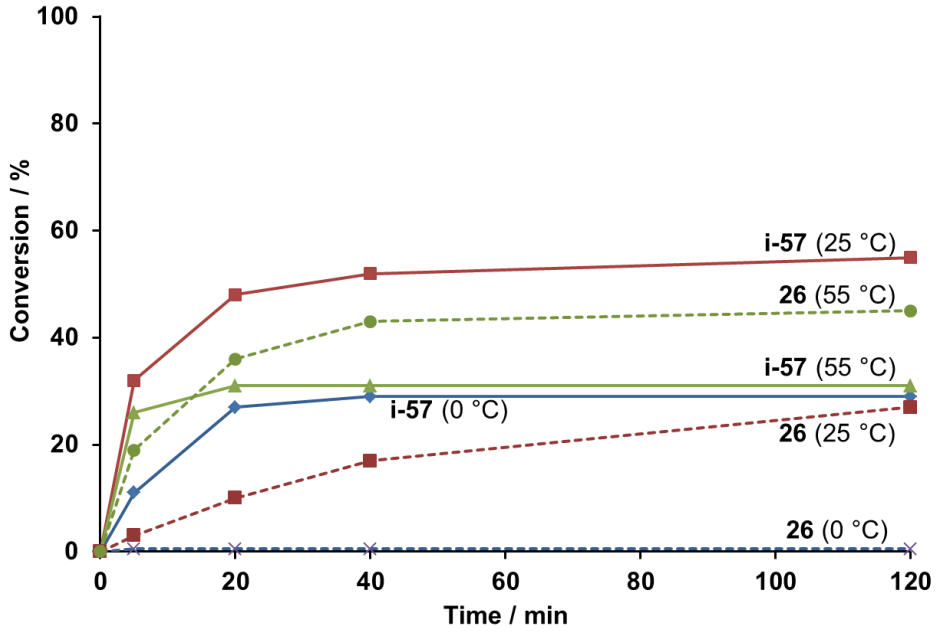

Figure 2.20. Alkene hydroacylation using **E** and 1-octene as substrates and **i-57** (solid line) or **26** (dashed line) as the catalyst. *Conditions: 10 mol% catalyst loading, acetone, 0.075 M aldehyde, aldehyde:alkene ratio = 1:1.5. Conversions were measured by HPLC.*

Table 2.7. Comparisons of the catalytic activity of the zwitterionic complex **i-57** and the cationic complex **26** at different temperatures for alkene hydroacylation.

Entry	Catalyst	Temperature / °C	Conversion / % (after 5 min)	Conversion / % (after 120 min)
1	**26**	0 °C	0	0
2	**26**	25 °C	3	27
3	**26**	55 °C	19	45
4	**i-57**	0 °C	11	29
5	**i-57**	25 °C	32	55
6	**i-57**	55 °C	27	31

Conditions: 10 mol% catalyst loading, acetone, 0.075 M aldehyde, aldehyde:alkene ratio = 1:1.5. Conversions were measured by HPLC.

Interestingly the highest conversion, in the case of **i-57**, was achieved at 25 °C (3 turnovers in 5 minutes and 5.5 turnovers in 2 h). Also, 3 turnovers were seen when the reaction was run at 0 °C, while no reactivity was seen for **26** under these low temperature conditions. This change of

reactivity with respect to the temperature could indicate that there is a fine balance between the relative barriers of hydroacylation and decarbonylation pathways for these zwitterionic catalysts, but as the reaction was still sluggish at 0 °C, we were not able to use the reaction temperature to shut down decarbonylation completely. The overall reactivity is summarised in Table 2.7.

2.4.2.2. *Intermolecular Alkyne Hydroacylation*

Alkyne hydroacylation was carried out using **i-57** and **26** as catalysts with **E** and 1-octyne as the substrates (Scheme 2.28, Table 2.8). Initial screening using **i-57** at 10 mol% (0.075 M, acetone, 25 °C, **E**:1-octyne ratio of 1:1.5) showed essentially 100% conversion after 2 hours. At 1 mol% (2 M aldehyde) the catalyst reached 83% conversion, similar to the small bite-angle isopropyl substituted complexes **11b** and **11c**, the catalyst was highly effective during the first 5 minutes (81% conversion) followed by presumably rapid decarbonylation. The cationic complex (**26**) also led to 100% conversion upon 10 mol% catalyst loading (0.075 M, acetone, 25 °C, **E**:1-octyne ratio of 1:1.5) but when the catalyst loading was dropped to 1 mol% (2 M aldehyde) only 37% conversion was seen. Both complexes allowed for excellent linear to branched product selectivity (32:1 linear:branched).

Table 2.8. Comparisons of the catalytic activity of the zwitterionic complex **i-57** and the cationic complex **26** at different concentrations for alkyne hydroacylation

Entry	Catalyst	Catalyst loading / mol%	Concentration / M	Conversion / % (after 5 min)	Conversion / % (after 120 min)
1	**26**	10	0.075	100	100
2	**i-57**	10	0.075	77	94
3	**26**	1	0.075	20	22
4	**i-57**	1	0.075	27	63
5	**26**	1	2.0	32	37
6	**i-57**	1	2.0	81	84

Conditions: 25 °C, acetone, aldehyde:alkyne ratio = 1:1.5. Conversions were measured by HPLC.

Although both catalysts (**i-57** and **26**) don't allow for full conversion at reduced catalyst loadings (1 mol%), it can be seen that the zwitterionic catalyst (**i-57**) results in much higher

conversions than the analogous cationic complex (**26**). Encouraged by these screening results using the large bite-angle zwitterionic complex it was decided to investigate the effect of the small bite-angle zwitterionic ligands on hydroacylation reaction using β-S-substituted aldehydes.

2.4.3. Synthesis of *Bis*(di-alkylphosphino)boronium Compounds

The potential ligand synthesis was based on compounds developed by Yamaguchi with the general motif of [*bis*(di-alkylphosphino)boronium][anion] (**27**-R-X, where R = ^{t}Bu, Cy or Ph; X = BAr^{F}_{4}, Br or OTf) and in particular the *bis*(di-tert-butyl-phosphino)boronium bromide (**27**-tBu-Br) was targeted.[53] The synthesis, depicted in Scheme 2.29, leads to the formation of the cationic species **27**-R-Br, which was postulated as the pro-ligand by deprotonation of one of the phosphine centres to yield the neutral species which could then be reacted with a suitable rhodium fragment. Another approach would be a direct complexation on rhodium by a reaction between **27**-R-Br and a suitable neutral rhodium starting material (*e.g.* $[Rh(cod)(OMe)]_2$). In order to achieve this, a range of PBP cations (where PBP = $R_2PBH_2PR_2$) with different counterions were synthesised, as for the hydroacylation reaction a non-coordinating counterion is desired (*e.g.* BAr^{F}_{4} or triflate) (Scheme 2.29).

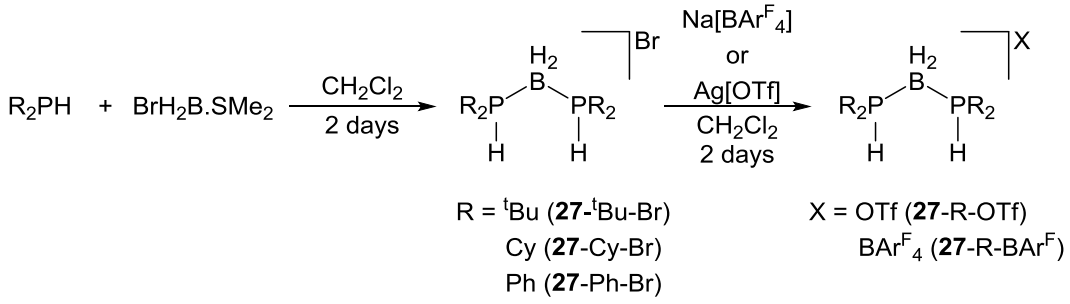

Scheme 2.29. Synthetic approach to a range of PBP complexes with different anions.

The bromide products (**27**-R-Br) were obtained as analytically pure white solids in good yield (approximately 70%). Similarly the second step yielded the desired salts (**27**-R-X, where R = ^{t}Bu, Cy or Ph; X = $BArF_4$ or OTf) in good yield (65 – 72%). All of these products were characterised using ^{1}H, ^{11}B and ^{31}P NMR spectroscopy, ESI-MS and elemental analysis. X-ray

structures were obtained for all the tert-butyl substituted complexes (**27**-tBu-X, X = Br, BAr^F_4 or OTf). The X-ray crystal structures all showed analogous structure for the PBP fragment but the interaction with the counterion was observed to be different. The solid state structure and the ^1H NMR spectra suggested that weak hydrogen bonds formed between the P–H units of the boronium cation and the anion (in the order of BAr^F_4 < OTf < Br).[54] The counterion effect was thoroughly investigated by Tim Shuttleworth, but this is outside the scope of this thesis. Important though, are the attempts to form the neutral PBP species, and the reactivity between rhodium complexes and the cationic PBP complexes.

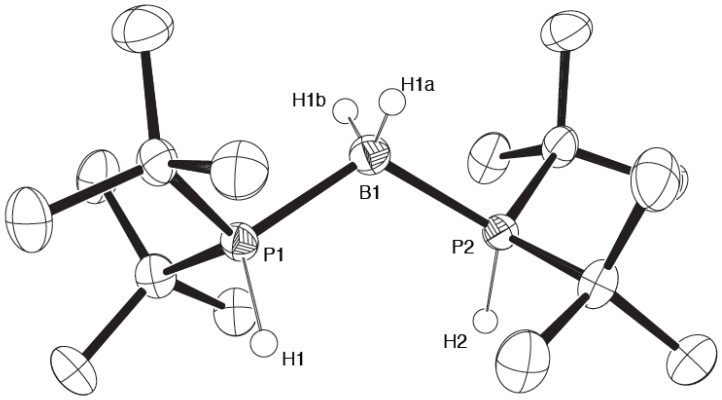

Figure 2.21. Solid state structure of the cation **27**-tBu-X. Displacement ellipsoids depicted at the 50% probability level. Most hydrogen atoms and anion and are omitted for clarity. All unlabelled atoms are carbon atoms. The X-ray data showed that the P-B bond lengths and P-B-P angle remain essentially unchanged upon changing the counterion (Br *vs.* OTf *vs*. BAr^F_4) Key bond lengths (Å) and angles (°): **27**-tBu-Br: P1-B1, 1.934(5); P2-B1, 1.948(5); P1-H1, 1.31(4); P2-H2, 1.31(4); P1-B1-P1, 118.9(3). **27**-tBu-OTf: P1-B1, 1.941(2); P2-B1, 1.938(2); P1-H1, 1.33(2); P2-H2, 1.30(2); P1-B1-P1, 118.8(1). **27**-tBu-BAr^F: P1-B1, 1.936(3); P2-B1, 1.933(3); P1-H1, 1.31(3); P2-H2, 1.31(2); P1-B1-P1, 118.7(1).

2.4.3.1. *Attempted Deprotonation of Cationic PBP Compounds*

The initial approach was to deprotonate one of the phosphonium groups of the PBP pro-ligand which could lead to a neutral ligand that could then be reacted with the suitable rhodium fragment. As it was noted that the phenyl-substituted PBP compounds (**27**-Ph-X) showed high stability, it was decided to probe the deprotonation using these pro-ligands.

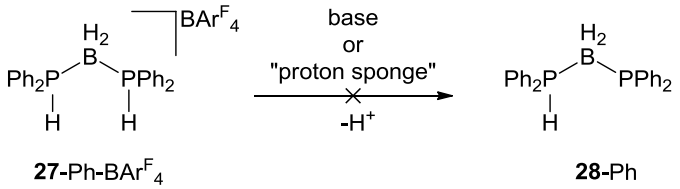

27-Ph-BAr$^F_4$ **28**-Ph

Scheme 2.30. General scheme of the attempted deprotonation of **27**-Ph-BAr$^F_4$.

The reactions were carried out using two very different bases: a weak base (Na_2CO_3) and much stronger base (^{n}BuLi). The use of ^{n}BuLi led to immediate decomposition of the **27**-Ph-BAr^F species (in THF solvent, 1.2 eq. of ^{n}BuLi) as indicated by the ^{31}P NMR spectrum: the P-B bond results in broad quadrupolar broadening of the ^{31}P NMR signals, while upon breaking the P-B bond, sharp signals were observed. When moving to the much weaker base (Na_2CO_3), no reactivity was seen initially, but after a few hours of stirring a small amount of decomposition products were seen (< 10 %, based on the ^{31}P{^{1}H} NMR spectrum) indicating that if any reaction is occurring, it leads to decomposition. In order to avoid nucleophilic bases, a "proton sponge" was used – 1,8-*bis*(dimethylamino)naphthalene.[55] This non-nucleophilic base was expected to allow for more gentle route to the deprotonation, but unfortunately similarly to the other bases, decomposition was observed over time by ^{31}P NMR spectroscopy.

2.4.3.2. *Attempted Complexation of PBP Cationic Species*

As the synthesis of neutral PBP compounds was not successful, it was decided to continue by direct synthesis of rhodium-PBP complexes using the cationic PBP compounds and neutral rhodium starting materials or via *in situ* deprotonation using the previously tested weak base, Na_2CO_3.

The direct synthesis was attempted using a route reported previously by Werner,[56, 57] in which he showed that reaction between $[Rh(cod)(OMe)]_2$ and *mono*-protonated phosphine cations (*e.g.* $[HP^tBu_2(CH_2CH_2OC_6H_5)][BF_4]$) leads to rhodium complexes (*e.g.* $[Rh(C_8H_{12})(\kappa\text{-O,P-MeOCH}_2CH_2P^tBu][BF_4]$). Upon reacting **27**-Ph-BAr^F with $[Rh(cod)(OMe)]_2$ overnight, only decomposition products were seen when using CH_2Cl_2 as the solvent (indicated by the formation of dark brown solution and ^{31}P NMR spectrum). When the same reaction was carried

out using C_6H_5F solvent a mixture of decomposition product, rhodium starting material and small quantities of new species was observed. ESI-MS shed light on the new species formed, which showed a major peak at m/z = 385.14 (the starting PBP(Ph) compound, **27**-Ph-BAr^F) and minor peaks at m/z = 594.14 and 979.27. These peaks correspond to the rhodium phosphine complexes with one or two *mono*-deprotonated PBP ligands, $[Rh(P(C_8H_{12})(PPh_2BH_2PHPh_2)]^+$ (**29**) and $[Rh(P(C_8H_{12})(PPh_2BH_2PHPh_2)_2]^+$ (**30**) respectively (Figure 2.22). Based on recent work reported by Weller using $[Rh(PPh_3)_3H]$ species, there might be an interaction between the B–H group and the rhodium metal in **29**, but only based on these ESI-MS data we are reluctant to propose this type of bonding occurring here.[54] Any attempts to produce these complexes in greater yields or to promote the coordination of the second phosphorus atom using bases led to decomposition.

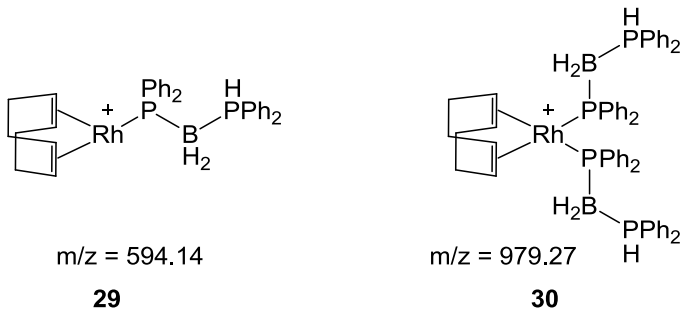

Figure 2.22. Minor species, seen using ESI-MS, synthesised by reacting **27**-Ph-BAr^F with $[Rh(cod)(OMe)]_2$. The $[BAr^F{}_4]^-$ counter-anion is not pictured for clarity.

Based on somewhat promising results upon using the weak base discussed above, $NaCO_3$, it was considered, whether it would be viable to carry out the reaction between $[Rh(nbd)Cl]_2$ and **27**-Ph-BAr^F with $NaCO_3$ present in the reaction mixture allowing for *in situ* deprotonation. This once again led to the formation of mixtures including decomposition products, which could not be identified by ESI-MS or NMR spectroscopy. Any attempts to isolate any of these products by crystallisation methods failed. Analogous problems were seen using other PBP compounds.

In light of all these challenges of these small bite-angle PBP compounds, any further research into using them as ligands for hydroacylation reaction were not pursued.

2.5. Conclusions

A thorough synthetic investigation has been undertaken in order to develop a range of novel small bite-angle ligands for the hydroacylation reaction. The investigation revealed that the synthesis is sterically nuanced, and the ligand design dictates whether the ligand itself or the metal complex can be synthesised. The successfully synthesised ligands were complexed on rhodium leading to a range of new rhodium complexes which have been proven to be highly active and linear product selective hydroacylation catalysts.

Screening studies showed that the best overall catalytic transformation (rate and regio-selectivity) was obtained upon using [Rh(^{i}Pr$_2$PNMeP^{i}Pr$_2$)(C$_6$H$_5$F)][BAr$^{F}_4$] (**11b**) as the catalyst, including excellent selectivity for alkynes over alkenes. **11b** was further studied to understand the mechanism of alkyne hydroacylation using small bite-angle phosphine ligands. NMR spectroscopy, ESI-MS, X-ray crystallography, catalytic and labelling studies helped to further understand the individual steps of the hydroacylation mechanism and formation of species during and at the end of the hydroacylation reaction. Although these studies revealed **11b** (and other isopropyl substituted complexes) to be highly effective alkyne hydroacylation catalysts, they also readily reductively decarbonylate to form catalytically inactive rhodium-carbonyl species.

The large bite-angle zwitterionic complexes developed by Peters were shown to be relatively good intermolecular hydroacylation catalysts upon using the β-S substituted aldehydes. Attempts to synthesise zwitterionic analogues of these cationic small bite-angle complexes failed due to the inherently unstable nature of the PBP motifs chosen.

Overall, these small bite-angle complexes allow for excellent reactivity with alkynes but have no defence against the catalyst deactivating reductive decarbonylation. Combining this high activity with a design that would allow for added stability towards deactivation, the small bite-angle motif has been upgraded and combined with the hemilability (motif that has proven to provide stability towards the reductive decarbonylation reaction). Ligands of this type are further investigated in Chapter 3.

2.6. References

1. R. J. Pawley, G. L. Moxham, R. Dallanegra, A. B. Chaplin, S. K. Brayshaw, A. S. Weller and M. C. Willis, *Organometallics*, 2010, **29**, 1717-1728.
2. P. D. Achord, P. Kiprof and B. Barker, *J. Mol. Struct. THEOCHEM*, 2008, **849**, 103-111.
3. S. M. Reid, J. T. Mague and M. J. Fink, *J. Am. Chem. Soc.*, 2001, **123**, 4081-4082.
4. P. Hofmann, C. Meier, U. Englert and M. U. Schmidt, *Chem. Ber.*, 1992, **125**, 353-365.
5. P. Hofmann, C. Meier, W. Hiller, M. Heckel, J. Riede and M. U. Schmidt, *J. Organomet. Chem.*, 1995, **490**, 51-70.
6. F. Eisentrager, A. Gothlich, I. Gruber, H. Heiss, C. A. Kiener, C. Kruger, J. U. Notheis, F. Rominger, G. Scherhag, M. Schultz, B. F. Straub, M. A. O. Volland and P. Hofmann, *New J. Chem.*, 2003, **27**, 540-550.
7. A. B. Chaplin, J. F. Hooper, A. S. Weller and M. C. Willis, *J. Am. Chem. Soc.*, 2012, **134**, 4885-4897.
8. C. A. Tolman, *Chem. Rev.*, 1977, **77**, 313-348.
9. L. E. Bowen, M. Charernsuk, T. W. Hey, C. L. McMullin, A. G. Orpen and D. F. Wass, *Dalton Trans.*, 2010, **39**, 560-567.
10. J. A. Bailey, M. F. Haddow and P. G. Pringle, *Chem. Commun.*, 2014, **50**, 1432-1434.
11. M. C. Maumela, K. Blann, H. de Bod, J. T. Dixon, W. F. Gabrielli and D. B. G. Williams, *Synthesis-Stuttgart*, 2007, 3863-3867.
12. E. W. Abel, M. A. Bennett and G. Wilkinson, *J. Chem. Soc.*, 1959, 3178-3182.
13. R. R. Schrock and J. A. Osborn, *J. Am. Chem. Soc.*, 1971, **93**, 2397-&.
14. J. L. Herde, J. C. Lambert, C. V. Senoff and M. A. Cushing, *Inorg. Synth.*, 1974, **15**, 18-20.
15. S. D. Pike, R. J. Pawley, A. B. Chaplin, A. L. Thompson, J. A. Hooper, M. C. Willis and A. S. Weller, *Eur. J. Inorg. Chem.*, 2011, 5558-5565.
16. J. L. Herde, J. C. Lambert, C. V. Senoff and M. A. Cushing, in *Inorg. Synth.*, 2007, pp. 18-20.
17. B. Guzela, M. A. Omarya, J. P. Fackler Jr and A. Akgermand, *Inorg. Chim. Acta*, 2001, **325**, 45-50.
18. M. A. Huertos and A. S. Weller, *Chem. Sci.*, 2013, **4**, 1881-1888.
19. L. D. Quin and A. J. Williams, *Practical Interpretation of P-31 NMR Spectra and Computer Assisted Structure Verification, Advanced Chemistry Development, Inc. Toronto, Canada*, 2004.
20. A. T. Lubben, J. S. McIndoe and A. S. Weller, *Organometallics*, 2008, **27**, 3303-3306.
21. W. Henderson and J. S. McIndoe, *Mass Spectrometry of Inorganic and Organometallic Compounds: Tools - Techniques - Tips, Wiley.*, 2005.
22. C. González-Rodríguez, R. J. Pawley, A. B. Chaplin, A. L. Thompson, A. S. Weller and M. C. Willis, *Angew. Chem. Int. Ed.*, 2011, **50**, 5134-5138.
23. A. C. Cooper, E. Clot, J. C. Huffman, W. E. Streib, F. Maseras, O. Eisenstein and K. G. Caulton, *J. Am. Chem. Soc.*, 1998, **121**, 97-106.
24. L. J. Sewell, A. B. Chaplin, J. A. B. Abdalla and A. S. Weller, *Dalton Trans.*, 2010, **39**, 7437-7439.
25. H. Urtel, C. Meier, F. Eisenträger, F. Rominger, J. P. Joschek and P. Hofmann, *Angew. Chem. Int. Ed.*, 2001, **40**, 781-784.
26. G. Ewart, A. P. Lane, J. McKechnie and D. S. Payne, *J. Am. Chem. Soc.*, 1964, 1543-1547.
27. K. Blann, A. Bollmann, H. de Bod, J. T. Dixon, E. Killian, P. Nongodlwana, M. C. Maumela, H. Maumela, A. E. McConnell, D. H. Morgan, M. J. Overett, M. Prétorius, S. Kuhlmann and P. Wasserscheid, *J. Catal.*, 2007, **249**, 244-249.
28. www.sigma-aldrich.com.
29. Thesis of Will Reilly. Unpublished data.
30. M. C. Willis, *Chem. Rev.*, 2010, **110**, 725-748.
31. S. Kozuch and J. M. L. Martin, *ACS Catal.*, 2012, **2**, 2787-2794.

32. D. F. Wass, *Dalton Trans.*, 2007, 816-819.
33. T. Agapie, *Coord. Chem. Rev.*, 2011, **255**, 861-880.
34. R. A. Mackay and W. Henderson, *Introduction to Modern Inorganic Chemistry, 6th editionIn, Nelson Thorness*, 1996.
35. B. K. H. Jeremy K. M. Sanders, *Modern NMR Spectroscopy, A Guide For Chemists,* OUP Oxford, 1989.
36. R. J. Pawley, M. A. Huertos, G. C. Lloyd-Jones, A. S. Weller and M. C. Willis, *Organometallics*, 2012, **31**, 5650-5659.
37. D. Milstein, *J. Am. Chem. Soc.*, 1982, **104**, 5227-5228.
38. A. B. Chaplin, A. I. Poblador-Bahamonde, H. A. Sparkes, J. A. K. Howard, S. A. Macgregor and A. S. Weller, *Chem. Commun.*, 2009, 244-246.
39. M. R. Buchner, E. Herdtweck and S. Schneider, *J. Organomet. Chem.*, 2008, **693**, 3943-3946.
40. A. C. Cooper, J. C. Huffman and K. G. Caulton, *Organometallics*, 1997, **16**, 1974-1978.
41. D. P. Fairlie and B. Bosnich, *Organometallics*, 1988, **7**, 946-954.
42. M. von Delius, C. M. Le and V. M. Dong, *J. Am. Chem. Soc.*, 2012, **134**, 15022-15032.
43. M. M. Coulter, K. G. M. Kou, B. Galligan and V. M. Dong, *J. Am. Chem. Soc.*, 2010, **132**, 16330-16333.
44. J. Hartwig, *Organotransition Metral Chemistry From Bonding to Catalysis*, University Science Books, 2010.
45. K. Tanaka and G. C. Fu, *J. Am. Chem. Soc.*, 2001, **123**, 11492-11493.
46. R. S. Tanke and R. H. Crabtree, *J. Am. Chem. Soc.*, 1990, **112**, 7984-7989.
47. D. P. Fairlie and B. Bosnich, *Organometallics*, 1988, **7**, 936-945.
48. R. Ghosh, X. Zhang, P. Achord, T. J. Emge, K. Krogh-Jespersen and A. S. Goldman, *J. Am. Chem. Soc.*, 2007, **129**, 853-866.
49. Z. Ahmadi and J. S. McIndoe, *Chem. Commun.*, 2013, **49**, 11488-11490.
50. J. Luo, A. G. Oliver and J. Scott McIndoe, *Dalton Trans.*, 2013, **42**, 11312-11318.
51. R. R. Schrock and J. A. Osborn, *J. Am. Chem. Soc.*, 1976, **98**, 2143-2147.
52. T. A. Betley and J. C. Peters, *Angew. Chem. Int. Ed.*, 2003, **42**, 2385-2389.
53. Y. Yamamoto, T. Koizumi, K. Katagiri, Y. Furuya, H. Danjo, T. Imamoto and K. Yamaguchi, *Org. Lett.*, 2006, **8**, 6103-6106.
54. T. A. Shuttleworth, M. A. Huertos, I. Pernik, R. D. Young and A. S. Weller, *Dalton Trans.*, 2013, **42**, 12917-12925.
55. R. W. Alder, P. S. Bowman, W. R. S. Steele and D. R. Winterman, *Chem. Commun.*, 1968, 723-724.
56. G. Canepa, C. D. Brandt, K. Ilg, J. Wolf and H. Werner, *Chem. Eur. J.*, 2003, **9**, 2502-2515.
57. E. Sola, J. Navarro, J. A. López, F. J. Lahoz, L. A. Oro and H. Werner, *Organometallics*, 1999, **18**, 3534-3546.

3. TOWARDS HEMILABILE PNP LIGANDS

3.1. Introduction

The small bite-angle ligand approach discussed in Chapter 2 was based around the concept that the postulated rate-limiting step of the hydroacylation reaction, reductive elimination, could selectively be sped-up in comparison to the catalyst deactivation pathway, reductive decarbonylation. This relative rate difference would allow the catalyst to essentially outrun the decarbonylation reaction under suitable conditions of high concentration of substrate (Scheme 1.6).[1, 2] Although this approach worked, and very fast hydroacylation catalysts were developed, the catalyst loadings are still limited to 0.5 mol% and decarbonylation still occurs.[3] One way to improve the relative ratio of productive hydroacylation with respect to reductive decarbonylation would be to fine tune the catalysis conditions by testing a range of additives or controlling the reaction temperature (for example this was shown to have substantial effect on zwitterionic systems, Section 2.4.2); but most likely this would result in only slight improvements in conversions. Another, more sophisticated, approach is to make these highly efficient catalysts more stable towards decarbonylation, hence potentially reducing the effect of the reductive decarbonylation during the hydroacylation reaction. As discussed in the Introduction Chapter, one of the most effective ways to reduce the effect of decarbonylation is to

temporarily block the free coordination site formed after the C-H activation of the aldehyde, which is needed for decarbonylation to occur, *i.e.* to form a 6-coordinate acyl-hydride intermediate.[4, 5] One way for this to happen would be to modify the substrates and add another tether to the aldehyde or to the alkyne, but this would significantly reduce the scope of the reaction.[6] An alternative is to use hemilabile ligands that can reversibly block free coordination-sites that are revealed during the catalytic cycle, hence inhibiting the effect of decarbonylation. However, an inherit problem with hemilabile systems is the relative strength of the binding of the hemilabile group; if it is too weak, decarbonylation can still readily occur, while if it binds too strongly, it can block the site required for the binding of the incoming alkene/akyne.

Over the recent years, the groups of Weller and Willis have been looking into the effect of hemilability by screening a range of hemilabile phosphine ligands for the hydroacylation reaction. In order to investigate the effect of binding strength of the hemilabile atom, and its effect on the hydroacylation reaction, three similar ligands with different backbone linkers were probed: $[Ph_2P(C_6H_4)]_2CH_2$ (**31**), $[Ph_2P(C_6H_4)]_2S$ (**32**) and $[Ph_2P(C_6H_4)]_2O$ (DPEphos) (Figure 3.1).[7]

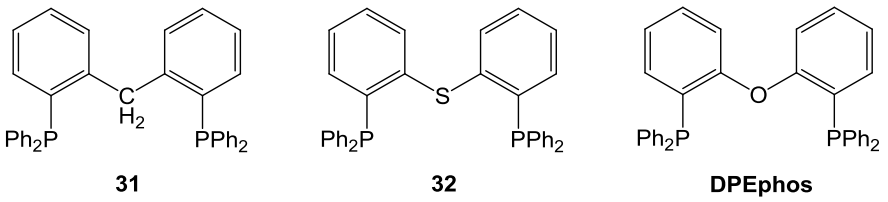

Figure 3.1. Ligands used by Weller in a comparative study to understand the strength of hemilabile bonding of different backbone linkers.

The catalytic reactions which compared these ligands in the hydroacylation reaction between β-SMe-propanal and methyl acrylate (Scheme 2.1) showed full conversion to product upon using DPEphos as the ligand, while no reactivity was seen when **31** and **32** were used as ligands (5 mol% catalyst loading, 1:2 ratio of aldehyde:alkene, acetone, 55 °C).[8]

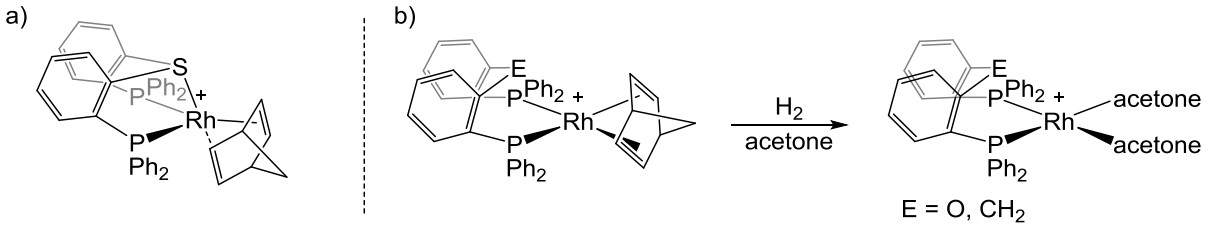

Scheme 3.1. a) The pseudo-trigonal bipyramidal coordination mode of the Rh(I) nbd-species adopted upon the use of the PSP ligand **32**. b) Hydrogenation reaction carried out using DPEphos ligand and **31**, to remove the strained nbd ligand in order to obtain the desired precatalyst. The $[BAr^F_4]^-$ counter-anion is not pictured for clarity.

The use of the complex containing a phosphine ligand with the sulfur backbone linker (**32**) on rhodium, $[Rh\{Ph_2P(C_6H_4)\}_2S(nbd)][BAr^F_4]$ (Scheme 3.1, a), did not lead to the formation of an active catalyst. The hydrogenation reaction that resulted in *bis*-acetone complexes in the case of ligands **31** and DPEphos (Scheme 3.1, b) did not lead to the formation of the desired $[Rh\{Ph_2P(C_6H_4)\}_2S(acetone)_2][BAr^F_4]$ precatalyst, instead the 18-electron configuration was retained even at high H_2 pressures (up to 100 bar H_2) (Scheme 3.1, a). This suggests that the sulfur atom is very strongly bound to the metal centre and this suggestion in strengthened by the inactivity of this complex in the hydroacylation reaction.

Although the desired *bis*-acetone precatalysts were formed in the case of both **31** and DPEphos (Scheme 3.1, b), the reactivity towards aldehydes was observed to be different. The addition of the aldehyde (3-(methylthio)propionaldehyde or 2-(methyl-thio)benzaldehyde (**E**)) to the complex containing a phosphine ligand with the carbon backbone linker (**31**), $[Rh\{Ph_2P(C_6H_4)\}_2CH_2(acetone)_2][BAr^F_4]$, resulted in only decomposition of the rhodium complex into unidentified products and no acyl-hydride intermediate was observed, demonstrating the importance of the hemilability as this phosphine ligand (**31**) provides the same electronic and steric environment as DPEphos but no hemilability.

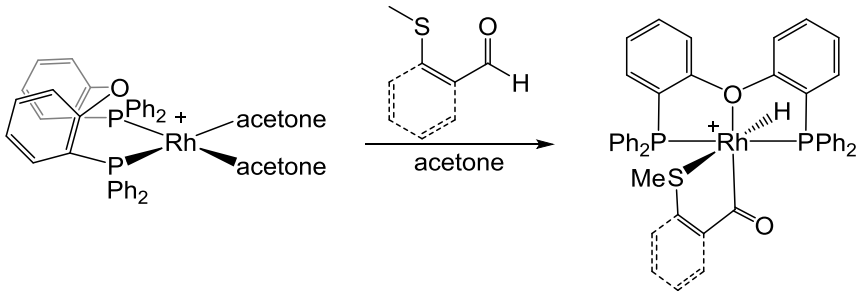

Scheme 3.2. Formation of stable acyl-hydride species using DPEphos ligand. The $[BAr^F_4]^-$ counter-anion is not pictured for clarity.

By contrast, the reaction of [Rh(DPEphos)(acetone)$_2$][BAr$^F{}_4$] with 3-(methylthio)propionaldehyde or 2-(methyl-thio)benzaldehyde (**E**), allowed for the formation and characterisation (including X-ray structure) of the acyl-hydride intermediate (Scheme 3.2). Upon leaving these acyl-hydride intermediates in acetone solution for a week, slow reductive decarbonylation into [Rh(DPEphos)(CO)(SEtMe)][BAr$^F{}_4$] or [Rh(DPEphos)(CO)(SPhMe)][BAr$^F{}_4$] occurs, respectively, demonstrating the stability of these complexes.

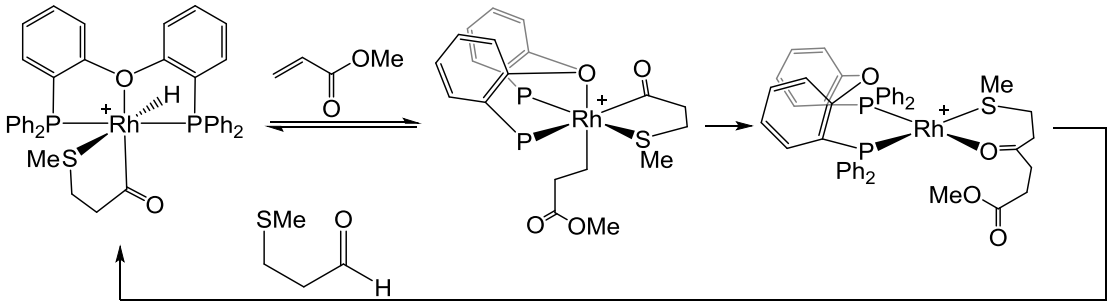

Scheme 3.3. The hydroacylation reaction between the acyl-hydride intermediate and methyl acrylate showing the flexibility of the ligand required to accommodate the reaction. The [BAr$^F{}_4$]$^-$ counter-anion is not pictured for clarity.

The addition of methyl acrylate to the 3-(methylthio)propionaldehyde activated acyl-hydride intermediate resulted in the hydride migration and an intermediate that adopts the *cis*-conformation followed by the reductive elimination to yield the 4-coordinate product-bound species (Scheme 3.3). This can then eliminate the product and the reaction with another equivalent of 3-(methylthio)propionaldehyde leads to the formation of the acyl-hydride intermediate (*trans*-conformation).

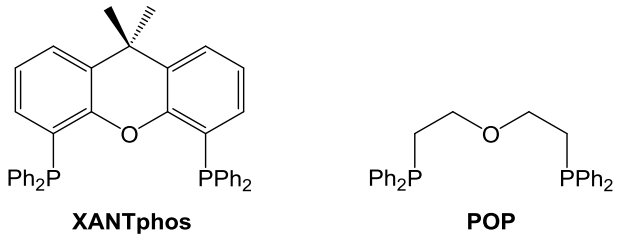

Figure 3.2. Hemilabile ligands tested for hydroacylation reaction.

Utilising these results, Weller and Willis continued investigating hemilabile ligands containing oxygen as the hemilabile unit.[7, 8] Additionally to DPEphos, other oxygen containing ligands were tested, in particular POP and the more rigid XANTphos ligands (Figure 3.2).[8-10] Even though

these other oxygen containing ligands allowed for hydroacylation reaction to happen, they yielded in much lower conversions of aldehyde to the ketone product (50% (165 h) and 30% (145 h) respectively at 10 mol% catalyst loading compared to full conversion seen upon using the DPEphos ligand (20 h)). Furthermore, the use of POP and XANTphos ligands led to the aldehyde hydroacylation (Tishcenko reaction) product being the major species at the end of the reaction (Scheme 1.2). This data demonstrated that both the hemilability and *trans-cis-trans* adjustments of the coordination geometry are required to result in active hydroacylation catalysis.

This lower activity was put down to XANTphos and POP being less able to de-coordinate the oxygen atom in the acyl-hydride complexes, thus not allowing for alkene or alkyne coordination for productive hydroacylation. Upon using POP and XANTphos ligands, the initial coordination and activation of the aldehyde is observed which leads to the formation of the *trans*-phosphine acyl-hydride complex analogous to the DPEphos system (Scheme 3.2). Unlike for DPEphos complex, no decarbonylation is observed upon leaving the acetone solution of the acyl-hydride complex standing for a week. However the acyl-hydride intermediates show no appreciable reactivity towards methyl acrylate over 24 h, indicating the strong binding of the ether linker, and thus unavailability of the free coordination site (*cf.* Scheme 3.3). This was further probed by the synthesis of the dihydride complex, to which the strongly binding acetonitrile was added (Scheme 3.4).

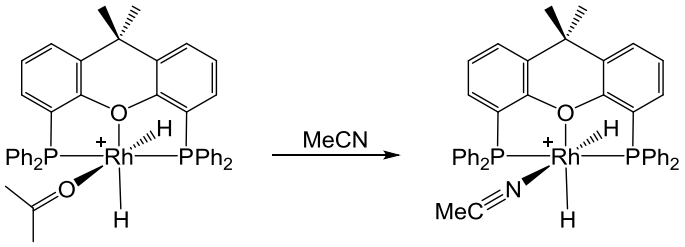

Scheme 3.4. Addition of MeCN to the rhodium XANTphos dihydride complex. The $[BAr^F{}_4]^-$ counter-anion is not pictured for clarity.

This resulted in the replacement of acetone with acetonitrile, while the ether linker remained attached to the metal centre, again demonstrating the strong bond formation between the oxygen atom of the ether group and the rhodium metal centre. Analogous result was obtained

upon using POP ligand when the same reaction with acetonitrile was carried out. In comparison, the addition of MeCN to the DPEphos ligated acyl-hydride intermediate led to the dissociation of the oxygen atom and the formation of a 6-coordinate MeCN bound complex (Scheme 3.5).

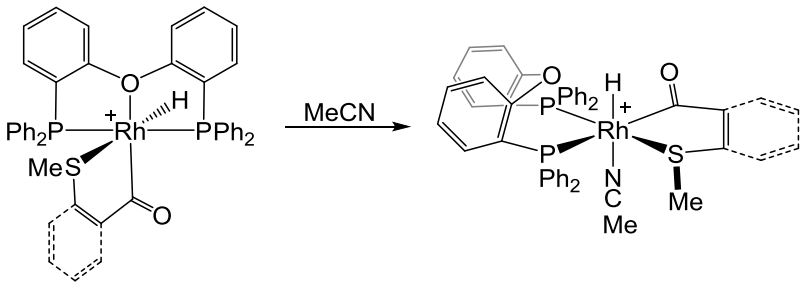

Scheme 3.5. Addition of acetonitrile to the rhodium DPEphos acyl-hydride complex. The $[BAr^{F}_{4}]^{-}$ counter-anion is not pictured for clarity.

Additionally to this flexibility and hemilability, the reaction rate of hydroacylation was shown to be linked to the P-M-P bite angle. This bite angle effect was shown using a range of diphenylphosphino based ligands (dpp2 – dpp5) (Scheme 1.45), and as discussed in the previous chapter, the small bite-angle ligands are highly selective towards alkene or alkyne hydroacylation over the unwanted aldehyde hydroacylation (Tishcenko reaction). Based on the gathered observations, it was decided to develop a cationic system combining both motifs: hemilability and small bite-angle, using rhodium *bis*-phosphine based complexes (Figure 3.3).

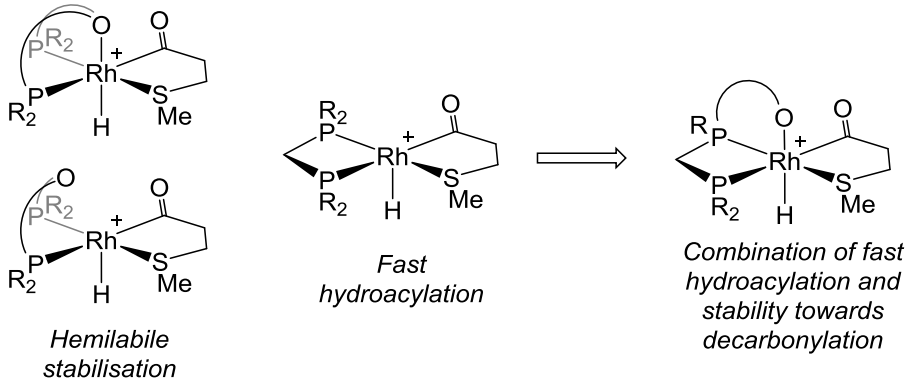

Figure 3.3. General scheme of the postulated ligand design that incorporates fast hydroacylation catalysis by speeding up the reductive elimination step with hemilability.

Upon combining the small bite-angle ligands with the hemilabile systems (Figure 3.3), it was decided that the best design that covers both requirements is provided by the N,N-*bis*(diarylphosphino)amine ligand, where the aryl groups are *ortho*-methoxy phenyls (**37**, Figure 3.4). These ligands have received a lot of attention over the recent years. Wass has

carried out an extensive study on small bite-angle PCP and PNP ligands, and has demonstrated that **37** and other similar PNP ligands ligated to chromium promote olefin trimerisation, allowing for highly selective catalysis at very low catalyst loadings.[11-14]

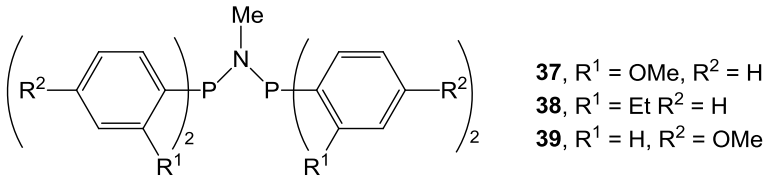

Figure 3.4. The general structure of the hemilabile small bite-angle ligand and the changes in the ligand design that allow the electronic and steric effects of this ligand motif to be probed.

Further encouragement for the potential benefits of using these *ortho*-methoxy unit containing PNP ligands comes from the work of Labinger and Bercaw,[15-19] who conducted a thorough study on the reasons behind the impressive activity of these ligands when complexed with chromium. They conducted a range of stoichiometric reaction to investigate the effect of the OMe-group. In particular relevance to this study, they were able to isolate complexes showing the coordination of the oxygen to the metal centre (Scheme 3.6) indicating that these ligands, when used in hydroacylation, could allow for the combination of the activity of the small bite-angle moiety and extra stabilisation against reductive decarbonylation via the coordination of the OMe during the catalytic process. These oxygen-chromium coordination containing species were synthesised and studied using the deuterated version of the PNP ligand where the OCH_3 groups on the phenyl rings were replaced with OCD_3 groups to allow for better NMR data. Using these ligands, three complexes (**33**, **34** and **35**) were synthesised, which were characterised by NMR spectroscopy, and by single crystal X-ray diffraction (Scheme 3.6). These structures clearly showed a bond between the chromium metal centre and the oxygen atom (2.27 – 2.43 Å, the corresponding van der Waals radii would be 3.63 Å).[19] The mixed aryl/halide complex **35** was synthesised by mixing two equivalents of **33** with one equivalent of **34** in dichloromethane. Complexes **33** and **35**, when reacted with $H[BAr^F_4]$ or $Na[BAr^F_4]$ respectively led to the formation of complex **36** (Scheme 3.6). Although **36** could not be isolated, based on the observation of the liberation of a benzene molecule in the case of **33**, or NaCl in the case of **35**, and the expected six-coordinate preference of the chromium(III) metal centre, they proposed the formation of **36**.

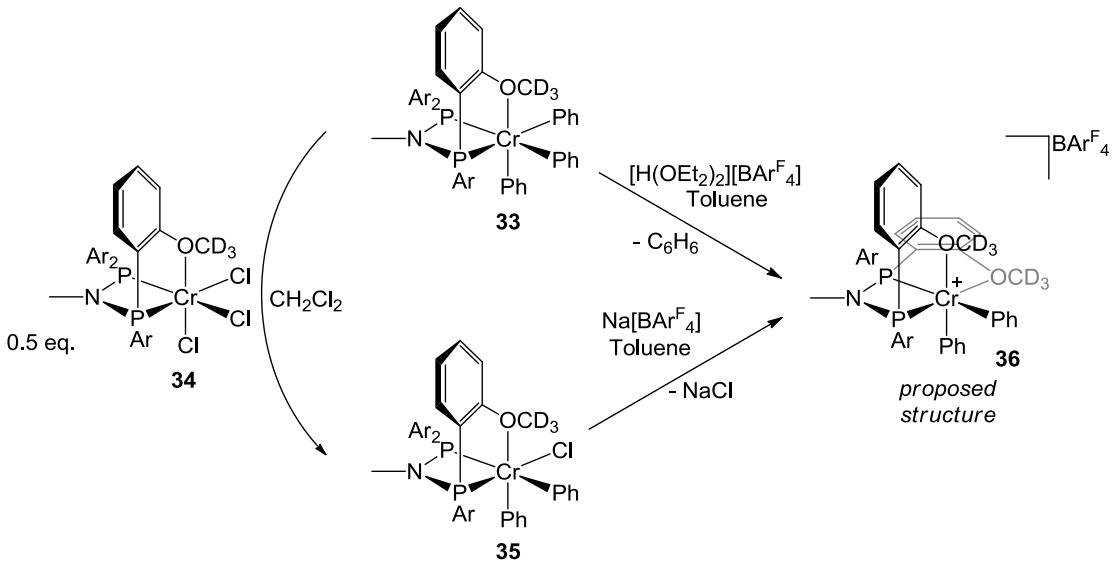

Scheme 3.6. The coordination modes of **33**, **34** and **35** showing the chromium-oxygen bonding occurring and the synthesis of the suggested doubly oxygen-bound species **36** via abstraction of the chloride or the benzene molecule.

Lavanant and co-workers have also been interested in the coordination mode of these PNP(*o*-OMe) ligands, as in some cases the enhancements of the catalytic activity and/or selectivity has been proposed to arise from steric effects of this type of ligands,[20, 21] while in other cases the *ortho*-methoxy groups have been reported as hemilabile.[12, 18, 22] Lavanant reported the bond-lengths of the four-coordinate [Ni((2-OMe-C_6H_4)$_2$PNMeP(2-OMe-C_6H_4)$_2$)Br_2] compound that adopts a distorted square-planar geometry. Upon investigating the nickel-oxygen distances they concluded that no interaction is occurring, as in all cases the Ni-O distances were longer than the corresponding van der Walls radii (3.66 Å *vs.* 3.15 Å). Presumably this lack of coordination of the oxygen atom is due to the 4-coordinate preference of the d^8 metal centre of Ni(II).[23]

3.2. Ligands

Based on the successful trimerisation results obtained by Wass using the PNP-type ligands, and the coordination modes reported by Labinger and Bercaw, it was decided to investigate the potential for hemilability of small bite-angle systems using Ar_2PNMePAr_2 as the ligand on appropriate rhodium fragment (Ar = 2-OMe-C_6H_4) (**37**).

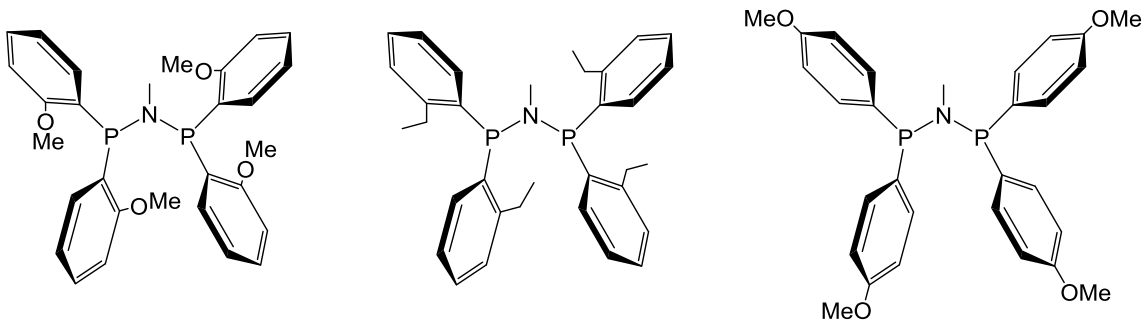

Figure 3.5. Three ligands synthesised to compare the steric and electronic effects of this motif.

In order to establish whether any coordination via the oxygen atom of the OMe group is occurring and to allow for direct comparison, the sterically similar $Ar_2PNMePAr_2$ ligand where Ar = 2-Et-C_6H_4 (**38**) was also synthesised. Additionally, to establish the electronic effect of the ligand the electronically similar yet sterically different $Ar_2PNMePAr_2$ ligand where Ar = 4-OMe-C_6H_4 (**39**) was synthesised (Figure 3.5). This *para*-substituted ligand should be electronically similar to 2-OMe, but due to the lack of a substituent at the *ortho* position, the steric influence and hemilability would be expected to be different. Also, Wass has shown that upon comparing the electronically related *ortho*-methoxy substituted PNP(*o*-OMe) **37** and *para*-methoxy substituted PNP(*p*-OMe) ligand **39**, a substantial difference in catalytic activity for the ethylene trimerisation reaction was observed.[12] In the case of **37** excellent activity was obtained, while the *para*-substituted **39** proved to be inactive under the same reaction conditions.

The combined data from the resulting metal-ligand complexes in catalysis was expected to allow for us to draw conclusions about this ligand motif and its effect on the intermolecular hydroacylation reaction to be drawn.

3.2.1. Ligand Synthesis

Although established, the synthesis of (2-OMe-C_6H_4)$_2$PNMeP(2-OMe-C_6H_4)$_2$ (**37**) initially proved difficult in our hands. We followed a procedure kindly provided by Prof. Duncan Wass, where initially $Cl_2PNMePCl_2$ is synthesised and the desired PNP product is obtained by reacting $Cl_2PNMePCl_2$ with the relevant Grignard reagent (Scheme 3.7). The usefulness of this approach

is the fact that upon synthesising the $Cl_2PNMePCl_2$ precursor, the new modified PNP ligands can be easily synthesised by reacting it with different Grignard reagents.[12, 24]

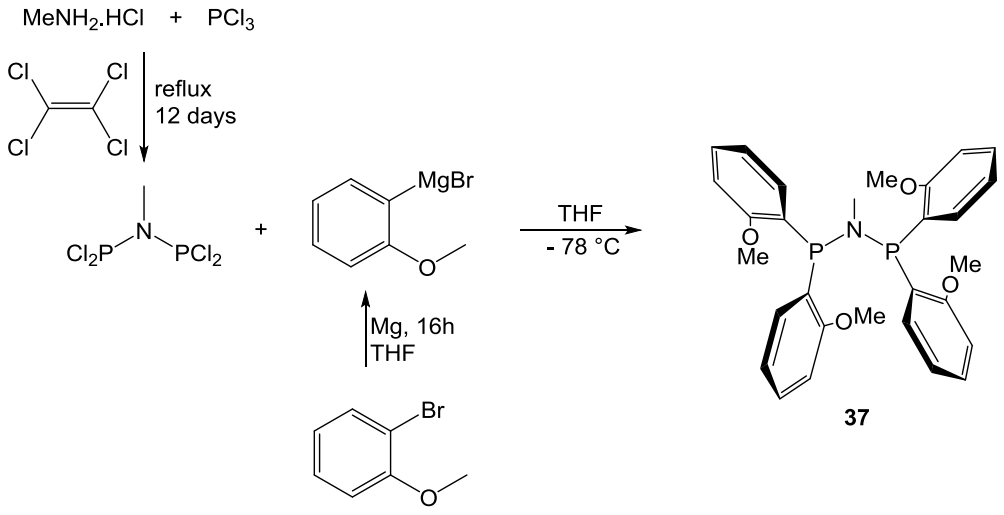

Scheme 3.7. The synthesis of the ligand **37**.

The synthesis of $Cl_2PNMePCl_2$ involved the dissolving of methylamine hydrochloride in 1,1,2,2-tetrachloroethylene (b.p. 121 °C). To this solution PCl_3 was then added and the mixture was set refluxing for 12 days (based on ^{31}P NMR spectral data the reaction had reached approximately 70% conversion after 5 days although no further reactivity was seen over the following 7 days). The solution was subsequently filtered and the solvent was removed *in vacuo*. The formation of a single product was confirmed by $^{13}C\{^1H\}$ and $^{31}P\{^1H\}$ NMR spectra, and these data were in agreement with the previously reported data.[25] To the obtained $Cl_2PNMePCl_2$ in THF (at –78 °C) (2-methoxyphenyl)magnesium bromide was added (synthesised from 1-bromo-2-methoxybenzene). This resulted in the formation of the desired ligand **37** in THF, which turned into a sticky wax-like brown product upon removing the THF under reduced pressure. This step caused a problem to our synthesis, as any THF left in the mixture can affect the formation of the desired rhodium complexes due to the coordinating ability of the THF molecule. Subsequental washing with cold methanol allowed for the removal of any excess Grignard reagent in the mixture, and most of the THF, resulting in white solid. Addition of fluorobenzene to this solid, followed by sonication, allowed the removal of any entrained THF and upon setting the solution under reduced pressure the product was obtained as white powder with no THF in the system (due to the higher boiling point of fluorobenzene compared to THF, 85 °C *vs.* 66 °C). The purity

of the ligand was confirmed by ^{1}H and ^{31}P NMR spectra ($^{31}P\{^{1}H\}$ NMR spectrum shows a singlet at δ 52.1.). The ligand was stored under an argon atmosphere in a glovebox (62% yield).

The synthesis of (2-Et-C_6H_4)$_2$PNMeP(2-Et-C_6H_4)$_2$ (**38**) was carried out in an analogous manner to **37**. (2-ethylphenyl)magnesium bromide was synthesised from the reaction between 1-bromo-2-ethylbenzene and magnesium metal in THF. This Grignard reaction is not straightforward and in order to initiate the reaction, a small iodine crystal had to be added to the reaction mixture and then in the presence of a small amount of 1-bromo-2-ethylbenzene the solution was heated until reactivity was noted. The resulting Grignard product was added to the previously prepared $Cl_2PNMePCl_2$ in THF (at –78 °C) to yield the desired product. The isolation procedure was analogous to that of **37**, and the ligand was obtained as a white solid (65% yield). The formation of **38** was confirmed by ^{1}H and ^{31}P NMR spectroscopy.[26] $^{31}P\{^{1}H\}$ NMR spectrum shows a singlet at δ 55.9. The ^{1}H NMR spectrum shows two environments for the CH_2 protons of the *ortho*-ethyl groups, corresponding to the previously published results.[27]

The synthesis of (4-OMe-C_6H_4)$_2$PNMeP(4-OMe-C_6H_4)$_2$ (**39**) was also carried out following the procedure set for **37**. (4-methoxyphenyl)magnesium bromide was synthesised from the reaction between 1-bromo-2-methoxybenzene and magnesium metal, and the resulting product was added to the previously prepared $Cl_2PNMePCl_2$ in THF (at –78 °C). The isolation process was analogous to **37** although relative solubility of **39** in methanol posed a problem during the isolation step, but this was overcome by use of less methanol and longer sonication times, and the ligand was obtained as a white solid (41% yield). The formation of **39** was confirmed by ^{1}H and ^{31}P NMR spectroscopy. The $^{31}P\{^{1}H\}$ NMR spectrum shows a singlet at δ 70.0.[25]

3.2.2. The Synthesis of the Rhodium Pre-Catalysts

3.2.2.1. *The synthesis of [Rh{(2-OMe-C_6H_4)$_2$PNMeP(2-OMe-C_6H_4)$_2$}(C_6H_5F)][BAr^F_4] (**41**)*

Similar to the small bite-angle ligands investigated in Chapter 2, the attempts to complex the **37** using neutral rhodium complexes [Rh(cod)Cl]$_2$ and [Rh(nbd)Cl]$_2$ and subsequent hydrogenation led to the formation of impure product; as shown by the resulting ^{31}P NMR spectra of the

reaction mixtures. The use of the preformed cationic starting material $[Rh(cod)_2][BAr^F_4]$ (**9**) allowed for the formation of the cod-complex **40** (Scheme 3.8) cleanly which was assigned by ^1H and $^{31}P\{^1H\}$ NMR spectroscopy. The ^1H NMR spectrum is consistent to the cod-bound complex and the $^{31}P\{^1H\}$ NMR spectrum shows a chemical shift at δ 39.2 [*J*(RhP) = 140 Hz], ESI-MS spectrum shows a peak at m/z = 730.17 with the expected isotopic pattern. Complex **40** was subsequently hydrogenated in fluorobenzene at 4 atm overnight in order to obtain the desired fluorobenzene complex **41** (Scheme 3.8). Interestingly this reaction is less prone to decomposition compared to the equivalent isopropyl and cyclohexyl ligands, *e.g.* decomposition of **11a** – **11e** was observed after only approximately 1h.[3, 28] This overnight hydrogenation reaction resulted in the formation of the desired η^6-coordinated fluorobenzene complex $[Rh(Ar_2PNMePAr_2)(\eta^6\text{-}C_6H_5F)][BAr^F_4]$ (Ar = 2-OMe-C_6H_4) (**41**), and a colour change of dissolved complex from deep orange (**40**) to pale orange (**41**).

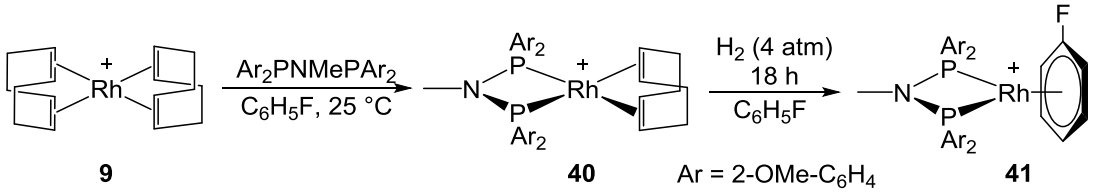

Scheme 3.8. The synthesis of the *ortho*-methoxy substituted **41** starting from $[Rh(cod)_2][BAr^F_4]$ (**9**). The $[BAr^F_4]^-$ counter-anion is not pictured for clarity.

Upon initial isolation **41** forms as an oily product. The purification was carried out by initially washing the oily product with pentane followed by a slow addition of pentane to the fluorobenzene solution of **41** with sonication. This allowed, over time, the formation of a pale orange solid which was then isolated by filtration. The product was obtained in good yield (60 – 70 %, repeated synthesis) and its formation was confirmed by analytical methods. The ^1H NMR spectrum (in C_6H_5F solvent) showed the coordination of the fluorobenzene ring (three environments in 2:2:1 ratio at δ 5.5 – 6.3, *cf.* a doublet and a multiplet centred at 7.1 observed for free fluorobenzene),[29] the aromatic protons on the 2-Me-phenyl groups at δ 6.5 – 7.5, the methoxy groups at δ 3.2 as a single environment (12H) and the NMe backbone at δ 2.7 (3H). The $^{31}P\{^1H\}$ NMR spectrum shows a single doublet at δ 45.4 showing coupling to ^{103}Rh [*J*(RhP) = 188 Hz] and to ^{19}F [*J*(PF) = 3.6 Hz], consistent with the formation of the fluorobenzene adduct.[3, 30] The

ESI-MS spectrum of the complex shows a peak at m/z = 718.12 corresponding to the calculated mass of the $[Rh((2\text{-}OMe\text{-}C_6H_4)_2PNMeP(2\text{-}OMe\text{-}C_6H_4)_2)(\eta^6\text{-}C_6H_5F)]^+$ fragment, which also shows the isotopic pattern corresponding to the desired species. The purity of the complex was confirmed by elemental analysis. Upon layering of the fluorobenzene solution of **41** with pentane, suitable crystals for X-ray crystallography were obtained and the structure was determined (Figure 3.6). The resulting crystal structure confirms the η^6-coordination mode of the fluorobenzene ligand. The P-Rh-P bite angle of 70.22(4)° is comparable to the ones reported for the analogous rhodium PNP(^{i}Pr) and PCP(^{i}Pr) complexes (70.36(4)° for **11b** and 72.64(5)° for **11c**) discussed in Chapter 2. It is interesting to note that the solid-state structure shows the methoxy-groups positioned in four different environments, while both the solution ^{1}H and ^{31}P{^{1}H} NMR spectra suggest only one chemical environment for these groups. This is indicative of rotation around the P-C(aryl) bond at room temperature. Unfortunately low temperature NMR spectrum was not collected for **41**.

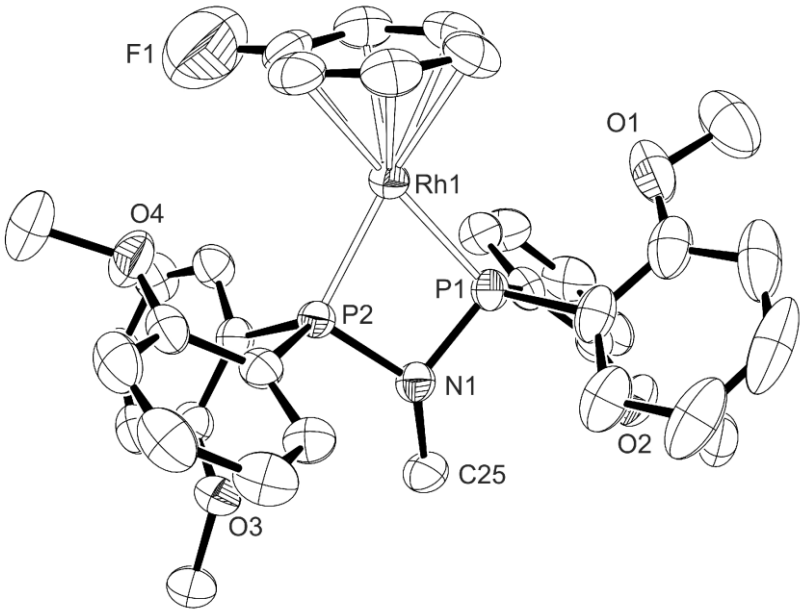

Figure 3.6. Solid state structure of the cation **41**. Displacement ellipsoids depicted at the 50% probability level. Hydrogen atoms, anion and disordered component (C_6H_5F ligand) omitted for clarity. All unlabelled atoms are carbon atoms. Key bond lengths (Å) and angles (°): Rh1-P1, 2.2142(10); Rh1-P2, 2.2132(11); Rh1-C, 2.278(4)-2.360(4); P1-Rh1-P2, 70.22(4); P1-N1-P2, 97.20(17).

It was found that the isolation of a solid of **41** could be achieved more easily by adding pentane to the dichloromethane solution instead of fluorobenzene solution of **41**, but this also resulted

in the formation of a substantial quantities of another species in the reaction mixture seen as a complicated set of peaks by $^{31}P\{^{1}H\}$ NMR spectroscopy (in CD_2Cl_2) at approximately δ 40 – 43 and δ 48 – 52 as shown in Figure 3.7; while the peak at δ 39.5 corresponds to the fluorobenzene species **41**. This same result is seen upon dissolving the isolated fluorobenzene complex **41** in dichloromethane.

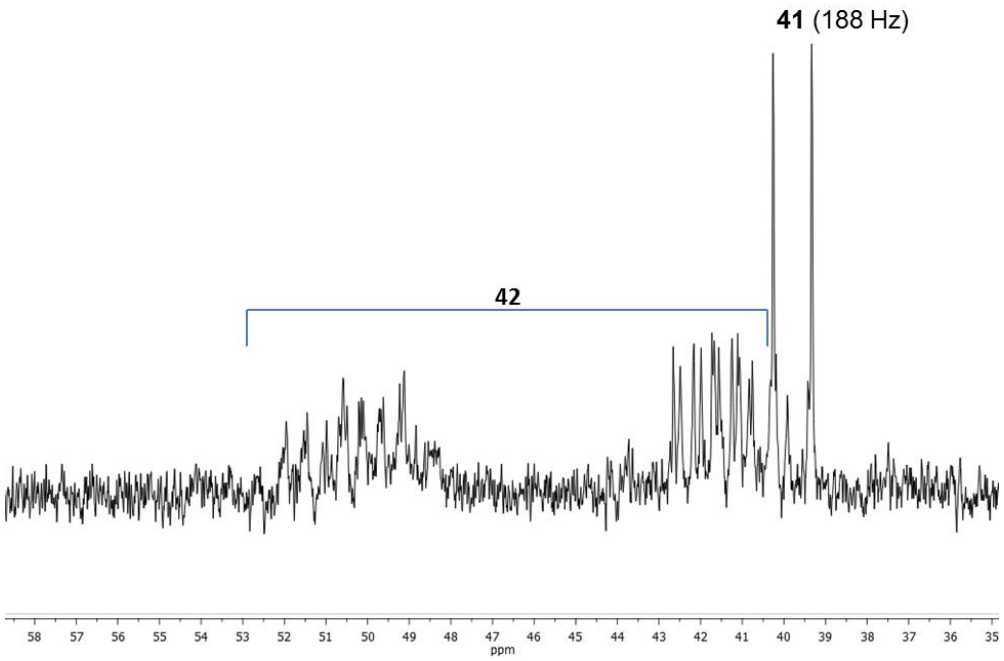

Figure 3.7. $^{31}P\{^{1}H\}$ NMR spectrum of **41** dissolved in CD_2Cl_2.

The formed solution was investigated by ESI-MS, which showed a peak for **41** (m/z = 718.12) but also a peak at m/z = 622.08 (where z = 2, shown by the half mass units in the isotopic pattern) corresponding to a dimeric species containing two rhodium phosphine fragments – $[Rh(Ar_2PNMePAr_2)]_2^{2+}$. We assign this species as the aryl-bound dimer **42** (Scheme 3.9), similar to the complex reported by Bosnich and Weller groups previously, both upon using the $[Rh(dpp3)]^+$ fragment, and by Pluth using $[Rh(dpp2)]^+$ fragment.[31-34] This complicated second order $^{31}P\{^{1}H\}$ NMR spectrum results from the different bonding modes the dimer can adopt. Based on the $^{31}P\{^{1}H\}$ NMR spectroscopy results Bosnich commented on the formation of isomers (in 88:12 ratio) which were seen as two sets of doublets of doublets corresponding to both isomers. The formation of stereoisomers arises from the possible enantiomeric forms the complex can take. The dimeric $[Rh(dpp3)]_2[BAr^F{}_4]_2$ complex can result as two enantiomeric

isomers (RR and SS) and the optically inactive superposable *meso* complex (RS/SR) (*cf.* **42** in Scheme 3.9). In the case of **42** analogous bonding modes can be expected, but additionally the presence of the *ortho*-methoxy groups on the phenyl rings leads to the formation of another set of isomers as the OMe group can point in two different directions, thus further complicating the $^{31}P\{^{1}H\}$ NMR spectrum of **42**.

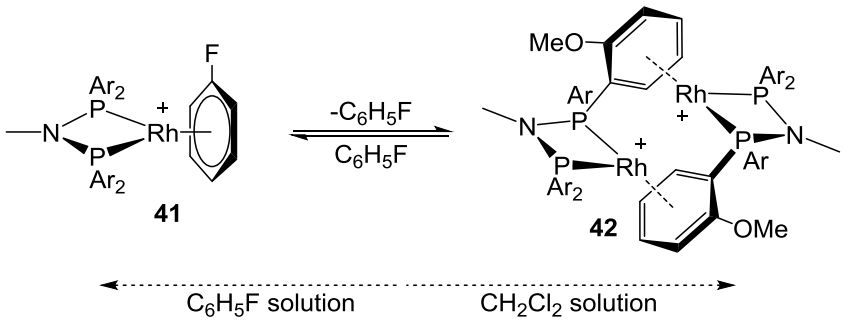

Scheme 3.9. Schematic representation of the equilibrium between **41** and **42** in different solvents. Ar = 2-OMe-C_6H_4. The $[BAr^F_4]^-$ counter-anion is not pictured for clarity.

The formation of this dimeric species (**42**) is no doubt caused by equilibrium between the fluorobenzene complex **41** and dimer **42** due to the similar η^6-binding modes (Scheme 3.9). Upon removing fluorobenzene solvent and dissolving the complex in CH_2Cl_2, the equilibrium is shifted towards the dimer as the relative amount of fluorobenzene in the solution is dramatically reduced. Interestingly, and as expected, no such dimers are observed for the alkyl substituted ligands.

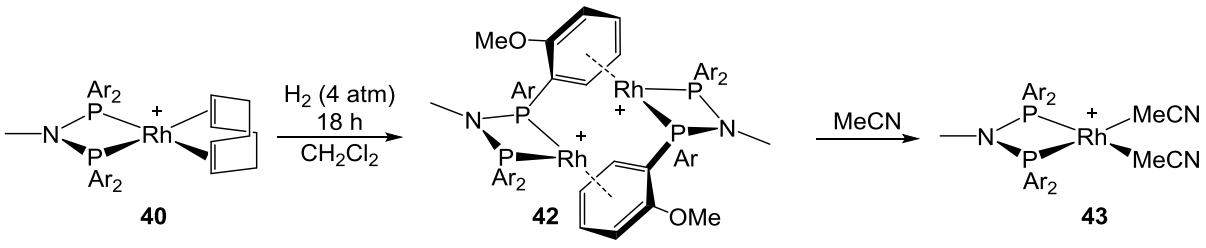

Scheme 3.10. The expected coordination mode of the formed species (**42**) upon carrying out the hydrogenation of **40** in CH_2Cl_2. Also the dimeric species **42** is formed upon dissolving the fluorobenzene complex in CH_2Cl_2. Upon dissolving **42** in acetonitrile, unique formation of **43** is observed. The $[BAr^F_4]^-$ counter-anion is not pictured for clarity.

The same complicated set of $^{31}P\{^{1}H\}$ NMR resonances (δ 40 – 43 and δ 48 – 52) were observed upon performing the hydrogenation reaction of **40** in CH_2Cl_2. Although the hydrogenation reaction conducted in CH_2Cl_2 leads to substantial decomposition (indicated by large amount of

the rhodium complex reduced to colloidal rhodium), by $^{31}P\{^{1}H\}$ NMR spectroscopy the distinctive pattern (*cf.* Figure 3.7), and the peak at m/z = 622.08 by ESI-MS were observed (corresponding to **42**). Upon addition of MeCN to this sample (or to the one showing equilibrium between **41** and **42**, Figure 3.7) full conversion into a *bis*-acetonitrile complex $[Rh(Ar_2PNMePAr_2)(MeCN)_2][BAr^F_4]$ (**43**) was observed by ^{1}H and $^{31}P\{^{1}H\}$ NMR spectroscopy. $^{31}P\{^{1}H\}$ NMR spectrum shows a clean product with a chemical shift at δ 49.1 [J(RhP) = 159 Hz] (Figure 3.8).

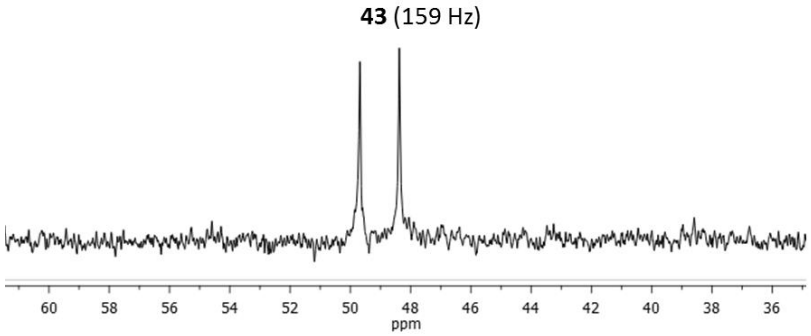

Figure 3.8. The $^{31}P\{^{1}H\}$ NMR spectrum of the bis-MeCN complex **43**.

Complex **43** was not observed by ESI-MS probably due to decomposition of the species under the ESI-MS conditions. Similar problems have been noted with $[Rh(bis\text{-phosphine})(L_2)]^+$ fragments previously, where L = acetone or MeCN. Unfortunately we were not able to grow crystals of either the dimeric species **42** or the *bis*-acetonitrile species **43**. However, the elemental analysis of the acetonitrile species **43** was obtained, and is consistent with the expected C, N, H ratio.

3.2.2.2. *The Synthesis of $[Rh\{(2\text{-}Et\text{-}C_6H_4)_2PNMeP(2\text{-}Et\text{-}C_6H_4)_2\}(C_6H_5F)][BAr^F_4]$* (**48**)

Using the established route that allowed for the synthesis of **41** and **11a** – **11e** (Chapter 2), the synthetic procedure was carried out using the *ortho*-ethyl ligand **38**. The initial addition of the ligand to $[Rh(cod)_2][BAr^F_4]$ (**9**) resulted in the expected $[Rh(Ar_2PNMePAr_2)(cod)][BAr^F_4]$ complex (**47**), but to our surprise, the hydrogenation (4 atm) in fluorobenzene did not allow for the formation of the desired fluorobenzene complex $[Rh(Ar_2PNMePAr_2)(\eta^6\text{-}C_6H_5F)][BAr^F_4]$ (**48**). Instead the $[Rh(Ar_2PNMePAr_2)(cod)][BAr^F_4]$ complex was seen as the only, unreacted, product.

Even heating the reaction at 40 °C for several days (in fluorobenzene solvent, 4 atm H_2) did not result in the formation of **48**.

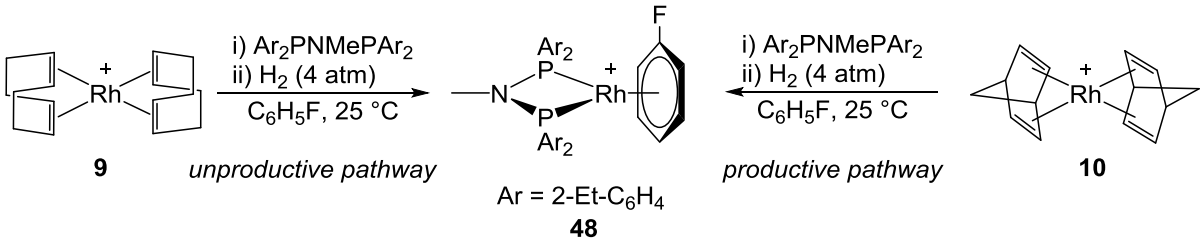

Scheme 3.11. Synthesis of the *ortho*-ethyl substituted catalyst **48**. Unproductive approach using the *bis*-cod starting material *vs.* productive approach using the *bis*-nbd starting material. The $[BAr^F_4]^-$ counter-anion is not pictured for clarity.

It is postulated that due to the bulky nature of *ortho*-substituted phenyl substituents on phosphorus atoms, this might be a steric effect. The hydrogenation step was also carried out in different solvents that would not lead to the formation of η^6-coordinated systems: the hydrogenation reaction was performed in acetone, acetonitrile and dichloromethane. Interestingly, all of these hydrogenation reactions led to decomposition indicated by the formation of colloidal rhodium in the solution. Although discouraging, the pursuit for the synthesis of the desired fluorobenzene complex **48** was continued with $[Rh(nbd)_2][BAr^F_4]$ (**10**) as the starting material.[35] Rhodium nbd species have been used successfully before in the Weller group in the synthesis of fluorobenzene complexes, and it has been shown that the hydrogenation of nbd is much faster compared to the hydrogenation of the cod ligand.[3, 9] This seemed like a potentially fruitful synthetic route, particularly as the main problem using nbd-ligand on rhodium with small bite-angle ligands is that they led to the formation of *bis*-substituted species with the general structure of [Rh(*bis*-phosphine)$_2$][BAr^F_4]. As this was not a problem for previously reported bulky tert-butyl ligand $^tBu_2PCH_2P^tBu_2$, it was speculated that the use of **10** in the case of bulky *ortho*-ethyl ligand **38** would not be problematic. Pleasingly $[Rh(Ar_2PNMePAr_2)(nbd)][BAr^F_4]$ (Ar = 2-Et-C_6H_4) could be synthesised cleanly, and upon placing it under hydrogen atmosphere (4 atm) overnight, the formation of the desired $[Rh(Ar_2PNMePAr_2)(\eta^6\text{-}C_6H_5F)][BAr^F_4]$ (**48**) was observed by colour change from deep orange to pale orange, and $^{31}P\{^1H\}$ NMR spectroscopy. The product was isolated from a fluorobenzene/pentane solution by sonication, and further washed with pentane, resulting in an

orange solid in 72% yield. The formation of **48** was also observed by ESI-MS (m/z = 710.20, with the observed isotope pattern corresponding to the expected pattern) and microanalysis. Unfortunately all attempts to crystallise the product failed.

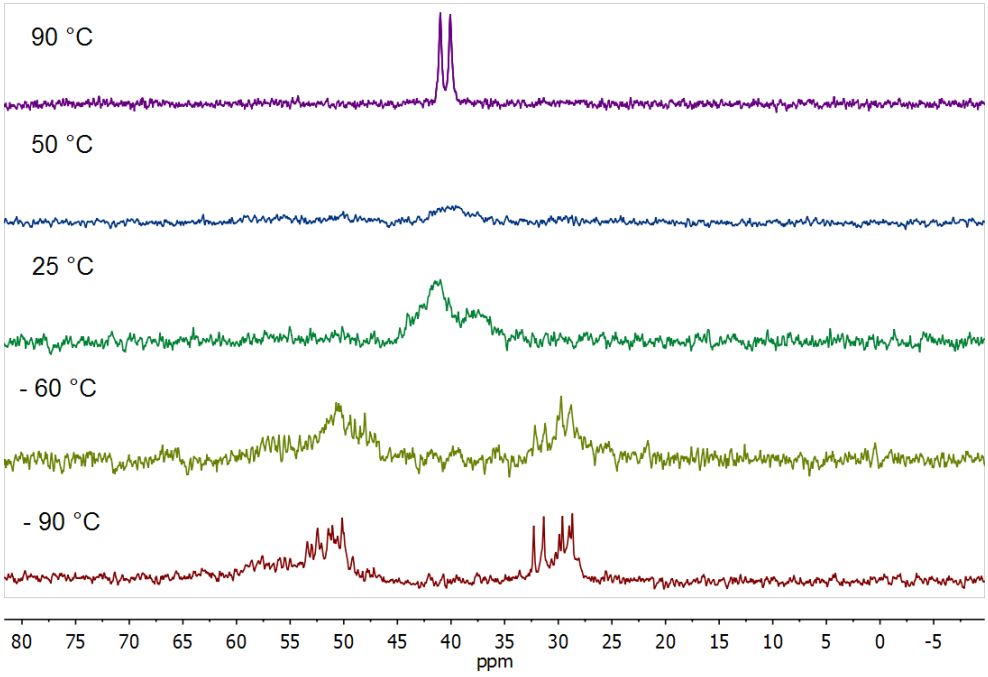

Figure 3.9. $^{31}P\{^{1}H\}$ NMR spectra of **48** at a range of different temperatures. Spectra at –90, –60 and 25 °C were acquired in CD_2Cl_2, while spectra at 50 and 90 °C were acquired in C_6H_5F, due to the relative boiling and melting points of these solvents. At 25 °C, the same spectrum is observed in both solvents.

Instead of the expected doublet of doublets due to rhodium phosphine and phosphorus fluorine coupling as was observed for **41**, in the $^{31}P\{^{1}H\}$ NMR spectrum (25 °C, C_6H_5F solvent) two broad signals were seen in an approximately 1:1 ratio (Figure 3.9). In CD_2Cl_2 solvent an analogous $^{31}P\{^{1}H\}$ NMR spectrum was obtained suggesting that this species was not observed due to an arene bridged dimer formation. Also **48** was seen as the only product formed by ESI-MS. Upon cooling the CD_2Cl_2 solution containing **48**, the initial two broad peaks resolved into two complicated multiplets, suggesting that at this low temperature regime, the product is not fluxional, and presumably due to the steric effects, the complex resolves in a number of conformations. Unfortunately no suitable crystals for X-ray crystallography were obtained, but as was previously commented for the crystal structure of **41**, where all the OMe groups were in different environments, this could also be the case for **48** at 25 °C, resulting in the multiplets in

the $^{31}P\{^{1}H\}$ NMR spectrum. Whereas heating the sample to as high as 90 °C (in fluorobenzene solvent) **48** becomes fluxional on the NMR timescale, and a simple doublet at δ 41.5 [*J*(RhP) = 188 Hz] was observed. Unfortunately even at such high temperature, phosphine fluorine coupling cannot be observed due to the relative broadness of these peaks (Figure 3.9).

3.2.2.3. *The Attempted Synthesis of [Rh{ (4-OMe-C_6H_4)$_2$PNMeP(4-OMe-C_6H_4)$_2$}(C_6H_5F)][BAr^F_4] (**50**)*

The attempted synthesis of [Rh(cod)(Ar_2PNMePAr_2)][BAr^F_4] complex, where Ar is 4-OMe-C_6H_4, was carried out by a reaction between [Rh(cod)$_2$][BAr^F_4] (**9**) and the relevant Ar_2PNMePAr_2 ligand **39** (Ar = 4-OMe-C_6H_4). Unfortunately this reaction followed the trend discussed in Section 2.2.2., where the formation of [Rh(*bis*-phosphine)$_2$][BAr^F_4] complexes dominates. Instead of the desired complex **50** the *bis*-substituted product, [Rh{(4-OMe-C_6H_4)$_2$PNMeP(4-OMe-C_6H_4)$_2$}$_2$][BAr^F_4], was observed in addition to some decomposition material. This adds further weight to that lower steric bulk on the phosphines promotes formation of the *bis*-chelate.

3.2.2.4. *Bis-Acetone Complexes of the Motif of [Rh(R_2PXPR_2)(acetone)$_2$][BAr^F_4]*

As hydroacylation catalysis is generally performed in acetone solvent, and as we had previously seen the formation of *bis*-acetone small bite-angle complexes of the general formula of [Rh(R_2PXPR_2)(acetone)$_2$][BAr^F_4] (**16a** – **16e**), the synthesis of the corresponding *bis*-acetone complex [Rh{(2-OMe-C_6H_4)$_2$PNMeP(2-OMe-C_6H_4)$_2$}(acetone)$_2$][BAr^F_4] (**44**) was attempted. Following the method used for **16a** – **16e**, the fluorobenzene complex **41** was dissolved in acetone. Instead of the formation of a single species, a range of peaks were seen by $^{31}P\{^{1}H\}$ NMR spectrum (Figure 3.10). Signals corresponding to the fluorobenzene complex **41** was also observed as a doublet of doublets at δ 42.1 [*J*(RhP) = 188 Hz, *J*(PF) = 3 Hz] suggesting a similar equilibrium between the fluorobenzene and the *bis*-acetone complexes as was observed in the case of **16a** – **16c**.[3] A major doublet at δ 50.5 [*J*(RhP) = 183 Hz] and additionally a smaller

doublet at δ 42.9 [*J*(RhP) = 191 Hz] were observed. Interestingly, surrounding both doublets there were additional small multiplets.

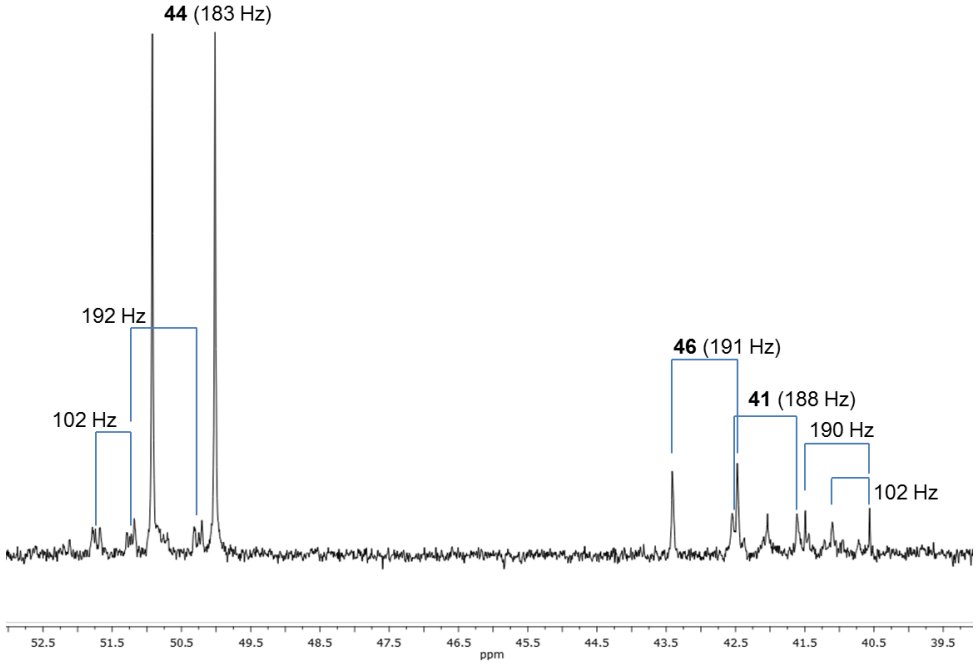

Figure 3.10. $^{31}P\{^{1}H\}$ NMR spectrum of the acetone complex **44** plus potential rhodium-oxygen bound species and the fluorobenzene complex **41**.

Based on NMR spectra the main species was assigned as the desired [Rh{(2-OMe-$C_6H_4)_2$PNMeP(2-OMe-$C_6H_4)_2$}(acetone)$_2$][$BAr^F{}_4$] complex (**44**) and potentially the other new species seen as a doublet at δ 42.9 could correspond to a *bis*-OMe coordinated species (**46**) (Scheme 3.12). This allows for the speculation that the small multiplets close to both doublets correspond to the two phosphorus environments created in case of *mono*-OMe coordinated complex **45**. This would result in a species where one phosphorus atom is in a similar environment as the phosphorus atoms in **44** and the other phosphorus atom is in a similar environment as the phosphorus atoms in **46** (Scheme 3.12). Unfortunately ESI-MS data for this mixture was inconclusive (acetone bound complexes often lead to decomposition under ESI-MS conditions) and any attempts to crystallise these complexes failed, thus we are cautious on commenting on this data any further.

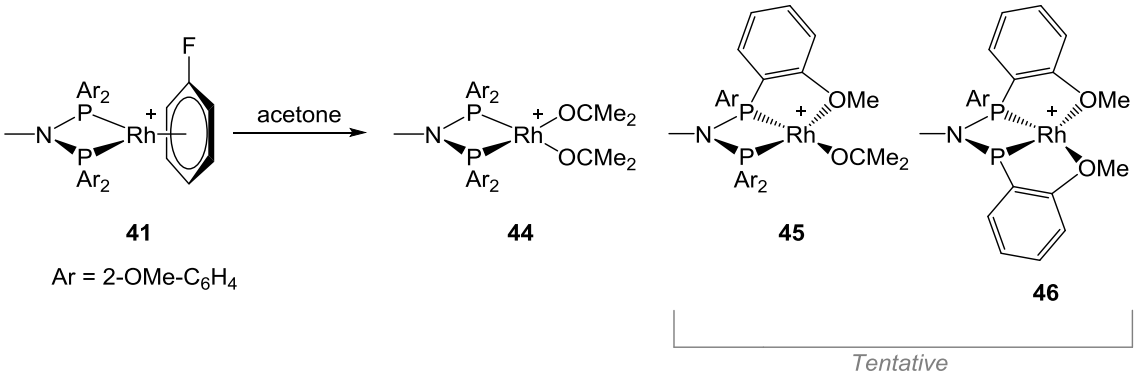

Scheme 3.12. The synthesis of the *bis*-acetone complex **44** and the suggested potential side-products that formed during the reaction. The $[BAr^F_4]^-$ counter-anion is not pictured for clarity.

Although it was not possible to confirm these bonding modes, the lability of these complexes was confirmed. By removing acetone solvent under reduced pressure and addition of MeCN to the obtained oil, an immediate colour change from orange to yellow was observed. By $^{31}P\{^1H\}$ NMR spectroscopy, this led to the formation of the *bis*-MeCN product (**43**) as the only species.

When the *ortho*-ethyl fluorobenzene complex **48** was dissolved in acetone the *bis*-acetone species, $[Rh((2\text{-Et-}C_6H_4)_2PNMeP(2\text{-Et-}C_6H_4)_2)(acetone)_2][BAr^F_4]$ (**49**) was formed. Unlike for **44**, only one species was observed and this was confirmed by ^1H and ^{31}P NMR spectra. $^{31}P\{^1H\}$ NMR spectrum shows a doublet at δ 45.4 [*J*(RhP) = 178 Hz].[3] This different reactivity compared to the *ortho*-methoxy complex **44**, further indicates that additional coordination to the metal centre might be occurring through the OMe groups rather than the aromatic rings.

3.3. Catalysis

3.3.1. Preliminary Catalytic Studies

Catalytic studies were carried out using the established benchmark reaction between 2-(methylthio)benzaldehyde (**E**) and 1-octene or 1-octyne (Scheme 3.13).

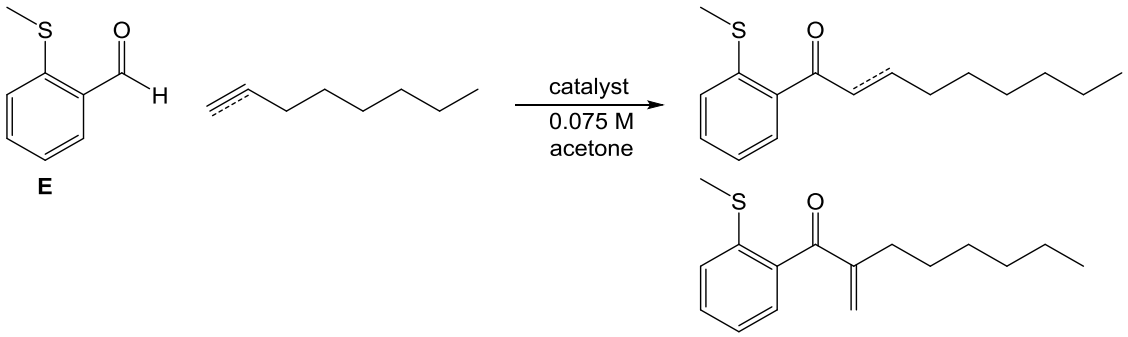

Scheme 3.13. Hydroacylation reaction using 2-(methylthio)benzaldehyde (**E**) and 1-octene or 1-octyne as the substrates. In case of alkyne hydroacylation also the branched product can be seen.

Table 3.1. Comparison of **41** to isopropyl substituted **11b** and tert-butyl substituted **5** in hydroacylation reaction of 2-(methylthio)benzaldehyde (**E**) and 1-octene or 1-octyne.

Entry	Catalyst	Substrate	Conversion / %	Time / min	Solvent	Temperature / °C
1	PNP(*o*-OMe) **41**	1-octene	< 5	120	acetone	55
2	PNP(^{i}Pr) **11b**	1-octene	64	60	acetone	55
3	PCP(^{t}Bu) **5**	1-octene	94	15	acetone	55
4	PNP(*o*-OMe) **41**	1-octyne	100	5	acetone	25
5	PNP(^{i}Pr) **11b**	1-octyne	100	5	acetone	25
6	PCP(^{t}Bu) **5**	1-octyne	90	360	acetone	25

*Conditions: 10 mol% catalyst, 0.075 M aldehyde, 1:1.5 **E**:1-octene/1-octyne. Conversions measured by HPLC.*

Initial catalytic screening was conducted under high catalyst loadings of 10 mol% and at low concentration of aldehyde (0.075 M of **E**) as previously used. First, the ability of **41** as the alkene hydroacylation catalyst was probed, as catalysts with bulky substituents on phosphorus atoms *e.g.* PCP(^{t}Bu) complex (**5**), have previously shown to be highly efficient alkene hydroacylation catalysts (Entry 3, Table 3.1).[1] Unexpectedly, the reaction between **E** and 1-octene, using **41** as the catalyst, resulted only in a negligible amount of conversion to the desired product even after 2 h of stirring at 55 °C (Entry 1, Table 3.1).

Similar poor abilities for alkene hydroacylation catalysis were previously seen using PNP(^{i}Pr) catalyst **11b**. As **11b** turned out to be in fact highly efficient alkyne hydroacylation catalysts, alkyne hydroacylation reaction using catalyst **41** was carried out. Under the same initial reaction conditions (10 mol% **41**, 0.075 M, 25 °C, 1:1.5 aldehyde:alkyne), using **E** and 1-octyne as substrates, full conversion to the desired product was observed within 5 minutes (Entry 4,

Table 3.1). Noteworthy is that under these conditions the analogous PNP(^{i}Pr) catalyst **11b** also led to 100% conversion in 5 minutes (Entry 5, Table 3.1). Encouraged by this rate of catalysis it was important to continue this investigation using lower catalyst loadings, which would allow for us to determine whether there is any difference in reactivity between **41** and the similar isopropyl complex **11b** that has no stabilising OMe group in its ligand design and that worked at 1 mol% catalyst loading.

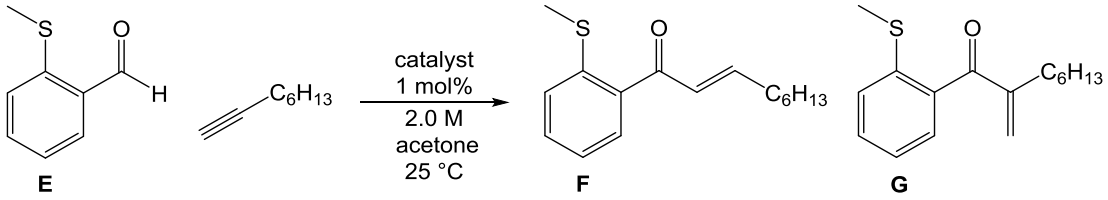

Scheme 3.14. Alkyne hydroacylation reaction using 2-(methylthio)benzaldehyde (**E**) and 1-octyne as the substrates under optimal conditions. The ratio of **E**:1-octyne is 1:1.5. At the end of the reaction linear (**F**) and branched product (**G**) were seen, while the ratio of the products is dependent on the catalyst used.

At 1 mol% catalyst loading of **41** (2 M aldehyde, 25 °C, 1:1.5 **E**:1-octyne, acetone) (Scheme 3.14) 52% conversion to the product was observed during the first 5 minutes, while after an hour approx. 90% conversion was seen, and full conversion in 3 h (Entry 3, Table 3.2) (*cf.* under the same reaction conditions **11b** allows for full conversion in less than 10 minutes, Entry 1, Table 3.2). As during the time between 5 minutes and 1 h, an extra 38% conversion to the product is seen we can argue that **41** is showing some extra stability towards decarbonylation compared to the previously studied small bite-angle complexes, *i.e.* **11c** shows rapid initial reaction and then shuts down (Entry 2, Table 3.2).

Table 3.2. Hydroacylation reaction between E and 1-octyne under optimal conditions using different small bite angle catalysts.

Entry	Catalyst	Conversion / % (after 5 min)	Conversion / % (after 60 min)	linear:branch ratio (**F**:**G**)
1	PNP(^{i}Pr) **11b**	97	100	21:1
2	PCP(^{i}Pr) **11c**	77	81	12:1
3	PNP(*o*-OMe) **41**	52	90 (100)[a]	2:1

*Conditions: 2 M aldehyde, 25 °C, 1:1.5 **E**:1-octyne, acetone. [a] = conversion after 3 h.*

Under these conditions the selectivity of **41** was also probed. HPLC analysis reveals, that compared to the highly selective PNP(Cy) catalysts (up to 69:1 linear:branched selectivity for **11a**), **41** is a much less selective catalyst, allowing for only a 2:1 linear (**F**) to branched (**G**) product ratio upon using **E** and 1-octyne as the substrates (Scheme 3.14). This reduced selectivity compared to **11a** suggests that the relative energy barriers for reductive elimination for both linear and branched pathway are closer than they are for **11a**.

As 100 % conversion was seen under the optimal conditions described above, it was important to lower the reaction concentration to see the effect of reductive decarbonylation to **41**. The reduced concentration is an useful way of probing the effect of this catalyst deactivation pathway, as decarbonylation is a first order process, and thus is not dependent on the substrate concentration (assuming that acyl-hydride formation is essentially 100%), while hydroacylation is. Hence, the catalysis was performed under dilute conditions used in Chapter 2 (1 mol% catalyst loading, 0.4 M aldehyde, 0 °C, 1:1.5 **E**:1-octyne, acetone). Also carrying out any investigative studies using 2 M concentration is challenging, as due to the small amount of solvent in the mixture any removal of a sample aliquot results in substantial change in the volume of the solution. This investigation at 0.4 M concentration resulted in catalytic conversion, but only 68% of the aldehyde had been converted to product during the transformation. In attempt to gain any extra activity by addition of substrates **E** and 1-octyne (100 eq.) after 1200 minutes resulted in no additional catalysis (Figure 3.11). This suggests that decarbonylation is occurring.

Upon carrying out the hydroacylation reaction under the same conditions as above (1 mol% catalyst loading, 0.4 M aldehyde, 0 °C, acetone), but with an **E** and 1-octyne ratio of 1.5 to 1, 91% conversion to the desired product was observed (Figure 3.11) (23% increase compared to the previous ratio of **E** to 1-octyne = 1:1.5). Although an increase in the overall reactivity was observed, still this did not lead to the full conversion. This additional conversion observed is presumably due to additional attenuation of the effect of the reductive decarbonylation provided by coordination of the aldehyde (discussed in later section). This data shows that even if **41** behaves as a hemilabile catalyst via the coordination of the OMe group to the metal, the

effect of hemilability is not good enough to reduce the effect of reductive decarbonylation substantially.

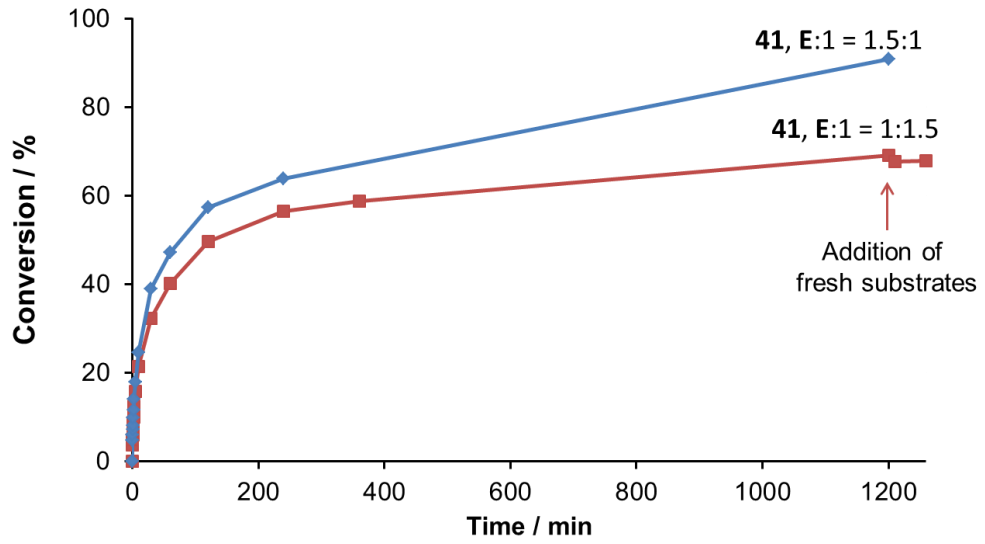

Figure 3.11. Hydroacylation reaction carried out using **E** and 1-octyne as substrates and **41** as the catalyst. Red squares, *aldehyde:alkyne ratio 1:1.5.* After 1200 min, 100 eq. of fresh **E** and 1-octyne were added to the reaction mixture. Blue diamonds, *aldehyde:alkyne ratio 1.5:1. Conditions: 1 mol% catalyst loading, 0.4 M aldehyde, 0 °C, acetone. Conversions were measured by HPLC.*

To further probe the catalytic activity of these species, hydroacylation catalysis was carried out at lower catalyst loading (*i.e.* 0.1 mol%). The use of the PNP(^{i}Pr) catalyst **11b** (in Chapter 2) showed 100% conversion at high concentration (2 M) upon lowering the catalyst loading to 0.5 mol%, while at 0.1 mol% catalyst loading, 30% conversion was seen. In the case of **41**, similar to **11b**, 100% conversion was achieved at 0.5 mol% catalyst loading, while at 0.1 mol% an impressive 70 % conversion was noted (700 turnovers), at the modified 1.5:1 **E**:1-octyne ratio. This impressive activity was tested further by carrying out a recycling experiment. As seen before, at 2 M concentration and 1 mol % catalyst loading **41** mediated the full conversion to product in approximately 3 h. Thus a reaction was carried out using **41** (1 mol%, 2 M, 25 °C, acetone, **E**:1-octyne 1.5:1) and the mixture was allowed to stir for 3 hours, after which additional 100 eq. of **E** and 1-octyne were added to the mixture (in 1:1 ratio). The reaction was followed by taking a small HPLC sample from the reaction mixture before addition of any fresh

substrates. The HPLC data showed that following the initial 100% conversion during the first 3 h, negligible further conversion was seen, *i.e.* **41** is inherently unstable during the hydroacylation reaction using **E** and 1-octyne.

Although the above data shows this catalyst not to be recyclable, it was crucial to try to understand whether the OMe-motif can provide any use in hydroacylation catalysis. For this a comparative catalytic study was performed using **41** and the previously synthesised *ortho*-ethyl complex **48**. Wass has previously reported upon a comparative result using the sterically similar *ortho*-methoxy **37** and *ortho*-ethyl **38** ligands.[12] In this it was shown that for ethylene trimerisation, on chromium (1:1 ratio of **37** or **38** and $[CrCl_3(THF)_3]$) **37** proved to be the best ligand, while the *ortho*-ethyl-group containing **38** on chromium was completely inactive under the same conditions. The two catalysts (**41** and **48**) were compared using **E** and 1-octyne as substrates under the optimal reaction conditions established for **41** (1 mol% catalyst loading, 2 M, acetone, 25 °C, **E**:1-octyne 1.5:1) (Figure 3.12).

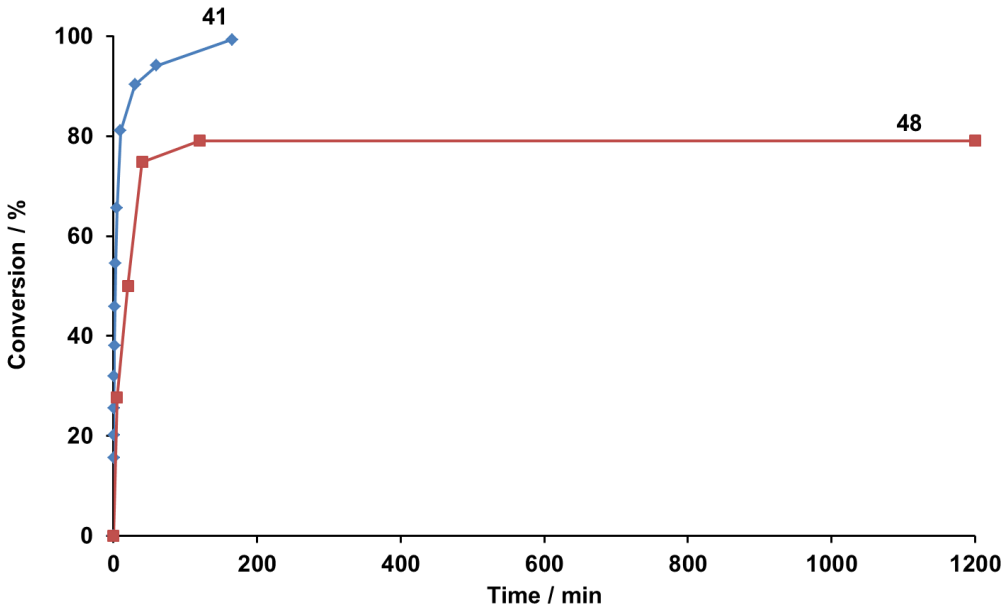

Figure 3.12. Comparison *bis*-phosphine small bite-angle catalysts (**41** and **48**) for the hydroacylation reaction of **E** and 1-octyne over time. Conditions: 1.0 mol% catalyst loading, acetone, 25 °C, 2.0 M aldehyde, **E**:1-octyne ratio = 1.5:1. Conversions were measured by HPLC. **41** = $[Rh\{(2\text{-}OMe\text{-}C_6H_4)_2PNMeP(2\text{-}OMe\text{-}C_6H_4)_2\}(C_6H_5F)][BAr^F{}_4]$, **48** = $[Rh\{(2\text{-}Et\text{-}C_6H_4)_2PNMeP(2\text{-}Et\text{-}C_6H_4)_2\}(C_6H_5F)][BAr^F{}_4]$.

Both **41** and **48** allow for good catalytic conversion of **E** and 1-octyne to the desired hydroacylation product in 100% and 80% conversion respectively. **41** shows still some activity after 1 h, allowing for further 9 % conversion, while **48** allows for another 3 % conversion after 1 h, but no further reactivity is seen after that. Although **41** is a slightly better hydroacylation catalyst than **48** (while both are much slower than PNP(^{i}Pr) catalyst **11b** which allowed for 100 % conversion in less than 10 min under the same reaction conditions) there is not much difference and based on this data we cannot comment on the hemilability of OMe having any significant effect on this hydroacylation catalysis. In comparison to **41**, **48** is even less selective alkyne hydroacylation catalyst, allowing for 1.4:1 linear:branced ratio (*cf.* 2:1 linear:branched ratio obtained for **41**).

On reviewing the above data we can show that **41** is an active alkyne hydroacylation catalyst that allows for high conversions. Unfortunately **41** does not allow for a long lived recyclable catalyst despite the fact that the OMe group was expected to act in a hemilabile manner during the reaction. However comparing the catalytic data to the isopropyl or cyclohexyl substituted PNP catalysts that led to reductive decarbonylation within minutes (**11b** and **11a** respectively) aryl-*o*-OMe and aryl-*o*-Et containing substituents are an important part of the ligand motif, allowing for longer lived catalysts.

3.4. Study of the Elemental Reactions in Hydroacylation with Aryl-*o*-OMe Ligand

This initial work showed that although **41** is an active alkyne hydroacylation catalyst, still over time decomposition occurs and the catalyst dies. To further understand the reasons behind this behaviour stoichiometric reactions were carried out to probe the hydroacylation reaction using **41**, but also to understand the decomposition pathways.

3.4.1. Reactions of 41 with Aldehyde E

Using **11b**, it was shown in Chapter 2 that the reaction with 2-(methylthio)benzaldehyde (**E**) leads to the formation of the decarbonylation product **16b** via the acyl-hydride intermediate **18b** (Scheme 3.15) and also the formation of analogous complexes has been reported upon using PCP(^{t}Bu) complex **5**.[1]

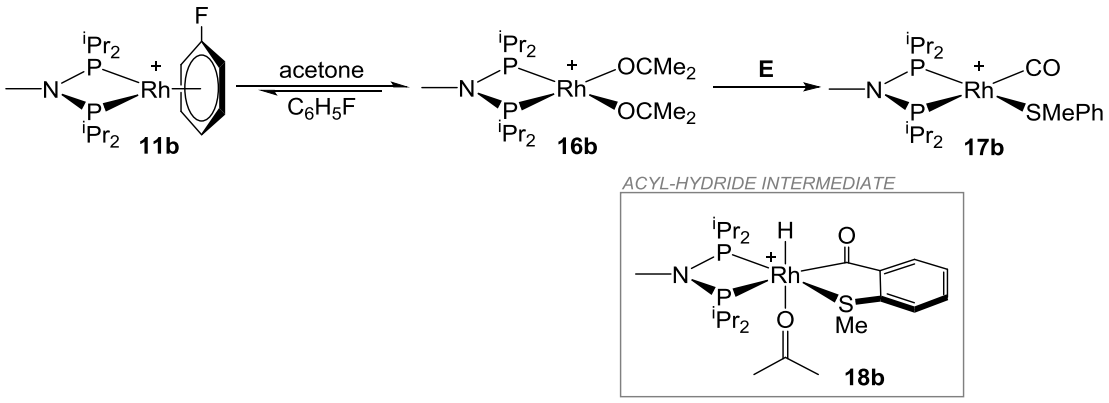

Scheme 3.15. Synthesis of the decarbonylation product (**17b**) via the initial formation of the *bis*-acetone complex (**16b**) followed by the formation of the acyl-hydride intermediate (**18b**), which can then undergo the reductive decarbonylation reaction to yield the desired product. The $[BAr^F{}_4]^-$ counter-anion is not pictured for clarity.

To compare the reactivity of **41** to **11b**, the same stoichiometric reaction with **E** was carried out to establish whether the catalyst deactivation demonstrated in Figure 3.11 could be caused by the reductive decarbonylation reaction. Instead of expected reaction pattern seen using the PNP(^{i}Pr) complex **11b** which formed the decarbonylation product **17b** (Scheme 3.15), the reaction between **41** and **E** led to a complicated $^{31}P\{^1H\}$ NMR spectrum consisting of a range of overlapping multiplets between δ 60 and 40 (which did not resolve at –60 °C) indicating a formation of a wide range of complexes. This reactivity was further probed using low temperature NMR spectroscopy at –60 °C on a freshly prepared mixture of **41** and **E** in acetone-d_6. In the case of **11b** mixed with **E**, this led to the observation of the acyl-hydride intermediate **18b** by ^1H NMR spectroscopy at –60 °C (Scheme 3.15). However, no formation of the analogous acyl-hydride intermediate (*e.g.* **52**, Scheme 3.16) was detected at –60 °C, indicated by the lack of signals at the hydride region in the ^1H NMR spectrum. The $^{31}P\{^1H\}$ NMR spectrum did reveal that there was no fluorobenzene starting material **41** present in the reaction mixture, but no

further information was obtained due to the overlapping signals. That a reaction had occurred was also displayed by the colour change from pale orange to deep brown.

Based on the acyl-hydride species not being formed and the colour change from orange to brown, we tentatively assign this complicated $^{31}P\{^{1}H\}$ NMR spectrum to correspond to the aldehyde bound species **59** (Scheme 3.16). The aldehyde could potentially coordinate in a range of ways (*i.e.* κ^2-S,O or κ^1 via oxygen or sulfur) which would lead to a complicated $^{31}P\{^{1}H\}$ NMR spectrum. The bonding modes for DMSO have been investigated previously, and the data show that both the bonding via oxygen or sulfur can occur to the transition metal centre.[36, 37] The presence of the coordinating solvent, acetone, and potentially coordinating OMe groups can lead to even greater range of products formed thus further complicating the $^{31}P\{^{1}H\}$ NMR spectrum.

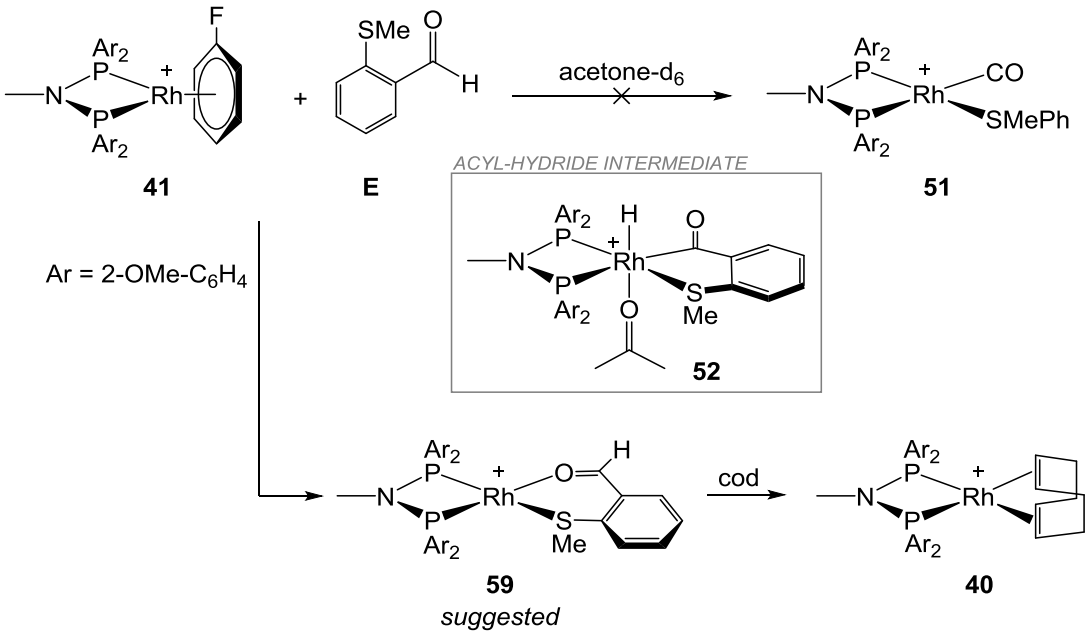

Scheme 3.16. The postulated reactivity between **41** and **E** resulting in the formation of **59** (proposed) and upon the addition of 1,5-cyclooctadiene (cod) to the solution, **40** is formed as the only product.

To exclude the possibility that the complex formed by reacting **41** and **E** was in fact a simple decomposition product, an excess of 1,5-cyclooctadiene (cod) was added to this reaction mixture, resulting in an immediate colour change from brown to orange. The $^{31}P\{^{1}H\}$ NMR spectrum and ESI-MS data confirmed that the addition of cod resulted in the formation of previously synthesised $[Rh\{(2\text{-}OMe\text{-}C_6H_4)_2PNMeP(2\text{-}OMe\text{-}C_6H_4)_2\}(cod)][BAr^F{}_4]$ (Scheme 3.16,

40) cleanly as one product, and ^{1}H NMR spectrum showed the liberation of free aldehyde **E** seen as a peak formation at δ 10.28 corresponding to the aldehylic proton. This allows us to further speculate that the addition of **E** to **41** results in the formation of the aldehyde bound complex (**59**) which does not undergo C-H activation unlike for **11b**, while the addition of the strongly binding 1,5-cyclooctadiene (cod) ligand to the formed species results in substitution of the aldehyde and the formation of **40** (Scheme 3.16). These results also indicate that reductive decarbonylation is not occurring upon reacting **E** with **41** when there is no 1-octyne present, but as C-H activation must be able to occur for the hydroacylation reaction to proceed, clearly 1-octyne is playing a role (as discussed further in later section).

The reaction between **41** and **E** was further investigated using *in-situ* real-time ESI-MS, in collaboration with Prof. Scott McIndoe (University of Victoria) (Figure 3.13). To follow the substrates as well as the rhodium complexes, the positively charged aldehyde mod-**E** was used instead of **E** (Figure 3.13). Upon the addition of **41** to a solution of mod-**E** in acetone immediately the formation of a species at m/z = 451.13 was observed, in addition to small amounts of the *mono*- and *bis*-acetone fragments, $[Rh(Ar_2PNMePAr_2)(acetone)]^+$ and $[Rh(Ar_2PNMePAr_2)(acetone)_2]^+$ respectively. The species at m/z = 451.13 (z = 2) corresponds to a fragment containing a $[Rh(Ar_2PNMePAr_2)]^+$ and an aldehyde (mod-**E**). ESI-MS/MS showed fragmentation of the peak at m/z = 451.13 to $[Rh(Ar_2PNMePAr_2)]^+$ and mod-**E** further supporting the formation of the aldehyde bound species (mod-**59**) upon a reaction between **41** and **E**. Interestingly, over time also another peak grows in at m/z = 508.11 (z = 3). ESI-MS/MS experiments on this peak showed that this product contains two $[Rh(Ar_2PNMePAr_2)]^+$ fragments plus one of mod-**E**. It is unclear whether this dimeric species is only seen due to ESI-MS conditions, or is it a real OMe-stabilised intermediate, but it could further explain the complicated $^{31}P\{^{1}H\}$ NMR spectrum that is seen upon carrying out the reaction between **41** and **E**.

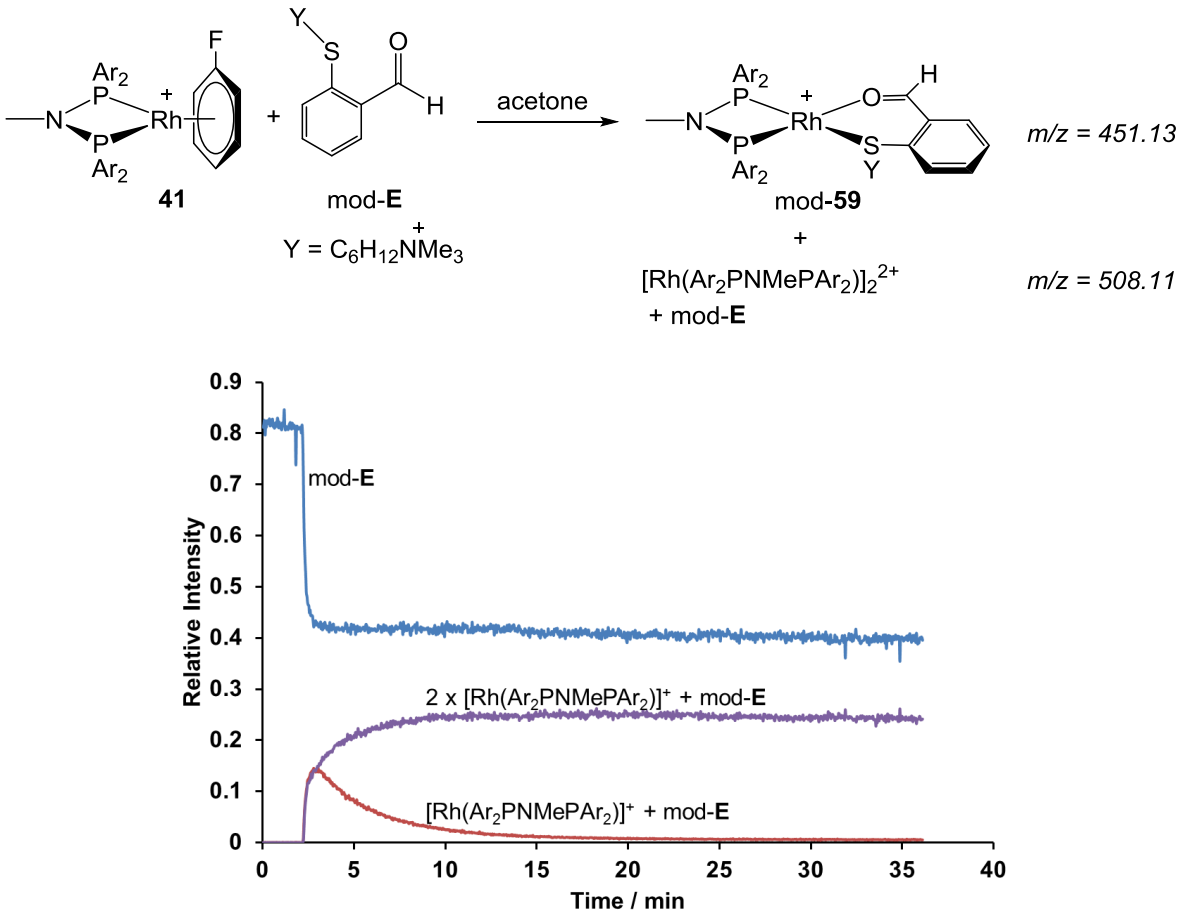

Figure 3.13. ESI-MS data for the hydroacylation reaction of mod-**E** with **41.** The $[BAr^F_4]^-$ counter-anion is not pictured for clarity.

It was rationalised that if no C-H activation and reductive decarbonylation is occurring upon reacting **41** with **E**, the formed complex should still be active in hydroacylation catalysis. To probe this, a stoichiometric reaction was conducted, where **41** was reacted with **E** in acetone, and the mixture was allowed to stir overnight (25 °C). The obtained solution was then added to a reaction mixture containing **E** and 1-octyne resulting in a catalytic mixture comparable to the reaction showed in Figure 3.11 (1 mol% catalyst loading, 0.4 M aldehyde, 0 °C, 1:1.5 **E**:1-octyne, acetone). HPLC data showed 70 % conversion in 20 h (same result was observed upon using **41** as the catalyst under the same catalytic conditions), indicating that no catalyst decomposition occurred during the overnight reaction with **E**.

For the *ortho*-ethyl substituted complex, the stoichiometric reaction between the [Rh{(2-Et-C_6H_4)$_2$PNMeP(2-Et-C_6H_4)$_2$}(C_6H_5F)][BAr^F_4] (**48**) and **E** was also conducted (Scheme 3.17).

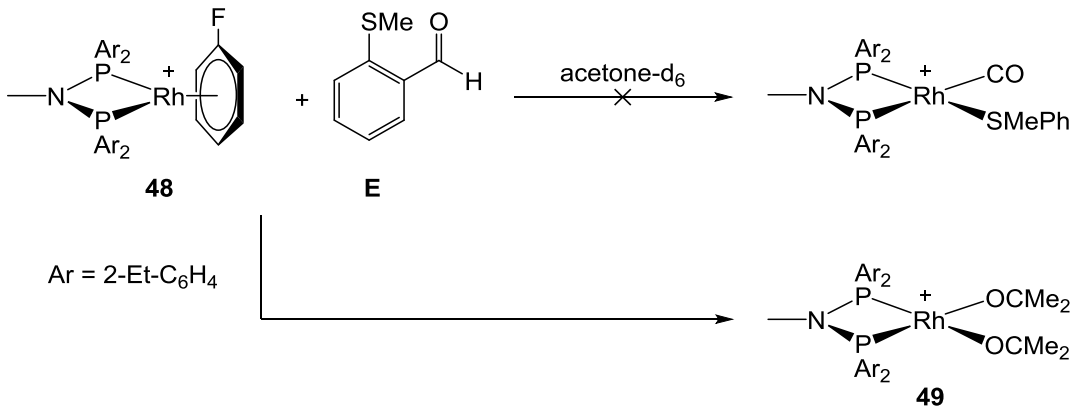

Scheme 3.17. Attempted synthesis of the decarbonylation product using **48** and **E**. The $[BAr^F_4]^-$ counter-anion is not pictured for clarity.

Similar to **41**, the stoichiometric reaction between [Rh{(2-Et-C_6H_4)$_2$PNMeP(2-Et-C_6H_4)$_2$}(C_6H_5F)][BAr^F_4] (**48**) and **E** does not lead to the formation of the decarbonylation product, [Rh{(2-Et-C_6H_4)$_2$PNMeP(2-Et-C_6H_4)$_2$}(CO)(SMePh)][BAr^F_4]. Interestingly in this case also the aldehyde coordinated species is not seen. Instead the formation of the *bis*-acetone species, [Rh{(2-Et-C_6H_4)$_2$PNMeP(2-Et-C_6H_4)$_2$}(acetone)$_2$][BAr^F_4] was observed by $^{31}P\{^1H\}$ NMR spectroscopy, showing a doublet at δ 45.4 [*J*(RhP) = 178 Hz] (**49**) (Scheme 3.17). Although the formation of the aldehyde-bound or C-H activated acyl-hydride species were not seen, **48** was still shown to be active in hydroacylation catalysis. The slower catalytic rate (Figure 3.12) might suggest that C-H activation is now rate limiting. What is clear is that alkyne is having a role to play in promoting the C-H activation process for those ligands.

Such difference in C-H activation abilities upon comparing the aryl complexes **41** and **48** to the isopropyl analogue **11b** has been noted previously. Similar substantial change in C-H activation ability of the catalyst upon slightly modifying the ligand has been shown by Yu.[38] They carried out a screening of a range of ligands on palladium for the C-H activation of arylation of an amide with *para*-iodotoluene (Scheme 3.18).

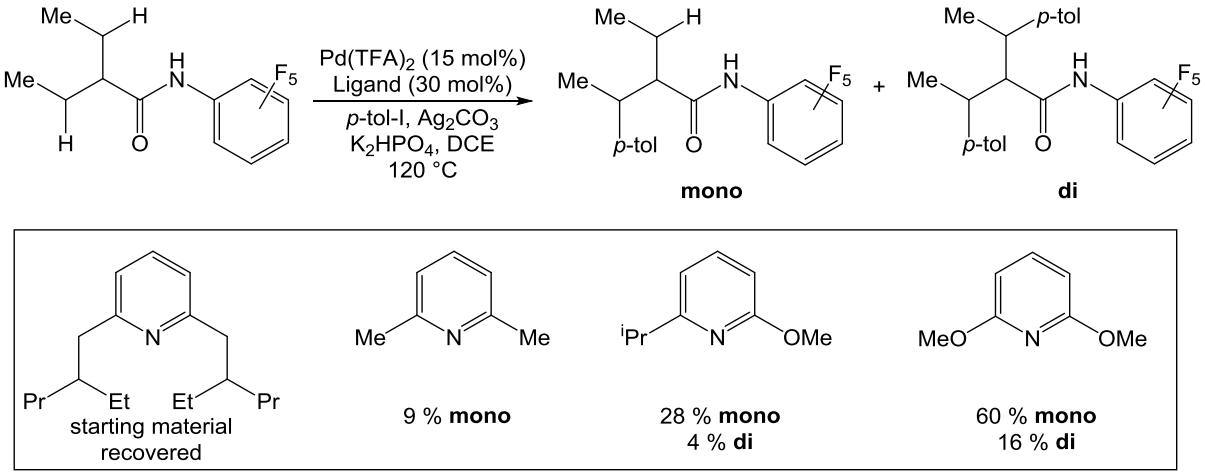

Scheme 3.18. Arylation of methylene C–H bond using palladium catalyst with different ligands.

The screening showed that slight changes in the ligand design resulted in substantial changes in the relative amount of product formed. Particularly noteworthy is the increased activity towards C-H activation upon using *ortho*-methoxy groups instead of methyl groups on the ligand.

3.4.2. Reactions of 41 with 1-octyne

To try to further understand the reasons for catalyst deactivation and the promotional effect during the hydroacylation reaction the reactivity with 1-octyne was probed. For this an excess of 1-octyne (3 eq.) was added to **41**.

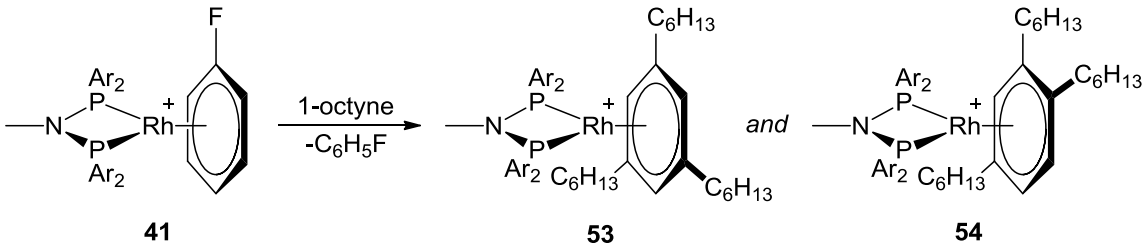

Scheme 3.19. The two products formed (**53** and **54**) by the reaction between **41** and excess of 1-octyne. The $[BAr^F_4]^-$ counter-anion is not pictured for clarity.

This resulted in the formation of two new doublets in the $^{31}P\{^1H\}$ NMR spectrum (major doublet at δ 50.6 [*J*(RhP) = 188 Hz], minor doublet at δ 50.2 [*J*(RhP) = 188 Hz] in 3:2 ratio), while ESI-MS spectrum only showed one species at m/z = 952.41. This mass and isotope pattern correspond

to $[Rh(Ar_2PNMePAr_2)]^+$ fragment plus three octynes, which are assumed to have formed an aromatic η^6-bound ligand presumably via alkyne cyclotrimerisation, thus resulting in the $[Rh(Ar_2PNMePAr_2)(trihexylbenzene)]^+$ fragment.[39] As there are two ways for the octynes to combine in order to form the aromatic rings (*i.e.* complexes **53** and **54**), the formation of two very similar species seen in the $^{31}P\{^1H\}$ NMR spectrum can be explained (Scheme 3.19). The coupling [*J*(RhP) = 188 Hz] is also analogous to **41**. Alkyne cyclotrimerisation has been shown for a range of transition metals, and the formation of both species has been reported previously.[39, 40] ^1H NMR spectral data support this, as the aromatic region shows two different multiplets at δ 7.50 and 7.40. Although in the case of 1:1 formation of **53** and **54** observation of 4 signals in 1:1:1:3 ratio by ^1H NMR spectroscopy would be expected, but this was not seen experimentally due to overlapping signals. This hypothesis of the formation of the η^6-bound species was further strengthened by the $^{31}P\{^1H\}$ NMR spectrum of the mesitylene-bound rhodium complex $[Rh(Ar_2PNMePAr_2)(\eta^6\text{-mesitylene})][BAr^F{}_4]$ (**55**), which was synthesised by an addition of excess mesitylene to **41**. The $^{31}P\{^1H\}$ NMR spectrum of **55** shows a single doublet at δ 51.6 [*J*(RhP) = 188 Hz].

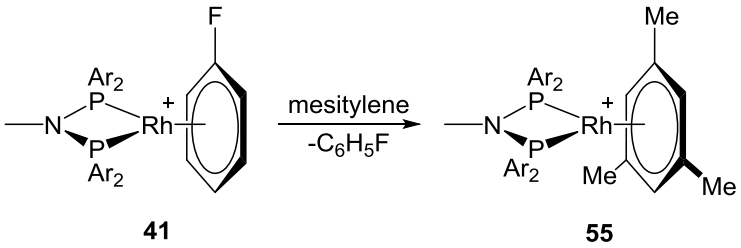

41 55

Scheme 3.20. The synthesis of the mesitylene-bound species **55**. The $[BAr^F{}_4]^-$ counter-anion is not pictured for clarity.

As alkyne trimerisation has previously been shown to be catalytic,[41] it was important to carry out reactions with 1-octyne using catalytic amount of **41**. Under catalytic conditions (1 mol% **41**, acetone, 0.4 M 1-octyne, 25 °C) **53** and **54** formed, but no further consumption of 1-octyne or formation of aromatic products were observed by ^1H NMR spectroscopy, showing that alkyne trimerisation is not catalytic for **41** under these reaction conditions. Most likely this is due to the formation of strongly bound arene species.

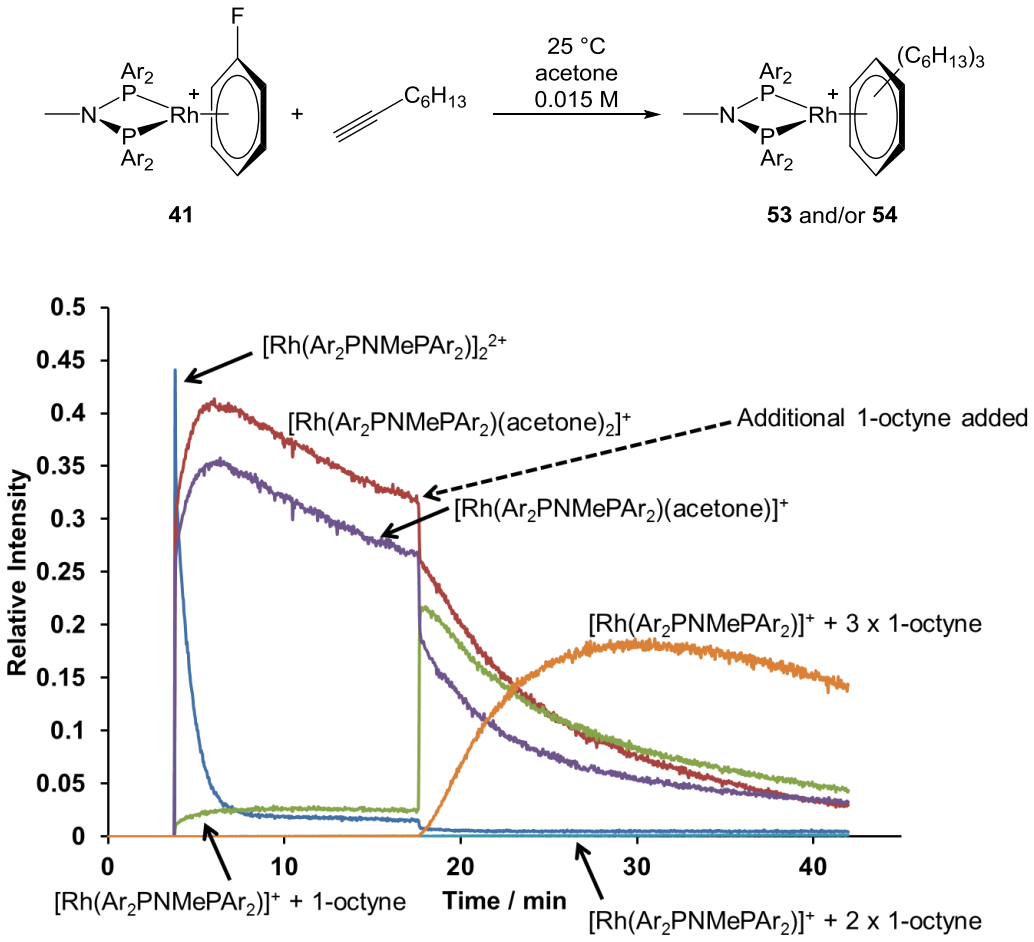

Figure 3.14. ESI-MS data for the hydroacylation reaction of 1-octyne with **41**. The $[BAr^F_4]^-$ counter-anion is not pictured for clarity.

The formation of **53** and **54** was also seen upon carrying out *in-situ* real-time ESI-MS studies. The reaction was initially set up with 1-octyne dissolved in acetone (0.015 M alkyne, 25 °C, acetone) (Figure 3.14) and the reaction mixture was allowed to stir and run into the ESI-MS. As neither of these species (1-octyne and acetone) is visible by ESI-MS there was no signal observed. After 3.5 minutes, the complex **41** was added (1 eq. with respect to the alkyne). This resulted in the appearance of peaks at m/z = 622.08, 680.12 and 738.16, plus a relatively small peak at 732.19 (Figure 3.14). The peak at m/z = 622.08, corresponds to the dimeric species of $[Rh(Ar_2PNMePAr_2)]_2^{2+}$ (**42**) which initially shows very high relative concentration, but upon the formation of the *mono*- and *bis*-acetone species ($[Rh\{(2\text{-}OMe\text{-}C_6H_4)_2PNMeP(2\text{-}OMe\text{-}C_6H_4)_2\}(acetone)][BAr^F_4]$ and $[Rh\{(2\text{-}OMe\text{-}C_6H_4)_2PNMeP(2\text{-}OMe\text{-}C_6H_4)_2\}(acetone)_2][BAr^F_4]$) (peaks at m/z = 680.12 and 738.16 respectively) the relative concentration of the dimer drops.

The additional peak seen during the reaction (m/z = 732.19), corresponds to the species containing the $[Rh(Ar_2PNMePAr_2)]^+$ fragment plus one 1-octyne. Presumably this species is also stabilised by acetone in the solution forming a 4-coordinate complex, but it fragments under the ESI-MS conditions. After 18 minutes of reaction time, another 10 eq. of 1-octyne was added to the reaction mixture resulting in the reduction of the relative concentration of both of the acetone species (*mono*- and *bis*-acetone). Immediately an increase in the concentration of the species containing the $[Rh(Ar_2PNMePAr_2)]^+$ fragment and one 1-octyne unit is observed and an increase in the relative intensity of a peak at m/z = 952.41 was observed. This peak corresponds to the $[Rh(Ar_2PNMePAr_2)(trihexylbenzene)]^+$ fragment (**53** and/or **54**). Interestingly, during the whole reaction the relative concentration of the species containing the $[Rh(Ar_2PNMePAr_2)]^+$ fragment and two 1-octyne units (m/z = 842.30) remained very low suggesting that it is an intermediate. The reaction process is depicted in Figure 3.14.[b]

Unfortunately due to 1-octyne not being charged, we were not able to see any free product formation to confirm whether the reaction is catalytic, but based on NMR spectra discussed previously this is not expected to be the case.

As for the aldehyde bound species **59**, the mixture containing **53** and **54** was used as the hydroacylation catalyst. Under the conditions used for **59** (1 mol% catalyst, 0.4 M aldehyde, 1:1.5 **E**:1-octyne, acetone, 0 °C) no reduction in catalytic activity was seen (analogously to **59** and the fluorobenzene complex **41**) and 70% conversion to the desired hydroacylation product was obtained, demonstrating that the formation of the aryl-bound species **53** and **54** does not lead to catalyst deactivation.

3.4.3. Reactions of 41 with E and 1-octyne

Establishing the reactions using only **E** or 1-octyne, it was thus a logical step to see whether the same products are seen during the hydroacylation reaction. Upon following the hydroacylation

[b] A noteworthy observation from Figure 3.14 is the overall decrease in relative concentration of all the visible species during the reaction. By ESI-MS, it was possible to see some impurities "growing in" but we were not able characterise these species and to fully understand what the decomposition products were

reaction by NMR spectroscopy, no sign of **53** or **54** was observed. Also, ESI-MS studies using both the **E** and mod-**E** with 1-octyne showed no signal corresponding to the $[Rh(Ar_2PNMePAr_2)(trihexylbenzene)]^+$ fragment, indicating that trimerisation of 1-octyne is not occurring during the hydroacylation reaction using **41** as the catalyst. An ESI-MS sample taken at the end of the hydroacylation reaction (2 M aldehyde, 25 °C, 1:1.5 **E**:1-octyne, acetone) did show the formation of a large range of species which were not identified, there were also peaks corresponding to the decarbonylation fragment of **51** with the formula of $[Rh(Ar_2PNMePAr_2)(SMePh)(CO)]^+$ (m/z = 743.09) and a peak at m/z = 771.11 corresponding to **51** missing a CO group, $[Rh(Ar_2PNMePAr_2)(SMePh)]^+$, the latter probably due to fragmentation occurring in the ESI-MS.

This was further probed using in *in-situ* real-time ESI-MS instrument at the McIndoe group. The hydroacylation reaction was carried out using **41**, 1-octyne and the cationic aldehyde mod-**E** (10 mol% catalyst loading, acetone, 25 °C, 0.015 M aldehyde, mod-**E**:1-octyne ratio = 1:1.5) (Scheme 3.21). The reaction leads to the initial formation of the *bis*- and *mono*-acetone complexes $[Rh(Ar_2PNMePAr_2)(acetone)_2]^+$ and $[Rh(Ar_2PNMePAr_2)(acetone)]^+$ which in this case are observed in very small quantities. In the case of **41** there is also some formation of the $[Rh(Ar_2PNMePAr_2)]_2^{2+}$ fragment (m/z = 622.08) which likely corresponds to the aryl-bridged dimer (**42**) discussed in Section 3.2.2.1. Also, immediately after the addition of **41** to the reaction mixture, the formation of a species at m/z = 451.13 is seen. This species (z = 2, based on the isotope pattern spacing) corresponds to the complex containing the $[Rh(Ar_2PNMePAr_2)]^+$ fragment and the aldehyde, mod-**E**. As was discussed in Chapter 2, this could correspond to the acyl-hydride intermediate (mod-**52**), aldehyde bound species (mod-**58**) or to the decarbonylation product (mod-**51**) as they all have the same mass to charge ratio (the weakly bound acetone is not included in the mass calculation, Scheme 3.21). Unfortunately, ESI-MS/MS experiments did not allow for us to discriminate between these species due to the relatively low concentration of this species observed. The resting state, as was seen for **11b**, is the product bound intermediate **58**, of which there is a relatively high concentration at the beginning of the catalysis, but its concentration slowly decays as the catalysis proceeds (Figure 3.15).

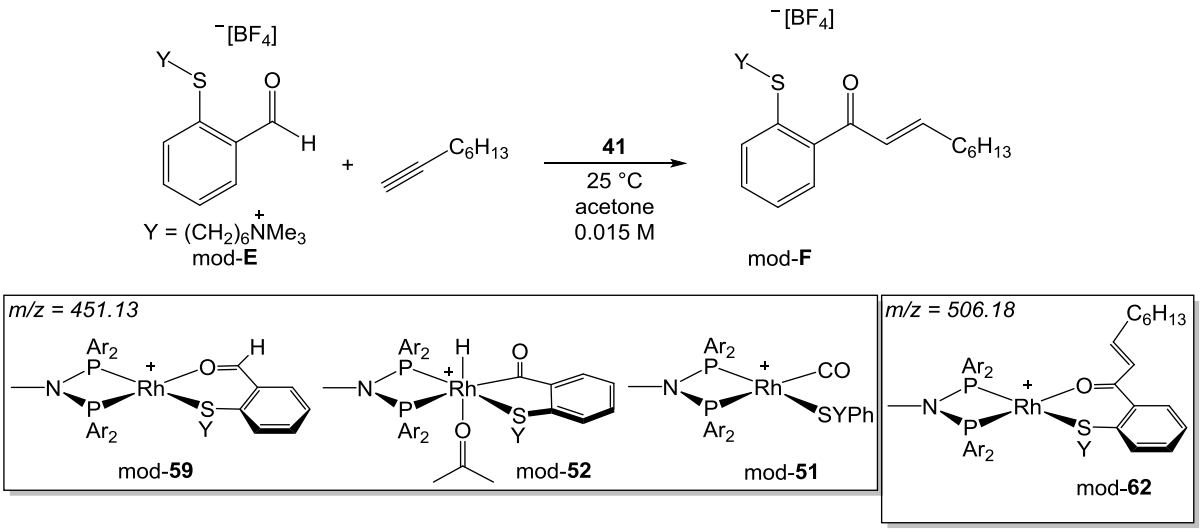

Scheme 3.21. Hydroacylation reaction using the cationic aldehyde, mod-**E** and 1-octyne as the substrates and **41** as the catalyst. Fragment corresponding to 451.13 (mod-**51** and/or mod-**52** and/or mod-**59**) and the product bound resting state mod-**62** are visible during the hydroacylation reaction upon following it by ESI-MS. The $[BAr^F_4]^-$ counter-anion is not pictured for clarity.

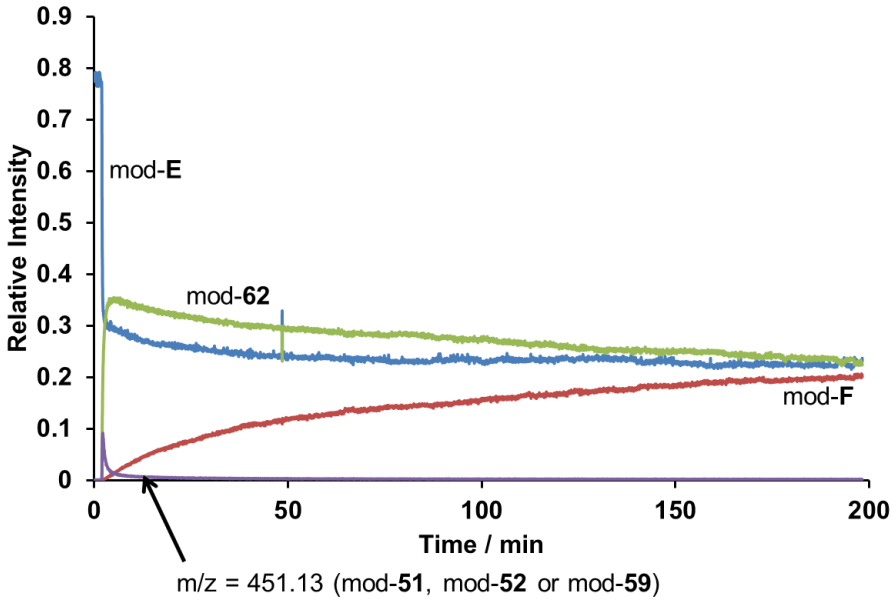

Figure 3.15. ESI-MS data for the hydroacylation reaction of mod-**E** and 1-octyne with **41** as the catalyst.

Although the reactions using just **41** and **E** or mod-**E** indicated that no reductive decarbonylation is occurring (overnight reaction between **41** and **E** retained the active catalyst), the catalytic investigation using **E**/mod-**E** and 1-octyne clearly showed that the catalyst is decomposing; catalytic hydroacylation reaction under low catalyst loading and concentration, 1 mol% **41**, 0.075 M **E**, did not allow for full conversion. To further understand the reactivity of

41, the work was continued on probing ways to mimic or find different routes to synthesise the metal complexes involved in the hydroacylation reaction mechanism. In particular we were interested in the synthesis of the acyl hydride intermediate and the decarbonylation product. Previous work reported by the groups of Weller and Jun using the phosphorus tethered 2-(diphenylphosphanyl)benzaldehyde (**H**) showed that a stabile acyl-hydride intermediate can be synthesised.[1, 42, 43] An *in situ* reaction was conducted using **41** and the phosphine based tethered aldehyde 2-(diphenylphosphanyl)benzaldehyde (**H**) in acetone (Scheme 3.22). This phosphorus-tethered species is particularly useful because of its stability against decarbonylation and the extra ^{31}P NMR spectral data it can provide. The expected acyl-hydride was observed as **56** by NMR spectroscopy.

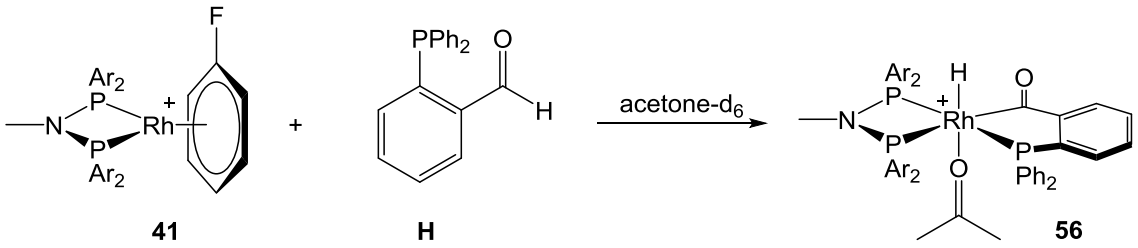

Scheme 3.22. Formation of the stabile acyl-hydride intermediate **56** by a reaction between **41** and 2-(diphenylphosphanyl)benzaldehyde (**H**). The $[BAr^F{}_4]^-$ counter-anion is not pictured for clarity.

The formation of this C-H activated species was assigned based on its ^{1}H NMR spectrum, especially the observation of the hydride signal at δ –18.5 (*cf.* δ –19.4 for the analogous acyl-hydride complex upon using ^{t}Bu$_2$PCH$_2$P^{t}Bu$_2$ ligand[1]) and the observation of four OMe environments (seen as singlets in 1:1:1:1 ratio at δ 3.65, 3.42, 3.24, 2.99) due to the loss in symmetry in the cation compared to **41**. The ^{31}P{^{1}H} NMR spectrum was expected to show three doublet of doublet of doublets corresponding to the three phosphorus environments, with rhodium phosphine and phosphorus phosphine couplings indicating the relative *cis*- and *trans*-positioning of these phosphorus atoms with respect to each other (*trans*-phosphine coupling expected around 300 Hz, while *cis*-phosphine coupling would result in much smaller coupling constant, *ca.* 30 Hz)[1, 8, 44] Instead a broad doublet is observed at δ 66 (FWHM: 210 Hz) and another broad signal centred at δ 51.2 (FWHM: 670 Hz) in 2:1 ratio. The 2:1 is ratio is seen presumably due to the phosphorus atoms in the complex being in very similar environments

and leading to the overlap of the signals. These results nevertheless show that C-H activation with these PNP ligands is possible.

Although the stoichiometric reactions with **41** and **E** showed no formation of the decarbonylation product (**51**), the ESI-MS data indicated that **51** was present at the end of the hydroacylation reaction. In order to further understand the role of **51** during the hydroacylation reaction, an alternative route to synthesise the decarbonylation product was required. **51** was synthesised via a route based upon one reported by Hofmann, starting from the neutral $[Rh(cod)Cl]_2$ precursor (Scheme 3.23).[45]

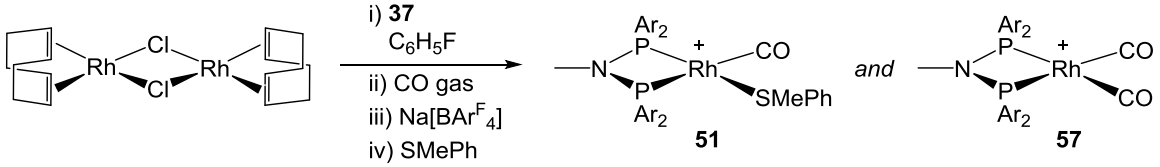

Scheme 3.23. Alternative synthetic route to synthesise the decarbonylation product **51**. The $[BAr^F_4]^-$ counter-anion is not pictured for clarity.

The first step was carried out via a very slow addition of the PNP(*o*-OMe) ligand **37** to $[Rh(cod)Cl]_2$ in fluorobenzene solvent (if CH_2Cl_2 is used as the solvent, decomposition is observed during the reaction). During the addition the colour changes from pale orange to deeper orange, and after the addition the reaction was allowed to stir for 2-3 hours. This was followed by bubbling CO gas though the solution for 1 minute during which the solution colour changed from orange to pale yellow. $Na[BAr^F_4]$ and thioanisole (SMePh) were then added to the formed product. The addition order is important as the addition of thioanisole first, or both of the reagents at the same time, leads to formation of less pure material, *i.e.* larger relative amount of the *bis*-CO product $[Rh(Ar_2PNMePAr_2)(CO)_2][BAr^F_4]$ (**57**) formed. The obtained product was a mixture of species as observed by the $^{31}P\{^1H\}$ NMR spectrum. Based on ESI-MS, the *bis*-CO complex (**57**) indicated by a peak at m/z = 678.07 corresponding to the $[Rh(Ar_2PNMePAr_2)(CO)_2]^+$ fragment and the desired decarbonylation product **5** (m/z = 771.11) were formed as the major species. Also the ESI-MS spectrum showed peaks for $[Rh(Ar_2PNMePAr_2)(CO)]^+$ and $[Rh(Ar_2PNMePAr_2)(SMePh)]^+$ fragments. For the purpose of this investigation this was not a problem and the isolated mixture was used in hydroacylation

catalysis. Also, the *bis*-CO product has been seen as a decarbonylation product using **11b**. At 1 mol% catalyst loading, the use of this mixture as the catalyst for a reaction between **E** and 1-octyne (2 M, 25 °C, **E**:1octyne 1:1.5, acetone) was conducted. No catalytic activity was observed after leaving the reaction stirring overnight, demonstrating that reductive decarbonylation is not reversible for catalyst **41**. This data further indicates that no C-H activation reaction is occurring upon reacting **41** with **E**, as if any C-H activation had occurred, this would have resulted in the acyl-hydride intermediate that would have readily decarbonylated as was demonstrated by the formation of the decarbonylation products during the hydroacylation catalysis.

3.5. Proposed Hydroacylation Mechanism Using 41 as the Catalyst

Based on the catalytic and stoichiometric reactions carried out and upon linking these to the previous studies conducted using small bite-angle and hemilabile ligands a mechanism for hydroacylation reaction using the *ortho*-methoxy substituted **41** is proposed (Scheme 3.24).

As for the small bite-angle ligands, **11a – 11e**, the 18 electron η^6-bound fluorobenzene rhodium complex was used as the precatalyst which is in equilibrium with **42** if dissolved in dichloromethane. Whereas upon dissolving the precatalyst, [Rh{(2-OMe-C_6H_4)$_2$PNMeP(2-OMe-C_6H_4)$_2$}(C_6H_5F)][BAr^F_4] (**41**) in acetone solvent, the formation of [Rh{(2-OMe-C_6H_4)$_2$PNMeP(2-OMe-C_6H_4)$_2$}(acetone)$_2$][BAr^F_4] (**44**) was observed, plus additional species tentatively assigned as complexes involving rhodium-oxygen bond to the OMe groups. The additional species could also be aryl-bridged dimers, but this is less likely as in the case of the *ortho*-ethyl substituted complex **48**, no additional species, other than the *bis*-acetone adduct **49**, were observed upon dissolving **48** in acetone. It was possible to confirm that although a number of species formed upon dissolving **41** in acetone, they were all labile, and the addition of acetonitrile resulted in the formation of one clean product (**43**). The addition of 1-octyne to the *bis*-acetone adduct (**44**) resulted in the formation of two regio-isomers **53** and **54**, but these isomers are not observed

during the hydroacylation catalysis presumably due to the preferred coordination of the sulfur-tethered aldehyde **E**.

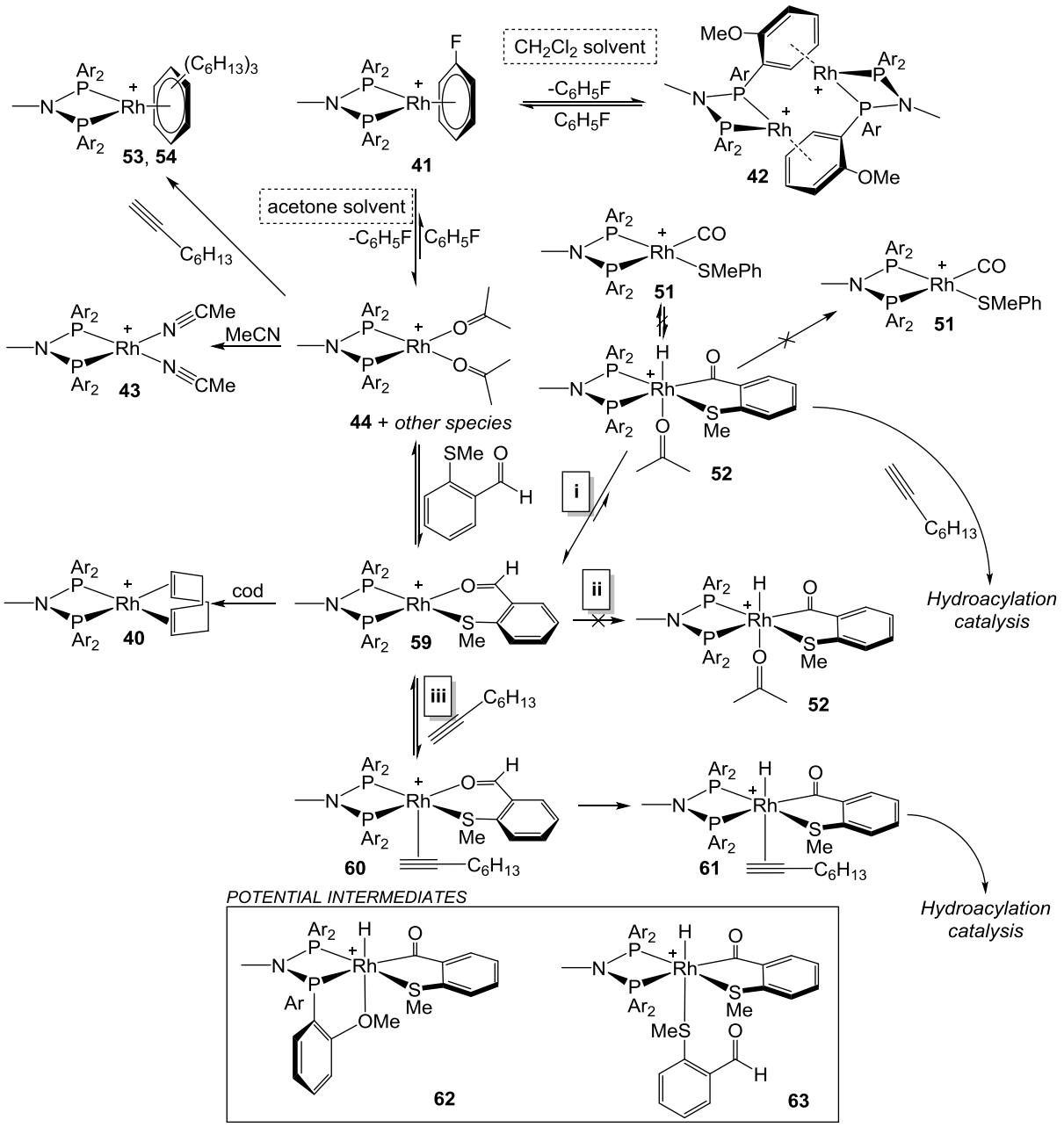

Scheme 3.24. Proposed hydroacylation reaction mechanism (excluding hydride migration and reductive elimination steps for clarity) upon using **E** and 1-octyne as substrates and **41** as the catalyst. The $[BAr^F_4]^-$ counter-anion is not pictured for clarity.

The addition of 2-(methylthio)benzaldehyde (**E**) to the *bis*-acetone species resulted in the formation of a species assigned as Rh(I) aldehyde-bound complex (**59**) based on NMR and ESI-MS/MS data (this does not occur in the case of the *ortho*-ethyl substituted **48**). Additionally the

formation of **59** was further tested by addition of 1,5-cyclooctadiene which resulted in the formation of the rhodium-cod complex **40** cleanly as one product. **59** was also shown to be catalytically active even after leaving it in acetone overnight. This was not the case for the analogous isopropyl or cyclohexyl substituted small bite-angle catalysts **11a** – **11c** which resulted in rapid reductive decarbonylation upon dissolved in acetone in the presence of **E**. To further understand this, three mechanistic possibilities (**i**, **ii** and **iii**) are proposed.

For pathway **i**, it is postulated that the C-H activation of the aldehyde **E** is occurring, but it is leads to an equilibrium between the acyl-hydride intermediate **52** and aldehyde bound species **59**, and if the equilibrium is strongly towards **59** this would explain the fact that no acyl-hydride species were seen by ^{1}H NMR spectroscopy. This assumption would be plausible if the acyl-hydride species (**52**) does not undergo decarbonylation, but this is highly unlikely, as the reductive decarbonylation products were seen by ESI-MS at the end of the hydroacylation catalysis. Additionally the decarbonylation from the acyl-hydride intermediate could be reversible, and thus no catalyst deactivation is occurring. This was shown also not to be the case by synthesising the decarbonylation product **51** via a separate route and then using it as a catalyst. This investigation demonstrated that the decarbonylation product **51** is inactive as a hydroacylation catalyst using **E** and 1-octyne as substrates.

Reaction pathway **ii** is assuming that no C-H activation occurs. Although this is the case upon reacting just **41** and **E** in acetone, metal based C-H activation is expected to occur during the hydroacylation catalysis based on similar reactivity to the other small bite-angle ligands investigated before in the Weller group.[1, 3] Moreover, productive C-H activation was observed upon using the phosphorus tethered aldehyde **H**.

In pathway **iii** oxidative addition of the aldehyde **E** is promoted by the coordination of the incoming alkyne (1-octyne). This fits the experimental data that shows that no C-H activation is occurring upon reacting **41** and **E**, while the presence of 1-octyne in the reaction mixture allows the hydroacylation catalysis to proceed. Milstein has reported a C-H activation reaction being promoted by the coordination of a CO molecule.[46, 47] He showed that the formation of a cationic

rhodium pincer hydride complex only forms via intramolecular C-H activation in the presence of a carbonyl (Scheme 3.25).

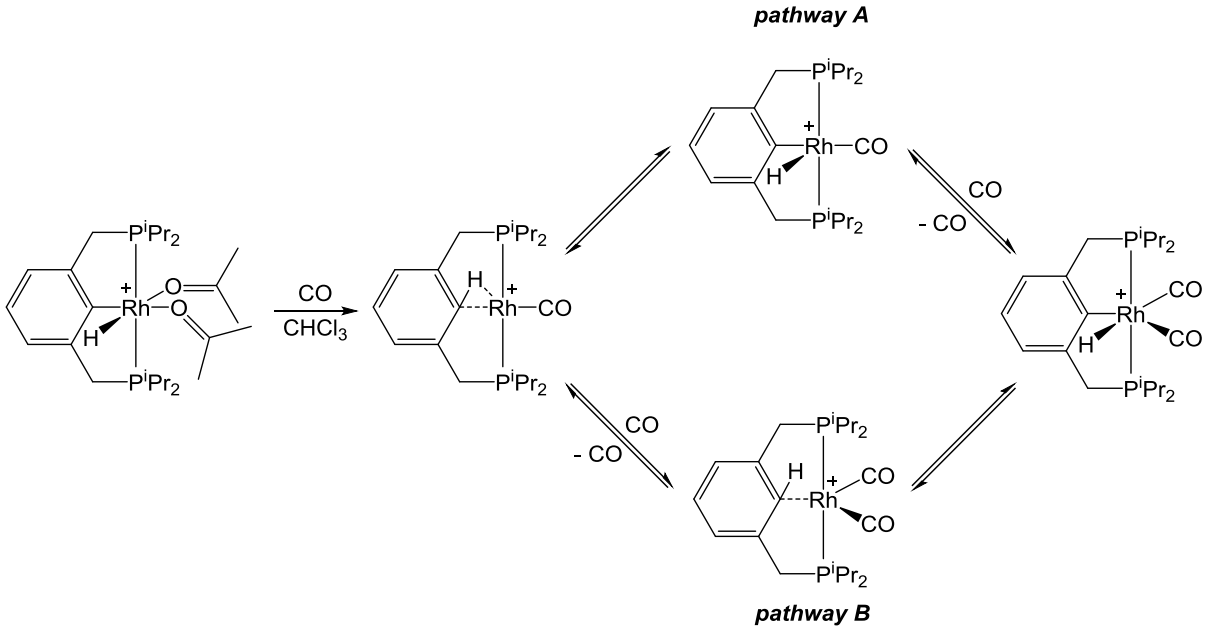

Scheme 3.25. The synthesis of the rhodium-CO complex and the two proposed reaction pathways for the agostic/aryl hydride equilibrium. The $[BF_4]^-$ counter-anion is not pictured for clarity.

Based on experimental and computational data they were able to show that CO promotes oxidative addition of a C-H bond in a cationic rhodium(I) complex. The computational data indicates that reaction via pathway **B** has a lower barrier than pathway **A**. Additionally they found that the addition of the first CO ligand inhibits C-H activation by stabilising the complex in an agostic motif, while the second CO ligand facilitates the C-H activation. Also the dissociation of rhodium-phosphine bond was investigated, but it was shown to go through a much higher energy pathway.

The formation of **60** can then undergo the C-H activation forming the suitable alkyne coordinated species (**61**) which upon carrying out hydride migration allows for branched or linear intermediates suitable for reductive elimination resulting in the desired linear and branched ketone products, as was seen during the catalytic transformations. Based on the higher catalytic conversion obtained upon using excess of aldehyde in the catalytic mixture, it can be proposed that the acyl-hydride intermediate can be stabilised by the coordination of

another equivalent of **E** forming the intermediate **63**. Additionally stabilisation of the acyl-hydride intermediate may occur via the OMe groups, forming **62**, as was shown by Bercaw, but it was not possible to prove that experimentally.

Thus this data overall suggest that the reaction pathway **iii** is operating as this fits best with the available data.

3.6. Future Work

This work carried out using the PNP(*o*-OMe) ligand **37** has shown both positive and negative results and the project using OMe motif on small bite-angle ligands has been further developed to use ligands that would allow for more stable complexes (Figure 3.16).

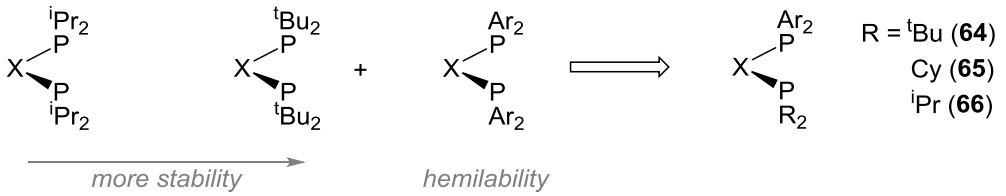

Figure 3.16. Development of the new potentially highly efficient hydroacylation catalysts by combining the benefits of different small bite-angle catalysts. X = NMe or CH_2. Ar = 2-OMe-C_6H_4.

The design of the new ligand system relies on two observations noted during this project: the low overall stability of the complex **41** and the extra stability towards reductive decarbonylation seen upon comparison to the analogous PNP(^{i}Pr) complex **11b**. Based on the experimental results seen in Chapter 2, a definite trend can be seen which indicates that bulky tert-butyl groups allow for a longer lived catalyst (**5**) compared to the less bulky isopropyl analogue (**11c**) (Figure 2.8). At the same time, based on the discussion above, the OMe groups on the ligand design are also beneficial. Upon combining this data, it can be postulated that a successful ligand incorporates both the tert-butyl and *ortho*-methoxy phenyl ligands on the phosphorus atoms of the small bite-angle phosphine ligand (Figure 3.16). A suitable initial ligand proved to be ^{t}Bu$_2$PNMeP(2-OMe-C_6H_4)$_2$ (**64**). As we have previously shown that the aliphatic substituents on the phosphorus atoms play a great role in the selectivity (alkyne *vs.*

alkene hydroacylation) of the catalyst, additionally to **64**, **65** and **66** were proposed to result in interesting chemistry (Figure 3.16). This work is being currently carried out by a post-doctoral researcher in the Weller group, Dr. Amparo Prades. Already the research using **64** has shown, that the combination of the electron-rich and bulky tert-butyl groups with the *ortho*-methoxy phenyl groups allows for highly active and substantially more stable catalyst. Furthermore, this new ligand (**64**) results in much more stable intermediates and cleaner stoichiometric reactions hence allowing us to study the reaction mechanism and the kinetics of the hydroacylation reaction more readily.

3.7. Conclusions

During this project a new hydroacylation catalyst [Rh{(2-OMe-C_6H_4)$_2$PNMeP(2-OMe-C_6H_4)$_2$}(C_6H_5F)][BAr^F_4] (**41**) was developed based on the small bite-angle ligand design containing an *ortho*-methoxy motif ((2-OMe-C_6H_4)$_2$PNMeP(2-OMe-C_6H_4)$_2$, **37**) shown previously to be highly active for alkene trimerisation by Wass. Subsequent research by Bercaw and Labinger has showed that this ligand motif allows for oxygen coordination to the metal centre, making it hemilabile.

The research described in this chapter showed **41** to be inactive as an alkene hydroacylation catalyst, but it is highly effective as an alkyne hydroacylation catalyst allowing for catalyst loadings as low as 0.5 mol%. Upon comparing to the previously developed isopropyl and cyclohexyl substituted rhodium PCP and PNP catalysts **11a** – **11e**, additional stability towards hydroacylation was seen to arise upon using **41**, whereas the regioselectivity is much lower (2:1 (**41**) *vs.* 69:1 (**11a**) linear:branched product ratio). While comparison to PNP(*o*-Et) complex [Rh{(2-OMe-C_6H_4)$_2$PNMeP(2-OMe-C_6H_4)$_2$}(C_6H_5F)][BAr^F_4] (**48**) only slightly higher overall conversion was observed. Although the catalyst (**41**) was shown to be more stable towards reductive decarbonylation, still it was deactivated during hydroacylation catalysis.

The mechanism of the hydroacylation reaction was investigated using **41**. It was found that the catalyst does not undergo C-H activation of the aldehyde (**E**) unless there is alkyne is present in the reaction mixture. This lack of reactivity towards **E** allows for the catalyst to be placed in a solution containing acetone and **E**, but any reactivity only occur upon the addition of 1-octyne. The mechanistic studies did not reveal the degree of hemilability provided by ligand **37** during the hydroacylation catalysis.

Overall, although not the best catalyst itself, **41** has allowed for us to probe the use of a small bite-angle catalyst combining the fast rate of the small bite-angle with the additional stability provided by the hemilability, and based on these studies a new generation of hydroacylation catalysts can be designed, that should allow for a wide range of reactivity with substantially reduced decomposition during the hydroacylation reaction.

3.8. References

1. A. B. Chaplin, J. F. Hooper, A. S. Weller and M. C. Willis, *J. Am. Chem. Soc.*, 2012, **134**, 4885-4897.
2. M. C. Willis, *Chem. Rev.*, 2010, **110**, 725-748.
3. I. Pernik, J. F. Hooper, A. B. Chaplin, A. S. Weller and M. C. Willis, *ACS Catal.*, 2012, **2**, 2779-2786.
4. D. Milstein, *J. Chem. Soc., Chem. Commun.*, 1982, 1357-1358.
5. D. Milstein, *Acc. Chem. Res.*, 1984, **17**, 221-226.
6. M. M. Coulter, K. G. M. Kou, B. Galligan and V. M. Dong, *J. Am. Chem. Soc.*, 2010, **132**, 16330-16333.
7. S. D. Pike, R. J. Pawley, A. B. Chaplin, A. L. Thompson, J. A. Hooper, M. C. Willis and A. S. Weller, *Eur. J. Inorg. Chem.*, 2011, 5558-5565.
8. G. L. Moxham, H. Randell-Sly, S. K. Brayshaw, A. S. Weller and M. C. Willis, *Chem. Eur. J.*, 2008, **14**, 8383-8397.
9. R. J. Pawley, G. L. Moxham, R. Dallanegra, A. B. Chaplin, S. K. Brayshaw, A. S. Weller and M. C. Willis, *Organometallics*, 2010, **29**, 1717-1728.
10. G. L. Moxham, H. E. Randell-Sly, S. K. Brayshaw, R. L. Woodward, A. S. Weller and M. C. Willis, *Angew. Chem. Int. Ed.*, 2006, **45**, 7618-7622.
11. L. E. Bowen, M. Charernsuk, T. W. Hey, C. L. McMullin, A. G. Orpen and D. F. Wass, *Dalton Trans.*, 2010, **39**, 560-567.
12. A. Carter, S. A. Cohen, N. A. Cooley, A. Murphy, J. Scutt and D. F. Wass, *Chem. Commun.*, 2002, 858-859.
13. A. Dulai, C. L. McMullin, K. Tenza and D. F. Wass, *Organometallics*, 2011, **30**, 935-941.
14. J. N. L. Dennett, A. L. Gillon, K. Heslop, D. J. Hyett, J. S. Fleming, C. E. Lloyd-Jones, A. G. Orpen, P. G. Pringle, D. F. Wass, J. N. Scutt and R. H. Weatherhead, *Organometallics*, 2004, **23**, 6077-6079.
15. J. E. B. Jay A. Labinger, *Nature*, 2002, **417**, 507-514.
16. T. Agapie, J. A. Labinger and J. E. Bercaw, *J. Am. Chem. Soc.*, 2007, **129**, 14281-14295.
17. T. Agapie, M. W. Day, L. M. Henling, J. A. Labinger and J. E. Bercaw, *Organometallics*, 2006, **25**, 2733-2742.
18. T. Agapie, S. J. Schofer, J. A. Labinger and J. E. Bercaw, *J. Am. Chem. Soc.*, 2004, **126**, 1304-1305.
19. S. J. Schofer, M. W. Day, L. M. Henling, J. A. Labinger and J. E. Bercaw, *Organometallics*, 2006, **25**, 2743-2749.
20. T. Kochi, A. Nakamura, H. Ida and K. Nozaki, *J. Am. Chem. Soc.*, 2007, **129**, 7770-7771.
21. Ingrid M. Angulo, E. Bouwman, Sandra M. Lok, M. Lutz, Wilhelmus P. Mul and Anthony L. Spek, *Eur. J. Inorg. Chem.*, 2001, **2001**, 1465-1473.
22. M. Nandi, J. Jin and T. V. RajanBabu, *J. Am. Chem. Soc.*, 1999, **121**, 9899-9900.
23. L. Lavanant, A.-S. Rodrigues, E. Kirillov, J.-F. Carpentier and R. F. Jordan, *Organometallics*, 2008, **27**, 2107-2117.
24. D. F. Wass, *Pat WO2002004119, 2002 (to British Petroleum Chemicals)*.
25. S. J. Dossett, A. Gillon, A. G. Orpen, J. S. Fleming, P. G. Pringle, D. F. Wass and M. D. Jones, *Chem. Commun.*, 2001, 699-700.
26. N. A. Cooley, S. M. Green, D. F. Wass, K. Heslop, A. G. Orpen and P. G. Pringle, *Organometallics*, 2001, **20**, 4769-4771.
27. C. A. Tolman, *Chem. Rev.*, 1977, **77**, 313-348.
28. A. T. Lubben, J. S. McIndoe and A. S. Weller, *Organometallics*, 2008, **27**, 3303-3306.
29. H. E. Gottlieb, V. Kotlyar and A. Nudelman, *J. Org. Chem.*, 1997, **62**, 7512-7515.
30. M. A. Huertos and A. S. Weller, *Chem. Sci.*, 2013, **4**, 1881-1888.
31. D. P. Fairlie and B. Bosnich, *Organometallics*, 1988, **7**, 936-945.
32. D. P. Fairlie and B. Bosnich, *Organometallics*, 1988, **7**, 946-954.

33. *Unpublished data, Thesis of Will Reilly*.
34. J. Halpern, D. P. Riley, A. S. C. Chan and J. J. Pluth, *J. Am. Chem. Soc.*, 1977, **99**, 8055-8057.
35. B. Guzela, M. A. Omarya, J. P. Fackler Jr and A. Akgermand, *Inorg. Chim. Acta*, 2001, **325**, 45-50.
36. A. Mercer and J. Trotter, *Journal of the Chemical Society, Dalton Transactions*, 1975, 2480-2483.
37. T. Diao, P. White, I. Guzei and S. S. Stahl, *Inorg. Chem.*, 2012, **51**, 11898-11909.
38. M. Wasa, K. S. L. Chan, X.-G. Zhang, J. He, M. Miura and J.-Q. Yu, *J. Am. Chem. Soc.*, 2012, **134**, 18570-18572.
39. O. V. Ozerov, F. T. Ladipo and B. O. Patrick, *J. Am. Chem. Soc.*, 1999, **121**, 7941-7942.
40. S. Kotha, E. Brahmachary and K. Lahiri, *European Journal of Organic Chemistry*, 2005, **2005**, 4741-4767.
41. S. Saito, T. Kawasaki, N. Tsuboya and Y. Yamamoto, *J. Org. Chem.*, 2001, **66**, 796-802.
42. H. Lee and C.-H. Jun, *Bull. Korean Chem. Soc.*, 1995, **16**, 1135-1138.
43. H. Lee and C.-H. Jun, *Bull. Korean Chem. Soc.*, 1995, **16**, 66-68.
44. C. González-Rodríguez, R. J. Pawley, A. B. Chaplin, A. L. Thompson, A. S. Weller and M. C. Willis, *Angew. Chem. Int. Ed.*, 2011, **50**, 5134-5138.
45. P. Hofmann, C. Meier, W. Hiller, M. Heckel, J. Riede and M. U. Schmidt, *J. Organomet. Chem.*, 1995, **490**, 51-70.
46. M. Montag, L. Schwartsburd, R. Cohen, G. Leitus, Y. Ben-David, J. M. L. Martin and D. Milstein, *Angew. Chem. Int. Ed.*, 2007, **46**, 1901-1904.
47. M. Montag, I. Efremenko, R. Cohen, G. Leitus, L. J. W. Shimon, Y. Diskin-Posner, Y. Ben-David, J. M. L. Martin and D. Milstein, *Chem. Eur. J.*, 2008, **14**, 8183-8194.

4. C-S ACTIVATION

4.1. Introduction

As discussed in Chapter 1, the hydroacylation reaction has been investigated by a number of research groups using a variety of methodologies in order to yield better conversions and reduce the effect of the deactivating side-reaction – reductive decarbonylation. Arguably, the best results have been obtained using tethered substrates (*i.e.* aldehydes or alkenes/alkynes), including –OH,[1-3] –NR_2[4-6] or –SR[7-11] based tethers (where the R group can be an alkyl or an aryl). Although the use of tethered substrates have allowed for highly efficient and selective hydroacylation catalysis, the inherit problem with this approach is the fact that unless the tether can be removed at the end of the reaction, the scope is substantially reduced.[12]

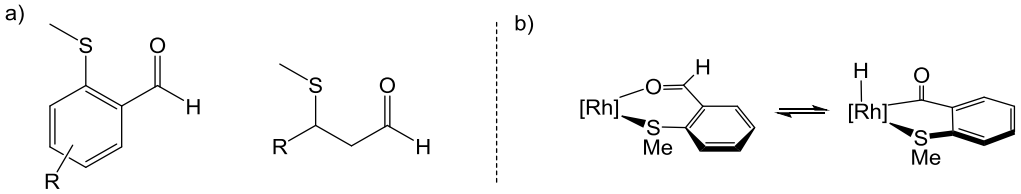

Figure 4.1. a) General scheme of tethered substrates used by Willis. b) Example of coordination of the aldehyde and C-H activation aided by the initial coordination of the sulfur atom to the rhodium metal centre.

Since 2004, Willis has been using β-sulfur-tethered aldehydes (Figure 4.1) for the hydroacylation reaction, that allow for initial coordination of the aldehyde substrate to the metal centre via the sulfur atom, followed by the intramolecular C-H activation, that in most cases does not happen without the tether.[8, 13] Just as important is that during the hydroacylation

reaction, the sulfur atom acts as a catalyst stabiliser, as it blocks one of the coordination sites on the metal centre, thus making the catalyst less susceptible for reductive decarbonylation (as was discussed in Section 1.4.12). This benefit upon using the sulfur-based tether was also shown by Bendorf for the intramolecular hydroacylation reaction in 2002,[7] they showed that these substrates allow for a range of intramolecular hydroacylation reactions to be performed (Scheme 4.1). Using these substrates the initial coordination of the sulfur atom to the rhodium centre occurred allowing for further reactivity, *i.e.* C-H activation. Another practical reason for the use of sulfur-based tethers is the simple synthetic procedure to obtain the desired aldehydes. For example, the benchmark aldehyde used in the Willis and Weller group, 2-(methylthio)benzaldehyde (**E**), is synthesised by a simple reaction between methanethiol sodium salt and 2-fluorobenzaldehyde.[8]

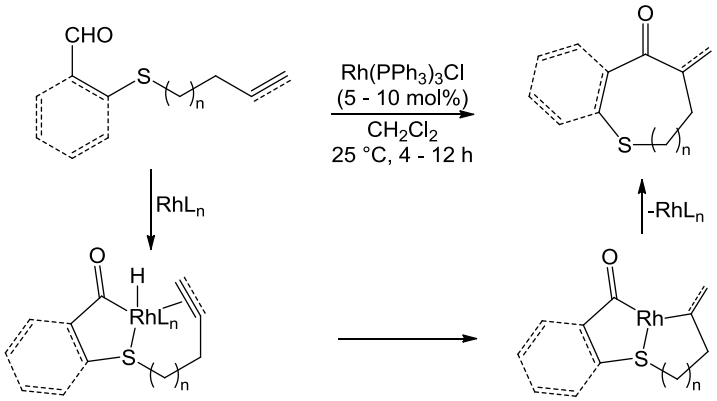

Scheme 4.1. Intramolecular hydroacylation catalysis using sulfur-tethered substrates as demonstrated by Bendorf and co-workers.[7]

Although the tethered substrates are relatively simple to synthesise and they are useful for initial studies, for developing a catalytic process that allows a catalyst to be used for a truly general range of different aldehydes and alkynes or alkenes, a more general method is needed. Ideally this method would be tether free, but as of yet successful tether free general approaches have not been developed.[12]

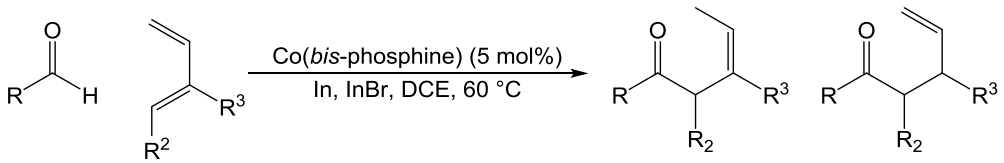

Scheme 4.2. Hydroacylation reaction using a range of tether-free aldehydes (R = aryl or alkyl) and 1,3-dienes reported by Dong and co-workers.[14]

Very recently Dong and co-workers reported a cobalt mediated hydroacylation reaction that allows hydroacylation catalysis without the need for an aldehyde tether. Although more general, as a range of aldehydes can be used, the reaction only works for 1,3-dienes which in this case act as chelating ligands and allow for the reaction to proceed. Additionally this reaction results in two different products (Scheme 4.2).[14] Dong has also recently reported another method that avoids tethers on aldehydes. Using small bite-angle neutral rhodium-PCP catalyst [Rh(dcpm)(OMe)] they were able to carry out intermolecular hydroacylation using non-tethered aldehyde and vinyl-phenols as starting materials.[1]

If the general method involves the use of a tether (*e.g.* a sulfur based tether), synthetic methodologies must be developed to cleave the carbon-based group (*e.g.* carbon-sulfur bond) at the end of the reaction, and replace the tether with a hydrogen atom or some other functional group (Scheme 4.3). Ideally this cleavage should be carried out by a catalytic process to reduce the waste generated during the reaction.

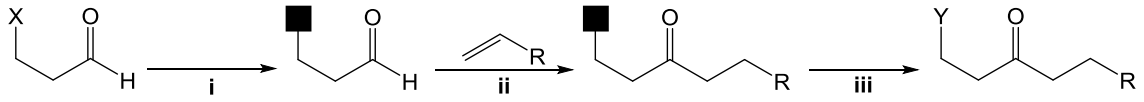

Scheme 4.3. General scheme of a tandem reaction where initially a tethering group (black square) is added to the substrate (**i**) followed by the hydroacylation reaction (**ii**) after which the tether is removed or replaced with another group Y (including hydrogen) (**iii**). X = a moiety that can be replaced with the tether.

Although C-S activation is a crucial part of organic chemistry, including natural product synthesis, drug and pesticide development and in approaches to turn simple unfunctionalised molecules to valuable chemicals, the use of transition metals for C-S activation has only been explored during the last two decades.[13, 15] In general, compared to C-H activation, C-S activation is considered to be relatively easier due to having smaller bond dissociation enthalpy (307.8 kcal.mol^{-1} for H_3C–S *vs.* 436.8 kcal.mol^{-1} for H_3C–H).[16] A number of C-S activation reactions under stoichiometric conditions using a range of transition metals have been reported, but only a limited number of catalytic C-S activations are known.[17] The lack of catalytic processes reported is due to the formation of a strong metal-sulfur bond during the reaction, which can prevent the catalytic turnover.

4.1.1. Historical Advances in Catalytic C-S Bond Activation

The first catalytic C-S cleavage reaction was reported by Liebeskind and Srogl in 2000.[18] They reported a synthesis of ketone products from thiol esters with organoboronic acids via palladium-catalysed, copper-mediated, cross-coupling reactions. It was shown that for this reaction to occur highly specific reaction conditions were needed. For example, the reaction occurred on using copper(I) carboxylate as a co-reagent, while the use of copper(I) halides led to no turnover. Additionally the use of sodium(I) and lithium(I) salts led to reduced conversions that both the copper(I) and the carboxylate are required to mediate the reaction. The proposed reaction mechanism for this C-S cleavage via this cross-coupling reaction is depicted in Scheme 4.4.

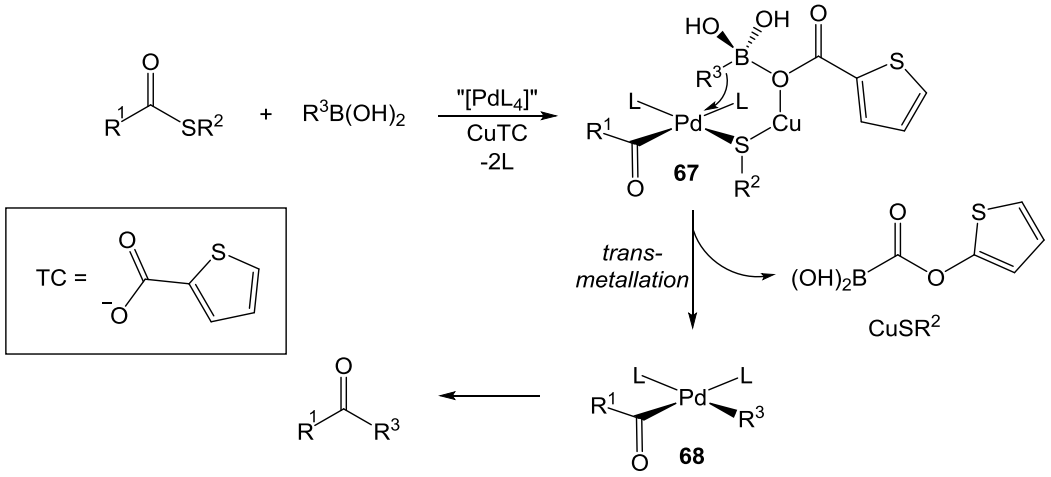

Scheme 4.4. Copper carboxylate mediated thiol ester boronic acid cross-coupling reaction mechanism. R^1, R^2 = alkyl or aryl, R^3 = aryl or styryl. 2L = dibenzylideneacetone.

The reaction involves an initial C-S activation by the palladium metal complex, which then forms the intermediate **67** that also incorporates the boronic acid and the copper carboxylate reagents. The formation of **67** allows for transmetallation through a 6-membered ring, while at the same time palladium-sulfur bond gets broken, resulting in the formation of the stable $CuSR^2$ species, which due to the strong Cu-S bond acts as a thermodynamic sink. This leads to the formation of **68**, from which reductive elimination occurs to yield the desired coupled product. The palladium catalyst loading was as low as 1 mol%, while stoichiometric amounts of copper reagent were required, consistent with the proposed mechanism.

Similar cross-coupling methodologies have been reported by the same group, and others, for a range of different C-S cleavage reactions.[19, 20] Furthermore, Liebeskind developed a methodology for C-S bond cleavage where the palladium catalyst is not required during the reaction (Scheme 4.5). The reaction occurs via initial coordination of Cu(I) to the thiol ester-oxime resulting in the S,N-chelated **69**. This is followed by the transmetallation reaction from boron or tin to Cu(I) which crucially leads to the proximity between the carbonyl carbon (**70**) of the thiol ester and the previously transmetallated R^2 group.

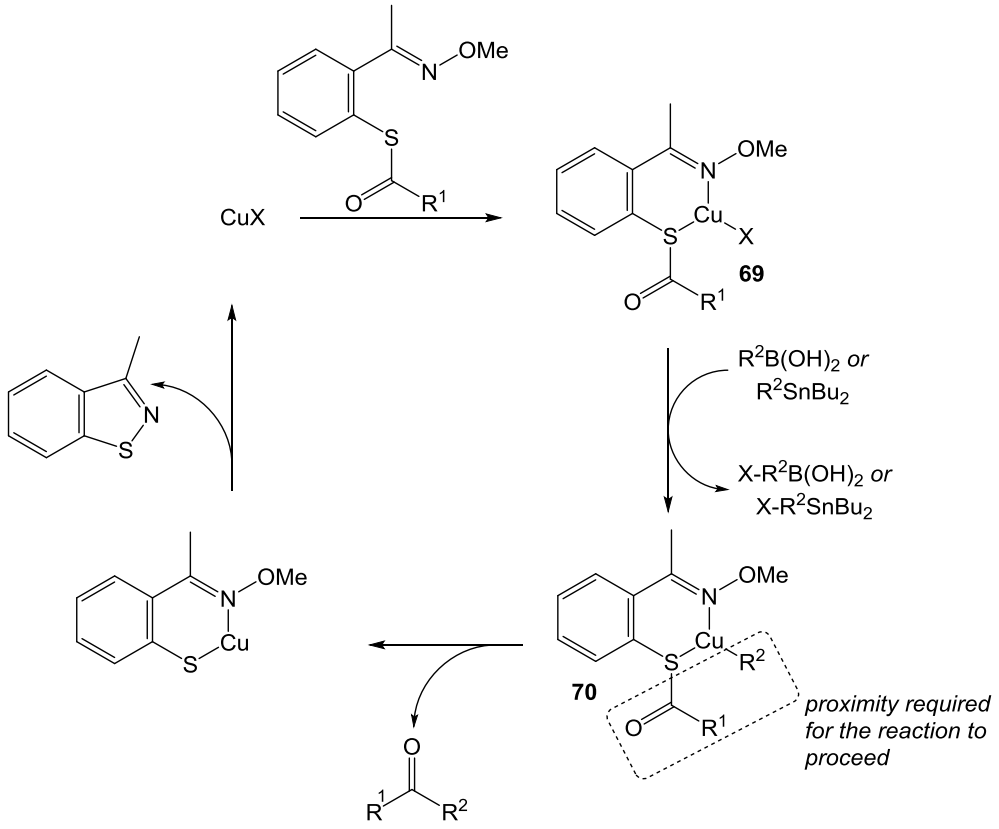

Scheme 4.5. Copper(I) catalysed C-C bond formation by desulfitative coupling via metallothionein mimicking.

This proximity allows for the coordination induced electrophilic activation of the thiol ester resulting in the formation of the ketone. The cycle is finished by the elimination of the ketone product that allows for the formation of the Cu-thiolate, which at 100 °C results in the formation of the S-N bond and liberation of the copper(I) catalyst.[21]

For similar cross-coupling reactions a range of different metal catalysts have been used (some of the most successful results have been obtained using nickel metal based catalysts),[22, 23] and a

range of different additives has also been investigated.[17] Although carbon-sulfur bonds are quite suitable for cross-coupling reactions, due to the strong bond formation between the transition-metal and the sulfur atom, there is a significant barrier to other reactivity when no co-reagent such as copper acetate is used.[24] Recently Willis and Weller used a rhodium(I) DPEphos based catalyst for combining aryl methyl sulfides with terminal alkynes, resulting in carbothiolation products.[25] This carbothiolation approach allowed for a wide range of substrates with different electronic and steric properties to be used. The mechanism is depicted in Scheme 4.6.

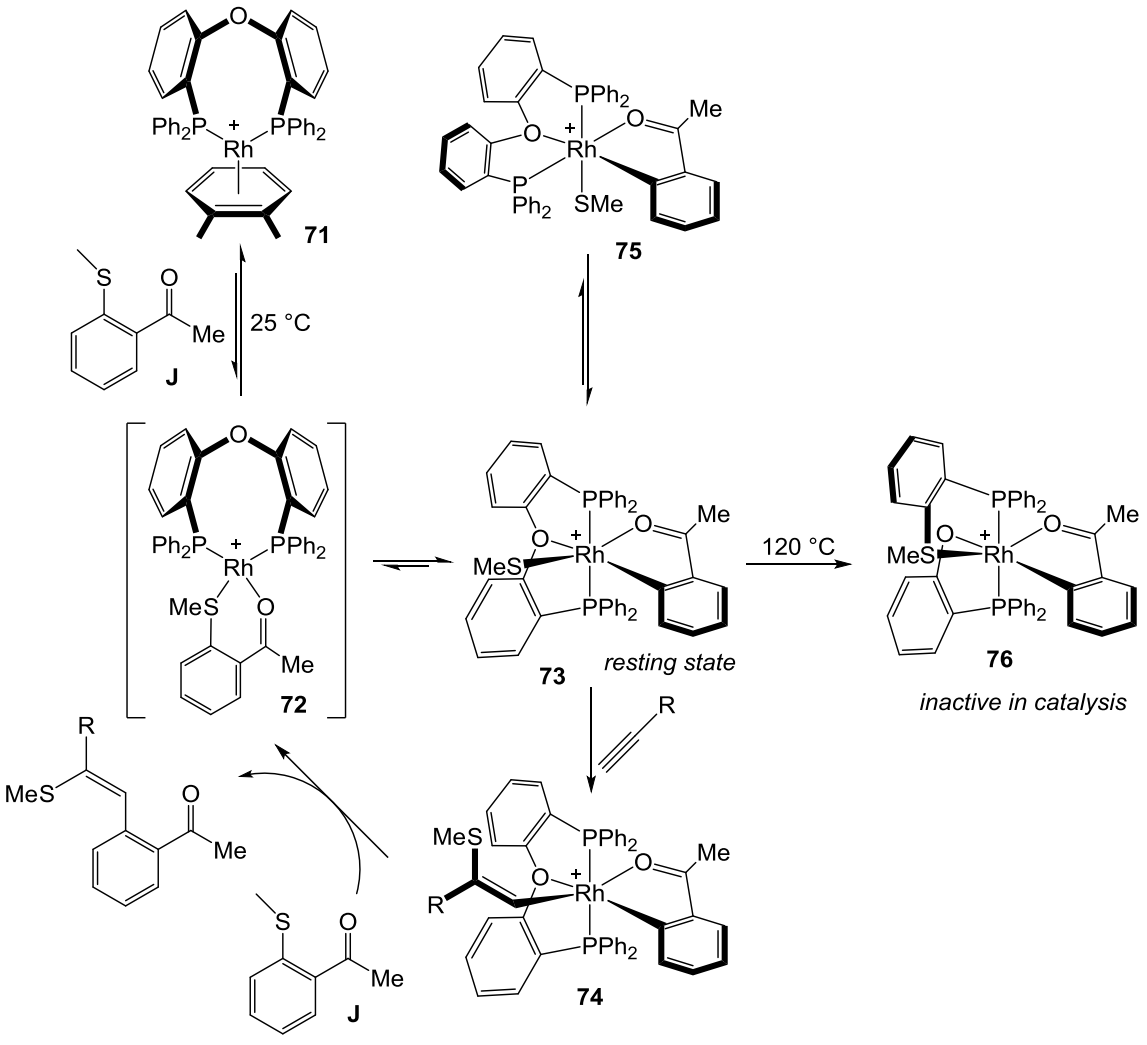

Scheme 4.6. The catalytic cycle for the alkyne insertion into the C-S bond of a β-S-substituted ketone, proposed by Willis and Weller. The $[BAr^F_4]^-$ counter-anion is not pictured for clarity.[25]

The mechanism proposed by Willis and Weller shows the initial equilibrium formed upon the addition of $MeSC_6H_4C(O)CH_3$ (**J**) to the rhodium(I) DPEphos catalyst (**71**) leading to the aryl-S bond cleavage and formation of **73**. This is followed by the insertion of the alkyne to the C-S

bond leading to **74** which can undergo reductive elimination resulting in the product formation and upon reaction with another equivalent of **J**, complex **72** is formed completing the cycle. During the catalytic cycle, also the formation of **75** and **76** can occur. The reversible formation of **75**, where the SMe migrates from being *trans* to acyl group to being *trans* to a phosphine, is likely to occur due to the hemilabile nature of the DPEphos ligand. The complex **76** was also formed during the catalysis, but was found to be to be off-cycle and inactive as a catalyst. The isolated **76** showed no catalytic activity upon being placed in the reaction mixture. The formation of **76** was observed to be much slower than the productive C-S activation pathway (6 h at 120 °C *vs*. 15 min. at 25 °C respectively), and hence is not considered to be problematic during the desired insertion reaction.

Interestingly, in particular with respect to this thesis, the authors were able to combine this reactivity with the hydroacylation reaction. Upon using **E** as the aldehyde and the electron rich alkyne **L**, they were able to show that the catalyst initially acts as the hydroacylation catalyst forming **M**, followed by C-S cleavage to form the final product in 66% overall yield (Scheme 4.7).

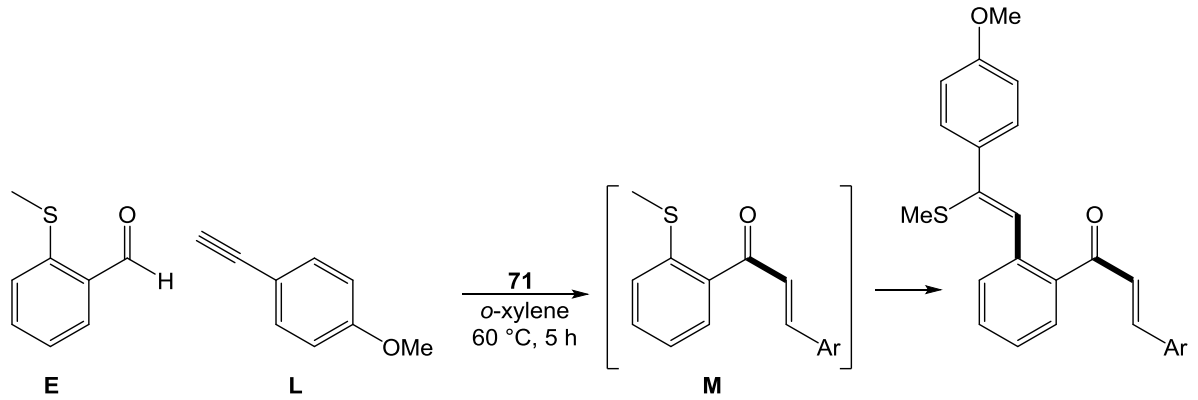

Scheme 4.7. Tandem hydroacylation/C-S insertion reaction reported by Willis and Weller.[25]

Other than cross-coupling reactions, another highly important field for C-S bond cleavage is C-S bond reduction to form the C-H bond. The development of this field is of particularly high importance for coal and petroleum industry, as currently available methods for removing of sulfur rely on reductants such as Raney nickel or $NiCl_2/NaBH_4$ which lead to poor yields and low selectivities.[26, 27] Furthermore the use stoichiometric amounts of metal species during the reduction reaction leads to additional waste being produced. Hence transition-metal based C-S

bond reduction has become increasingly important. Martin has reported a C-S reduction of aromatic substrates containing a C-SMe bond using $Ni(cod)_2$ as the catalyst (10 mol%) and $EtMe_2SiH$ as the reducing agent (2 eq.) (Scheme 4.8).[28] They reported that the mechanism of this reaction initially involves oxidative addition of the C-SMe to form an aryl-nickel(II)-SMe intermediate, which then undergoes σ-bond metathesis with the Si–H bond followed by reductive elimination from the nickel(II) hydride, resulting in the desired product.

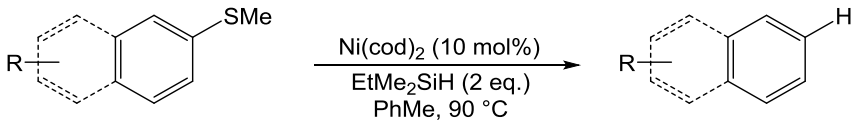

Scheme 4.8. C–S bond reduction reported by Martin.[28] Only examples with aromatic substrates were reported.

4.1.2. C-S Activation Using Small Bite-Angle Ligands

Weller and Willis recently reported C–S bond reduction using small bite-angle phosphine ligands on rhodium(I) metal centres as the catalysts.[29] This work continued from previous success reported by the same groups for the hydroacylation reaction using small bite-angle phosphine ligands on rhodium.[10, 11] Over the last few years, a "toolbox" of highly efficient hydroacylation catalysts have been reported by these groups which are highly efficient upon carrying the hydroacylation reaction out using sulfur tethered aldehydes (Figure 4.1, b), but they are inactive towards tether-free substrates.

Hence a method was required to catalytically cleave the C-S bond in order to remove the tether at the end of the hydroacylation reaction. The first example of hydroacylation reaction with traceless tether control was reported.[29] This means, that although during the hydroacylation reaction the sulfur tether is present, at the end of the reaction, C-S cleavage occurs and the tether is removed. This approach allowed for a broad substrate scope (due to chelation of the sulfur-tether) but the resulting products lacked a redundant coordinating group (Scheme 4.9).

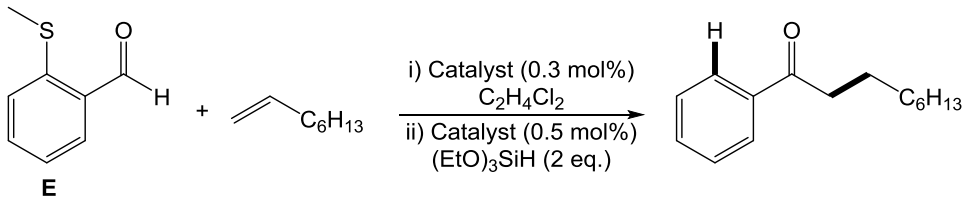

Scheme 4.9. Benchmark reaction between **E** and 1-octene, where initially the small bite-angle catalyst carries out the hydroacylation reaction and then the same catalyst can be in combination with the reducing agent, $(EtO)_3SiH$, to mediate the C-S reduction reaction.

This C-S activation reaction was screened using a range of different ligands on rhodium (5 mol % catalyst loading, 1 eq. of Et_2SiH, CH_2Cl_2, 25 °C). Both hemilabile ligand complexes containing DPEphos and XANTphos led to 33 % and 15 % conversion respectively (by NMR spectra). The best result (100% conversion) was observed upon using the $Cy_2PCH_2PCy_2$ ligand, while the similar small bite-angle ligand $^tBu_2PCH_2P^tBu_2$ only afforded negligible conversion in sulfide reduction. The reducing agents were also screened. The use of hydrogen gas (1 atm) resulted in < 10 % conversion, and the use of phenyl-substituted silanes led to no reactivity, whereas $(EtO)_3SiH$ allowed for high conversions even at very low catalyst loadings (< 1 mol%). Upon establishing these conditions, mechanistic studies were conducted, which led to the proposed mechanism depicted in Scheme 4.10. The experimental study indicated that there are two reaction pathways operating in parallel: C-S bond cleavage followed by the addition of silane (cycle A), and initial silane addition followed by C-S cleavage (cycle B). Addition of **J** to the rhodium fragment (**6**) in MeCN a reaction allows for the formation of **77,** which can continue to undergo a reaction with the silane to yield the desired product (**N**) and the *bis*-MeCN or ketone (**J**) bound rhodium fragment **78** (cycle A). Upon carrying out the same reaction in non-coordinating CH_2Cl_2 solvent, instead of the monomeric **77**, a dimeric Rh(III) species is formed, proposed as $[Rh(Cy_2PCH_2PCy_2)(\mu\text{-}SMe)(\sigma,\kappa\text{-}C_6H_4(OCMe))]_2[BAr^F{}_4]_2$ (**82**) (based on the NMR spectra and the ESI-MS). Due to the formation of oily products, suitable X-ray crystals were not obtained. To confirm the dimeric structure of the proposed **82**, a pyridyl containing ketone was used instead of **J** as the substrate, which allowed for extra stabilisation and resulted in the formation of **79** (Scheme 4.10), which was fully characterised and the crystal structure was obtained. The NMR spectra and ESI-MS data of **79** were analogous to the proposed dimeric species (**82**) formed when using **J** as the substrate. Both **79** and **82** were demonstrated to be

inactive in catalysis, once formed they represented a deactivation pathway for the C-S activation process in CH_2Cl_2.

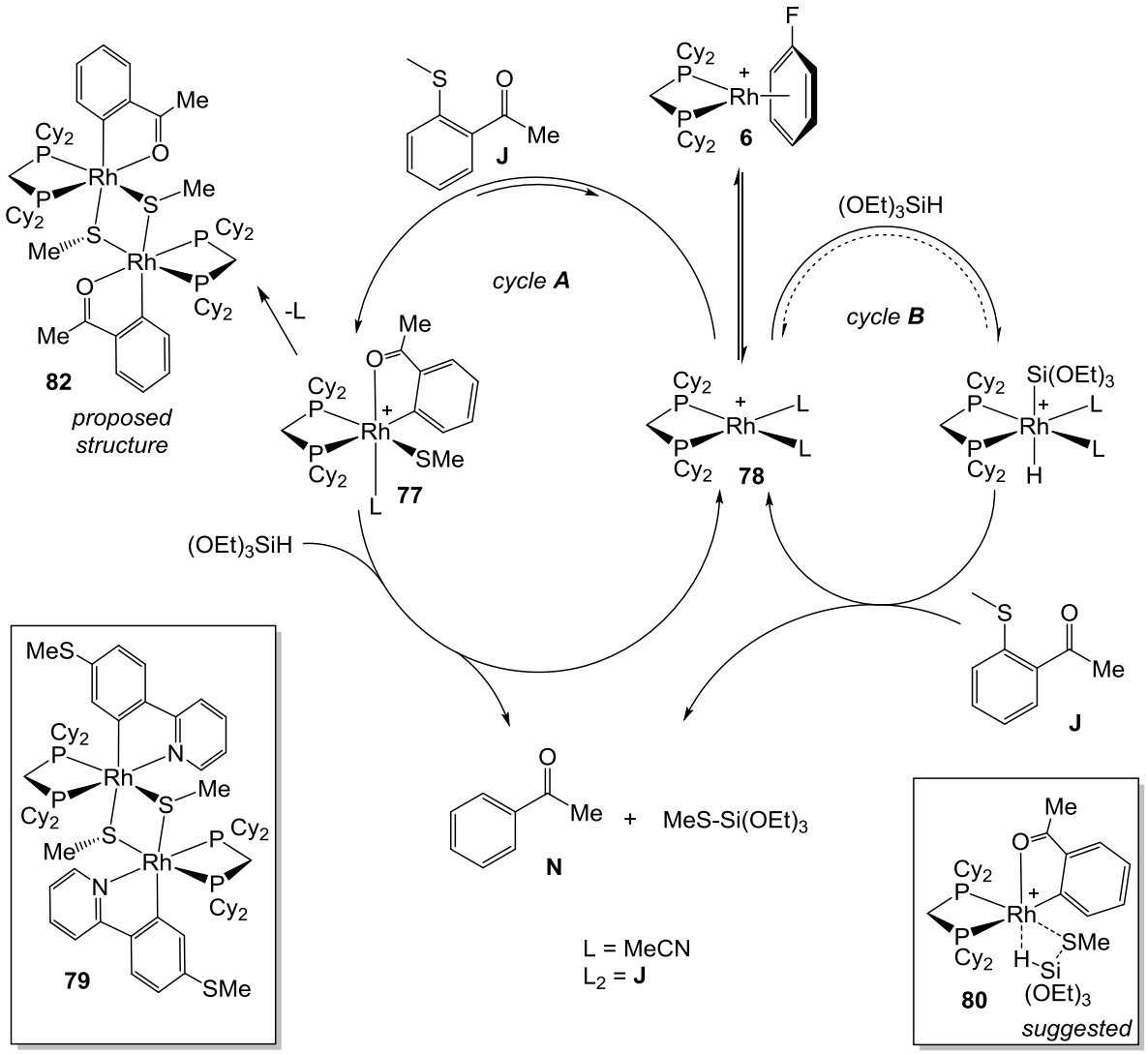

Scheme 4.10. The suggested mechanism of the tandem hydroacylation, C-S bond reduction using small bite-angle rhodium phosphine catalyst **6**. Cycle B turns over when L = CH_2Cl_2, $(OEt)_3SiH$ or agostic interaction. The $[BAr^F{}_4]^-$ counter-anion is not pictured for clarity.

The reduction of the C-S bond is expected to go via σ-bond metathesis through an η^2-silane (suggested intermediate **80**), this type of intermediate has been reported previously.[30] The process could also involve oxidative addition, but this would result in a Rh(V) intermediate, which is rare for rhodium species.[31] It was proposed that the $(OEt)_3SiH$ addition to **78** is much slower than the addition of **J** to **78** and thus cycle A mainly operates.

The promising results from the C-S bond reduction led Weller and Willis to further investigate the C-S activation ability of these small bite-angle rhodium *bis*-phosphine complexes to construct C-C bonds using boronic acids and methyl sulfides.[32] Additionally to the C-C bond formation, they were interested in developing a system incorporating orthogonal reactivity, as these rhodium complexes are inert with respect to aryl-bromide activating groups. In quest for orthogonal reactivity involving cross-coupling, a reaction process was investigated where substrates could be designed so that different active sites would attract specific metal complexes only. In particular a reaction combining rhodium(I) catalysed coupling of aryl and alkyl methyl sulfides with aryl and alkenyl boronic acids, which displays orthogonal reactivity towards palladium catalysed coupling of aryl bromides (Scheme 4.11).

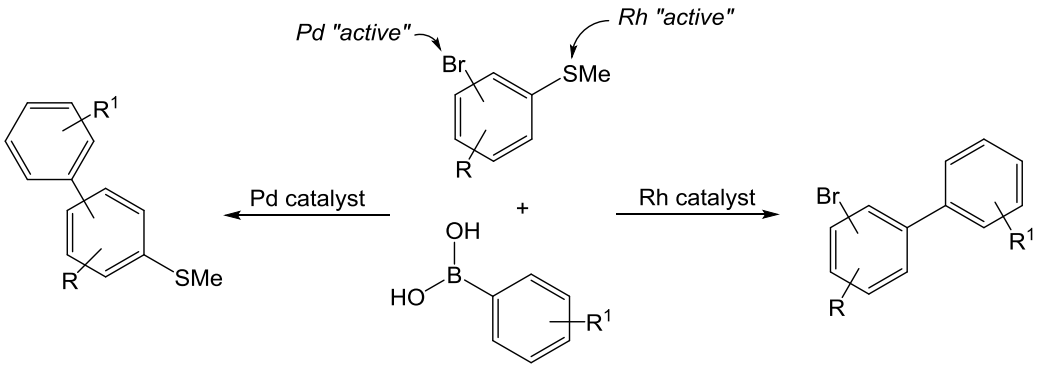

Scheme 4.11. Orthogonal reactivity in Pd- and Rh-catalysed cross-coupling reaction using halogenated methyl sulfides and boronic acids as substrates.

Initial screening using $MeSC_6H_4C(O)CH_3$ (**J**) and phenyl boronic acid as substrates (5 mol % catalyst loading, acetone, 55 °C) was carried out using the previously reported small bite-angle rhodium complexes $[Rh(^tBu_2PCH_2P^tBu_2)(C_6H_5F)][BAr^F_4]$ (**5**) and $[Rh(Cy_2PCH_2PCy_2)(C_6H_5F)][BAr^F_4]$ (**6**). Additionally, to investigate the effect the isopropyl groups have on the C-S activation reaction, screening was carried out using the catalyst developed for this thesis, $[Rh(^iPr_2PCH_2P^iPr_2)(C_6H_5F)][BAr^F_4]$ (**11c**). The screening demonstrated that **6** and **11c** both resulted in high conversions (> 70%), while the PCP(^{t}Bu) catalyst (**5**) led to a negligible amount of conversion to the product (Scheme 4.12).

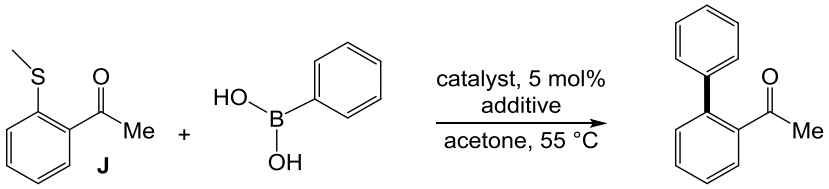

Scheme 4.12. Benchmark reaction of the coupling of the aryl-methyl sulfide (**J**) and phenyl boronic acid using a rhodium *bis*-phosphine catalyst.

Also, the screening of a range of additives (including Cs_2CO_3, $Cu(OAc)_2$, $Zn(OTf)_2$ and Ag_2CO_3) revealed that the best results were obtained upon using Ag_2CO_3. The combination of **11b** or **6** and Ag_2CO_3 allowed for a wide scope of boronic acids (aryl and alkyl) to be used (5 mol% catalyst loading, acetone, 16 h, 55 °C, 0.075 M **J**, 1 eq. Ag_2CO_3, **J**:boronic acid 1:1.5). Similarly to reaction described above (depicted in Scheme 4.9), the tandem reaction involving hydroacylation followed by Suzuki coupling[33, 34] was carried out (Scheme 4.13). First the rhodium *bis*-phosphine catalyst **6** or **11c** mediates the hydroacylation reaction between **E** and 1-octyne, and this is then followed by the cleavage of the C-S bond (carried out by the same catalyst) forming a new aryl-aryl complex as depicted in Scheme 4.13.

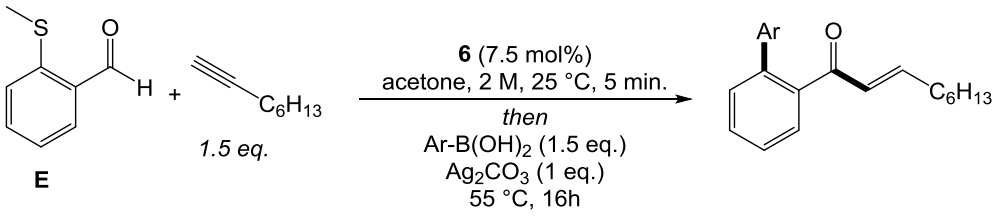

Scheme 4.13. Tandem hydroacylation/Suzuki coupling reaction using **E** and 1-octyne as the substrates.

The mechanistic studies carried out using the $Cy_2PCH_2PCy_2$ ligand allowed for a similar reaction mechanism seen for the reduction of C-S bonds to be proposed (Scheme 4.14).[29]

Upon carrying out the C-S activation in acetone, initially the formation of an equilibrium is observed between **6** and **81**. The *bis*-acetone complex **81** then undergoes a reaction with **J** that results in the off-cycle dimer **82** that is in a rapid equilibrium with the monomeric species **83**, unlike for the C-S reduction mechanism, where the dimer led to the catalyst deactivation in CH_2Cl_2 (**77**, Scheme 4.10). The addition of the boronic acid to **83** is rate-limiting, and requires the presence of an additive (Ag_2CO_3 or equivalent) in order to result in the desired coupled product. The step is suggested to go via the intermediate **84** that allows for transmetallation to

occur. Upon the addition of boronic acid to the *bis*-acetone complex **81**, formation of **85** is observed (cycle B). It was proposed that **85** is off-cycle and not productive in catalysis, and based on experimental data it appeared to be in equilibrium with the dimeric species **82**.

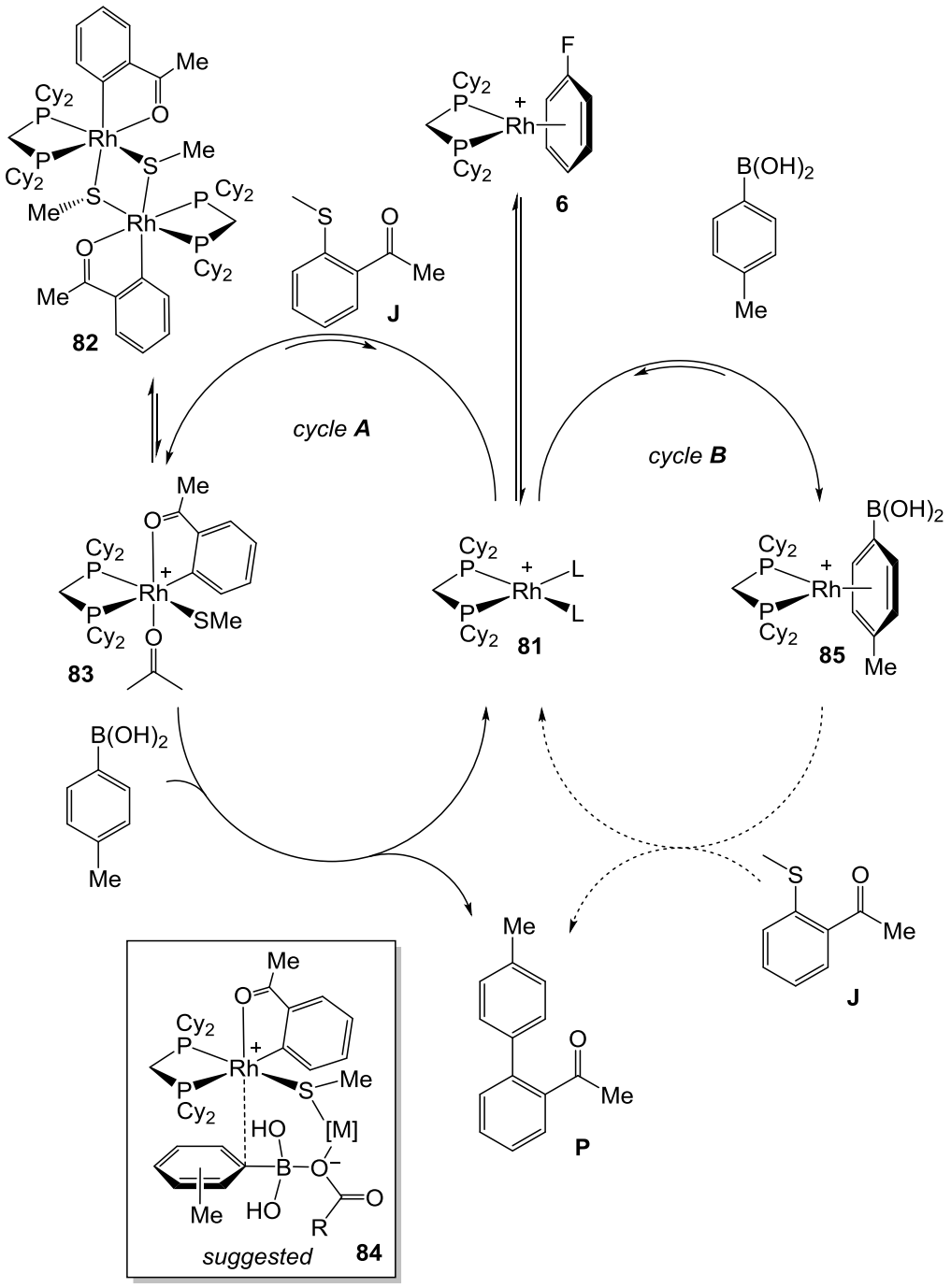

Scheme 4.14. Proposed catalytic cycles for C-S activation/cross-coupling reaction using **6**. M = Ag^+ or Cu^+. $[RCO_2]^-$ = acetate or carbocylate. The $[BAr^F_4]^-$ counter-anion is not pictured for clarity. Acetone-d_6 solution. L = acetone.

4.2. C-S Activation via the Formation of Dimeric Species

4.2.1. The Aim of the Project

Based on the successful results obtained in C-S activation of β-sulfur tethered ketones using rhodium centres complexed with small bite-angle phosphine ligands, it was particularly important to further probe the formation of the dimeric species observed during the reaction (*e.g.* **82**, Scheme 4.15).

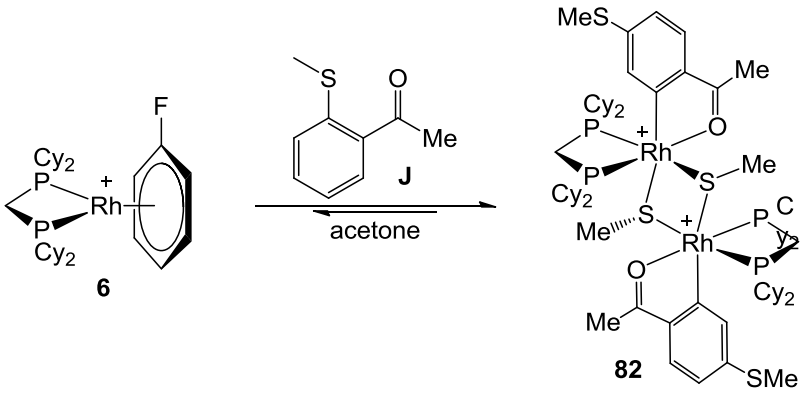

Scheme 4.15. Formation of the dimeric species during the C-S activation reaction using **6** and **J**. The $[BAr^F_4]^-$ counter-anion is not pictured for clarity.

As the formation of the dimer (*e.g.* **82**) can occur without the presence of additives needed for the reaction involving the cross coupling or C-S bond reduction reactions, it was important to understand how the formation of the dimeric species via C-S activation can affect the hydroacylation reaction as ultimately the ketone product of hydroacylation can form such dimer with the catalyst. Hence the aim was to probe the formation of these C-S activated dimeric species using different rhodium *bis*-phosphine complexes as previous comparison between similar PCP(^{t}Bu) complex **5**, PCP(Cy) complex **6** and PCP(^{i}Pr) complex **11c** led to different reactivity (Table 2.1).

Table 2.1. Comparison of reactivity between complexes **5** and **6** and **11c**.[10, 11, 29, 32]

	Hydroacylation	C-S activation
PCP(^{t}Bu) **5**	✓	×
PCP(Cy) **6**	✓	✓
PCP(^{i}Pr) **11c**	✓	✓

Is the dimer formation important for C-S activation?

Is the dimer formation affecting the hydroacylation reaction?

Continuing on the work reported in Chapter 2, the investigation was carried out using the isopropyl substituted catalysts [Rh(^{i}Pr$_2$PNMeP^{i}Pr$_2$)(C$_6$H$_5$F)][BAr$^{F}_4$] (**11b**) and [Rh(^{i}Pr$_2$PCH$_2$P^{i}Pr$_2$)(C$_6$H$_5$F)][BAr$^{F}_4$] (**11c**) and as will become apparent, they show dramatically different reactivity in the C-S activation.

4.2.2. C-S Activation Using 11b and 11c

Under the reaction conditions that were used for screening the catalysts in the C-S activation/Suzuki cross-coupling reaction (5 mol% catalyst loading, acetone, 16 h, 55 °C, 0.075 M **J**, 1 eq. Ag_2CO_3, **J**:boronic acid 1:1.5), the catalyst [Rh(^{i}Pr$_2$PNMeP^{i}Pr$_2$)(C$_6$H$_5$F)][BAr$^{F}_4$] (**11b**) was tested (Scheme 4.16).

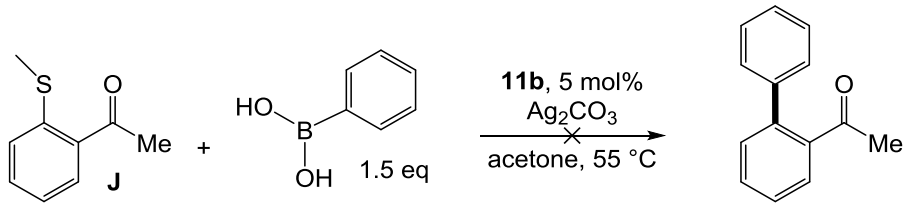

Scheme 4.16. Benchmark reaction of the coupling of the aryl-methyl sulfide (**J**) and phenyl boronic acid using **11b** as the catalyst.

Although **11b** has been shown to behave similarly to **11c** as a hydroacylation catalyst and is structurally similar (Chapter 2), no cross-coupling was observed upon using **11b** (*cf.* **11c** has been shown to act as a highly active cross-coupling catalyst, Scheme 4.13). It was decided to further compare these isopropyl substituted catalysts **11b** and **11c** in particular with respect to the PCP(^{t}Bu) **5** (previously shown to be sluggish C-S activation catalyst) and to the highly active C-S activation catalyst PCP(Cy) complex [Rh(Cy$_2$PCH$_2$PCy$_2$)(C$_6$H$_5$F)][BAr$^{F}_4$] **6**.

The addition of the isolated hydroacylation product (**F**) to the fluorobenzene complexes **5**, **6**, **11b** or **11c**, led to the formation of the product-ligated species which was indicated by ^{1}H and ^{31}P{^{1}H} NMR spectra (Scheme 4.17). Although the ^{1}H NMR spectra are very similar for the product bound and C-S activated dimer the ^{31}P{^{1}H} NMR spectra clearly show the formation of C-S activated rhodium(III) species over the ketone-bound rhodium(I) species for **6** and **11c**, while in the case of **5** and **11b** rhodium(I) species form. This is demonstrated by the smaller Rh-

P coupling (*e.g.* *J*[RhP] = 165 and 159 Hz for **5** while *J*[RhP] = 121 and 90 Hz for **6**).[11, 29, 35] Additional confirmation to the formation of C-S activated dimer formation was provided by ESI-MS data. As the dimeric species (z = 2) show different isotopic pattern compared to the monomers (z = 1), ESI-MS clearly showed the formation of the monomers in case of **5** [m/z = 669.28, calc. m/z 669.29 (**86**) with the correct isotopic pattern] and **11b** [m/z = 628.24, calc. m/z 628.24 (**25b**) with the correct isotopic pattern], whereas the reaction between **F** and the PCP(^{i}Pr) complex **11c** led to the formation of a dimer with a $[M_2]^{2+}$ parent ion at m/z = 613.23 (calc. m/z = 613.23 (**89**) with the correct isotopic pattern) analogous to the reactivity observed upon using **6** (**82**) (Scheme 4.17).[11, 32] These data match well with the cross-coupling reactions, which showed **5** and **11b** to be inactive while **6** and **11c** proved to be efficient cross-coupling catalysts – presumably the dimer cannot form.

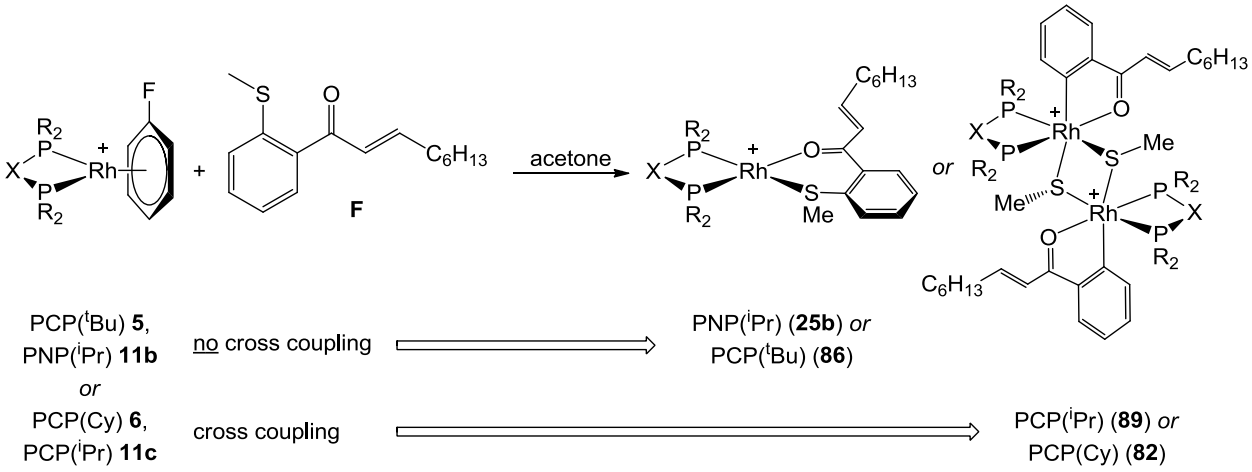

Scheme 4.17. Reactivity of rhodium phosphine complexes, with different backbone linkers or the substituents on the phosphorus atoms, towards the sulfur-tethered ketone **F**. The $[BAr^F_4]^-$ counter-anion is not pictured for clarity.

In order to simplify the mechanistic studies, the previously reported investigation using **6** was carried out using the simple methyl-ketone, 1-(2-(methylthio)phenyl)ethan-1-one (**J**) instead of the isolated hydroacylation product (**F**).[29] The stoichiometric reaction using **11c** and **J** was carried out in acetone solvent resulting in the formation of the C-S activated dimeric species **87** (Scheme 4.18) analogous to **89** which was observed upon a reaction between **11c** and the hydroacylation product **F** (Scheme 4.17).

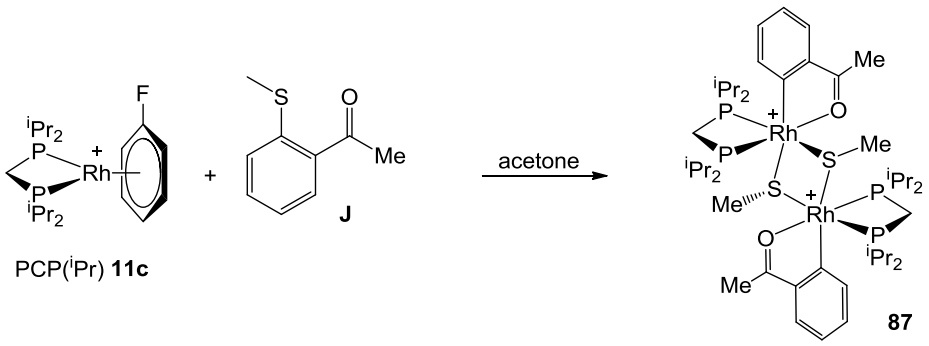

Scheme 4.18. C-S activation of **J** using the rhodium *bis*-phosphine complex **11c**. The $[BAr^F_4]^-$ counter-anion is not pictured for clarity.

Upon the addition of a stoichiometric amount of **J** to **11c** in acetone-d_6, the $^{31}P\{^1H\}$ NMR spectrum resulted initially in a very complicated spectrum showing multiple species had formed with very similar Rh-P and P-P couplings indicating the formation of a range of stereoisomers. No substantial change is seen upon leaving the sample for 2 h, but after the mixture was allowed to stand for 24 h this resolved into a spectrum that displayed one major species showing two doublet of doublets at δ 5.3 [*J*(RhP) = 116 Hz and *J*(PP) = 53 Hz] and at δ –11.4 [*J*(RhP) = 90 Hz and *J*(PP) = 53 Hz]. This data is almost identical to the $^{31}P\{^1H\}$ NMR data published for **82** (formed by a reaction between **6** and **J**) and is fully consistent with rhodium phosphine coupling expected for dimeric rhodium(III) *bis*-phosphine species.[11, 35, 36] In the case of **11c** additionally a minor set of doublet of doublets was seen at δ 4.3 [*J*(RhP) = 118 Hz and *J*(PP) = 54 Hz] and δ –13.9 [*J*(RhP) = 90 Hz and *J*(PP) = 54 Hz] showing essentially identical couplings to the pattern described above. We believe that this is due to the formation of a stereoisomer, where the methyl group on the sulfur atom is pointing in a different direction (*syn vs. anti*), especially as ESI-MS data on the same sample shows the formation of only one product immediately after mixing **11c** and **J** at m/z = 517.14 (calc. 517.14 for the ketone bound species $[Rh(^iPr_2PCH_2P^iPr_2)(\mu\text{-}SMe)(\sigma,\kappa\text{-}C_6H_4(C(O)Me))]_2[BAr^F_4]_2$) (**87**). The formation of stereoisomers due to the different orientation of the bridging SMe substituents has been previously reported.[37]

The timescale of this reaction between **11c** and **J** was investigated under the hydroacylation screening conditions using ESI-MS (10 mol% **11c**, 0.075 M **J**, acetone, 25 °C). For this, a solution containing **J** and acetone was prepared inside a glovebox that was interfaced with an ESI-MS instrument.[38] This prepared solution was added to the solid **11c**, and an aliquot was sampled,

diluted and injected to the ESI-MS instrument. During this reaction period (less than 30 s), full conversion into the dimer **87** had occurred (as was found under the stoichiometric conditions). The control reaction using the hydroacylation product (**F**) instead of **J** was carried out. Once again the formation of the corresponding dimer, $[Rh(^{i}Pr_2PCH_2P^{i}Pr_2)(\mu\text{-}SMe)(\sigma,\kappa\text{-}C_6H_4(C(O)CHCHC_6H_{13}))]_2[BAr^{F}_4]_2$ (**89**) had occurred before the first sample was taken from the reaction mixture. Building upon these results the reactions were designed to allow us to further understand C-S activation reaction using these catalysts. First the analytical approach was devised, as the stoichiometric reactions using **11c** and **J** showed that due to the formation of stereoisomers, NMR spectroscopy is not a suitable technique to follow this reactivity. Additionally the dynamic range of $^{31}P\{^{1}H\}$ NMR is too low for following these reactions under catalytic conditions. Thus it was found that the most suitable analytical method for following the C-S activation reactions is ESI-MS, allowing for discrimination between dimers and monomers and detection of mixtures in the cases where reaction mixtures include more than one ketone reagent.[39]

The reaction between **11c** and both ketones **J** and **F** was carried out (10 mol% **11c**, 0.075 M **J**, **J**:**F** 1:1, acetone, 25 °C). Interestingly in the case of addition of **11c** to a solution containing **J** and **F**, a mixture of products was observed. The main product obtained was the species formed via the activation of two equivalents of **J** (**87**) while the mixed C-S activated product (**88**) was observed in an intermediate concentration and the lowest relative concentration was detected for the **89** (in approximately 3:2:1 ratio) (Scheme 4.19). Presumably this selectivity arises from steric factors provided by a longer alkyl chain in the case of **F**. As this steric effect is useful for predicting potential reactivity of different substrates in C-S activation reactions, a range of ketones (**Q**, **R** and **S**), based on the general structure of **J** with small changes in the structure were prepared (Scheme 4.20). These particular ketones were synthesised to additionally investigate the steric effect observed upon comparing **J** and **F**. The substitution of SMe for SEt (**J** *vs.* **Q**) allows to investigate the sterics close to the metal centre, while the addition of *para*-Me to the phenyl ring (**J** *vs.* **R**) allows to obtain information about the effect the *para*-position has and additionally allows for a comparison of reactivity of two ketones with analogous sterics at the reaction centre. Additionally ketone **S** was synthesised that incorporates both motifs.

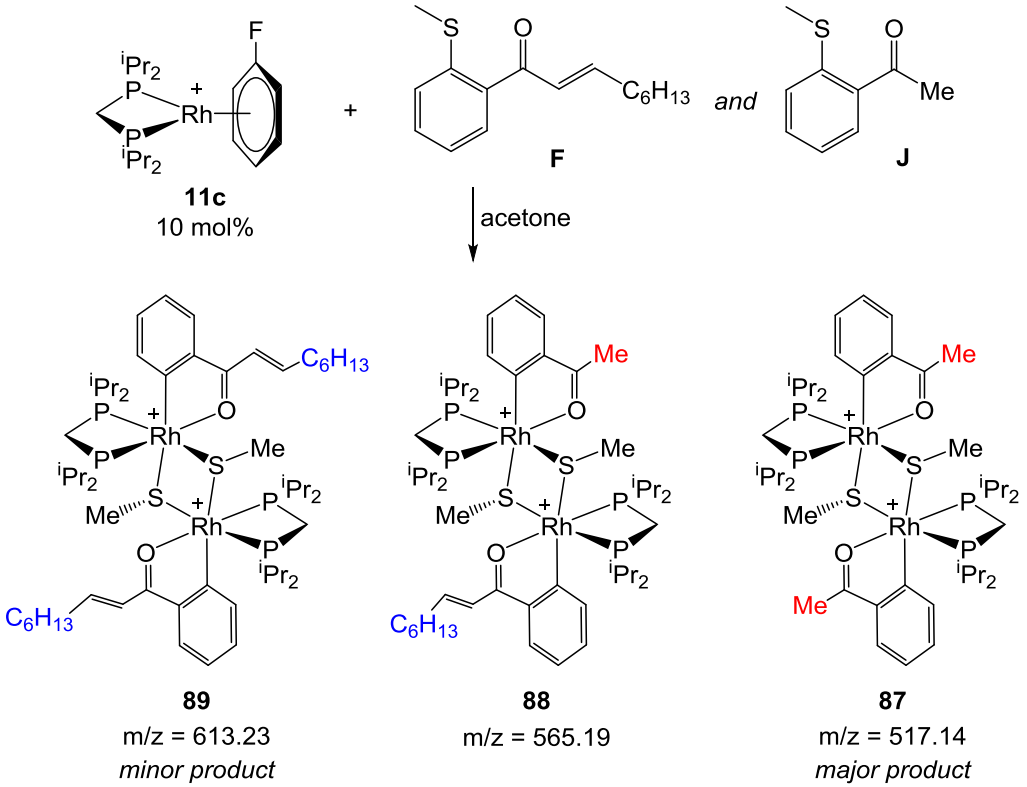

Scheme 4.19. Reaction of **11c** with a mixture containing **F** and **J**, and the formed products as observed by ESI-MS. The $[BAr^F_4]^-$ counter-anion is not pictured for clarity.

The effect of the ethyl group on the sulfur atom {*e.g.* $EtSC_6H_4C(O)CH_3$ (**Q**)} was of particular interest, as no C-S reduction reactions or cross-coupling reactions using this motif were reported by Willis and Weller.[29, 32] The ESI-MS control reactions carried out with each ketone (**Q**, **R** and **S**) individually using the rhodium complex **11c** resulted in the expected dimers which corresponded to the calculated masses {m/z = 531.15 (**90**), 531.15 (**91**) and 545.16 (**92**), *cf.* m/z = 517.13 was observed for **87** (reaction between **11c** and **J**) (Scheme 4.20)}. In all cases the charge of z = 2, and the correct isotopic pattern were observed.

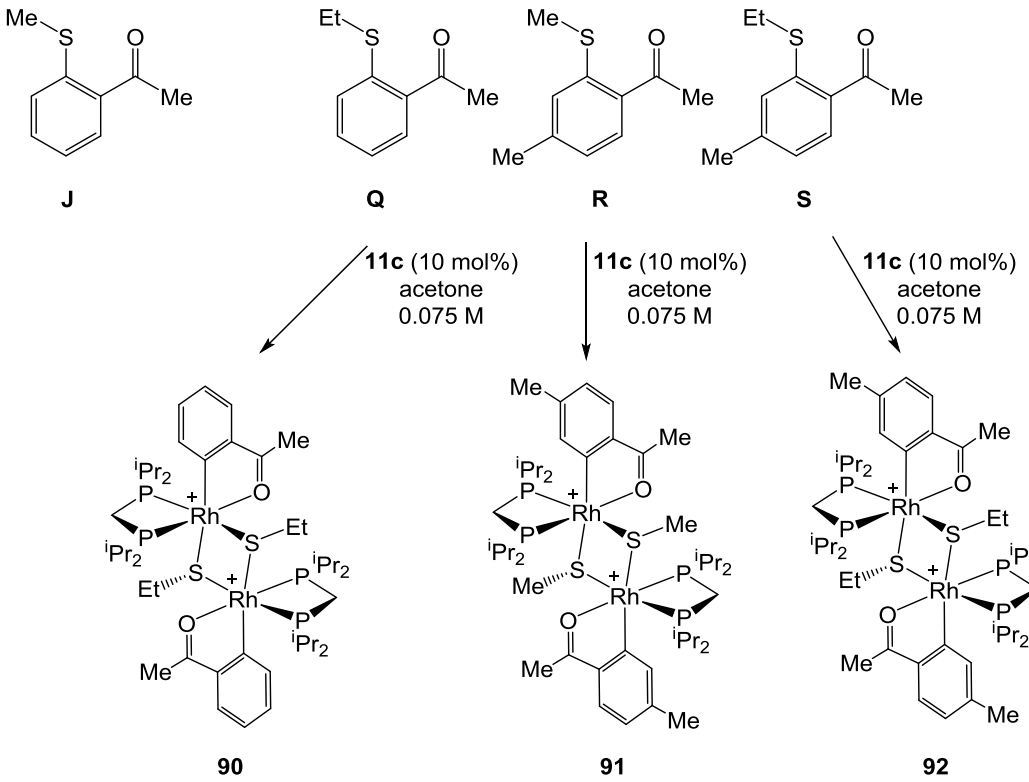

Scheme 4.20. Modified ketones (**Q**, **R** and **S**) synthesised by Milan Arambasic (Willis group) to investigate the steric effect on C-S activation, and the C-S activated dimeric species (**90** – **92**) formed upon the reaction between the ketone and **11c** in acetone. The $[BAr^F_4]^-$ counter-anion is not pictured for clarity.

Upon adding **11c** to an acetone solution containing **J** (*Me*$SC_6H_4C(O)CH_3$) and **Q** (*Et*$SC_6H_4C(O)CH_3$) (10 mol% **11c**, 0.075M **J**, 1:1 **J**:**Q**, 25 °C, acetone), a mixture of the three species was seen, with the main product being the dimer **87**, which was formed via the C-S activation of two equivalents of the least sterically demanding ketone **J**, while the dimer formed by the C-S activation of two equivalents of the sterically more demanding ketone (**Q**) present in this solution, **90**, is observed in very low intensity (Figure 4.2). The intermediate complex resulting in C-S activation of one equivalent of **J** and one equivalent of **Q** (**93**) would, based on a statistical distribution, be expected to be observed in double quantity compared to **87** and **90**, but this is not seen experimentally. These data indicate that the sterics close to the sulfur atom of the ketone substrates play a role in the C-S activation process, as the electronics of **J** and **Q** would be expected to be similar.

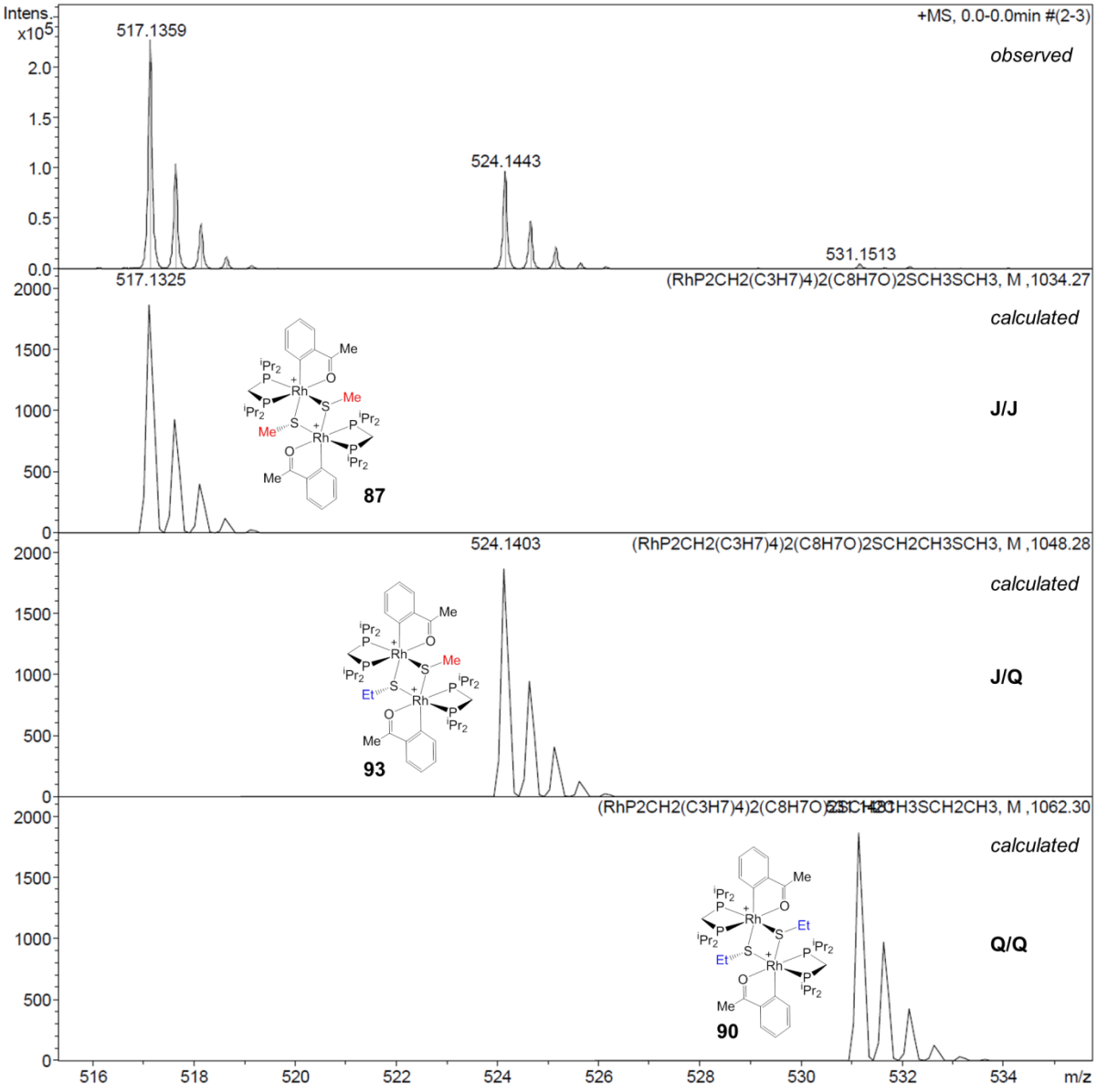

Figure 4.2. The formation of dimeric species (and their relative ratios) seen upon a reaction between **11c**, **J** and **Q**. The top spectrum is the experimental data, while all the spectra below consist of the simulated data. Acetone solvent.

In comparison, upon changing the sterics at the *para*-position of the thio-phenyl group of the aldehyde (**J** *vs.* **R**) a different distribution of products is seen. The reaction between **11c**, **J** and **R** (10 mol% **11c**, 0.075M **J**, 1:1 **J**:**R**, 25 °C, acetone) resulted in the formation of the three C-S activated dimeric species (**87**, **94** and **91**) in the approximately statistically expected 1:2:1 ratio by ESI-MS, although the species containing two *para*-methyl units (**91**) was formed in the lowest relative concentration (Figure 4.3), which could be indicative of steric interaction

between the isopropyl groups and the Me-substituent in the *para* position of the ketone-fragment.

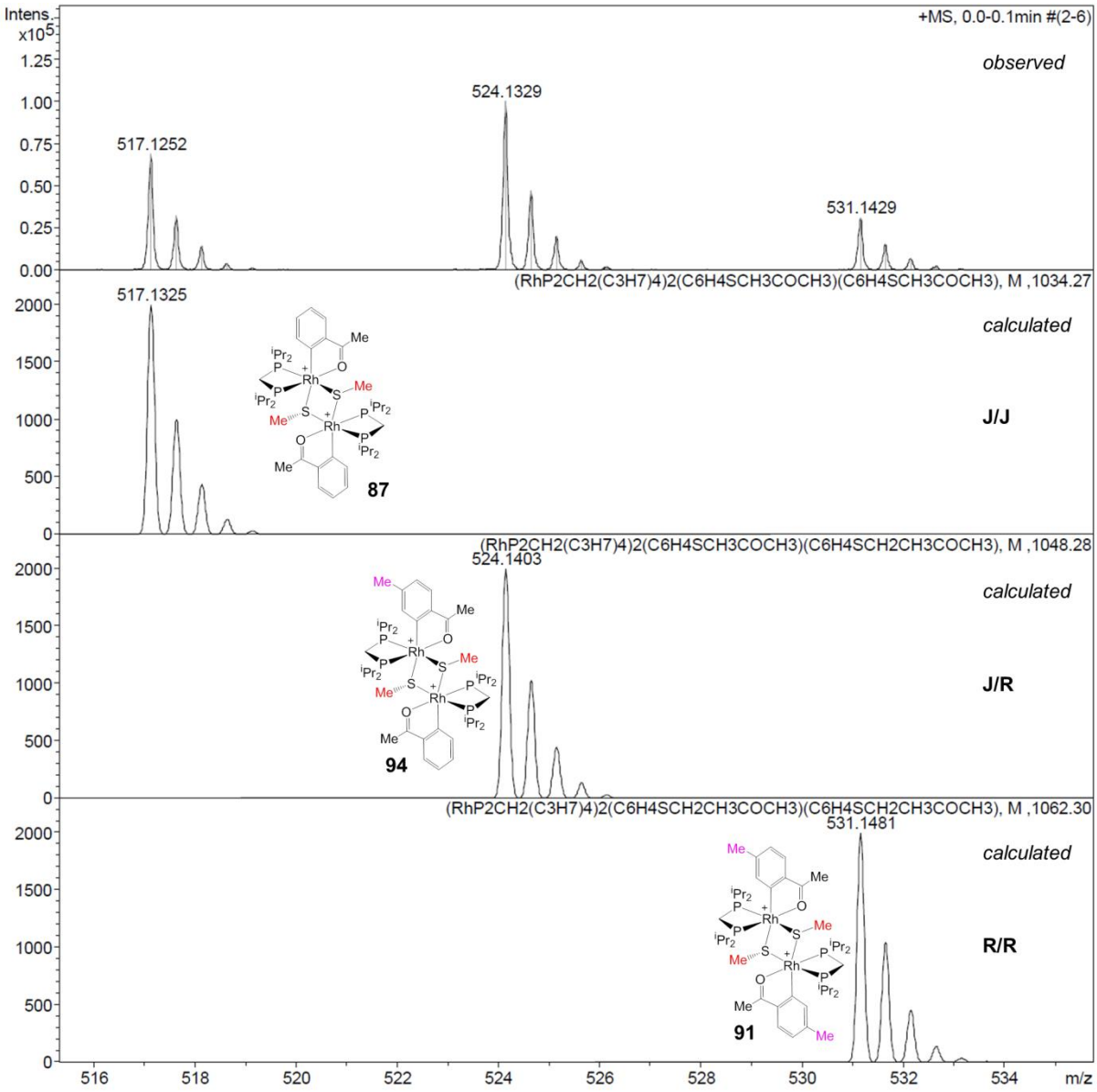

Figure 4.3. The formation of dimeric species (and their relative ratios) seen upon a reaction between **11c**, **J** and **R**. The top spectrum is the experimental data, while all the spectra below consist of the simulated data. Acetone solvent.

Additionally to the steric effects, these different ketones (**J**, **Q**, **R** and **S**) could be used to see if the formation of the dimeric species can subsequently undergo reductive elimination which would allow for reversibility. If that were the case, the addition of a third ketone to the mixture obtained from a reaction with **11c** and two ketones would lead to the formation of a new

dimeric rhodium species containing the third ketone (Scheme 4.21). This would occur via the initial dissociation of the dimeric species to form the corresponding monomers. These monomers can then undergo reductive elimination to eliminate a ketone species followed by the C-S activation of either the same or a new sulfur-tethered ketone forming a new C-S activated monomer, which, in combination with another monomeric species, can recombine to form a dimeric sulfur-bridged dimer.

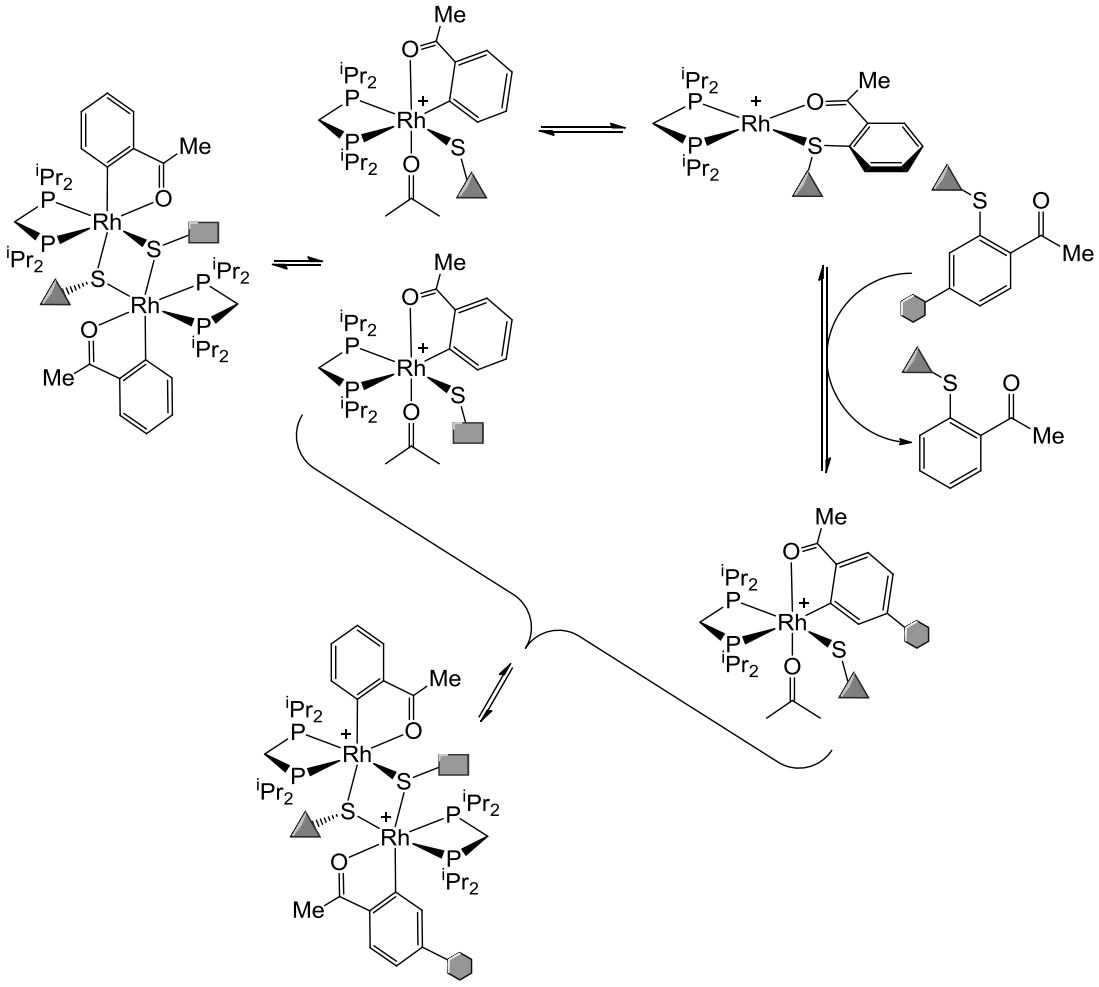

Scheme 4.21. The general scheme showing the scrambling via initial dissociation of the dimer to two monomeric species, which can then undergo reductive elimination and react with another ketone. The $[BAr^F_4]^-$ counter-anion is not pictured for clarity.

To probe this reversible reactivity, a third ketone (**S**) was added to the mixture shown in Figure 4.3 and the obtained solution was stirred at room temperature. After 10 minutes of stirring no change was observed by ESI-MS. Whereas upon stirring overnight, a peak at m/z = 538.17 (**96**) and a smaller peak at m/z = 545.17 (**92**) appeared showing the formation of species containing

ketone **S** (Figure 4.4). This result indicates that the C-S activation of these ketones using **11c** is reversible but slow, although it cannot be discriminated whether the slow step is due to the breaking of the C-S activated dimer to a C-S activated monomer or is it due to slow reductive elimination of the C-S bond.

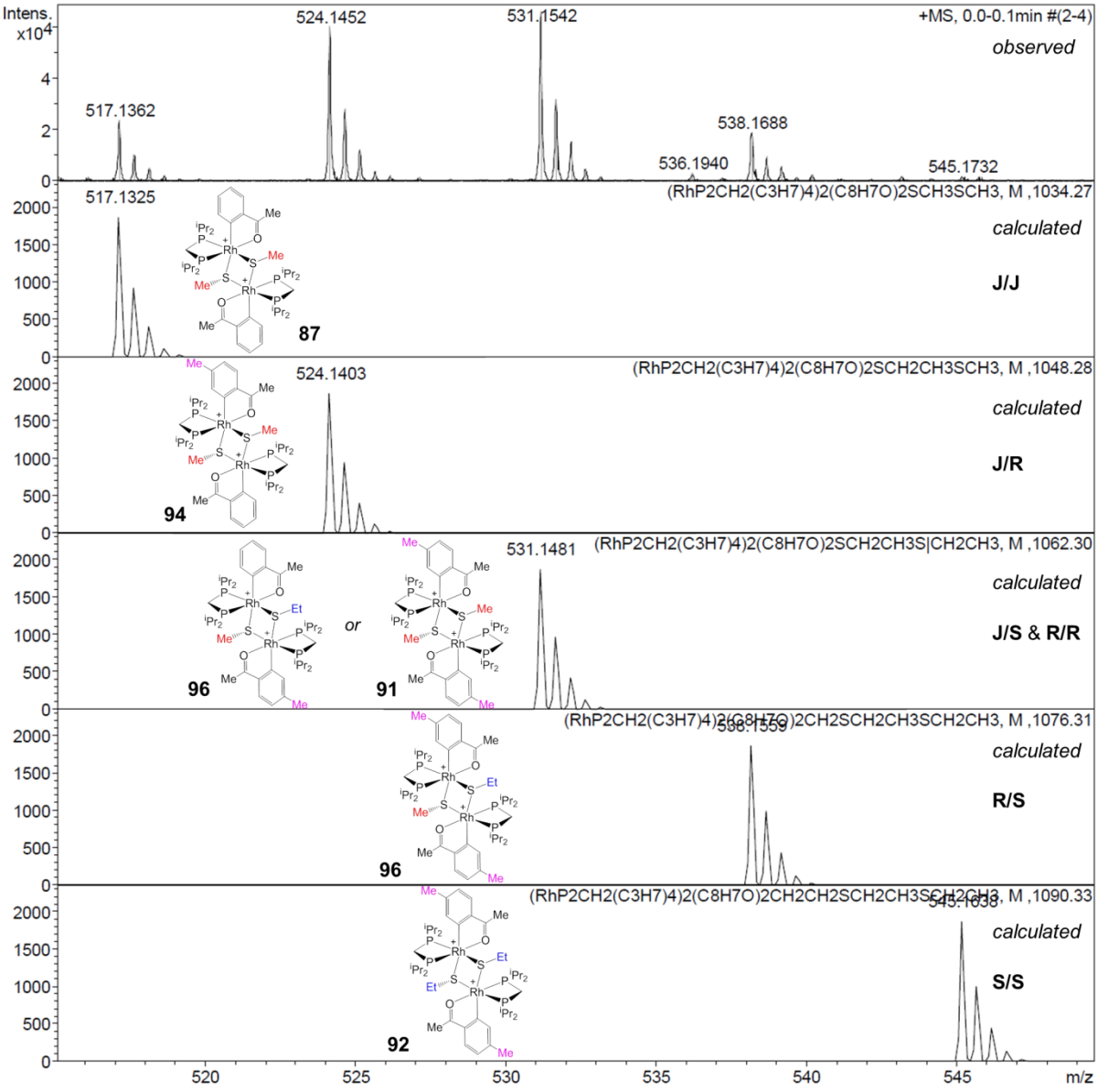

Figure 4.4. The formation of dimeric species (and their relative ratios) seen upon a reaction between **11c**, **J** and **R** followed by an addition of **S** which was allowed to react for 24 h. The top spectrum is the experimental data, while all the spectra below consist of the simulated data. Acetone solvent.

Based on these initial results indicating the potential reversibility of this dimer formation (Figure 4.4), two of the modified ketones, $EtSC_6H_4C(O)CH_3$ (**Q**) and $MeSC_6H_3$(*p*-Me)$C(O)CH_3$ (**R**), were used to see whether initial C-S activation reaction forming the dimer is catalytically reversible. For this a reaction was devised where **Q** and **R** were allowed to stir in acetone solution at the presence of **11c** (10 mol% **11c**, 0.075M **Q**, **Q**:**R** 1:1, acetone, 25 °C) and the reaction was followed using GC-MS enabling the detection of substrates. Reversibility would result in the formation of **J** and **S** via scrambling, and these would be observed by GC-MS (Scheme 4.22). The different retention times observed for all the ketones proved GC-MS to be a good technique for probing this reactivity.

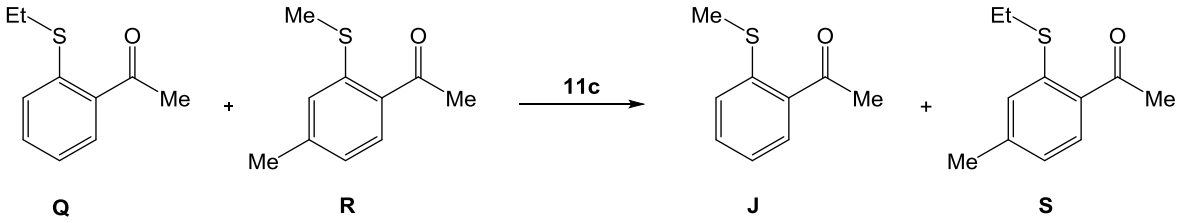

Scheme 4.22. Scrambling experiment to confirm the reversibility of the C-S activation process using small bite-angle ligands. *Conditions: 10 mol% catalyst, 0.075 M **Q**, acetone, 25 °C, 1:1 ratio of **Q** and **R**.*

The initial test-reaction was carried out using **Q** and **R** without the presence of any catalyst in acetone (stirring at 25 °C for 24 h), which confirmed that no reactivity is occurring without the presence of a metal species, demonstrated by no formation of **J** and **S**. Upon adding **11c** to the solution, based on GC-MS data, no scrambling was observed during the first 10 minutes, whereas when leaving the reaction stirring for 24 h, a mixture was obtained in which all four ketones (**J**, **Q**, **R** and **S**) were present in approximately equal quantities. This shows that the C-S activation and the formation of the dimeric species is reversible but the relative timescales between the formations of the C-S activated dimer (occurring in less than 30 s) and the overall reductive elimination process are very different (Scheme 4.23).

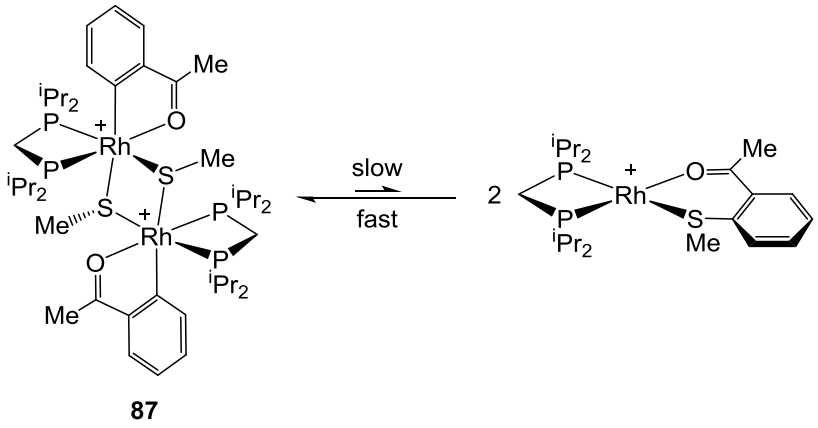

Scheme 4.23. The relative timescales for the formation of the C-S activated dimer and the ketone bound monomer. The $[BAr^{F}{}_{4}]^{-}$ counter-anion is not pictured for clarity.

As discussed previously, **5** and **11b** were inactive as cross-coupling catalysts. Also the use of **5** and **11b** resulted in the formation of product-ligated monomers upon reacting with **F** (**86** and **25b** respectively, Scheme 4.17) instead of the C-S activated dimers. Therefore, the cross-over experiment (Scheme 4.22) was carried out using **5** and **11b** as catalysts under the same reaction conditions. In either case no scrambling (*i.e.* formation of **J** and **S**) was observed even after the solution was allowed to stir for 24 h at 25 °C, consistent with the previous results that indicated no C-S activation (Scheme 4.24).

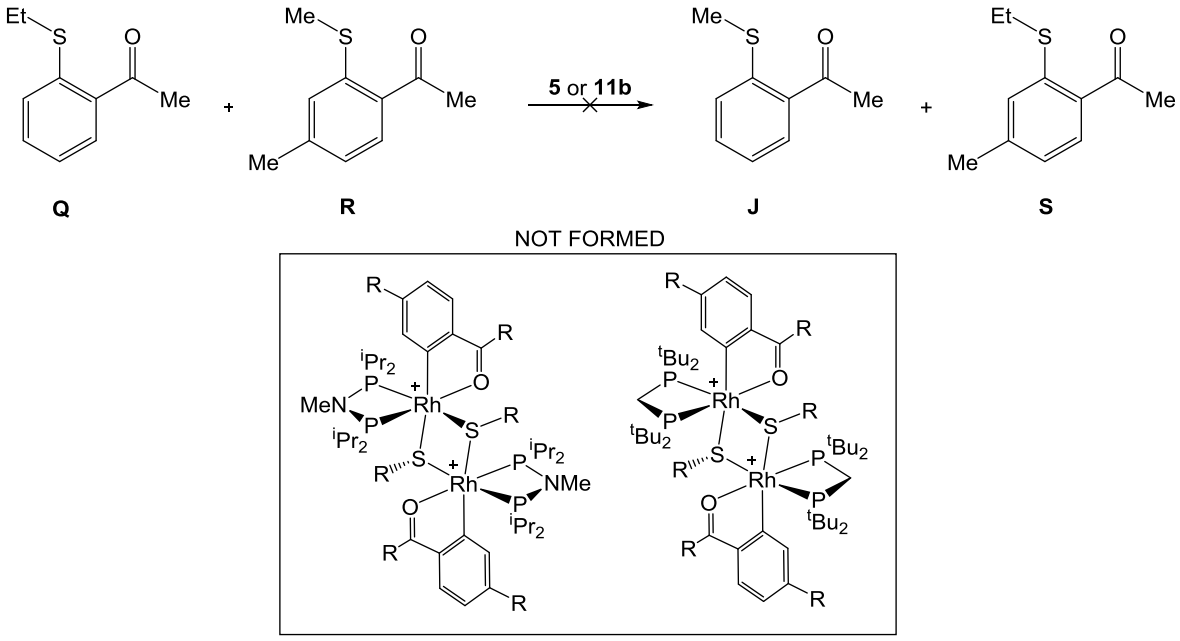

Scheme 4.24. The cross-over experiment is not occurring upon using PCP(^{t}Bu) complex **5** or PNP(^{i}Pr) complex **11b** as catalysts. The C-S activated dimers are not observed for **11c** and **5**. The $[BAr^{F}{}_{4}]^{-}$ counter-anion is not pictured for clarity.

4.2.3. C-S Activation During the Hydroacylation Reaction

With this understanding on which complexes carry out C-S activation, and the relative rate of C-S activation with respect to the reversible step, overall reductive elimination, next it was explored how this readily occurring C-S activation affects the hydroacylation reaction upon using β-sulfur tethered aldehydes (*i.e.* **E**) as substrates.

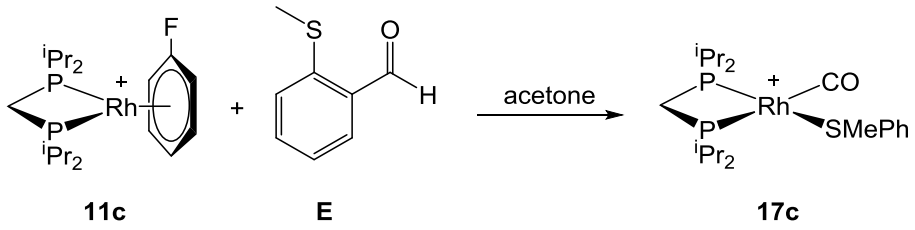

Scheme 4.25. The synthesis and the proposed structure of the PCP(^{i}Pr) based decarbonylation product **17c**. The $[BAr^{F}_{4}]^{-}$ counter-anion is not pictured for clarity.

The ^{1}H and ^{31}P{^{1}H} NMR have previously showed the formation of the decarbonylation product **17c** upon a reaction between **11c** and **E** (Scheme 4.25). Interestingly under ESI-MS conditions the decarbonylation product is seen as dimer with m/z = 503.11 (calc. m/z = 503.11, with the correct isotopic pattern, z = 2) corresponding to $[Rh(^{i}Pr_2PCH_2P^{i}Pr_2)(SMePh)(CO)]_2[BAr^{F}_{4}]_2$. This is presumably only the case in ESI-MS, as the ^{31}P{^{1}H} NMR spectrum showed similar rhodium phosphine coupling (indicative of rhodium(I) complex formation) to that was seen for PNP(^{i}Pr) complex **17b**, of which the X-ray structure was obtained (Figure 2.10).

Upon carrying out the hydroacylation reaction using **E** and 1-octyne with **11c** as the catalyst (10 mol% catalyst, 0.075 M **E**, acetone, 25 °C, 1:1.5 **E**:1-octyne) and following by ESI-MS the formation of the hydroacylation product (**F**) C-S activated dimer (**89**) was observed within a minute (Scheme 4.26). This corresponds to the hydroacylation catalysis data (Section 2.3.1) showing that hydroacylation under these conditions using **11c** as the catalyst allows for full conversion in less than a minute. Unfortunately we could not go any lower in catalyst loading, as this would have brought a relatively high concentration of **E** into the ESI-MS instrument, and the viscous nature of **E** has shown to lead to contamination problems. Nevertheless, the formation of this dimer clearly showed that the C-S activation readily occurs under the hydroacylation conditions. However, this data does not allow us to discuss at which point during the

hydroacylation reaction C-S activation occurs, and whether this leads to the formation of an inactive catalyst.

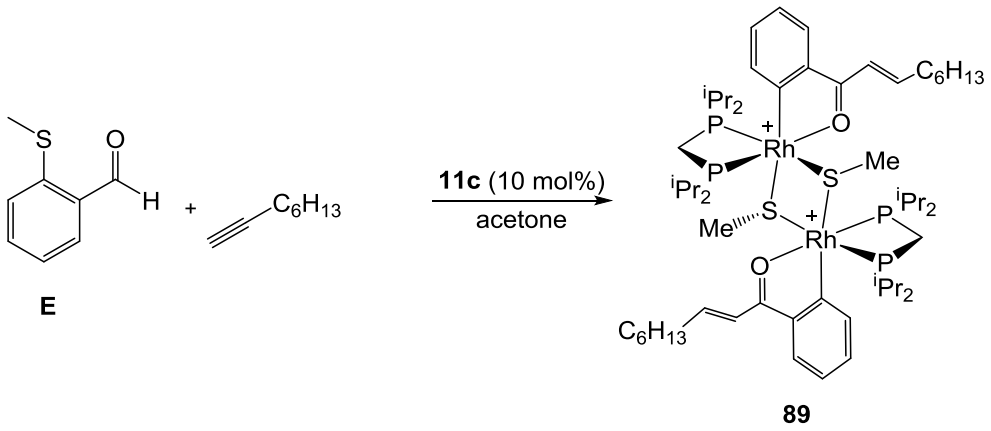

Scheme 4.26. Hydroacylation using **E** and 1-octyne as substrates and **11c** as the catalyst followed by ESI-MS. *Conditions: 10 mol% **11c**, 0.075 M **E**, 1:1.5 **E**:1-octyne, 25 °C, acetone.* The $[BAr^F{}_4]^-$ counter-anion is not pictured for clarity.

Similar timescale issues were observed upon attempting to follow the reaction by NMR spectroscopy. At 10 mol% catalyst loading and a large enough sample volume for acquiring a NMR spectrum (0.075 M) the hydroacylation reaction occurs within less than a minute, which is longer than it takes to tune the NMR spectrometer and lock and shim the sample. Lower catalyst loadings do not allow us to obtain any reliable NMR spectra for the active catalyst (due to the low dynamic range of this analytical method). A further problem using NMR spectroscopy is the formation of the C-S activated dimer in acetone. As was discussed above, the initial formation of the dimer from a preformed ketone results in a complicated set of data (presumably due to the formation of stereoisomers as ESI-MS only shows one product (**89**) being formed) that resolves over time (24 h). This behaviour is also seen upon carrying out the hydroacylation reaction in acetone and following it by NMR spectroscopy (one peak in ESI-MS corresponding to **89** is observed). Instead, upon carrying out the hydroacylation reaction in CD_2Cl_2 (at 10 °C), the disappearance of the aldehyde can be observed in the ^1H NMR spectrum and by $^{31}P\{^1H\}$ NMR spectroscopy the appearance of the decarbonylation product (**17c**) is observed. The better data upon using dichloromethane as the solvent is presumably due to the low coordinating ability of dichloromethane compared to acetone. Additionally, the formation of a new species is seen after the full consumption of the aldehyde **E** which is assigned as the C-S activated dimer **89**. For this

species, the $^{31}P\{^{1}H\}$ NMR spectrum shows two doublet of doublets at δ 12.8 (J(RhP) = 131 Hz and J(PP) = 40 Hz) and at δ –14.9 (J(RhP) = 62 Hz and J(PP) = 40 Hz). Unfortunately we could not compare this data to that of the separately formed dimer **89** in CH_2Cl_2 as **11c** is inert towards the **J** or hydroacylation product (**F**) in CH_2Cl_2, but the ESI-MS of the final product of the hydroacylation reaction shows the formation of the hydroacylation product activated dimeric species **89**. Overall, this data allows us to propose that the formation of **89** only occurs after the completion of the hydroacylation reaction, but it does not allow us to discuss the catalytic activity of the dimer.

Based on previously reported work (Section 4.1.2), the dimer **89** is expected to "sit" off-cycle, but as we have shown that the formation of the dimer is reversible, an experiment where the dimer formed via C-S activation of the hydroacylation product **F** (**89**) was used as the hydroacylation catalyst was conducted (10 mol% catalyst loading, 0.075 M, 25 °C, acetone, **E**:1-octyne 1:1.5) (Scheme 4.27).[32]

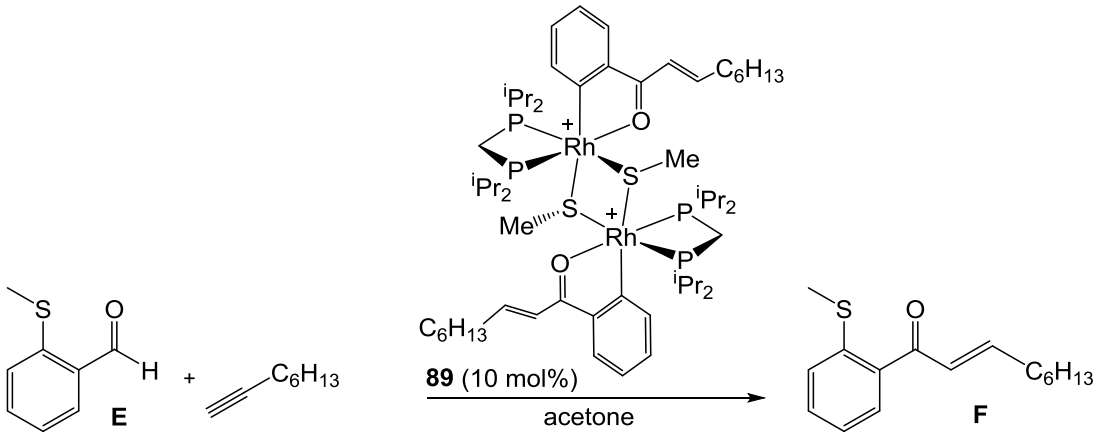

Scheme 4.27. Hydroacylation reaction using E and 1-octyne as substrates, and the C-S activated dimer **89** as the catalyst. The $[BAr^F_4]^-$ counter-anion is not pictured for clarity. *Conditions: 10 mol% catalyst loading, 0.075 M **E**, 25 °C, **E**:1-octyne 1:1.5, acetone.*

The reaction was followed by HPLC. This data (Figure 4.5) shows approx. 92% conversion after 20 h, but interestingly during the first 5 minutes only 3% conversion of **E** to the product (**F**) was seen. Under the same conditions full conversion into the hydroacylation product upon using **11c** as the catalyst was achieved in less than a minute. This slow catalysis and the induction period seen during the first 5 minutes corresponds well to the reversibility experiments carried out

above (GC-MS cross-over experiments) showing that the overall C-S reductive elimination from the dimeric species is slow. Initially most of the catalyst in the reaction mixture stays as the C-S activated dimer (**89**) (observed when following the catalysis by ESI-MS), thus showing the initial slow reaction rate, but over time more of **89** undergoes reductive elimination and the active catalyst concentration increases shown by faster catalysis. Comparison of this data to the data with **11c** indicates that if significant C-S activation to form **89** were to occur during the hydroacylation reaction, the hydroacylation process would be slowed down significantly, but also that the formation of the dimeric species **89** is reversible under the hydroacylation conditions.

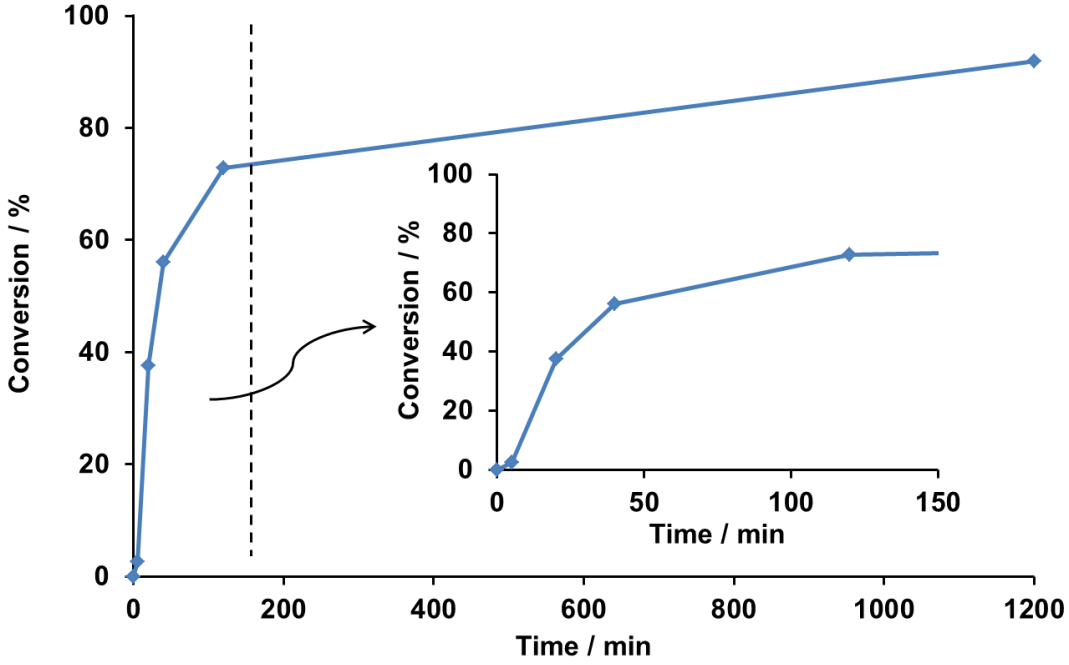

Figure 4.5. Hydroacylation reaction carried out using the dimer **89** as the catalyst. *Conditions: 10 mol% catalyst loading, 0.075 M **E**, 25 °C, acetone, **E**:1-octyne 1:1.5.*

4.2.4. Real-Time ESI-MS Experiments on C-S Activation *vs.* Hydroacylation

As previously observed (Chapter 2 and 3), real-time ESI-MS experiments, carried out in collaboration with the McIndoe group, were useful for investigating the fast hydroacylation reaction.[39] In light of this, an investigation was also conducted to probe the C-S activation reaction upon using **11c** as the catalyst. The strength of the real-time ESI-MS is its dynamic

range, as discussed previously, but also its ability to record a spectrum every second. This high density of data can be useful for investigating the fast rate of hydroacylation/C-S activation tandem reaction. As with the experiments carried out in Chapters 2 and 3, the reaction was conducted using the charged aldehyde (mod-**E**) and 1-octyne, with **11c** as the catalyst (Scheme 4.28).

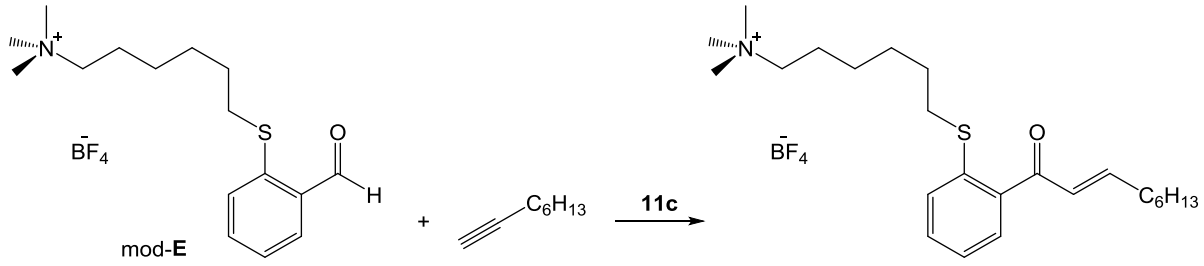

Scheme 4.28. Hydroacylation reaction carried out using mod-**E** and 1-octyne as the substrates and 11c as the catalyst. *Conditions: 10 mol% catalyst loading, acetone, 25 °C, 0.015 M aldehyde, mod-**E**:1-octyne ratio = 1:1.5.*

The hydroacylation reaction was followed and the hydroacylation products/intermediates seen are summarised in Section 2.3.2.5 but no peaks corresponding to the formation of C-S activated dimers were observed. The control reaction using **5** and **11b** (which had been shown to be inactive in C-S activation reactions) also led to no formation of the C-S activated dimers, as expected. As the C-S activated dimer (**89**) formation was readily seen upon reaction between **11c** and the neutral aldehyde **E**, it was speculated that the charged aldehyde (mod-**E**) could be the reason for this unexpected lack of C-S activation reactivity. If the C-S activated dimer (mod-**89**) did form, this would result in an overall +4 charged complex which we postulate would be less likely to form due to charge repulsion.

The collaboration between Weller and McIndoe groups has continued, and currently studies are being carried out in the McIndoe group to allow us to further understand the occurrence of C-S activation during the hydroacylation reaction in real time. So far, they have conducted reactions using the neutral aldehyde (**E**) and 1-octyne as the substrates and **11b** and **11c** as the catalysts to confirm the formation of the dimeric species only in the case of **11c**. Furthermore, they have been able to carry out experiments where during the reaction (using **11c**, **E** and 1-octyne) initially the product bound species, [Rh(^{i}Pr$_2$PCH$_2$P^{i}Pr$_2$)(κ^2-*O,S*-

$CO(C_6H_4SMeCH{=}CH(CH)_5Me)][BAr^F{}_4]$ (**25c**), is formed followed by the reduced relative concentration of **25c** and the formation of the C-S activated dimer **89**. Additionally, McIndoe group has developed a new set-up combining the real-time ESI-MS with real-time IR spectroscopy. This combination allows for the use of neutral substrates, as the cationic fragments can be followed by ESI-MS, while at the same time the neutral species (starting aldehyde **E** and product **F**) can be followed by IR (in particular the CO-fingerprint region is observed). Currently this is an ongoing project and the conditions yet to be optimised, so we are cautious about interpreting this data any further.

Upon combining the results gathered with the mechanism based on **11b** (Chapter 2), an overall mechanism involving C-S activation during hydroacylation is proposed (Scheme 4.29). Mixing the fluorobenzene complex with the general formula of $[Rh(R_2PXPR_2)(C_6H_5F)][BAr^F{}_4]$ with **E** and 1-octyne in acetone leads to the rhodium phosphine catalyst mediating the hydroacylation reaction. Based on NMR data and ongoing work at the McIndoe group using ESI-MS and IR techniques, the hydroacylation reaction is not affected by the C-S activation. The C-S activation reaction only becomes competitive after all the available aldehyde (*i.e.* **E**) is used up. The complexes **5** and **11b** are inactive as C-S activation catalysts and any remaining active catalyst in the reaction mixture stay as product-ligated complexes (*i.e.* **25b** and **86**, Scheme 4.17). In case of **6** and **11c**, the product bound species readily forms the C-S activated dimer (*i.e.* **82** and **89**, Scheme 4.17) which itself has been shown to be inactive in the C-S activation reactions[29, 32] but in acetone it has been reported to be in equilibrium with the C-S activated monomer (*e.g.* **97**), which in the presence of additives needed for the particular reaction, can lead to the formation of the C-S cleaved reduction or cross-coupling products discussed in Section 4.1.2. The formation of the C-S activated dimer was shown to be reversible, but hydroacylation catalysis data and the cross-over experiments demonstrated that the reversible step is slow.

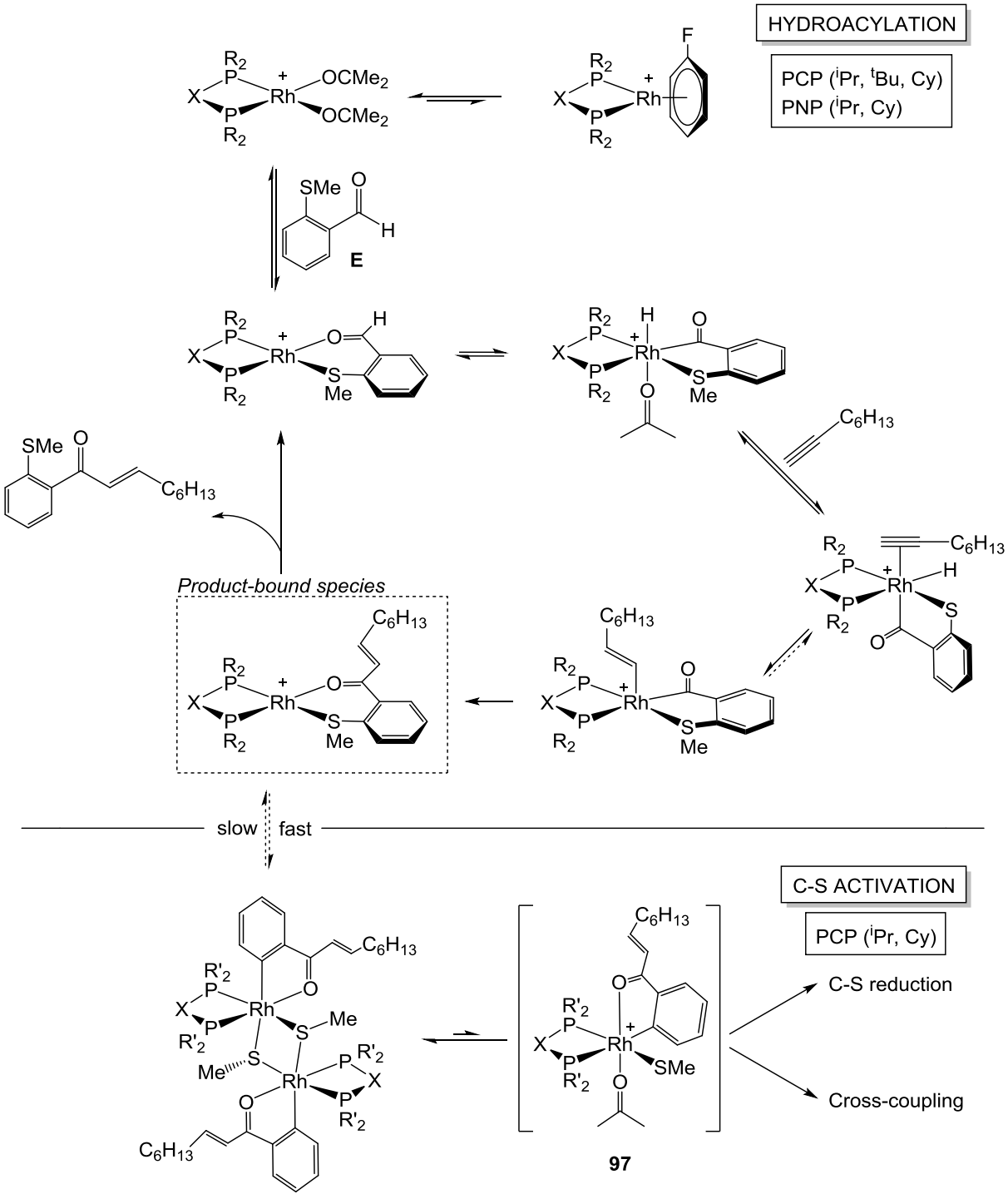

Scheme 4.29. Simplified hydroacylation mechanism based on the mechanism proposed for **11b** combined with the reversible C-S activation reaction that readily occurs, although C-S activation is not preferred as long as there is aldehyde left in the reaction mixture. X = CH_2 or NMe; R = ^{t}Bu, Cy or ^{i}Pr; R' = Cy or ^{i}Pr. The $[BAr^{F}_4]^-$ counter-anion is not pictured for clarity.

4.2.5. Summary

The C-S activation investigation showed that the use of similar small bite-angle catalysts (**5**, **6**, **11b** and **11c**) with slightly modified ligand structures led to substantially different reactivity.

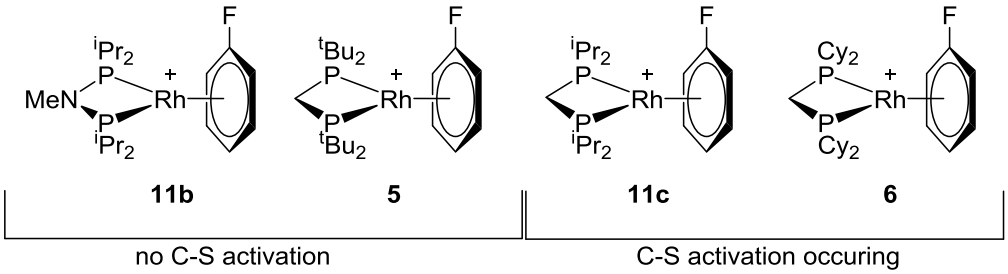

Figure 4.6. Comparison of similar small bite-angle catalysts. The $[BAr^F{}_4]^-$ counter-anion is not pictured for clarity.

Based on the data gathered it is not possible to state the reasons behind the different reactivity of these complexes, but clearly it must be due to fine balance between sterics and electronics, as the change of carbon to nitrogen in the backbone allowed for very different reactivity although for example the comparison of *bis*-CO complexes $[Rh(^iPr_2PXP^iPr_2)(CO)_2][BAr^F{}_4]$ (where X = CH_2 or NMe) showed very similar CO stretching frequencies. This could be a bite angle effect as Hofmann has commented that even small changes in the bite angle for small bite-angle complexes allow for different reactivity due to already strained metal centre.[40] Additionally changing the substituents on the phosphorus atoms of PCP ligand to tert-butyls result in complete deactivation of the catalyst which might indicate that the ligand flexibility has a role to play.

Upon using the complexes **6** and **11c**, that allow C-S activation, it was seen that the reaction with sulfur-tethered ketones (**J** or **F**) allow for immediate C-S activation observed as the formation of the C-S activated dimer whereas the overall reductive elimination from the dimeric species is slow. The previous work has shown that the formation of the dimer is not problematic for C-S activation reactions in acetone[32] and this work has demonstrated that the formation of the C-S activated dimer also does not affect the hydroacylation reaction in acetone, as the dimer is only formed upon the hydroacylation reaction has finished and if any C-S activated dimer is formed, the formation is reversible, thus not leading to catalyst deactivation.

4.3. Conclusions

Due to the catalyst deactivating side reaction accompanying the hydroacylation catalysis, reductive decarbonylation, research groups have been trying to find ways to modify the reaction to allow for more efficient hydroacylation and longer lived catalysts. As discussed in the Introduction Chapter, one of the most fruitful modifications is the use of tethered substrates. This additional coordination to the metal centre of the catalyst allows for faster initial reaction, but also, as it blocks one of the metal active sites, the effect of reductive decarbonylation is attenuated. The Weller and Willis groups have been using a sulfur moiety as this tether, and the use of this sulfur tether has allowed for highly active and selective hydroacylation catalysis.

Although the tether is useful for carrying out the hydroacylation reaction, it is not desirable in the products. Over the last few years, Weller and Willis have reported work on cleaving the C-S bond using small bite-angle *bis*-phosphine ligands on rhodium metal. As these ligands are also used for hydroacylation, an investigation was carried out to understand the effect of C-S activation during the hydroacylation reaction.

The results presented in this chapter show that the C-S activation is occurring rapidly upon adding the hydroacylation ketone product to the catalyst. At the same time, although present in the reaction mixture, when in competition with the hydroacylation reaction, hydroacylation is preferred. It was also shown that even if the dimerisation is occurring, it is reversible and does not deactivate the catalyst, but would slow it down.

Interestingly, it was observed that although some small bite-angle rhodium *bis*-phosphine catalysts (**6** and **11c**) allow for efficient C-S activation catalysis, other catalysts with similar motif (**5** and **11b**) resulted as essentially inactive C-S activation catalysts, which was seen to be due to the lack of C-S activation occurring upon using **5** or **11b**. This relative selectivity can be highly useful upon carrying out hydroacylation reaction where the sulfur containing tether is desired at the end of the reaction as **5** (active alkene hydroacylation catalyst) and **11b** (active alkyne hydroacylation catalyst) are inert towards the hydroacylation product.

4.4. References

1. S. K. Murphy, A. Bruch and V. M. Dong, *Angew. Chem. Int. Ed.*, 2014, **53**, 2455-2459.
2. M. von Delius, C. M. Le and V. M. Dong, *J. Am. Chem. Soc.*, 2012, **134**, 15022-15032.
3. M. M. Coulter, K. G. M. Kou, B. Galligan and V. M. Dong, *J. Am. Chem. Soc.*, 2010, **132**, 16330-16333.
4. J. W. Suggs, M. J. Wovkulich and S. D. Cox, *Organometallics*, 1985, **4**, 1101-1107.
5. J. Chul-Ho, H. Jong-Soo, K. Jung-Bu and K. Sun-Il, *J. Organomet. Chem.*, 1994, **474**, 183-189.
6. C. H. Jun, D. Y. Lee, H. Lee and J. B. Hong, *Angew. Chem. Int. Ed.*, 2000, **39**, 3070-3072.
7. H. D. Bendorf, C. M. Colella, E. C. Dixon, M. Marchetti, A. N. Matukonis, J. D. Musselman and T. A. Tiley, *Tetrahedron Lett.*, 2002, **43**, 7031-7034.
8. M. C. Willis, S. J. McNally and P. J. Beswick, *Angew. Chem. Int. Ed.*, 2004, **43**, 340-343.
9. G. L. Moxham, H. E. Randell-Sly, S. K. Brayshaw, R. L. Woodward, A. S. Weller and M. C. Willis, *Angew. Chem. Int. Ed.*, 2006, **45**, 7618-7622.
10. I. Pernik, J. F. Hooper, A. B. Chaplin, A. S. Weller and M. C. Willis, *ACS Catal.*, 2012, **2**, 2779-2786.
11. A. B. Chaplin, J. F. Hooper, A. S. Weller and M. C. Willis, *J. Am. Chem. Soc.*, 2012, **134**, 4885-4897.
12. M. C. Willis, *Chem. Rev.*, 2010, **110**, 725-748.
13. D. A. Colby, R. G. Bergman and J. A. Ellman, *Chem. Rev.*, 2009, **110**, 624-655.
14. Q.-A. Chen, D. K. Kim and V. M. Dong, *J. Am. Chem. Soc.*, 2014, **136**, 3772-3775.
15. D. Alberico, M. E. Scott and M. Lautens, *Chem. Rev.*, 2007, **107**, 174-238.
16. A. Cherkasov and M. Jonsson, *J. Chem. Inf. Comput. Sci.*, 2000, **40**, 1222-1226.
17. F. Pan and Z.-J. Shi, *ACS Catal.*, 2013, **4**, 280-288.
18. L. S. Liebeskind and J. Srogl, *J. Am. Chem. Soc.*, 2000, **122**, 11260-11261.
19. H. Yang, H. Li, R. Wittenberg, M. Egi, W. Huang and L. S. Liebeskind, *J. Am. Chem. Soc.*, 2007, **129**, 1132-1140.
20. J. M. Villalobos, J. Srogl and L. S. Liebeskind, *J. Am. Chem. Soc.*, 2007, **129**, 15734-15735.
21. Z. Zhang, M. G. Lindale and L. S. Liebeskind, *J. Am. Chem. Soc.*, 2011, **133**, 6403-6410.
22. K. Lee, C. M. Counceller and J. P. Stambuli, *Org. Lett.*, 2009, **11**, 1457-1459.
23. J. Torres-Nieto, A. Arévalo, P. García-Gutiérrez, A. Acosta-Ramírez and J. J. García, *Organometallics*, 2004, **23**, 4534-4536.
24. S. R. Dubbaka and P. Vogel, *Angew. Chem. Int. Ed.*, 2005, **44**, 7674-7684.
25. J. F. Hooper, A. B. Chaplin, C. González-Rodríguez, A. L. Thompson, A. S. Weller and M. C. Willis, *J. Am. Chem. Soc.*, 2012, **134**, 2906-2909.
26. C. M. Shafer and T. F. Molinski, *J. Org. Chem.*, 1998, **63**, 551-555.
27. I. Kawasaki, N. Sakaguchi, A. Khadeer, M. Yamashita and S. Ohta, *Tetrahedron*, 2006, **62**, 10182-10192.
28. N. Barbero and R. Martin, *Org. Lett.*, 2012, **14**, 796-799.
29. J. F. Hooper, R. D. Young, A. S. Weller and M. C. Willis, *Chem. Eur. J.*, 2013, **19**, 3125-3130.
30. H. F. T. Klare, M. Oestreich, J.-i. Ito, H. Nishiyama, Y. Ohki and K. Tatsumi, *J. Am. Chem. Soc.*, 2011, **133**, 3312-3315.
31. J. L. McBee, J. Escalada and T. D. Tilley, *J. Am. Chem. Soc.*, 2009, **131**, 12703-12713.
32. J. F. Hooper, R. D. Young, I. Pernik, A. S. Weller and M. C. Willis, *Chem. Sci.*, 2013, **4**, 1568-1572.
33. N. Miyaura, K. Yamada and A. Suzuki, *Tetrahedron Lett.*, 1979, **20**, 3437-3440.
34. N. Miyaura and A. Suzuki, *J. Chem. Soc., Chem. Commun.*, 1979, 866-867.
35. M. A. Huertos and A. S. Weller, *Chem. Sci.*, 2013, **4**, 1881-1888.
36. L. D. Quin and A. J. Williams, *Practical Interpretation of P-31 NMR Spectra and Computer Assisted Structure Verification, Advanced Chemistry Development, Inc. Toronto, Canada*, 2004.

37. P. Schollhammer, E. Guénin, F. Y. Pétillon, J. Talarmin, K. W. Muir and D. S. Yufit, *Organometallics*, 1998, **17**, 1922-1924.
38. A. T. Lubben, J. S. McIndoe and A. S. Weller, *Organometallics*, 2008, **27**, 3303-3306.
39. W. Henderson and J. S. McIndoe, *Mass Spectrometry of Inorganic and Organometallic Compounds: Tools - Techniques - Tips, Wiley.*, 2005.
40. P. Hofmann, C. Meier, U. Englert and M. U. Schmidt, *Chem. Ber.*, 1992, **125**, 353-365.

5. EXPERIMENTAL

5.1. General Considerations

All manipulations, unless otherwise stated, were performed under an atmosphere of argon, using standard Schlenk-line and glove-box techniques. Glassware was oven dried at 130 °C overnight and flamed under vacuum prior to use. Dichloromethane, tetrahydrofuran, acetonitrile, diethyl ether, pentane, hexane and toluene were dried over activated alumina, copper or molecular sieves as necessary using an MBraun solvent purification system (MBraun SPS-800) and degassed by successive freeze-pump-thaw cycles.[1] CD_2Cl_2 and C_6H_5F were distilled under vacuum from CaH_2 and stored over 3Å molecular sieves. Dry acetone (99.8%) was purchased from Acros and degassed by successive freeze-pump-thaw cycles.[2] Acetone-d_6 was dried over B_2O_6 and vacuum distilled twice.[3] Norbornadiene (nbd) was dried over sodium, vacuum distilled and stored over 3Å molecular sieves. 2-(methylthio)benzaldehyde was purchased from Sigma-Aldrich and purified by flash chromatography (5% Et_2O/petrol, matrix 60 silica) and distilled (145 °C, 13 mmHg) prior to use and was stored at –18 °C.[4] Microanalyses were performed by London Metropolitan University.

5.2. Nuclear Magnetic Resonance Spectroscopy

NMR spectra were recorded on Varian 500 (500 MHz), Varian 300 (300 MHz), Bruker AC-250 (250 MHz), Bruker DQX-400 (400 MHz) or Bruker AVC-500 (500 MHz) spectrometers at room temperature unless otherwise stated. Chemical shifts are given in δ (ppm), coupling constants (*J*)are given in Hz. ^{31}P NMR spectra were referenced against 85% H_3PO_4 (external). Residual protio solvent was used as reference for ^{1}H NMR spectra in deuterated solvent samples, while in C_6H_5F, ^{1}H NMR spectra were referenced to the centre of the solvent multiplet at δ 7.11.

5.3. Other Analytical Methods

Electrospray Ionization Mass Spectrometry (ESI-MS) experiments were carried out using a Bruker electrospray MicroTOF spectrometer directly connected to a modified Innovative Technologies glove box.[5] Prior to use, the spectrometer was calibrated in positive ion mode using a mixture of tetra(alkyl)ammonium bromide salts as the calibrant.

Electrospray Ionization Mass Spectrometry (ESI-MS) at the McIndoe lab were carried out under the given conditions: Capillary voltage: 2900 V. Cone voltage: 10 V. Extraction voltage: 0.5 V. Source temperature: 70 °C. Desolvation temperature: 150 °C. Cone gas flow: 100 L/h. Desolvation gas flow: 200 L/h. Collision voltage: 2 V (for MS experiments). Collision voltage: 15-25 V (for MS/MS experiments). During PSI experiments, overpressure in the flask was held at 3.5 psi (Ar) throughout the reaction. The reaction mixture was transferred to ESI-MS without further dilution through PEEK tubing (200 mm in length, i.d. 0.055 mm). About 3600 spectra were collected per hour of monitoring (1 s^{-1}).

Gas Chromatography-Mass Spectrometry (GC-MS) experimets were carried out using a set-up combining GC (Agilent Technologies 7890B) and MS (Agilent Technologies 7260). The mass was acquired using EI and CI methods. The measurements were carried out by mass-spectrometry service techicians.

High-Performance Liquid Chromatography (HPLC) experimets were performed using a reverse phase HPLC on a Agilent Zorbax SB-C18 5μm column (4.6 x 150mm), eluted in 85% MeCN/H_2O (under mildly acidic conditions), 1 mL/min. The samples of the reaction mixture (10 μL) were taken under argon and quenched by dilution with 1.5 mL of MeCN. Retention times: alkyne hydroacylation: t_1 (2-(methylthio)benzaldehyde, **E**) = 2.0 min, t_2 (linear 1-octyne product) = 5.0 min, t_3 (branched 1-octyne product) = 5.5 min. Alkene hydroacylation: t_1 (2-(methylthio)benzaldehyde, **E**) = 2.0 min, t_2 (1-hexene product) = 3.9 min, t_3 (1-octene product) = 6.3 min. The quenching with MeCN was tested by monitoring the conversion of an early sample from catalysis mixture diluted by MeCN over time and it remained unchanged, whereas the rest of the catalysis mixture (without MeCN) continued turning over.

Infrared Spectroscopy (IR) data were recorded on solid samples in Nujol mulls. The mulls were made up inside an inert-atmosphere glovebox and the KBr plates placed in an airtight sample holder prior to data collection. Spectra were recorded on a Thermo Scientific Nicolet iS5 FT-IR spectrometer in absorbance mode

5.4. X-ray Crystallography

The X-ray data were collected on an Enraf Nonius Kappa CCD diffractometer by myself or Dr. Adrian B. Chaplin using graphite monochromated Mo Kα radiation (λ = 0.71073 Å) and a low-temperature device [150(2) K][6] data were collected using COLLECT, reduction and cell refinement was performed using DENZO/SCALEPACK.[7] The structures were solved by direct methods using SIR92[8] or SIR2004[9] and refined full-matrix least squares on F^2 using SHELXL-97.[10] All non-hydrogen atoms were refined anisotropically. Hydrogen atoms were placed in calculated positions using the riding model.

5.5. Starting materials

The starting materials $Na[BAr^F_4]$,[11] $[Rh(nbd)Cl]_2$[12, 13] $[Rh(cod)Cl]_2$,[14] $[Rh(cod)_2][BAr^F_4]$[15] and $[Rh(nbd)_2][BAr^F_4]$[15] were prepared using published literature methods or variations thereof. All other reagents were used as received from Sigma-Aldrich, Acros, Fisher, Fluka or Strem Chemicals. Catalysts **5** and **6** were prepared following previously published procedures.[16] Starting aldehydes **E** and mod-**E**, and ketones **J**, **P**, **Q** and **R** were synthesised and purified by Willis group members. The hydroacylation product, **F**, was isolated and purified by column chromatography by Willis group members.

5.6. Synthetic Procedures

Chapter 2

1,1-dicyclohexyl-N-(dicyclohexylphosphino)-N-methylphosphinamine (**8a**) (based on the synthesis of ligand **8b**[17])

Under argon atmosphere, Cy_2PCl (0.47 mL, 2.15 mmol) was added drop-wise to a solution of $MeNH_2.HCl$ (0.064 g, 0.95 mmol) and Et_3N (0.42 mL, 3.04 mmol) in CH_2Cl_2 (5 mL). The resulting solution was stirred at room temperature for 16 hours. The obtained suspension was filtered through a short alumina column (CH_2Cl_2 as eluent) and washed with further 2 x 10 mL of CH_2Cl_2. The solvent was removed *in vacuo* and the ligand was obtained as white solid (0.200 g, 50%). The solid was stored at room temperature under argon atmosphere.

^{1}H NMR (300 MHz, CD_2Cl_2): δ 2.63 (t, ^3J(PH) 2.6 Hz, 3H, NMe), 1.94-1.61 (m, 24H, PCy), 1.25 (m, 20H, PCy).

^{31}P{^{1}H} NMR (121 MHz, CD_2Cl_2): δ 85.8 (s)

Microanalysis: Requires: C, 70.89; H, 11.18; N, 3.31. Found: C, 70.84; H, 11.32; N, 3.16.

N-(diisopropylphosphino)-1,1-diisopropyl-N-methylphosphinamine (**8b**) (modified synthetic route[17])

Under argon atmosphere, $^{i}Pr_2PCl$ (1.0 g, 6.55 mmol) was added drop-wise to a solution of $MeNH_2.HCl$ (0.196 g, 2.90 mmol) and Et_3N (1.29 mL, 9.28 mmol) in CH_2Cl_2 (20 mL). The resulting solution was stirred at room temperature for 16 hours. The obtained suspension was filtered through a short alumina column using CH_2Cl_2 as the eluent and washed with further 2 x 10 mL of CH_2Cl_2. The solvent was removed *in vacuo* and the ligand was obtained as colourless oil (0.456 g, 60%). The oil was stored under argon atmosphere at 0 °C. NMR data is consistent with the published data.[17]

^{1}H NMR (300 MHz, CD_2Cl_2): δ 2.66 (t, 3H, NMe), 1.96 (m, 4H, CH), 1.16-1.02 (m, 24H, CH_3).

$^{31}P\{^{1}H\}$ NMR (121 MHz, CD_2Cl_2): δ 92.06 (s).

Bis(diisopropylphosphino)methane (**8c**) (Modified synthetic route[18, 19])

Under argon atmosphere, a 2 M solution of $^{i}PrMgCl$ in THF (2.825 mL, 5.65 mmol) was added drop-wise at –78 °C to a solution of $H_2C(PCl_2)_2$ (0.30 g, 1.38 mmol) in THF (5 mL). The mixture was allowed to stir for 10 minutes and then reach the room temperature at which the mixture was allowed to stir for further 30 minutes. Then the mixture was heated to 50 °C and stirred for 3 hours. The solvent was removed *in vacuo*, and the obtained oil/solid was suspended in CH_2Cl_2. The mixture was run through a short alumina column (CH_2Cl_2 as eluent) and washed with further 2 x 10 mL of CH_2Cl_2. The solvent was removed *in vacuo* and the ligand was obtained as colourless oil (0.190 g, 56%). The oil was stored under argon atmosphere at 0 °C. NMR data is consistent with the published data.[18]

^{1}H NMR (300 MHz, CD_2Cl_2): δ 1.76 (m, 4H, CH), 1.37 (s, 2H, CH_2), 1.13-1.04 (m, 24H, CH_3).

$^{31}P\{^{1}H\}$ NMR (121 MHz, CD_2Cl_2): δ –2.29 (s)

1,2-bis(diisopropylphosphino)ethane (**8d**) (Modified synthetic route[20, 21])

Under argon atmosphere, a 2 M solution of ^{i}PrMgCl in THF (3.56 mL, 7.12 mmol) was added drop-wise at 0 °C to a solution of $(PCl_2)CH_2CH_2(PCl_2)$ (0.30 g, 1.29 mmol) in THF (10 mL). The mixture was allowed to stir for 10 minutes and then reach the room temperature at which the mixture was stirred for 16 hours. Degassed saturated ammonium chloride solution (20 mL) was added. The product was extracted using Et_2O (2 x 20 mL). To the combined solution of THF/Et_2O, Na_2SO_4 was added and the mixture was stirred for 30 minutes. The solvent was removed *in vacuo*, and the obtained oil/solid was suspended in CH_2Cl_2. The mixture was run through a short alumina column (CH_2Cl_2 as eluent) and washed with further 2 x 10 mL of CH_2Cl_2. The solvent was removed *in vacuo* and the ligand was obtained as colourless oil (0.228 g, 67%). The oil was stored under argon atmosphere at 0 °C. NMR data is consistent with the published data.

^{1}H NMR (300 MHz, CD_2Cl_2): δ 1.72 (m, 4H, CH), 1.47 (m, 4H, CH_2), 1.09-1.03 (m, 24H, CH_3).

^{31}P{^{1}H} NMR (121 MHz, CD_2Cl_2): δ 11.64 (s)

N-(diethylphosphino)-1,1-diethyl-N-methylphosphinamine (**8f**)

Under argon atmosphere, Et_2PCl (0.29 mL, 2.41 mmol) was added drop-wise to a solution of $MeNH_2$.HCl (0.079 g, 1.17 mmol) and Et_3N (0.52 mL, 3.76 mmol) in CH_2Cl_2 (5 mL). The resulting solution was stirred at room temperature for 16 hours. The obtained suspension was filtered through a short alumina column (CH_2Cl_2 as eluent) and washed with further 2 x 10 mL of CH_2Cl_2. The solvent was removed *in vacuo* and the ligand was obtained as white solid (0.153 g, 63%). The solid was stored at room temperature under argon atmosphere.

^{1}H NMR (300 MHz, CD_2Cl_2): δ 2.45 (t, 3H, NMe), 1.65 (m, 4H, CH), 1.02 (m, 12H, CH_3).

^{31}P{^{1}H} NMR (121 MHz, CD_2Cl_2): δ 68.5 (s)

[Rh{$Cy_2PN(CH_3)PCy_2$}(η^6-C_6H_5F)][BAr^F_4] (**11a**) (based on the synthesis of **11b**).

Under argon atmosphere, in a Schlenk flask **8a** (0.0716 g, 0.169 mmol) was dissolved in C_6H_5F (5 mL). In a Young's flask [$Rh(cod)_2$][BAr^F_4] (0.200 g, 0.169 mmol) was dissolved in C_6H_5F (1.5 mL). The solution from the Schlenk flask was slowly added to the solution in the Young's flask during which the colour changes from deep red to bright orange. The obtained solution was allowed to stir for 1 hour. The mixture was then set under hydrogen atmosphere (4 atm) and allowed to stir for 1.5 hours. Slight colour change from bright orange to pare orange was observed (decomposition is observed upon leaving the complex under hydrogen atmosphere for prolonged periods). The solvent was removed *in vacuo*. The obtained oily solid was washed and sonicated using hexane (10 mL). The obtained solid was recrystallized from fluorobenzene/hexane. The solid was filtered and then further washed and sonicated using hexane. The analytically pure yellow solid was dried *in vacuo* (180 mg, 74%). The compound was stored under inert atmosphere.

^{1}H NMR (500 MHz, C_6H_5F): δ 8.36 (s, 8H, Bar^F_4), 7.67 (s, 4H, Bar^F_4), 6.30 (t, 2H, η^6-C_6H_5F), 6.18 (dd, 2H, η^6-C_6H_5F), 5.63 (t, 1H, η^6-C_6H_5F), 2.31 (t, ^3J(PH) 9.8 Hz, 3H, NMe), 1,73 (m, 24H, PCy), 1,25-1.07 (m, 20H, PCy).

^{1}H NMR (300 MHz, CD_2Cl_2): δ 7.72 (s, 8H, Bar^F_4), 7.56 (s, 4H, Bar^F_4), 6.74 (t, 2H, η^6-C_6H_5F), 6.65 (m, 2H, η^6-C_6H_5F), 6.03 (tm, 1H, η^6-C_6H_5F), 2.58 (t, ^3J(PH) 9.8 Hz, 3H, NMe), 1,95-1.68 (m, 24H, PCy), 1,41-1.06 (m, 20H, PCy).

^{19}F NMR (300 MHz, CD_2Cl_2): δ –62.9 (s, 24F, BAr^F), –122.7 (s, 1F, η^6-C_6H_5F)

^{31}P{^{1}H} NMR (121 MHz, CD_2Cl_2): δ 73.5 [dd, *J*(RhP) 178 Hz, *J*(PF) 3.6 Hz]

^{31}P{^{1}H} NMR (202 MHz, C_6H_5F): δ 74.0 [d, *J*(RhP) 182 Hz]

ESI-MS (C_6H_5F, 60 °C, 4.5 kV): calc. for $[C_{31}H_{52}FNP_2Rh]^+$ 622.26, obs. m/z, 622.27. The observed isotopomer pattern (3 lines) is fully consistent with the molecular formula.

Microanalysis: Requires: C, 59.93; H, 4.34; N, 0.94. Found: C, 50.82; H, 4.37; N, 1.04.

Crystals suitable for X-ray diffraction were grown from a C_6H_5F solution of the complex layered with hexane at 0 °C.

[Rh{^{i}Pr$_2$PN(CH$_3$)P^{i}Pr$_2$}(η^6-C$_6$H$_5$F)][BAr$^F_4$] (11b)

Under argon atmosphere, a 0.09 M solution of **8b** (2.83 mL, 0.254 mmol) in C_6H_5F was added to a solution of [Rh(cod)$_2$][BAr$^F_4$] (0.300 g, 0.254 mmol) in C_6H_5F (1 mL). The obtained orange homogeneous solution was allowed to stir for 1 hour. The mixture was then set under hydrogen atmosphere (4 atm) and allowed to stir for 1.5 hours (decomposition is observed upon leaving the complex under hydrogen atmosphere for prolonged periods) during which the colour of the solution changes from orange to yellow. The solvent was removed *in vacuo*. The obtained oily solid was washed and sonicated using hexane (10 mL). The obtained solid was recrystallized from fluorobenzene/hexane. The solid was filtered and then further washed and sonicated using hexane. The analytically pure yellow solid was dried *in vacuo* (0.241 g, 72%)

^{1}H NMR (500 MHz, C$_6$H$_5$F): δ 8.35 (s, 8H, BAr$^F_4$), 7.65 (s, 4H, BAr$^F_4$), 6.22 (t, 2H, η^6-C$_6$H$_5$F), 6.10 (m, 2H, η^6-C$_6$H$_5$F), 5.49 (t, 1H, η^6-C$_6$H$_5$F), 2.19 (t, ^3J(PH) 9.7 Hz, 3H, NMe$_3$), 1.76 (m, 4H, CH), 0.91-0.81 (m, 24H, CH$_3$).

^{1}H NMR (300 MHz, CD$_2$Cl$_2$): δ 7.73 (s, 8H, BAr$^F_4$), 7.57 (s, 4H, BAr$^F_4$), 6.78 (m, 2H, η^6-C$_6$H$_5$F), 6.69 (m, 2H, η^6-C$_6$H$_5$F), 6.03 (t, 1H, η^6-C$_6$H$_5$F), 2.61 (t, ^3J(PH) 9.7 Hz, 3H, NMe$_3$), 2.17 (m, 4H, CH), 1.23-1.07 (m, 24H, CH$_3$).

^{19}F NMR (300 MHz, CD$_2$Cl$_2$): δ –62.9 (s, 24F, BAr^F), –122.3 (s, 1F, η^6-C$_6$H$_5$F)

^{31}P{^{1}H} NMR (121 MHz, CD$_2$Cl$_2$): δ 80.9 [dd, J(RhP) 178 Hz, J(PF) 3.8 Hz]

^{31}P{^{1}H} NMR (202 MHz, C$_6$H$_5$F): δ 82.44 [d, J(RhP) 183 Hz]

ESI-MS (C$_6$H$_5$F, 60 °C, 4.5 kV): calc. for $[C_{20}H_{39}FNP_2Rh]^+$ 462.13, obs. m/z, 462.13. The observed isotopomer pattern (3 lines) is fully consistent with the molecular formula.

Microanalysis: Requires: C, 46.21; H, 3.65; N, 1.06. Found: C, 46.64; H, 3.96; N, 1.02.

Crystals suitable for X-ray diffraction were grown from a C_6H_5F solution of the complex layered with hexane at 0 °C.

[Rh(*i*Pr$_2$PCH$_2$P*i*Pr$_2$)(η^6-C$_6$H$_5$F)][BAr$^F{}_4$] (11c)

Under argon atmosphere, a 0.06 M solution of **8c** (3.05 mL, 0.186 mmol) in C_6H_5F was added to a solution of [Rh(cod)$_2$][BAr$^F{}_4$] (0.200 g, 0.169 mmol) in C_6H_5F (1 mL). The obtained rusty-orange homogeneous solution was allowed to stir for 1 hour. The mixture was then set under hydrogen atmosphere (4 atm) and allowed to stir for 1 hour (decomposition is observed upon leaving the complex under hydrogen atmosphere for prolonged periods) during which the colour of the solution changes from rusty-orange to yellow. The solvent was removed *in vacuo*. The obtained oily solid was washed and sonicated using pentane (10 mL). The obtained solid was recrystallized from fluorobenzene/pentane. The solid was filtered and then further washed and sonicated using pentane. The analytically pure yellow solid was dried *in vacuo* (0.149 g, 67%).

^{1}H NMR (500 MHz, C$_6$H$_5$F): δ 8.35 (s, 8H, BAr$^F{}_4$), 7.66 (s, 4H, BAr$^F{}_4$), 6.21 (t, 2H, η^6-C$_6$H$_5$F), 6.07 (m, 2H, η^6-C$_6$H$_5$F), 5.49 (t, 1H, η^6-C$_6$H$_5$F), 2.17 (dt, ^2J(PH) 10.7 Hz, ^3J(RhH) 1.7 Hz, 2H, CH$_2$), 1.55 (m, 4H, CH), 0.88-0.80 (m, 24H, CH$_3$).

^{1}H NMR (300 MHz, CD$_2$Cl$_2$): δ 7.73 (s, 8H, BAr$^F{}_4$), 7.57 (s, 4H, BAr$^F{}_4$), 6.67 (t, 2H, η^6-C$_6$H$_5$F), 6.64 (m, 2H, η^6-C$_6$H$_5$F), 6.04 (tt, 1H, η^6-C$_6$H$_5$F), 2.63 (dt, ^2J(PH) 10.7 Hz, ^3J(RhH) 1.7 Hz, 2H, CH$_2$), 1.96 (m, 4H, CH), 1.17-1.07 (m, 24H, CH$_3$).

^{19}F NMR (300 MHz, CD$_2$Cl$_2$): δ –62.9 (s, 24F, BAr^F), –122.8 (s, 1F, η^6-C$_6$H$_5$F)

^{31}P{^{1}H} NMR (202 MHz, C$_6$H$_5$F): δ –2.1 [d, J(RhP) 175 Hz]

^{31}P{^{1}H} NMR (202 MHz, CH$_2$Cl$_2$): δ 0.7 [dd, J(RhP) 171 Hz, J(PF) 3.8 Hz]

ESI-MS (C$_6$H$_5$F, 60 °C, 4.5 kV): calc for [C$_{19}$H$_{35}$FP$_2$Rh]$^+$ 447.12, obs. m/z, 447.12. The observed isotopomer pattern (3 lines) is fully consistent with the molecular formula.

Microanalysis: Requires: C, 46.74; H, 3.61. Found: C, 46.98; H, 3.93.

Crystals suitable for X-ray diffraction were grown from a C_6H_5F solution of the complex layered with pentane at 0 °C.

[Rh{^{i}Pr$_2$P(CH$_2$)$_2$P^{i}Pr$_2$}(η^6-C$_6$H$_5$F)][BAr$^F{}_4$] (**11d**)

Under argon atmosphere, a 0.09M solution of **8d** (2.1 mL, 0.186 mmol) in C_6H_5F was added to a solution of [Rh(cod)$_2$][BAr$^F{}_4$] (0.200 g, 0.169 mmol) in C_6H_5F (1 mL). The obtained bright-orange homogeneous solution was allowed to stir for 1.5 hours. The mixture was then set under hydrogen atmosphere (4 atm) and allowed to stir for 2 hours (decomposition is observed upon leaving the complex under hydrogen atmosphere for prolonged periods) during which the color of the solution changes from bright-orange to yellow. The solvent was removed *in vacuo*. The obtained oily solid was washed and sonicated using hexane (10 mL). The obtained solid was recrystallized from fluorobenzene/hexane. The solid was filtered and then further washed and sonicated using hexane. The analytically pure yellow solid was dried *in vacuo* (0.180 g, 80%).

^{1}H NMR (500 MHz, C$_6$H$_5$F): δ 8.33 (s, 8H, BAr$^F{}_4$), 7.64 (s, 4H, BAr$^F{}_4$), 6.17 (t, 2H, η^6-C$_6$H$_5$F), 6.05 (m, 2H, η^6-C$_6$H$_5$F), 5.52 (t, 1H, η^6-C$_6$H$_5$F), 1.50 (m, 4H, CH), 1.13 (d, ^2J(PH) 13.5 Hz, 4H, CH$_2$CH$_2$), 0.80-0.68 (m, 24H, CH$_3$).

^{1}H NMR (300 MHz, CD$_2$Cl$_2$): δ 7.72 (s, 8H, BAr$^F{}_4$), 7.56 (s, 4H, BAr$^F{}_4$), 6.76 (m, 2H, η^6-C$_6$H$_5$F), 6.67 (m, 2H, η^6-C$_6$H$_5$F), 6.09 (tm, 1H, η^6-C$_6$H$_5$F), 1.99 (m, 4H, CH), 1.64 (dd, ^2J(PH) 13.4 Hz, 4H, CH$_2$CH$_2$), 1.17-0.99 (m, 24H, CH$_3$).

^{19}F NMR (300 MHz, CD$_2$Cl$_2$): δ –62.4 (s, 24F, BAr^F), –121.9 (s, 1F, η^6-C$_6$H$_5$F)

^{31}P{^{1}H} NMR (121 MHz, CD$_2$Cl$_2$): δ 107.5 [dd, *J*(RhP) 201 Hz, *J*(PF) 2.4 Hz]

^{31}P{^{1}H} NMR (202 MHz, C$_6$H$_5$F): δ 108.8 [d, *J*(RhP) 205 Hz]

ESI-MS (C_6H_5F, 60 °C, 4.5 kV): calc. for $[C_{20}H_{37}FP_2Rh]^+$ 461.14, obs. m/z, 461.14. The observed isotopomer pattern (3 lines) is fully consistent with the molecular formula.

Microanalysis: Requires: C, 47.15; H, 3.73. Found: C, 47.44; H, 3.86.

Crystals suitable for X-ray diffraction were grown from a C_6H_5F solution of the complex layered with hexane at 0 °C.

$[Rh\{^iPr_2P(CH_2)_3P^iPr_2\}(\eta^6\text{-}C_6H_5F)][BAr^F{}_4]$ (11e)

Under argon atmosphere, a 0.12 M solution of **8e** (1.37 mL, 0.169 mmol) in C_6H_5F was added to a solution of $[Rh(cod)_2][BAr^F{}_4]$ (0.200 g, 0.169 mmol) in C_6H_5F (1 mL). The obtained rusty-red homogeneous solution was allowed to stir for 1 hour. The mixture was then set under hydrogen atmosphere (4 atm) and allowed to stir for 2 hours (Decomposition is observed upon leaving the complex under hydrogen atmosphere for prolonged periods) during which the color of the solution changes from rusty-red to orange. The solvent is removed *in vacuo*. The obtained oily solid was washed and sonicated using hexane (10 mL). The obtained solid was recrystallized from fluorobenzene/hexane. The solid was filtered and then further washed and sonicated using hexane. The analytically pure peachy-orange solid was dried *in vacuo* (0.156 g, 69%).

^{1}H NMR (500 MHz, C_6H_5F): δ 8.34 (s, 8H, $BAr^F{}_4$), 7.64 (s, 4H, $BAr^F{}_4$), 6.13 (t, 2H, η^6-C_6H_5F), 6.06 (m, 2H, η^6-C_6H_5F), 5.66 (t, 1H, η^6-C_6H_5F), 1.37 (m, 4H, CH), 0.91-0.80 (m, 6H, $CH_2CH_2CH_2$), 0.91-0.73 (m, 24H, CH_3).

^{1}H NMR (300 MHz, CD_2Cl_2): δ 7.73 (s, 8H, $BAr^F{}_4$), 7.57 (s, 4H, $BAr^F{}_4$), 6.76-6.64 (m, 4H, η^6-C_6H_5F), 6.23 (tm, 1H, η^6-C_6H_5F), 1.83 (m, 6H, $CH_2CH_2CH_2$), 1.40-1.30 (m, 4H, CH), 1.23-1.05 (m, 24H, CH_3).

^{19}F NMR (300 MHz, CD_2Cl_2): δ –62.9 (s, 24F, BAr^F), –120.9 (s, 1F, η^6-C_6H_5F)

^{31}P{^{1}H} NMR (121 MHz, CD_2Cl_2): δ 46.7 [dd, *J*(RhP) 194 Hz, *J*(PF) 1.2 Hz]

^{31}P{^{1}H} NMR (202 MHz, C_6H_5F): δ 47.0 [d, *J*(RhP) 199 Hz]

ESI-MS (C_6H_5F, 60 °C, 4.5 kV): calc for $[C_{21}H_{39}FP_2Rh]^+$ 475.15, obs. m/z, 475.15. The observed isotopomer pattern (3 lines) is fully consistent with the molecular formula.

Microanalysis: Requires: C, 47.55; H, 3.84. Found: C, 47.83; H, 3.94.

Crystals suitable for X-ray diffraction were grown from a C_6H_5F solution of the complex layered with hexane at 0 °C.

[Rh(^{i}Pr$_2$P(X)P^{i}Pr$_2$)(CO)$_2$][BAr$^F_4$], X = NMe (**12b**), X = CH_2 (**12c**)

Under argon atmosphere a J. Youngs NMR tube was charged with 15 mg of [Rh(^{i}Pr$_2$P(X)P^{i}Pr$_2$)(C_6H_5F)][BAr$^F_4$]. To the solid 0.6 mL of C_6H_5F was added. CO gas was bubbled through the formed solution for 1 min resulting in a slight colour change from yellow to pale yellow (during which also the formation of colloidal rhodium was observed). The solution was filtered and the obtained yellow solution was layered with hexane resulting in the formation of crystalline material over 16 h. The solution was decanted and the product was obtained as yellow crystalline material.

Analytical data:

12b:

^{1}H NMR (400 MHz, CD_2Cl_2): δ 7.72 (s, 8H, BAr$^F_4$), 7.57 (s, 4H, BAr$^F_4$), 2.84 (t, NMe, 3H), 2.51 (br, 4H, CH), 1.40 (br, 12H, CH_3).

^{31}P{^{1}H} NMR (162 MHz, CD_2Cl_2): δ 78.8 [d, *J*(RhP) 107 Hz]

ESI-MS (C_6H_5F, 60 °C, 4.5 kV): calc. for $[C_{15}H_{31}NO_2P_2Rh]^+$ 422.09, obs. m/z, 422.09. The observed isotopomer pattern (3 lines) is fully consistent with the molecular formula.

IR (solid, selected data): υ (CO), 2100 and 2058 cm^{-1}

12c:

^{1}H NMR (400 MHz, CD_2Cl_2): δ 7.71 (s, 8H, BAr^F_4), 7.56 (s, 4H, BAr^F_4), 3.22 (t, NMe, 3H), 2.32 (br, 4H, CH), 1.30 (br, 12H, CH_3).

^{31}P{^{1}H} NMR (162 MHz, CD_2Cl_2): δ –15.2 [d, *J*(RhP) 101 Hz]

ESI-MS (C_6H_5F, 60 °C, 4.5 kV): calc. for $[C_{15}H_{30}O_2P_2Rh]^+$ 407.08, obs. m/z, 407.08. The observed isotopomer pattern (3 lines) is fully consistent with the molecular formula.

IR (solid, selected data): υ (CO), 2100 2102 and 2057 cm^{-1}

The complexes **16a – 16e** were formed by dissolving isolated complexes **11a - 11e** (10 mg) in acetone (0.6 mL). Equilibria between complexes **11a – 11e** and **16a – 16e** were observed.

NMR data:

$[Rh(Cy_2P(NMe)PCy_2)(OCMe_2)_2][BAr^F_4]$ (**16a**)

^{1}H NMR (300 MHz, acetone-d_6, selected data): δ 7.79 (s, 8H, Bar^F_4), 7.67 (s, 4H, Bar^F_4), 7.41 (m, 2H, free C_6H_5F), 7.23-7.08 (m, 2H, free C_6H_5F), 7.23-7.08 (m, 1H, free C_6H_5F), 2.78 (t, ^{3}J(PH) 10.1 Hz, 3H, NMe, **11a**), 2.68 (t, ^{3}J(PH) 9.3 Hz, 3H, NMe, **16a**) 2.27-1.60 (m, 24H, PCy), 1,36 (m, 20H, PCy)

^{19}F NMR (300 MHz, acetone-d_6): δ –63.3 (s, 24F, BAr^F), –114.8 (m, 1F, free C_6H_5F)

^{31}P{^{1}H} NMR (121 MHz, acetone-d_6): δ 79.2 [d, *J*(RhP) 179 Hz, **10b**], 73.9 [dd, *J*(RhP) 178 Hz, *J*(PF) 3.4 Hz, **10a**] **11a:16a** 13:87.

[Rh(^{i}Pr$_2$P(NMe)P^{i}Pr$_2$)(OCMe$_2$)$_2$][BAr$^F_4$] (**16b**)

^{1}H NMR (300 MHz, acetone-d$_6$, selected data): δ 7.79 (s, 8H, Bar$^F_4$), 7.67 (s, 4H, Bar$^F_4$), 7.41 (q, 2H, free C_6H_5F), 7.22-7.09 (m, 2H, free C_6H_5F), 7.22-7.09 (m, 1H, free C_6H_5F), 2.70 (t, ^3J(PH) 9.5 Hz, 3H, NMe), 2.28 (m, 4H, CH), 1,27 (m, 12H, CH_3), 1.19 (m, 12H, CH_3).

^{19}F NMR (300 MHz, acetone-d$_6$): δ –63.3 (s, 24F, BAr^F), –114.8 (m, 1F, free C_6H_5F)

^{31}P{^{1}H} NMR (121 MHz, acetone-d$_6$): δ 86.5 [d, *J*(RhP) 181 Hz, **16b**], 81.2 [d, *J*(RhP) 181 Hz, **11b**]. **11b:16b** 25:75.

[Rh(^{i}Pr$_2$PCH$_2$P^{i}Pr$_2$)(OCMe$_2$)$_2$][BAr$^F_4$] (**16c**)

^{1}H NMR (300 MHz, acetone-d$_6$, selected data): δ 7.79 (s, 8H, Bar$^F_4$), 7.68 (s, 4H, Bar$^F_4$), 7.41 (q, 2H, free C_6H_5F), 7.22-7.09 (m, 2H, free C_6H_5F), 7.22-7.09 (m, 1H, free C_6H_5F), 2.71 (dt, ^2J(PH) 10.3 Hz, ^3J(RhH) 2.2 Hz, 3H, CH_2 of **11c**) 2.71 (dt, ^2J(PH) 10.3 Hz, ^3J(RhH) 2.7 Hz, 3H, CH_2 of **16c**), 2.13 (m, 4H, CH), 1,40-1.15 (m, 24H, CH_3)

^{19}F NMR (300 MHz, acetone-d$_6$): δ –63.3 (s, 24F, BAr^F), –114.8 (m, 1F, free C_6H_5F)

^{31}P{^{1}H} NMR (121 MHz, acetone-d$_6$): δ 5.3 [d, *J*(RhP) 170 Hz, **16c**], 0.7 [dd, *J*(RhP) 171 Hz, *J*(PF) 4 Hz, **11c**]. **11c:16c** 24:76.

[Rh(^{i}Pr$_2$CH$_2$CH$_2$^{i}Pr$_2$)(OCMe$_2$)$_2$][BAr$^F_4$] (**16d**)

^{1}H NMR (300 MHz, acetone-d$_6$): δ 7.79 (s, 8H, Bar$^F_4$), 7.67 (s, 4H, Bar$^F_4$), 7.40 (q, 2H, free C_6H_5F), 7.24-7.06 (m, 2H, free C_6H_5F), 7.24-7.06 (m, 1H, free C_6H_5F), 2.04 (m, 4H, CH), 1.62 (dd, ^2J(PH) 12.0 Hz, ^3J(RhH) 1.4 Hz, 4H, CH_2), 1,40-1.15 (m, 24H, CH_3)

^{19}F NMR (300 MHz, acetone-d$_6$): δ –63.3 (s, 24F, BAr^F), –114.8 (m, 1F, free C_6H_5F)

^{31}P{^{1}H} NMR (121 MHz, acetone-d$_6$): δ 105.1 [d, *J*(RhP) 203 Hz]

[Rh(^{i}Pr$_2$PCH$_2$CH$_2$CH$_2$P^{i}Pr$_2$)(OCMe$_2$)$_2$][BAr$^F_4$] (**16e**)

^{1}H NMR (300 MHz, acetone-d$_6$): δ 7.78 (s, 8H, Bar$^F_4$), 7.67 (s, 4H, Bar$^F_4$), 7.41 (q, 2H, free C_6H_5F), 7.24-7.08 (m, 2H, free C_6H_5F), 7.24-7.08 (m, 1H, free C_6H_5F), 1.94 (m, 6H, CH_2), 1.44 (m, 4H, CH), 1,39-1.19 (m, 24H, CH_3)

^{19}F NMR (300 MHz, acetone-d$_6$): δ –63.3 (s, 24F, BAr^F), –114.8 (m, 1F, free C_6H_5F)

^{31}P{^{1}H} NMR (121 MHz, acetone-d$_6$): δ 51.9 [d, *J*(RhP) 193 Hz]

[Rh(R$_2$PXPR$_2$)(CO)(SMePh)][BAr$^F_4$] (**17a – 17e**)

In a J. Youngs NMR tube to a solution of **11a – 11e** (10mg) in acetone-d$_6$ (0.4 mL) 1.1eq of 2-(methylthio)benzaldehyde (**E**) was added. Immediately the yellow homogeneous solution turns brown, over time the color changes back to yellow. The reaction was followed by ^{1}H and ^{31}P{1H} NMR spectroscopy. During the reaction, a mixture of products is formed, including compounds with hydride signals. Over 10 min the reaction results in decarbonylated products on rhodium complexes and other unidentified decomposition products.

Analytical data:

[Rh(Cy$_2$P(NMe)PCy$_2$)(CO)(SMePh)][BAr$^F_4$] (**17a**)

^{1}H NMR (300 MHz, acetone-d$_6$): Due to the formation of side products, it was not possible to obtain definitive ^{1}H NMR spectrum of this mixture.

^{31}P{^{1}H} NMR (121 MHz, acetone-d$_6$): A range of species (currently uncharacterized) δ 85 to 58.

[Rh(^{i}Pr$_2$P(NMe)P^{i}Pr$_2$)(CO)(SMePh)][BAr$^{F}_4$] (17b)

^{1}H NMR (500 MHz, acetone-d$_6$, selected data): Due to the formation of side products, it was not possible to obtain definitive ^{1}H NMR spectrum of this mixture.

^{31}P{^{1}H} NMR (202 MHz, acetone-d$_6$): δ 93.4 [dd, *J*(RhP) 112 Hz, *J*(PP) 59 Hz, P$_A$], 69.3 [dd, *J*(RhP) 113 Hz, *J*(PP) 58 Hz, P$_B$]

The ^{31}P{^{1}H} NMR spectrum (202 MHz, acetone-d$_6$) shows other compounds formed at: δ 88.1 [dd, *J*(RhP) 63 Hz, *J*(PP) 29 Hz] and 70.5 [d *J*(RhP) 108 Hz – assigned as [Rh(^{i}Pr$_2$P(NMe)P^{i}Pr$_2$)(CO)$_2$][BAr$^{F}_4$]]

ESI-MS (C$_6$H$_5$F, 60 °C, 4.5 kV): calc for [C$_{21}$H$_{39}$NOP$_2$RhS]$^+$ 518.12, obs. m/z, 518.12. The observed isotopomer pattern (4 lines) is fully consistent with the molecular formula. A low intensity peak at m/z, 422.09 (corresponding to [Rh(^{i}Pr$_2$P(NMe)P^{i}Pr$_2$)(CO)$_2$][BAr$^{F}_4$], calc: 422.09). The observed isotopomer pattern (3 lines) is fully consistent with the molecular formula.

A small number of crystals suitable for X-ray diffraction were grown overnight from a CH_2Cl_2 solution of the complex layered with pentane at 0 °C.

NMR data of the crystals grown, washed with hexane and dissolved in CD_2Cl_2:

^{1}H NMR (500 MHz, CD_2Cl_2, selected data): δ 7.72 (s, 8H, BAr$^{F}_4$), 7.56 (s, 4H, BAr$^{F}_4$), 7.37-7.03 (m, 5H, SPh), 3.03 (br, 3H, SMe), 2.71 (t, 3H, NMe), 2.28 (dm, 4H, CH), 1.34 (dq, *J* 7.15, *J*(PH) 12.7 Hz, 12H, ^{i}PrP$_A$), 1.13 (dq, *J* 7.15, *J*(PH) 16.4 Hz, 12H, ^{i}PrP$_B$).

^{31}P{^{1}H} NMR (202 MHz, CD_2Cl_2): δ 91.4 [dd, *J*(RhP) 125 Hz, *J*(PP) 59 Hz, P$_A$], 69.5 [dd, *J*(RhP) 114 Hz, *J*(PP) 59 Hz, P$_B$]

[Rh(^{i}Pr$_2$PCH$_2$P^{i}Pr$_2$)(CO)(SMePh)][BAr$^{F}_4$] (**17c**)

^{1}H NMR (500 MHz, acetone-d$_6$): Due to the formation of side products, it was not possible to obtain definitive ^{1}H NMR spectrum of this mixture.

^{31}P{^{1}H} NMR (202 MHz, acetone-d$_6$): mixture of compounds: δ 17.3 [dd, *J*(RhP) 107 Hz, *J*(PP) 29 Hz], 1.3 [dd, *J*(RhP) 63 Hz, *J*(PP) 29 Hz], δ 2.0 [br], δ –4.4 [dd, *J*(RhP) 94 Hz, *J*(PP) 58 Hz] (See NMR Appendix)

^{31}P{^{1}H} NMR (202 MHz, CD$_2$Cl$_2$): mixture of compounds: δ 17.0 [dd, *J*(RhP) 107 Hz, *J*(PP) 28 Hz], 3.6 [br], δ 0.7 [ddd, *J*(RhP) 62 Hz, *J*(PP) 27 Hz, J(PH) 9 Hz], δ –4.9 [br].

ESI-MS (C$_6$H$_5$F, 60 °C, 4.5 kV): calc for $[C_{21}H_{38}OP_2RhS]^+$ 503.11 obs. m/z, 503.11. The observed isotopomer pattern (4 lines) is fully consistent with the molecular formula.

[Rh(^{i}Pr$_2$PCH$_2$CH$_2$P^{i}Pr$_2$)(CO)(SMePh)][BAr$^{F}_4$] (**17d**)

^{1}H NMR (500 MHz, acetone-d$_6$): δ 7.72 (s, 8H, BAr$^{F}_4$), 7.56 (s, 4H, BAr$^{F}_4$), 7.49-7.47 (m, 4H, Ph), 2.93 (dt, 3H, SMe), 2.33-2.0 (m, 4H, CH$_2$), 2.05-1.79 (m, 4H, CH), 1.34-1.00 (m, 24H, CH$_3$).

^{31}P{^{1}H} NMR (202 MHz, acetone-d$_6$): δ 103.3 [dd, *J*(RhP) 141 Hz, *J*(PP) 20 Hz, P$_A$], δ 80.4 [dd, *J*(RhP) 126 Hz , *J*(PP) 20 Hz, P$_B$]

The ^{31}P{^{1}H} NMR spectrum (202 MHz, acetone-d$_6$) shows a small impurity (less than 10%): δ 95.5 [d, *J*(RhP) 121 Hz] – assigned as [Rh(^{i}Pr$_2$PCH$_2$CH$_2$P^{i}Pr$_2$)(CO)$_2$][BAr$^{F}_4$] (See NMR appendix)

^{31}P{^{1}H} NMR (121 MHz, CD$_2$Cl$_2$): δ 101.9 [dd, *J*(RhP) 142 Hz, *J*(PP) 22 Hz, P$_A$], δ 79.5 [dd, *J*(RhP) 126 Hz, *J*(PP) 22 Hz, P$_B$]

The ^{31}P{^{1}H} NMR spectrum (202 MHz, CD$_2$Cl$_2$) shows a small impurity (less than 10%): δ 95.5 [d, *J*(RhP) 121 Hz] – assigned as [Rh(^{i}Pr$_2$PCH$_2$CH$_2$P^{i}Pr$_2$)(CO)$_2$][BAr$^{F}_4$]

ESI-MS (C$_6$H$_5$F, 60 °C, 4.5 kV): calc for $[C_{22}H_{40}OP_2RhS]^+$ 517.13 obs. m/z, 517.13. The observed isotopomer pattern (4 lines) is fully consistent with the molecular formula.

A low intensity peak at m/z, 421.09 (corresponding to [Rh(^{i}Pr$_2$PCH$_2$CH$_2$P^{i}Pr$_2$)(CO)$_2$][BAr$^F_4$], calc: 421.09). The observed isotopomer pattern (2 lines) is fully consistent with the molecular formula.

[Rh(^{i}Pr$_2$PCH$_2$CH$_2$CH$_2$P^{i}Pr$_2$)(CO)(SMePh)][BAr$^F_4$] (**17e**)

^{1}H NMR (500 MHz, acetone-d$_6$, selected data): δ 7.79 (s, 8H, BAr$^F_4$), 7.68 (s, 4H, BAr$^F_4$), 7.69-7.10 (m, 4H, Ph), 3.13 (dt, 3H, SMe), 2.60-2.20 (m, 6H, CH$_2$), 2.10-1.75 (m, 4H, CH), 1.44-1.23 (m, 24H, CH$_3$).

^{1}H NMR (500 MHz, CD$_2$Cl$_2$, selected data): δ 7.72 (s, 8H, BAr$^F_4$), 7.56 (s, 4H, BAr$^F_4$), 7.51-7.48 (m, 5H, Ph), 2.90 (dt, 3H, SMe), 2.30-2.04 (m, 6H, CH$_2$), 1.74-1.54 (m, 4H, CH), 1.20 (m, 24H, CH$_3$).

^{31}P{^{1}H} NMR (202 MHz, acetone-d$_6$): δ 43.5 [br.d, *J*(RhP) 146 Hz, P$_A$], δ 16.9 [br.d, *J*(RhP) 125 Hz , P$_B$]

^{31}P{^{1}H} NMR (202 MHz, CD$_2$Cl$_2$): δ 43.4 [dd, *J*(RhP) 141 Hz, *J*(PP) 44 Hz, P$_A$], δ 17.0 [dd, *J*(RhP) 121 Hz, *J*(PP) 44 Hz, P$_B$]

The ^{31}P{^{1}H} NMR spectra show a small impurity (30%): δ 27.9 [d, *J*(RhP) 117 Hz] – assigned as [Rh(^{i}Pr$_2$PCH$_2$CH$_2$CH$_2$P^{i}Pr$_2$)(CO)$_2$][BAr$^F_4$]

ESI-MS (C$_6$H$_5$F, 60 °C, 4.5 kV): ESI-MS: calc for [C$_{23}$H$_{42}$OP$_2$RhS]$^+$ 531.15 obs. m/z, 531.15. The observed isotopomer pattern (4 lines) is fully consistent with the molecular formula.

A low intensity peak is observed at m/z, 435.11 (corresponding to [Rh(^{i}Pr$_2$PCH$_2$CH$_2$CH$_2$P^{i}Pr$_2$)(CO)$_2$][BAr$^F_4$], calc: 435.10). The observed isotopomer pattern (2 lines) is fully consistent with the molecular formula.

[Rh(R_2PXPR_2)H{$\kappa^2_{(S,C)}$-SMe(C_6H_4CO)}($OCMe_2$)][BAr^F_4] (**18a – 18e**)

In a Youngs NMR tube 1.1eq of 2-(methylthio)benzaldehyde (**E**) was added to a frozen mixture of precatalyst (**11a – 11e**) in acetone-d_6. The mixture was allowed to reach room temperature and then the NMR tube was inverted a number of times to ensure to formation of homogeneous solution. Immediately a colour change from yellow to dark yellow was observed. Within a minute from mixing the NMR tube was placed into a pre-cooled NMR spectrometer (–60 °C). Immediately ^{1}H and ^{31}P{^{1}H} NMR spectra were acquired, followed by a ^{31}P{^{1}H} NMR spectrum 30 min later. Based on the integrations of the ^{1}H and ^{1}H{^{31}P} NMR spectra we can determine that the reaction does not proceed at –60 °C. Upon warming the reaction continues reductive decarbonylation to form **17a – 17e** (respectively), with other unidentified decomposition products.

[Rh($Cy_2P(NMe)PCy_2$)H{$\kappa^2_{(S,C)}$-SMe(C_6H_4CO)}($OCMe_2$)][BAr^F_4] (**18a**)

^{1}H NMR (300 MHz, acetone-d_6, –60 °C, selected data): δ 7.84 (s, 8H, Bar^F_4), 7.75 (s, 4H, Bar^F_4), 2.92 (t, ^4J(PH) 7.5 Hz, 3H, NMe), 2.72 (d, ^4J(PH) 4.3 Hz, 3H, SMe), –20.14 (ddd, 1H, J(RhH) 29.8 Hz, J(PH) 13.0 Hz, J(PH) 10.5 Hz, RhH)*

^{1}H{^{31}P} NMR (300 MHz, acetone-d_6, –60 °C, selected data): δ –19.91 (d, 1H, J(RhH) 32.1 Hz, RhH_A), –20.14 (d, 1H, J(RhH) 29.8 Hz, RhH_B).*

^{31}P{^{1}H} NMR (121 MHz, acetone-d_6, –60 °C): δ –118.1 (ddd, J(RhP) 134.1 Hz, J(PP) 34.1 Hz, J(PH) 13.0 Hz, P_B), 107.7 (ddd, J(RhP) 63.1 Hz, J(PP) 34.1 Hz, J(PH) 10.5 Hz, P_A).

* - Based on ^{1}H{^{31}P} NMR spectra, two hydride environments are observed, which are assigned to the isomers formed by the relative orientation of the SMe group. Ratio: 28:72 RhH_A:RhH_B. The smaller hydride peak cannot be seen in ^{1}H NMR spectra, as the peaks overlap when coupling to ^{31}P.

[Rh(^{i}Pr$_2$P(NMe)P^{i}Pr$_2$)H{κ^2$_{(S,C)}$-SMe(C$_6$H$_4$CO)}(OCMe$_2$)][BAr$^F_4$] (18b)

^{1}H NMR (300 MHz, acetone-d$_6$, –60 °C, selected data): δ 7.84 (s, 8H, Bar$^F_4$), 7.75 (s, 4H, Bar$^F_4$), 2.93 (t, ^{4}*J*(PH) 7.6 Hz, 3H, NMe), 2.72 (d, ^{4}*J*(PH) 4.3 Hz, 3H, SMe), –20.09 (ddd, 1H, ^{1}*J*(RhH) 29.5 Hz, ^{2}*J*(PH) 12.5 Hz, ^{2}*J*(PH) 9.7 Hz, RhH)*

^{1}H{^{31}P} NMR (300 MHz, acetone-d$_6$, –60 °C, selected data): δ –19.89 (d, *J*(RhH) 29.5 Hz, 1H, RhH$_A$), –20.09 (d, 1H, *J*(RhH) 29.5 Hz, RhH$_B$).*

^{31}P{^{1}H} NMR (121 MHz, acetone-d$_6$, –60 °C): δ 92.2 (ddd, *J*(RhP) 132.9 Hz, *J*(PP) 36.4 Hz, *J*(PH) 12.5 Hz, P$_B$), 83.5 (ddd, *J*(RhP) 63.1 Hz, *J*(PP) 36.4 Hz, *J*(PH) 9.0 Hz, P$_A$).

* - Based on ^{1}H{^{31}P} NMR spectra, two hydride environments are observed, which are assigned to the isomers formed by the relative orientation of the SMe group. Ratio: 13:87 RhH$_A$:RhH$_B$. The smaller hydride peak cannot be seen in ^{1}H NMR spectra, as the peaks overlap when coupling to ^{31}P.

[Rh(^{i}Pr$_2$PCH$_2$P^{i}Pr$_2$)H{κ^2$_{(S,C)}$-SMe(C$_6$H$_4$CO)}(OCMe$_2$)][BAr$^F_4$] (18c)

^{1}H NMR (300 MHz, acetone-d$_6$, –60 °C, selected data): δ 7.84 (s, 8H, Bar$^F_4$), 7.75 (s, 4H, Bar$^F_4$), 2.72 (d, ^{4}*J*(PH) 4.1 Hz, 3H, SMe), –19.87 (ddd, 1H, *J*(RhH) 30.0 Hz, *J*(PH) 9.5 Hz, *J*(PH) 9.5 Hz, RhH)*

^{1}H{^{31}P} NMR (300 MHz, acetone-d$_6$, –60 °C, selected data): δ –19.58 (d, 1H, *J*(RhH) 32.0 Hz, RhH$_A$), –19.87 (d, 1H, *J*(RhH) 30.0 Hz, RhH$_B$).*

^{31}P{^{1}H} NMR (121 MHz, acetone-d$_6$, –60 °C): δ –8.7 (ddd, *J*(RhP) 130.0 Hz, *J*(PP) 38.1 Hz, *J*(PH) 9.5 Hz, P$_B$), –37.5 (ddd, *J*(RhP) 59.0 Hz, *J*(PP) 38.1 Hz, *J*(PH) 9.0 Hz, P$_A$).

* - Based on ^{1}H{^{31}P} NMR spectra, two hydride environments are observed, which are assigned to the isomers formed by the relative orientation of the SMe group. Ratio: 17:83 RhH$_A$:RhH$_B$. The smaller hydride peak cannot be seen in ^{1}H NMR spectra, as the peaks overlap when coupling to ^{31}P.

[Rh(^{i}Pr$_2$PCH$_2$CH$_2$P^{i}Pr$_2$)H{κ^2$_{(S,C)}$-SMe(C$_6$H$_4$CO)}(OCMe$_2$)][BAr^F$_4$] (**18d**)

^{1}H NMR (300 MHz, acetone-d$_6$, –60 °C, selected data): Multiple species, including hydride signals at: δ –7.25 (ddd, *J*(trans-PH) 161.5 Hz, *J*(RhH) 21.5 Hz, *J*(cis-PH) 5.5 Hz, RhH), –22.1 (br m, RhH) and –22.4 (br m, RhH)

^{31}P{^{1}H} NMR (121 MHz, acetone-d$_6$, –60 °C): A range of species (currently uncharacterized) δ 108 to 46.

[Rh(^{i}Pr$_2$PCH$_2$CH$_2$CH$_2$P^{i}Pr$_2$)H{κ^2$_{(S,C)}$-SMe(C$_6$H$_4$CO)}(OCMe$_2$)][BAr^F$_4$] (**18e**)

^{1}H NMR (300 MHz, acetone-d$_6$, –60 °C, selected data): Multiple species, including hydride signals at: δ –7.9 (m) and -8.5 (m) – most likely hydride signals for species with the hydride *trans* to a phosphorous.

^{31}P{^{1}H} NMR (121 MHz, acetone-d$_6$, –60 °C): A range of species (currently uncharacterized) δ 55 to 0.

[Rh(^{i}Pr$_2$P(NMe)P^{i}Pr$_2$)Cl{κ^2$_{(S,C)}$-SMe(C$_6$H$_4$CO)}(OCMe$_2$)][BAr^F$_4$] (**21b**)

Under argon atmosphere a Schlenk flask was charged with **11b** (100 mg, 0.075 mmol) and 2-(methylthio)benzoyl chloride (Cl-**E**) (35.2 mg, 0.189 mmol). The solids were dissolved in acetone (5 mL), resulting in a pale yellow solution. The solvent was removed in vacuo, and hexane (15 mL) was added followed by sonication. The supernatant was filtered of and the product was obtained as a yellow solid from CH_2Cl_2/hexane solution. The obtained solid was further washed/sonicated with 2 x 5 mL of hexane. The product was isolated as microcrystalline solid (67 mg, 63%). The compound was stored under inert atmosphere.

^{1}H NMR (300 MHz, CD$_2$Cl$_2$): δ 7.79 [d, *J*(HH) = 7.8 Hz, 1H, Aryl-H], 7.79 [d, J(HH) = 9.2 Hz, 2H, Aryl-H], 7.74-7.71 (m, 1H + 8H, Aryl-H and BAr^F$_4$), 7.56 (s, 4H, BAr^F$_4$), 7.50 (m, 2H, free-C_6H_5F), 7.32 (m, 3H, free-C_6H_5F), 3.2 [m, 1H, C*H*$(CH_3)_2$], 3.03 (m, 3H, SMe), 2.86 [m, 2H, C*H*$(CH_3)_2$], 2.59

[m, 1H, C*H*(CH_3)$_2$], 2.4 (s, 3H, NMe), 1.6 (m, 3H, CH_3), 1.44 (m, 3H, CH_3), 1.03 (m, 3H, CH_3), 0.87 (m, 3H, CH_3).

^{31}P{^{1}H} NMR (121 MHz, CD_2Cl_2): δ 73.2 [dd, *J*(RhP) 120 Hz, *J*(PP) 36 Hz], 69.8 [dd, *J*(RhP) 120 Hz, *J*(PP) 36 Hz]

ESI-MS (C_6H_5F, 60 °C, 4.5 kV): calc. for $[C_{31}H_{52}FNP_2Rh]^+$ 552.09, obs. m/z, 552.08. The observed isotopomer pattern (5 lines) is fully consistent with the molecular formula.

Crystals suitable for X-ray diffraction were grown from a C_6H_5F solution of the complex layered with hexane at 0 °C.

[(PR_2H)$_2BH_2$]Br, R = ^{t}Bu (**27**-^{t}Bu-Br), Cy (**27**-Cy-Br), Ph (**27**-Ph-Br).

In a typical experiment, HPR_2 (2 eq., 0.6 mmol) was added to CH_2Cl_2 (5 mL) in a Schlenk flask. To this, a CH_2Cl_2 solution (1 M) of BrH2B·SMe2 (1 eq., 0.3 mL, 0.3 mmol) was added drop-wise and the reaction was stirred for 48 h. Removal of the solvent in vacuo yielded a colourless oil. Addition of hexane (3 mL) to the oil, and sonication, resulted in the precipitation of the product as a white solid, which was filtered and washed with hexane (2 x 3 mL) and then dried in vacuo, resulting in a white solid which was stored under argon in a glove box. Yield: **27**-^{t}Bu-Br (81 mg, 70%), **27**-Cy-Br (102 mg, 69%), **27**-Ph-Br (100 mg, 72%).

Analytical data:

27-^{t}Bu-Br:

^{1}H NMR (500 MHz, CD_2Cl_2): δ 5.73 [dm, *J*(PH) = 403 Hz, 2H, PH], 1.61-1.31 [m, 38H, C(CH_3) and BH_2].

^{31}P{^{1}H}NMR (202 MHz, CD_2Cl_2): δ 26.8 [m, AX2, J(PB) = 102 Hz, 2P].

11B NMR (160 MHz, CD_2Cl_2): δ −41.2 [br, BH_2].

ESI-MS (C_6H_5F, 60 °C, 4.5 kV): calc. for $[C_{16}H_{40}BP_2]^+$ 305.27; found m/z, 305.27.

Microanalysis: Requires: C, 49.89; H, 10.47. Found: C, 49.85; H, 10.40.

Crystals suitable for X-ray diffraction were grown from CH_2Cl_2 solution of the complex layered with hexane at 0 °C.

27-Cy-Br:

^{1}H NMR (500 MHz, CD_2Cl_2): δ 5.80 [dm, *J*(PH) = 405 Hz, 2H, PH], 2.33-0.80 [m, 46H, $(C_6H_{11})4$ and BH_2].

^{31}P{^{1}H} NMR (202 MHz, CD_2Cl_2): δ −1.2 [br, 2P]. ^{11}B NMR (160 MHz, CD_2Cl_2): δ −44.0 [br, BH_2].

ESI-MS (C_6H_5F, 60 °C, 4.5 kV): calc. for $[C_{24}H_{48}BP_2]^+$ 409.33; found m/z, 409.34.

Microanalysis: Requires: C, 58.91; H, 9.89. Found: C, 58.72; H, 10.02.

27-Ph-Br:

^{1}H NMR (500 MHz, CD_2Cl_2): δ 8.96 [dm, *J*(PH) = 457 Hz, 2H, PH], 7.74-7.21 [m, 20H, Ph], 2.35 [br, 2H, BH_2].

^{1}H{^{11}B} NMR (300 MHz, CD_2Cl_2, selected data): δ 2.35 [br.t, 2H, BH_2].

^{11}B NMR (160 MHz, CD_2Cl_2): δ −36.5 [br, BH_2].

^{31}P{^{1}H} NMR (202 MHz, CD_2Cl_2): δ −18.5 [m, AX2, J(PB) = 143 Hz, 2P].

ESI-MS (C_6H_5F, 60 °C, 4.5 kV): calc. for $[C_{24}H_{24}BP_2]^+$ 385.14; found m/z, 385.15.

Microanalysis: Requires: C, 61.98; H, 5.20. Found: C, 61.78; H, 5.17.

[(PR$_2$H)$_2$BH$_2$]OTf, R = tBu (**27**-^{t}Bu-OTf), Cy (**27**-Cy-OTf), Ph (**27**-Cy-OTf).

In a typical experiment, a Schlenk flask was charged with [H$_2$B(PR$_2$H)$_2$]Br (20 mg) and AgOTf (1 eq.). The solids were dissolved in CH_2Cl_2 (3 mL) and stirred for 2 hours, during which precipitation of solid, assigned as AgBr, was observed. The solution was filtered through a Celite® pad, and the solvent was removed in vacuo to yield a colourless oil. Addition of hexane (3 mL) and subsequent sonication resulted in precipitation of the product. After drying in vacuo, the pure product was obtained as a white solid and stored under argon in a glove box. Yield: **27**-^{t}Bu-OTf (16 mg, 69%), **27**-Cy-OTf (13 mg, 55%), **27**-Cy-OTf (16 mg, 67%).

Analytical data:

27-^{t}Bu-OTf:

^{1}H NMR (500 MHz, CD_2Cl_2): δ 4.93 (dm, *J*(PH) = 393, 2H, P-H), 1.60-1.14 (m, 38H, C(CH_3)$_3$ and BH_2).

^{31}P{^{1}H} NMR (202 MHz, CD_2Cl_2): δ 31.6 [br, 2P].

^{11}B NMR (160 MHz, CD_2Cl_2): δ −42.0 [br].

ESI-MS (C_6H_5F, 60 °C, 4.5 kV): calc. for [$C_{16}H_{40}BP_2$]$^+$ 305.27; found m/z, 305.27.

Microanalysis: Requires: C, 44.94; H, 8.87. Found: C, 44.92; H, 8.69.

Crystals suitable for X-ray diffraction were grown from CH_2Cl_2 solution of the complex layered with hexane at 0 °C.

27-Cy-OTf:

^{1}H NMR (500 MHz, CD_2Cl_2): δ 4.86 [dm, *J*(PH) = 395 Hz, 2H, P-H], 2.20-0.80 [m, 46H, (C_6H_{11})$_4$ and BH_2].

$^{31}P\{^{1}H\}$NMR (202 MHz, CD_2Cl_2): δ 2.8 [m, AX2, J(PB) = 101 Hz, 2P].

^{11}BNMR (160 MHz, CD_2Cl_2): δ −44.1 [br].

ESI-MS (C_6H_5F, 60 °C, 4.5 kV): calc. for $[C_{24}H_{48}BP_2]^+$ 409.33; found m/z, 409.34.

Microanalysis: Requires: C, 53.77; H, 8.66. Found: C, 53.61; H, 8.42.

27-Ph-OTf:

^{1}H NMR (500 MHz, CD_2Cl_2): δ 7.73–7.19 [m, 20H, Ph], 7.52 [dm, *J*(PH) = 442 Hz, 2H, PH], 2.40 [br, 2H, BH_2].

$^{31}P\{1H\}$ NMR (202 MHz, CD_2Cl_2): δ −13.3 [m, AX2, J(PB) = 154 Hz, 2P].

^{11}B NMR (160 MHz, CD_2Cl_2): δ −41.6 [br].

ESI-MS (C_6H_5F,60 °C, 4.5 kV): calc. for $[C_{24}H_{24}BP_2]^+$ 385.14; found m/z, 385.15.

Microanalysis: Requires: C, 56.20; H, 4.53. Found: C, 56.12; H, 4.83.

$[(PR_2H)_2BH_2][BAr^F{}_4]$, R = tBu (**27**-^{t}Bu-BAr^F), Cy (**27**-Cy-BAr^F), Ph (**27**-Cy-BAr^F).

In a typical experiment, a Schlenk flask was charged with $[(PR_2H)_2BH_2]Br$ (20 mg) and $Na[BAr^F{}_4]$ (1 eq.). The solids were dissolved in CH_2Cl_2 (3 mL) and stirred for 2 h, during which precipitation of solid, assigned as NaBr, was observed. The solution was removed *in vacuo* to yield colourless oil. Addition of hexane (3 mL) and subsequent sonication resulted in precipitation of the product. After drying *in vacuo*, the pure product was obtained as a white solid and stored under argon in a glove box. Yield: **27**-^{t}Bu-BAr^F (16 mg, 69%), **27**-Cy-BAr^F (13 mg, 55%), **27**-Ph-BAr^F (16 mg, 67%).

Analytical data:

27-^{t}Bu-BAr^{F}:

^{1}H NMR (500 MHz, CD_2Cl_2): δ 4.93 (dm, *J*(PH) = 393 Hz, 2H, P-H), 1.60-1.14 (m, 38H, $C(CH_3)_3$ and BH_2).

^{31}P{^{1}H} NMR (202 MHz, CD_2Cl_2): δ 31.6 [br, 2P].

^{11}B NMR (160 MHz, CD_2Cl_2): δ −42.0 [br].

ESI-MS (C_6H_5F, 60 °C, 4.5 kV): calc. for $[C_{16}H_{40}BP_2]^+$ 305.27; found m/z, 305.27.

Microanalysis: Requires: C, 44.94; H, 8.87. Found: C, 44.92; H, 8.69.

Crystals suitable for X-ray diffraction were grown from CH_2Cl_2 solution of the complex layered with hexane at 0 °C.

27-Cy-BAr^{F}:

^{1}H NMR (500 MHz, CD_2Cl_2): δ 4.86 [dm, *J*(PH) = 395 Hz, 2H, P-H], 2.20-0.80 [m, 46H, $(C_6H_{11})_4$ and BH_2].

^{31}P{^{1}H} NMR (202 MHz, CD_2Cl_2): δ 2.8 [m, AX2, J(PB) = 101 Hz, 2P].

^{11}B NMR (160 MHz, CD_2Cl_2): δ −44.1 [br].

ESI-MS (C_6H_5F, 60 °C, 4.5 kV): calc. for $[C_{24}H_{48}BP_2]^+$ 409.33; found m/z, 409.34.

Microanalysis: Requires: C, 53.77; H, 8.66. Found: C, 53.61; H, 8.42.

27-Ph-BAr^{F}:

^{1}H NMR (500 MHz, CD_2Cl_2): δ 7.73–7.19 [m, 20H, Ph], 7.52 [dm, *J*(PH) = 442 Hz, 2H, PH], 2.40 [br, 2H, BH_2].

$^{31}P\{^{1}H\}$ NMR (202 MHz, CD_2Cl_2): δ −13.3 [m, AX2, J(PB) = 154 Hz, 2P].

$^{11}B\{^{1}H\}$ NMR (160 MHz, CD_2Cl_2, selected data): δ −39.0 [t, 1 J(PB) = 73].

^{11}B NMR (160 MHz, CD_2Cl_2): δ −41.6 [br].

ESI-MS (C_6H_5F, 60 °C, 4.5 kV): calc. for $[C_{24}H_{24}BP_2]^+$ 385.14; found m/z, 385.15.

Microanalysis: Requires: C, 53.88; H, 2.91. Found: C, 53.76; H, 3.00.

Chapter 3

N-(bis(2-methoxyphenyl)phosphino)-1,1-bis(2-methoxyphenyl)-N-methylphosphinamine (37)[22, 23]

(2-methoxyphenyl)magnesium bromide: A Schlenk flask was charged with 2-bromo-anisole (3.75 mL, 0.030 mol) and THF (25 mL) and then degassed by bubbling argon gas through the solution for 15 min. A three-necked round bottomed flask, equipped with an argon inlet, condenser and a suba-seal was charged (under argon) with magnesium turnings (0.875 g, 0.036 mol) and degassed THF (3 mL). Also a small crystal of iodine was added. Slowly a few drops of the anisole solution were added to the round-bottomed flask, and heated with a heat-gun to initiate the reaction. When bubbling started slowly the rest of the anisole solution was added drop-wise to keep a steady reflux. When the addition was complete, the reaction was allowed to continue reflux at 75 °C (oil-bath) for 16 h. The obtained yellow/grey solution was filtered and stored in a freezer.

1,1-dichloro-N-(dichlorophosphino)-N-methylphosphinamine: A two-necked round-bottomed flask, equipped with a condenser with an argon inlet at the top and a suba-seal was charged with $MeNH_2$.HCl (5.0 g, 0.074 mol) (dried over-night *in vacuo* at room-temperature) and 1,1,2,2-tetrachloroethylene (60 mL). To the mixture PCl_3 (26.5 mL, 0.304 mol) was added. The mixture

was allowed to reflux for 10 days. The mixture was then filtered at room-temperature and the solvent was removed *in vacuo*. The spectral data corresponds to the previously published data.

N-(bis(2-methoxyphenyl)phosphino)-1,1-bis(2-methoxyphenyl)-N-methylphosphinamine: In a pump-filled Schlenk flask 1,1-dichloro-N-(dichlorophosphino)-N-methylphosphinamine (0.5 mL, 3.25 mmol) was dissolved in THF (5 mL). The solution was cooled to –78 °C, and drop-wise the (2-methoxyphenyl)magnesium bromide solution in THF (20 mL, 19.49 mmol) was added. The dry-ice bath was removed and the reaction mixture was left stirring, while slowly reaching room temperature. After 2 hours of stirring the solvent was removed *in vacuo*, and the resulting brown sticky solid was washed with ice-cold methanol yielding a white powder. To remove any methanol 2 x 10 mL wash/sonication and removal *in vacuo* can be carried out followed by a wash with hexane and filtration. The spectral data corresponds to the previously published data.

^{1}H NMR (300 MHz, CD_2Cl_2): δ 7.28 (t, 4H, aromatic H), 6.97 (m, 4H, aromatic H), 6.81 (m, 8H, aromatic H), 3.54 (s, 12H, OCH_3), 2.26 (t, 3H, NCH_3).

^{31}P{^{1}H} NMR (121 MHz, CD_2Cl_2): δ 52.1 [s]

N-(bis(2-ethylphenyl)phosphino)-1,1-bis(2-ethylphenyl)-N-methylphosphinamine (38)[24, 25]

1,1-dichloro-N-(dichlorophosphino)-N-methylphosphinamine was synthesised as described above.

(2-ethylphenyl)magnesium bromide: A Schlenk flask was charged with 1-bromoethylbenzene (1.49 mL, 0.011 mol) and THF (10 mL) and then degassed by freeze-pump-thaw cycles. A three-necked round bottomed flask, equipped with an argon inlet, condenser and a suba-seal was

charged (under argon) with magnesium turnings (0.323 g, 0.013 mol) and degassed THF (3 mL). Also a small crystal of iodine was added. Slowly a few drops of the bromide solution were added to the round-bottomed flask, and heated with a heat-gun to initiate the reaction. When bubbling started slowly the rest of the bromide solution was added drop-wise to keep a steady reflux. When the addition was complete, the reaction was allowed to continue reflux at 75 °C (oil-bath) for 14h. The obtained yellow/grey solution was filtered and stored in a freezer.

N-(bis(2-ethylphenyl)phosphino)-1,1-bis(2-ethylphenyl)-N-methylphosphinamine:

In a pump-filled Schlenk flask 1,1-dichloro-N-(dichlorophosphino)-N-methylphosphinamine (0.14 mL, 0.9 mmol) was dissolved in THF (3 mL). The solution was cooled to –78 °C, and drop-wise the (2-methoxyphenyl)magnesium bromide solution in THF (5.5 mL, 5.4 mmol) was added. The dry-ice bath was removed and the reaction mixture was left stirring, while slowly reaching room temperature. The solution was then allowed to stir for at 40 °C for 14 h. The solvent was removed *in vacuo*, and the resulting brown sticky solid was washed with ice-cold methanol yielding a white powder. To remove any methanol 2 x 10 mL wash/sonication and removal *in vacuo* can be carried out followed by a wash with hexane and filtration (the obtained solid is quite soluble in methanol, so care should be taken during the washing). The spectral data corresponds to the previously published data.

^{1}H NMR (500 MHz, CD_2Cl_2): δ 7.37 – 7.31 (m, 8H, aromatic H), 7.15 – 7.05 (m, 8H, aromatic H), 2.78 (dq, 4H, CH(*H*)CH_3), 2.57 (dq, 4H, C(*H*)HCH_3) 1.17 [t, 3H, *J*(PH) 7.6 Hz, NCH_3].

^{31}P{^{1}H} NMR (202 MHz, CD_2Cl_2): δ 55.9 [s]

N-(bis(4-methoxyphenyl)phosphino)-1,1-bis(4-methoxyphenyl)-N-methylphosphinamine (**39**)[26]

1,1-dichloro-N-(dichlorophosphino)-N-methylphosphinamine was synthesised as described above.

(4-methoxyphenyl)magnesium bromide: A Schlenk flask was charged with 4-bromo-anisole (3.75 mL, 0.030 mol) and THF (25 mL) and then degassed by bubbling argon gas through the solution for 15 min. A three-necked round bottomed flask, equipped with an argon inlet, condenser and a suba-seal was charged (under argon) with magnesium turnings (0.875 g, 0.036 mol) and degassed THF (3 mL). Also a small crystal of iodine was added. Slowly a few drops of the anisole solution were added to the round-bottomed flask, and heated with a heat-gun to initiate the reaction. When bubbling started slowly the rest of the anisole solution was added drop-wise to keep a steady reflux. When the addition was complete, the reaction was allowed to continue reflux at 75 °C (oil-bath) for 16 h. The obtained yellow/grey solution was filtered and stored in a freezer.

N-(bis(4-methoxyphenyl)phosphino)-1,1-bis(4-methoxyphenyl)-N-methylphosphinamine:

In a pump-filled Schlenk flask 1,1-dichloro-N-(dichlorophosphino)-N-methylphosphinamine (0.5 mL, 3.25 mmol) was dissolved in THF (5 mL). The solution was cooled to –78 °C, and drop-wise the (2-methoxyphenyl)magnesium bromide solution in THF (20 mL, 19.49 mmol) was added. The dry-ice bath was removed and the reaction mixture was left stirring, while slowly reaching room temperature. After 2 hours of stirring the solvent was removed *in vacuo*, and the resulting brown sticky solid was washed with ice-cold methanol yielding a white powder. To remove any methanol 2 x 10 mL wash/sonication and removal *in vacuo* can be carried out followed by a wash with hexane and filtration. The spectral data corresponds to the previously published data.

^{1}H NMR (400 MHz, CD_2Cl_2): δ 7.22-7.16 (m, 8H, aromatic H), 6.81-6.79 (d, 8H, aromatic H), 3.75 (s, 12H, OCH_3), 2.26 [t, 3H, *J*(PH) 3.1 Hz, NCH_3].

^{31}P{^{1}H} NMR (162 MHz, CD_2Cl_2): δ 70.0 [s]

[Rh{(2-OMe-C_6H_4)$_2$PNMeP(2-OMe-C_6H_4)$_2$}(cod)][BAr^F_4] (**40**)

Under argon atmosphere, **37** (1.2 mL, 0.085 mmol) in C_6H_5F was added to a solution of [Rh(cod)$_2$][BAr^F_4] (0.100 g, 0.085 mmol) in C_6H_5F (1 mL). The obtained orange homogeneous solution was allowed to stir for 1 hour. Subsequently the solvent was removed *in vacuo*. The obtained oily solid was washed and sonicated using pentane (10 mL). The solid was recrystallized from fluorobenzene/pentane. The solid was filtered and then further washed and sonicated using pentane. The analytically pure orange solid was dried *in vacuo* (0.81 g, 73% yield)

^{1}H NMR (250 MHz, C_6H_5F): δ 8.33 (s, 8H, BAr^F_4), 7.64 (s, 4H, BAr^F_4), 7.48-6.48 (m, 16H, aromatic H and free C_6H_5F), 4.55 (br, 4H, cod-CH), 3.24 (s, 12H, OCH_3), 2.34 (t, ^{3}J(PH) = 9.6 Hz, 3H, NCH_3) 1.95 (br, 8H, cod-CH_2).

^{31}P{^{1}H} NMR (101 MHz, C_6H_5F): δ 42.7 [d, *J*(RhP) 131 Hz]

ESI-MS (C_6H_5F, 60 °C, 4.5 kV): calc for $[C_{20}H_{39}FNP_2Rh]^+$ 730.17, obs. m/z, 730.17. The observed isotopomer pattern (3 lines) is fully consistent with the molecular formula.

Microanalysis: Requires: C, 52.00; H, 3.48; N, 0.88. Found: C, 50.80; H, 3.19; N, 1.00.

[Rh{(2-OMe-C_6H_4)$_2$PNMeP(2-OMe-C_6H_4)$_2$}(C_6H_5F)][BAr^F_4] (**41**)

Under argon atmosphere, **37** (1.2 mL, 0.085 mmol) in C_6H_5F was added to a solution of [Rh(cod)$_2$][BAr^F_4] (0.100 g, 0.085 mmol) in C_6H_5F (1 mL). The obtained orange homogeneous solution was allowed to stir for 1 hour. The mixture was then set under hydrogen atmosphere

(4 atm) and allowed to stir for 16 hours during which the colour of the solution changes from orange to pale orange. The solvent was removed *in vacuo*. The obtained oily solid was washed and sonicated using pentane (10 mL). The obtained solid was recrystallized from fluorobenzene/pentane. The solid was filtered and then further washed and sonicated using petane. The analytically pure pale orange solid was dried *in vacuo* (0.81 g, 73% yield)

Crystals suitable for X-ray diffraction were grown from a C_6H_5F solution of the complex layered with pentane at 0 °C.

^{1}H NMR (250 MHz, C_6H_5F): δ 8.32 (s, 8H, BAr^F_4), 7.67 (s, 4H, BAr^F_4), 7.50-6.45 (m, C_6H_5F solvent and ArH), 6.22 (t, 2H, η^6-C_6H_5F), 6.05 (m, 2H, η^6-C_6H_5F), 5.58 (t, 1H, η^6-C_6H_5F), 3.14 (s, 12H, OCH_3), 2.67 (t, ^3J(PH) 11.1 Hz, 3H, NCH_3).

^{31}P{^{1}H} NMR (101 MHz, C_6H_5F): δ 45.5 [d, *J*(RhP) 187 Hz, *J*(PF) 2.9 Hz]

ESI-MS (C_6H_5F, 60 °C, 4.5 kV): calc for $[C_{20}H_{39}FNP_2Rh]^+$ 718.12, obs. m/z, 718.12. The observed isotopomer pattern (3 lines) is fully consistent with the molecular formula.

Microanalysis: Requires: C, 58.51; H, 5.05; N, 1.95. Found: C, 58.14; H, 4.89; N, 1.94.

$[Rh\{(2\text{-}OMe\text{-}C_6H_4)_2PNMeP(2\text{-}OMe\text{-}C_6H_4)_2\}(acetone)_2][BAr^F_4]$ (**44 – 46**) (*in situ*)

In a J. Youngs NMR tube **41** was dissolved in acetone-d_6. The obtained orange solution was allowed to stand for 5 min.

^{1}H NMR (500 MHz, acetone-d_6, selected data): δ 7.82 (s, 8H, BAr^F_4), 7.70 (s, 4H, BAr^F_4), 7.11 (m, free C_6H_5F), 3.50 (m, 12H, OCH_3), 2.67 (t, ^3J(PH) 11.1 Hz, 3H, NCH_3).

^{31}P{^{1}H} NMR (202 MHz, acetone): δ 51.0 [dm, *J*(RhP) 193 Hz, *J*(PP) 105 Hz], 50.2 [d, *J*(RhP) 188 Hz], 43.0 [d, *J*(RhP) 188 Hz], 42.0 [d, *J*(RhP) 188 Hz], 41.4 [dm, *J*(RhP) 188 Hz, *J*(PP) 105 Hz].

[Rh{(2-OMe-C_6H_4)$_2$PNMeP(2-OMe-C_6H_4)$_2$}(MeCN)$_2$][BAr^F_4] (**43**)

In a J.Youngs NMR tube from the acetone solution of **44**-**46** the solvent was removed under reduced pressure and the obtained oily product was dissolved in MeCN-d_2. This resulted in immediate colour change from orange to yellow. The solvent was removed under reduced pressure and the obtained wax-like product was washed with hexane and recrystallised from dichloromethane/hexane solution.

^{1}H NMR (300 MHz, MeCN-d_2): δ 7.99-7.43 (m, 28H, Ar-H and BAr^F_4), 7.03 (m, 5H, free C_6H_5F), 3.39 (s, 12H, OCH_3), 2.71 (t, ^3J(PH) 11.0 Hz, 3H, NCH_3).

^{31}P{^{1}H} NMR (121 MHz, MeCN-d_2): δ 49.0 [d, *J*(RhP) 160Hz].

Microanalysis: Requires: C, 49.61; H, 3.52; N, 2.67. Found: C, 50.04; H, 3.59; N, 2.55.

[Rh{(2-Et-C_6H_4)$_2$PNMeP(2-Et-C_6H_4)$_2$}(cod)][BAr^F_4] (**47**)

Under argon atmosphere, **38** (0.050, 0.098 mmol) in C_6H_5F (5 mL) was added to a solution of [Rh(cod)$_2$][BAr^F_4] (0.116 g, 0.098 mmol) in C_6H_5F (1 mL). The obtained orange homogeneous solution was allowed to stir for 1 hour. The solvent was removed *in vacuo*. The obtained oily solid was washed and sonicated using pentane (10 mL). The obtained solid was recrystallized from fluorobenzene/pentane. The solid was filtered and then further washed and sonicated using pentane. The analytically pure orange solid was dried *in vacuo* (0.124 g, 80% yield).

^{1}H NMR (300 MHz, CD_2Cl_2): δ 7.75 (s, 8H, BAr^F_4), 7.69-7.60 (m, 4H, Ar-H), 7.57 (s, 4H, BAr^F_4), 7.55-7.00 (m, 12H, Ar-H), 4.44 (m, cod, 2H), 3.30 (m, cod, 2H), 2.57 (t, 3H, NCH_3), 2.57-2.30 (m, 8H, CH_2), 1.37 (br, 6H, CH_3), 0.93 (br, 6H, CH_3).

^{31}P{^{1}H} (121 MHz, CD_2Cl_2): δ 38.6 [d, *J*(RhP) 135 Hz]

ESI-MS (C_6H_5F, 60 °C, 4.5 kV): calc for $[C_{41}H_{51}NP_2Rh]^+$ 722.26, obs. m/z, 722.26. The observed isotopomer pattern (4 lines) is fully consistent with the molecular formula.

Microanalysis: Requires: C, 55.29; H, 4.00; N, 0.88. Found: C, 54.05; H, 3.63; N, 0.94.

[Rh{(2-Et-C_6H_4)$_2$PNMeP(2-Et-C_6H_4)$_2$}(nbd)][BAr^F_4]

Under argon atmosphere, **38** (0.070, 0.136 mmol) in C_6H_5F (5 mL) was added to a solution of [Rh(nbd)$_2$][BAr^F_4] (0.157 g, 0.136 mmol) in C_6H_5F (1 mL). The obtained orange homogeneous solution was allowed to stir for 1 hour. The solvent was removed *in vacuo*. The obtained oily solid was washed and sonicated using pentane (10 mL). The obtained solid was recrystallized from fluorobenzene/pentane. The solid was filtered and then further washed and sonicated using pentane. The analytically pure orange solid was dried *in vacuo* (0.160 g, 75% yield).

^{1}H NMR (500 MHz, CD_2Cl_2): δ 7.76 (s, 8H, BAr^F_4), 7.61 (s, 4H, BAr^F_4), 7.61-7.00 (br.m, 16H, Ar-H), 4.14 (br, nbd, 2H), 3.33 (br, nbd, 2H), 2.45 (br, 3H, NCH_3), 2.10-1.82 (br, 4H, CH_2), 1.48 (br, 4H, CH_2), 1.32 (br, 4H, CH_3), 0.92 (br, 8H, CH_3).

^{31}P{^{1}H} (202 MHz, CD_2Cl_2): δ 43.0 [d, *J*(RhP) 140 Hz]

ESI-MS (C_6H_5F, 60 °C, 4.5 kV): calc for $[C_{40}H_{47}NP_2Rh]^+$ 706.22, obs. m/z, 706.22. The observed isotopomer pattern (4 lines) is fully consistent with the molecular formula.

Microanalysis: Requires: C, 55.09; H, 3.79; N, 0.89. Found: C, 54.93; H, 3.90; N, 0.94.

[Rh{(2-Et-C_6H_4)$_2$PNMeP(2-Et-C_6H_4)$_2$}(C_6H_5F)][BAr^F_4] (**48**)

Under argon atmosphere, **38** (0.070, 0.136 mmol) in C_6H_5F (5 mL) was added to a solution of [Rh(cod)$_2$][BAr^F_4] (0.157 g, 0.136 mmol) in C_6H_5F (1 mL). The obtained orange homogeneous solution was allowed to stir for 1 hour. The mixture was then set under hydrogen atmosphere (4 atm) and allowed to stir for 16 hours during which the colour of the solution changes from orange to pale orange. The solvent was removed *in vacuo*. The obtained oily solid was washed and sonicated using pentane (10 mL). The obtained solid was recrystallized from

fluorobenzene/pentane. The solid was filtered and then further washed and sonicated using petane. The analytically pure pale orange solid was dried *in vacuo* (0.150 g, 70% yield)

^{1}H NMR (500 MHz, CD_2Cl_2): δ 7.76 (s, 8H, BAr^F_4), 7.54 (s, 4H, BAr^F_4), 7.52-7.04 (br.m, 16H, Ar-H), 6.63-6.00 (m, η^6-C_6H_5F, 2H), 2.95-2.10 (br, CH_2, 2H), 2.47 (br, 3H, NCH_3), 1.31-0.86 (br, 12H, CH_3).

^{31}P{^{1}H} (202 MHz, CD_2Cl_2): δ 44.5-35.4 [br.d]

^{31}P{^{1}H} (202 MHz, CD_2Cl_2, –60 °C): δ 53.6-49.6 [br.m, 1P], 32.5-27.9 [m, 1P].

^{31}P{^{1}H} (202 MHz, CD_2Cl_2, –90 °C): δ 53.6-49.6 [m, 1P], 32.5-27.9 [m, 1P].

^{31}P{^{1}H} (202 MHz, C_6H_5F): δ 41.9-36.4 [br.d]

^{31}P{^{1}H} (202 MHz, C_6H_5F, 90 °C): δ 40.6 [d, *J*(RhP) 188 Hz)

ESI-MS (C_6H_5F, 60 °C, 4.5 kV): calc for $[C_{40}H_{47}NP_2Rh]^+$ 710.20, obs. m/z, 710.20. The observed isotopomer pattern (4 lines) is fully consistent with the molecular formula.

Microanalysis: Requires: C, 54.18; H, 3.59; N, 0.89. Found: C, 54.32; H, 3.44; N, 0.95.

$[Rh\{(2\text{-}Et\text{-}C_6H_4)_2PNMeP(2\text{-}Et\text{-}C_6H_4)_2\}(acetone)_2][BAr^F_4]$ (**49**) (*in-situ*)

Under argon atmosphere the fluorobenzene complex (**48**) was dissolved in acetone-d_6. The reaction was allowed to stand for 5 minutes.

^{1}H NMR (500 MHz, acetone-d_6): δ 7.83 (s, 8H, BAr^F_4), 7.69 (s, 4H, BAr^F_4), 7.62-7.13 (m, 21H, aromatic H and free C_6H_5F), 2.82 (br, 3H, NCH_3), 2.53 (m, 8H, CH_2), 1.14-0.92 (br, 12H, CH_3).

^{31}P{^{1}H} NMR (202 MHz, acetone-d_6): δ 45.4 [d, *J*(RhP) 178 Hz]

41 + 2-(diphenylphosphino)benzaldehyde (**56**) (*in-situ*)

A J. Youngs NMR tube was charged with **41** (11mg, 0.007 mmol) and 2–(diphenylphosphino)benzaldehyde (**G**) (2 mg, 0.007 mmol). The solids were dissolved in acetone-d_6 (0.6 mL). This resulted in a colour change from orange to pale orange.

^{1}H NMR (500 MHz, acetone-d_6): δ 7.83 (s, 8H, $BAr^F{}_4$), 7.69 (s, 4H, $BAr^F{}_4$), 7.65-6.64 (m, 20H, ArH), 3.65 (s, 3H, OMe), 3.42 (s, 3H, OMe), 3.24 (s, 3H, OMe), 2.99 (s, 3H, OMe), 2.87 (m, 3H, NMe), –18.56 (br, 1H, RhH).

^{31}P{^{1}H} NMR (202 MHz, acetone-d_6): δ 65.8 [br.d, 2P, *J*(RhP) 127 Hz], 50.0 [br, 1P].

ESI-MS (C_6H_5F, 60 °C, 4.5 kV): calc for $[C_{40}H_{47}NP_2Rh]^+$ 912.16, obs. m/z, 912.16. The observed isotopomer pattern (3 lines) is fully consistent with the molecular formula.

Chapter 4

$[Rh(^iPr_2PCH_2P^iPr_2)(SMe)(C_6H_4(C(O)Me)]_2[BAr^F{}_4]_2$ (**87**)

A J. Youngs NMR tube was charged with $[Rh(^iPr_2PCH_2P^iPr_2)(C_6H_5F)][BAr^F{}_4]$ **6** (10.0 mg, 0.0076 mmol) and $MeSC_6H_4C(O)CH_3$ (**J**) (1.3 mg, 0.0076 mmol). The solids were dissolved in acetone-d_6 (0.6 mL). The mixture was allowed to rotate for 24 h. The mixture contains two isomers.

^{1}H NMR (500 MHz, acetone-d_6, selected data): δ 8.32-7.95 [m, 6H, C_6H_4(C(O)Me)], 7.81 [s, 16H, $BAr^F{}_4$], 7.70 [s, 8H, $BAr^F{}_4$], 7.59-7.12 [m, 12H, C_6H_4(C(O)Me) and free C_6H_5F], 3.28 [s, 3H, C(O)Me], 3.23 [s, 3H, C(O)Me], 1.83-1.29 [m, 44H, CH_2 and CH_3], 1.02 [m, 6H, CH_3], 0.78 [m, 6H, CH_3].

^{31}P{^{1}H} NMR (500 MHz, acetone-d_6): δ 5.1 [dd, *J*(RhP) 116 Hz, *J*(PP) 53 Hz, major isomer], 4.2 [dd, *J*(RhP) 116 Hz, *J*(PP) 53 Hz, minor isomer], –11.4 [dd, *J*(RhP) 90 Hz, *J*(PP) 53 Hz, major isomer], -13.9 [dd, *J*(RhP) 90 Hz, *J*(PP) 53 Hz, minor isomer]. The isomers were formed in 64:36 ratio.

ESI-MS (acetone, 60 °C, 4.5 kV): ESI-MS: calc for $[C_{23}H_{42}OP_2RhS]^+$ 517.13 obs. m/z, 517.13. The observed isotopomer pattern (5 lines) is fully consistent with the molecular formula.

$[Rh(^iPr_2PCH_2P^iPr_2)(SMe)(C_6H_4(C(O)CHCHC_6H_{13})]_2[BAr^F_4]_2$ (89)

A J. Youngs NMR tube was charged with $[Rh(^iPr_2PCH_2P^iPr_2)(C_6H_5F)][BAr^F_4]$ **6** (10.0 mg, 0.0076 mmol) and $MeSC_6H_4C(O)CHCHC_6H_{13}$ (**F**) (2.0 μL, 0.0076 mmol). The mixture was dissolved in acetone-d_6 (0.6 mL). The mixture was allowed to rotate for 24 h. The mixture contains two isomers.

^{1}H NMR (500 MHz, acetone-d_6, selected data): δ 8.34 [m, 4H, $C_6H_4(C(O)Me)$], 8.05 [m, 2H, $C_6H_4(C(O)Me)$], 7.81 [s, 16H, BAr^F_4], 7.70-7.04 [s, 22H, BAr^F_4 and $C_6H_4(C(O)Me)$], 7.13 [m, 10H, C_6H_5F].

^{31}P{^{1}H} NMR (500 MHz, acetone-d_6): δ 2.5 [dd, *J*(RhP) 118 Hz, *J*(PP) 53 Hz, minor isomer], 1.4 [dd, *J*(RhP) 113 Hz, *J*(PP) 53 Hz, major isomer], –8.7 [dd, *J*(RhP) 92 Hz, *J*(PP) 53 Hz, minor isomer], -13.4 [dd, *J*(RhP) 90 Hz, *J*(PP) 53 Hz, major isomer]. The isomers were formed in 79:21 ratio.

ESI-MS (acetone, 60 °C, 4.5 kV): ESI-MS: calc for $[C_{23}H_{42}OP_2RhS]^+$ 613.23 obs. m/z, 613.23. The observed isotopomer pattern (5 lines) is fully consistent with the molecular formula.

5.7. Catalysis

The catalytic reactions were run in a small vial equipped with a magnetic stirrer and sealed with a septum. The vial was charged with the catalyst in a glovebox and sealed under argon atmosphere. The reagents were measured into a small Schlenk flask, dissolved in acetone solvent and thoroughly degassed prior to the catalysis using the freeze-pump-thaw method. The reaction was initiated by cannula transfer of the substrates in acetone to the solid catalyst. The samples were periodically taken using a micro-syringe (10 μL) out and quenched in acetonitrile

(1.5 mL) (we have shown that excess acetonitrile inhibits the reaction. Upon leaving the sample in acetonitrile overnight no change in aldehyde to ketone ratio is seen by HPLC).

5.8. References

1. A. B. Pangborn, M. A. Giardello, R. H. Grubbs, R. K. Rosen and F. J. Timmers, *Organometallics*, 1996, **15**, 1518-1520.
2. www.acros.com.
3. D. R. Burfield and R. H. Smithers, *J. Org. Chem.*, 1978, **43**, 3966-3968.
4. www.sigma-aldrich.com.
5. A. T. Lubben, J. S. McIndoe and A. S. Weller, *Organometallics*, 2008, **27**, 3303-3306.
6. J. Cosier and A. M. Glazer, *J. Appl. Crystallogr.*, 1986, **19**, 105-107.
7. Z. Otwinowski, W. Minor and C. W. Carter, *Methods Enzymol.*, **276**, 307-326
8. A. Altomare, G. Cascarano, C. Giacovazzo, A. Guagliardi, M. C. Burla, G. Polidori and M. Camalli, *J. Appl. Crystallogr.*, 1994, **27**, 435.
9. M. C. Burla, R. Caliandro, M. Camalli, B. Carrozzini, G. L. Cascarano, L. De Caro, C. Giacovazzo, G. Polidori and R. Spagna, *J. Appl. Crystallogr.*, 2005, **38**, 381-388.
10. G. M. Sheldrick, *Acta Crystallogr. Sect. A*, 2008, **64**, 112-122.
11. W. E. Buschmann and J. S. Miller, *Inorg. Synth.*, 2002, **33**, 83-91.
12. E. W. Abel, M. A. Bennett and G. Wilkinson, *J. Chem. Soc.*, 1959, 3178-3182.
13. R. R. Schrock and J. A. Osborn, *J. Am. Chem. Soc.*, 1971, **93**, 2397-&.
14. J. L. Herde, J. C. Lambert, C. V. Senoff and M. A. Cushing, *Inorg. Synth.*, 1974, **15**, 18-20.
15. B. Guzela, M. A. Omarya, J. P. Fackler Jr and A. Akgermand, *Inorg. Chim. Acta*, 2001, **325**, 45-50.
16. A. B. Chaplin, J. F. Hooper, A. S. Weller and M. C. Willis, *J. Am. Chem. Soc.*, 2012, **134**, 4885-4897.
17. M. C. Maumela, K. Blann, H. de Bod, J. T. Dixon, W. F. Gabrielli and D. B. G. Williams, *Synthesis-Stuttgart*, 2007, 3863-3867.
18. J. Wolf, M. Manger, U. Schmidt, G. Fries, D. Barth, B. Weberndorfer, D. A. Vicic, W. D. Jones and H. Werner, *J. Chem. Soc.-Dalton Trans.*, 1999, 1867-1875.
19. Z. S. Novikova, A. A. Prishchenko and I. F. Lutsenko, *Zhurnal Obshchei Khimii*, 1977, **47**, 775-781.
20. M. D. Fryzuk, T. Jones and F. W. B. Einstein, *Organometallics*, 1984, **3**, 185-191.
21. R. J. Burt, J. Chatt, W. Hussain and G. J. Leigh, *J. Organomet. Chem.*, 1979, **182**, 203-206.
22. A. Carter, S. A. Cohen, N. A. Cooley, A. Murphy, J. Scutt and D. F. Wass, *Chem. Commun.*, 2002, 858-859.
23. D. F. Wass, *Pat WO2002004119, 2002 (to British Petroleum Chemicals)*.
24. N. A. Cooley, S. M. Green, D. F. Wass, K. Heslop, A. G. Orpen and P. G. Pringle, *Organometallics*, 2001, **20**, 4769-4771.
25. C. A. Tolman, *Chem. Rev.*, 1977, **77**, 313-348.
26. S. J. Dossett, A. Gillon, A. G. Orpen, J. S. Fleming, P. G. Pringle, D. F. Wass and M. D. Jones, *Chem. Commun.*, 2001, 699-700.

6. APPENDICES

6.1. Crystallographic Data

Table 6.1. Crystallographic data for **11a**, **11b**, **11c**, **11d**, **11e**, **17b**, **21b**, **27**-^{t}Bu-Br, **27**-^{t}Bu-OTf, **27**-^{t}Bu-BAr^{F} and **41**.

	11a	**11b**	**11c**
CCDC number	894726	894729	894729
Formula	$C_{63}H_{64}BF_{25}NP_2Rh$	$C_{52}H_{49}BF_{25}P_2Rh$	$C_{51}H_{47}BF_{25}P_2Rh$
M	1485.81	1324.57	1406.55
Crystal system	Monoclinic	Monoclinic	Tetragonal
Space group	P2(1)/c	P2(1)/c	P4(3)
T / K	150	150	150
a / Å	13.81620(10)	17.2281(2)	13.14030(10)
b / Å	18.09510(10)	17.5318(2)	13.14030(10)
c / Å	26.4511(3)	18.8880(2)	34.4622(2)
α / °	90	90	90
β / °	92.0377(3)	104.5329(5)	90
γ / °	90	90	90
V / Å^3	6608.74(9)	5522.39(11)	5950.50(7)
Z	4	4	4
Density / g.cm^{-3}	1.493	1.594	1.570
μ / mm^{-1}	0.417	0.488	0.460
θ range / °	5.13 ≤ θ ≤ 26.37	5.15 ≤ θ ≤ 26.37	5.18 ≤ θ ≤ 25.02
Reflns collected	25748	20198	10231
R_{int}	0.0330	0.0161	0.042
Completeness / %	99.1	99.2	98.8
Data/restr/param	13392 / 714 / 962	11199/ 825 / 891	10231 / 714 / 918
R_1 [I > 2σ(I)]	0.0584	0.0395	0.0392
wR_2 [all data]	0.1536	0.1044	0.0996
GoF	1.078	1.033	1.023
Largest diff. pk and hole / eÅ^{-3}	2.226, -0.768	0.528, -0.540	0.580, -0.450

11d	**11e**	**17b**	**21b**
894730	894731	894728	N/A
$C_{52}H_{49}BF_{25}P_2Rh$	$C_{53}H_{51}BF_{25}P_2Rh$	$C_{53}H_{51}BF_{24}NOP_2RhS$	$C_{52}H_{47}ClBF_{24}NOP_2RhS$
1324.21	1434.70	1381.67	1419.00
Monoclinic	Triclinic	Triclinic	Triclinic
P2(1)/c	P-1	P-1	P-1
150	150	150	150
17.79940(10)	12.65720(10)	12.2384(2)	12.41860(40)
17.3901(2)	13.24700(10)	15.4948(3)	15.47660(50)
19.0524(2)	19.6804(2)	17.5543(3)	17.47910(59)
90	104.2749(5)	103.6034(7)	104.5485(16)
109.3280	106.4945(5)	109.8639(8)	109.8009(16)
90	91.3854(4)	98.8340(7)	100.0350(17)
5564.97(9)	3050.53(5)	2942.02(9)	2932.790(177)
4	2	2	2
1.581	1.562	1.560	1.607
0.484	0.450	0.495	0.556
$5.11 \leq \theta \leq 27.88$	$5.12 \leq \theta \leq 27.88$	$5.13 \leq \theta \leq 25.03$	$5.19 \leq \theta \leq 21.91$
25692	25950	18611	12045
0.0188	0.0292	0.0313	0.0504
99.2	99.3	98.9	97.9
13170 / 675 / 828	14468 / 423 / 894	10291 / 788 / 949	6961 /1323 / 861
0.0474	0.0454	0.0660	0.0550
0.1337	0.1193	0.1787	0.1378
1.015	1.033	1.033	1.025
0.928, -1.021	0.847, -0.514	2.251, -1.592	0.788, -0.537

27-^{t}Bu-Br	**27**-^{t}Bu-OTf	**27**-^{t}Bu-BAr^{F}	**41**
912134	912135	912136	N/A
$C_{16}H_{40}BP_2Br$	$C_{17}H_{40}BF_3O_3P_2S$	$C_{50}H_{58}B_2F_{24}P_2$	$C_{67}H_{48}B_1F_{24}N_1O_4P_2Rh_1$
385.14	454.30	1204.53	1581.72
orthorhombic	monoclinic	monoclinic	monoclinic
P 21 21 21	P 21/n	P 21/n	P 2(1)/c
150	150	150	150
10.6330(3)	8.84740(10)	15.97400(10)	9.95430(10)
11.8889(3)	11.19090(20)	18.19600(10)	17.46540(10)
17.0844(7)	25.10740(40)	20.96500(20)	39.37000(29)
90	90	90	90
90	2.6590(10)	111.8041(3)	92.6529(3)
90	90	90	90
2159.72(12)	2483.27(7)	5657.79(7)	6837.368(94)
4	4	4	4
1.184	1.215	1.414	1.518
2.044	0.295	0.190	0.410
5.14 ≤ θ ≤ 27.49	5.10 ≤ θ ≤ 27.51	5.11 ≤ θ ≤ 27.48	5.10 ≤ θ ≤ 27.50
2684	9241	25113	28893
0.0487	0.0303	0.0214	0.0599
98.0	99.1	99.1	98.7
4859 / 0 / 197	5676 / 0 / 260	12867 / 816 / 854	15482 / 447 / 1000
0.0489	0.0438	0.0561	0.0549
0.0762	0.1176	0.1502	0.1540
0.993	0.881	1.054	1.045
0.360, -0.580	0.352, -0.295	0.673, -0.452	1.367, 0.680

6.2. Publications

I. Pernik, J. F. Hooper, A. B. Chaplin, A. S. Weller* and M. C. Willis, Exploring small bite–angle ligands for the rhodium–catalyzed intermolecular hydroacylation of β–S–substituted aldehydes with 1–octene and 1–octyne, *ACS Catalysis* **2012**, *2*, 2779.

J. F. Hooper, R. D. Young, I. Pernik, A. S. Weller* and M. C. Willis* Carbon-carbon bond construction using boronic acids and aryl methyl sulfides: Orthogonal reactivity in Suzuki-type couplings, *Chem. Sci.* **2013**, *4*, 1568. Highlighted in *SYNFACTS.*

T. A. Shuttleworth, M. A. Huertos, I. Pernik, R. D. Young, A. S. Weller* Bis(phosphine)boronium salts. Synthesis, Structures and Co-ordination Chemistry, *Dalton Trans.* **2013**, *42*, 12917.